Heat, Bearings, and Lubrication

Springer Science+Business Media, LLC

Ralph A. Burton

Heat, Bearings, and Lubrication

Engineering Analysis of Thermally Coupled Shear Flows and Elastic Solid Boundaries

With **75** Figures

Springer

Ralph A. Burton
Burton Technologies
PO Box 33809
Raleigh, NC 27636

rburton@me1.egr.duke.edu

Library of Congress Cataloging-in-Publication Data
Burton, Ralph A.
Heat, bearings, and lubrication
p. cm.
ISBN 978-1-4612-7060-7 ISBN 978-1-4612-1248-5 (eBook)
DOI 10.1007/978-1-4612-1248-5
1. Bearings (Machinery) 2. Lubrication and lubricants. 3. Heat—
Transmission. 4. Shear flow.
TJ267.5.B43H43 1999
621.8'22—dc21 99-18597

Printed on acid-free paper.

Originally published by Springer-Verlag New York Berlin Heidelberg in 2000
Softcover reprint of the hardcover 1st edition 2000

Production managed by Robert Bruni; manufacturing supervised by Nancy Wu.
Typeset by TechBooks, Fairfax, VA.

9 8 7 6 5 4 3 2 1

ISBN 978-1-4612-7060-7 SPIN 10715746

Preface

This book is about failure mechanisms in bearings and seals when high speeds or loads cause significant frictional heating. It is about how to predict and avoid these kinds of failures. The text is intended for the designer and mechanical engineer responsible for high-performance machinery. The subject matter is analytical and interdisciplinary. It incorporates transient heat flow, thermal deformation, and the fluid mechanics of thin films. A systematic effort has been made to define and condense these contributions into a set of tools that can solve practical problems.

The primary goal of this book is to give modern engineers a set of guidelines and design criteria to help them avoid thermally coupled failures in machines. The most important features are (1) the systematic definition and treatment of specific phenomena, (2) the use of consistent nomenclature, and (3) the worked examples. Recent publications are incorporated, and completely new work is presented to fill in gaps in the existing literature.

When thin viscous films are sheared at high rates, viscous heating can distort the solid boundary surfaces. The simplest configuration that shows this effect is the flow around a cylindrical journal that turns in a cylindrical bore. Thermal deformation can be the same magnitude as film thickness and can cause changes in the distribution of viscous heating. As a consequence, heating may be concentrated at small areas on the solid boundary surfaces and thus cause seizure when the critical temperature for a given material is reached.

Analyses of these phenomena are sparse in the design literature. For example, Pinkus (1990), in his definitive book on thermal aspects of tribology, mentions only one instance of coupled thermal deformation (Fillon et al., 1985). Treatment of thermoelastic effects is absent from the main body of fluid mechanics literature. In either case, the analyses require the blending of thermoelastic behavior of boundary solids and coupled changes in viscous heating of the shear flows restricted between the solid boundaries.

As documented by Ling (1990), much of the recent progress in contact and surface mechanics has been in numerical analysis by computer. The findings are similar to well-instrumented experiments. The computations yield vivid results, yet many effects remain hidden in the complexities of thermoelastic and thermoviscous interactions. Examples are the early works of Hahn and Kettleborough (1968),

Ettles (1982), Bishop and Ettles (1982), Gethen (1985), Medwell and Gethen (1985), and Dufrane and Kannell (1989). More recent works are those of Salant and Hassan (1989), Khonsari and Kim (1989), and Hazlett and Khonsari (1992a and b). Similar effects in seals are addressed by Etsion (1992, 1993, 1996) and Banerjee and Burton (1976a and b).

The engineering analyses presented here are intended to isolate and conceptualize the major thermoelastic interactions in shear flows between elastic boundary solids. The models are intended to be sufficiently comprehensive to inspire confidence in the conclusions, and effort has been made to keep them simple.

Acknowledgments

Thanks to Carol and Gaines for your help and patience. Thanks also to Martha Keravuori, in whose studio the first draft was written, and to the students whose bright minds and enthusiasm made this work significant.

Contents

1
Bearings and Seals

This chapter describes journal bearings and face seals, and introduces terminology that is used throughout this book. It explains the idea of relative curvature along with other assumptions that are implicit in the analysis of lubricant films. Important modes of thermal deformation are identified, and the implications of thermal failure mechanisms are discussed relative to each geometric configuration.

Full Journal Bearings

The principal distinction between machines and structures is at the moving junctions. Structures have tiny displacements at pins or sliding supports to accommodate thermal expansion or elastic deformation, or to simplify the loads that are transferred from one solid to another. In machines the relative displacements are large and often continuous. This movement is resisted by friction, and the work required to sustain motion is largely converted to heat. The passage of heat away from the junction usually leads to relative deformation, which can have large effects on the conditions of contact and the freedom of movement.

The simplest configuration for such a junction is the symmetric journal bearing, which consists of a cylindrical shaft (the journal) passing through a bore (the bearing). This is illustrated in Fig. 1-1, which shows a common electric motor, with an axisymmetric journal suspended on two bearings. The clearances around the journal are exaggerated. In household appliances the journal radius may be about 1 cm, and the clearance is $\approx 10^{-3}$ cm. Fans, pumps, and appliances operate at rotational speeds from 1000 to 3600 rpm, with sliding speed (surface speed of the journal) up to 3.6 m/sec. Grinders, routers, and centrifuges operate at much higher speeds, which may exceed 15 m/s. For typical applications the loads and speeds are below the limit required to cause large thermal deformation. Although the journal may reach temperatures in excess of the mean temperature of the end-cap of the motor, this rise is usually not large enough to eliminate the clearance in the bearing, and seizure is uncommon.

The bearings themselves may be sealed at each end to retain lubricant from a small sump. Fluid may be wicked from the sump to the journal and provide a

R. A. Burton, *Heat, Bearings, and Lubrication*

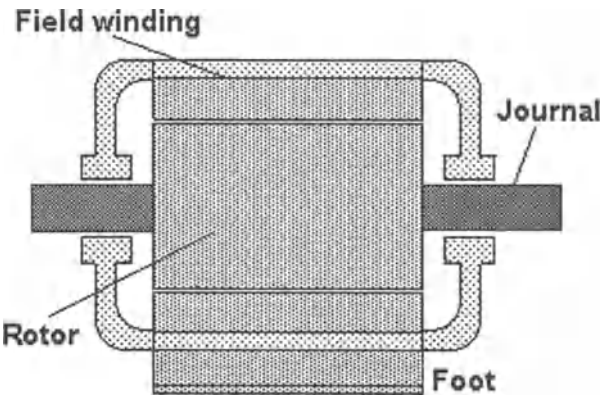

FIGURE 1-1. An electric motor illustrates an axisymmetric journal suspended on two cylindrical bearings.

fully effective film to lift the weight of the rotor and avoid solid contact. Grease may also serve as lubricant, offering a structure that is solid at rest and becomes a liquid under the rapid shearing in the annular film. Ball bearings may be employed; although these provide less "stiffness" than journal bearings, they accommodate relative expansion readily. Dry or boundary-lubricated bearings operate with solid contact against the journal and offer acceptable levels of friction when coated with molecule-thick films of organic material or thicker films of solid lubricants such as graphite or molybdenum disulfide. Dry contact occurs in the event of lubricant loss.

Only exceptional dry bearings operate at the low friction levels offered by liquid lubricants, and failure may come in the form of elevated temperature. This may be compounded by the rise of friction and softening of the bearing structure, if it is a polymeric material. Other factors that exacerbate failure mechanisms are the use of the massive housings and bearing bosses sometimes found in machine tools and scientific instruments. When the machine is started from rest, thermal inertia slows the rise in bearing temperature. A transient loss of clearance may be gradual or it may be part of an instability that feeds on increased heating as closure approaches, resulting in a catastrophic lock-up.

Bearings are challenged more severely in turbomachines, where the rotating member may operate at a vane temperature approaching 1000°C, and sliding speed may rise above 100 m/s. Rolling-contact bearings, copiously lubricated, avoid some of the thermal deformation problems; but fluid film bearings are chosen for many applications, particularly those that are small and have high power density. Figure 1-2 shows a schematic drawing of the rotor of a turbocompressor. Air enters at the left and flows radially along vanes on the impeller, rising in pressure and increasing in kinetic energy. In the stationary diffuser (not shown), the kinetic energy is converted into an additional pressure rise, and the air flows to the intake valves of a piston engine. Exhaust from the engine is collected and expanded through a nozzle ring from which it moves to the turbine buckets or blades, giving

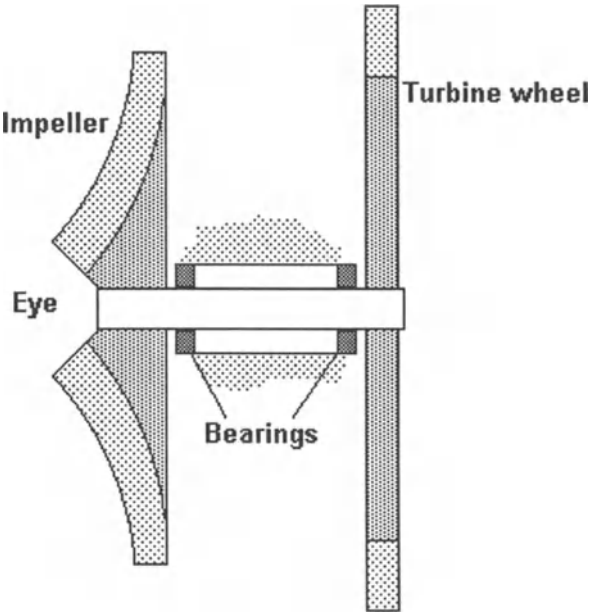

FIGURE 1-2. Rotating parts of a simple turbocompressor. Vanes on the impeller compress air entering at the eye of the compressor. Hot exhaust gas passes from nozzles through vanes on the turbine wheel, where they give up sufficient energy to drive the assembly.

up sufficient energy to drive the impeller and overcome bearing friction. The bearings are shown in a central quill, supported by structural connections to the stator and housing. They are sealed against leakage at both ends of the quill. Cooled lubricant is circulated into the quill and delivered to the bearings and seals. When the quill is properly designed, there is no problem of seizure, but this is not always the case for the small clearances, high speeds, and large radial heat flow encountered in the continual search for improved performance.

Not all bearings are conveniently symmetric. The example shown in Fig. 1-3 is intended to be bolted to a frame or a table, and shows considerable departure from axial symmetry, both mechanically and thermally. In practice, the temperature lag of the massive central structure is more important than the asymmetry, however, and seizure is most likely to result from the loss of radial clearance rather than from distortion. The bearing is most likely to fail when starting or when lubrication is interrupted.

Seals

The face seal represents a configuration in which the lubricant film lies in a plane between the ends of two concentric solid cylinders. A temperature difference between the two solids does not threaten the loss of clearance because the surfaces are

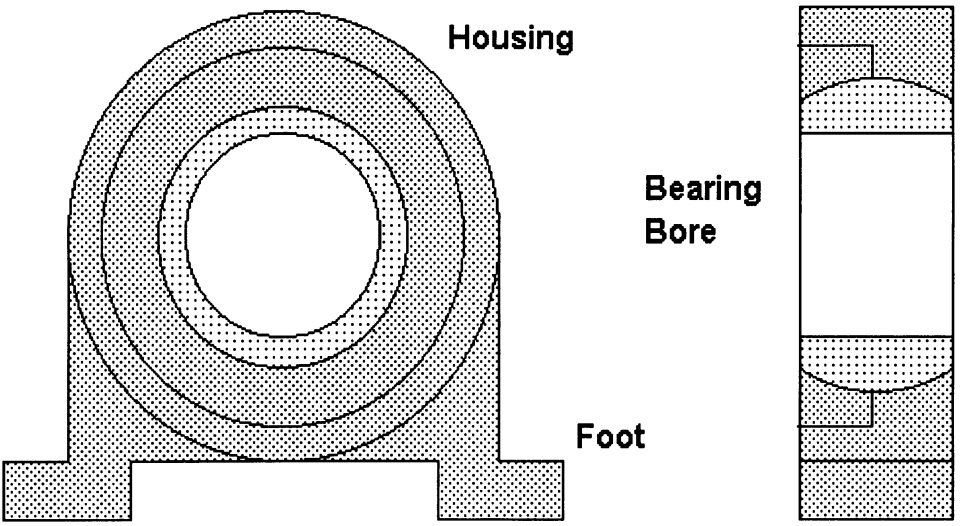

FIGURE 1-3. A bearing intended to be fastened to a frame, with asymmetric cooling and deformation. The example is self-aligning, with the bearing somewhat free to tilt in a spherical mount.

not confined axially and are free to accommodate fluid film forces by displacements relative to one another. The seal illustrated in Fig. 1-4 shows the principal elements, with some dimensions exaggerated for clarity. The rotating shaft has a vertical axis, and a cylindrical fin pressed onto it engages the seal ring. The seal ring is typically made of a nonmetal, such as carbon, a ceramic, or a self-lubricating composite. Rather than having contact over its full radial extent, it is contracted into a thin

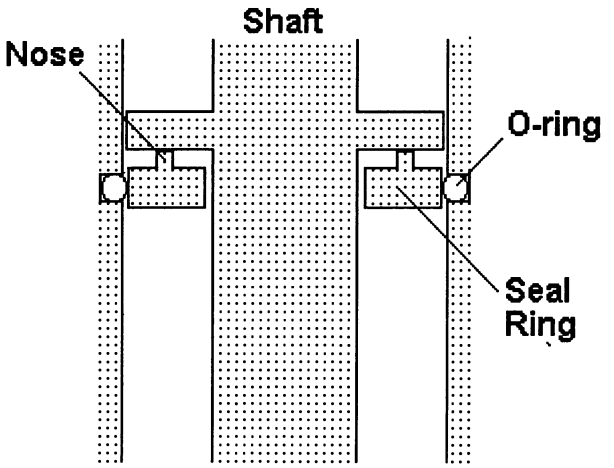

FIGURE 1-4. A face seal arrangement in which the nose of the seal ring presses against an annular face that is attached to the vertical shaft.

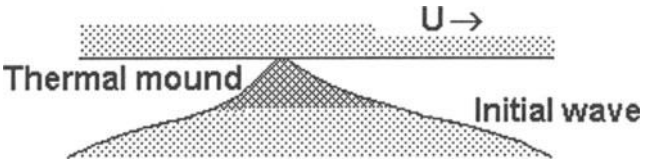

FIGURE 1-5. Illustration of a thermal mound forming at the peak of a surface wave on a nominally flat surface. The second surface (the counterface) slides at speed U and is separated from the wavy surface by a lubricant film. A similar waviness and thermal deformation may occur on the counterface, where the present stationary surface has relative velocity $-U$.

band of contact at the tip of an annular "nose." The seal ring is joined to the stator surface by an O-ring, which allows small displacements of the seal ring to accommodate wear or tilt of the mating face. As shown, fluid pressure from below presses the seal ring upward against the face. A liquid film may lie in the interface between the rings and keep the solids apart, as a consequence of hydrodynamic forces in the fluid. The mating surfaces are typically lapped flat within a tolerance of around 10^{-2} μm.

Face seals may have sliding speeds up to 50 m/s in turbomachines, and considerable frictional heating takes place. If face seals experience thermal failure it is because initial waviness on the surfaces becomes amplified. The wave peaks support the elevated load and receive more heat than the wave troughs. This can lead to an instability by which the peak becomes sharpened to form a small highly loaded contact patch. Temperature can rise to red heat due to friction on the patch, and then can rise farther as the lubricant is degraded. This is illustrated in Fig. 1-5, which shows an initial waviness (much exaggerated), and the distortion of the wave by a "thermal mound." In reality the wavelength may be a centimeter or more, whereas the wave amplitude may be only 10^{-4} cm.

Similar surface distress may occur in cylindrical bearings even when clearance is maintained by careful thermal design. Waves on the surfaces can be amplified to produce hot spots. This phenomenon may also appear in thrust bearings where a textured surface presses against a flat face much like the seal, but under a high load. Thrust bearings in hydraulic turbines support several tons.

Surface Waves

No machined surface is perfectly cylindrical or perfectly flat. The *nominal* geometry may be thought of as the mean surface supplemented by a spectrum of zero-average excursions. This spectrum may be visualized as an assembly of sine waves, and its distribution is determined by the technique used for surface formation. Typically, there will be waves of the order of 1 cm in length, and 10^{-3} to 10^{-4} cm in amplitude. Independently, there is roughness, with waves ranging around 10^{-4} to 10^{-5} cm in amplitude and 10^{-3} cm in wavelength. The longer wavelengths tend

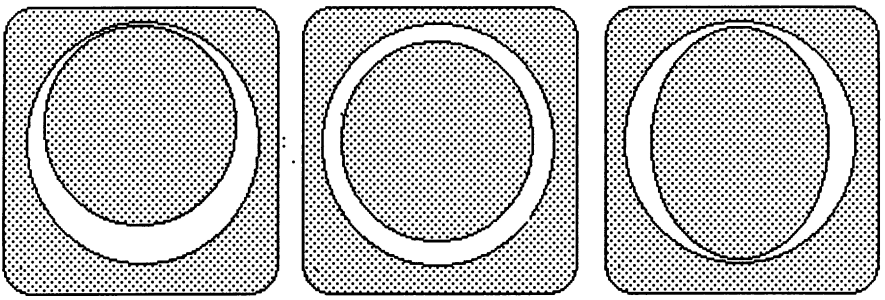

FIGURE 1-6. Three configurations of a journal bearing: eccentricity, concentricity, and ellipticity of the journal. Ellipticity of the bearing is also possible as well as multilobe configurations.

to participate in thermal deformation instabilities, and the roughness determines the nature of the ultimate contact on the patch or hot spot.

Surface waves have a special significance in the cylindrical bearing, and may give rise to a kind of seizure that is more severe than in the face seal. Figure 1-6 illustrates three configurations, one with eccentric journal placement, one with symmetry, and one with ellipticity of the journal.

There is a major difference between the effects of waviness on the journal and on the bearing. In the eccentric configuration, the eccentricity may rotate with the journal (as when the shaft is unbalanced), or it may be stationary with the journal surface passing through cooler and hotter regions. The latter eccentricity may cause an eccentric displacement of the bore of the bearing, but this does not typically affect the mechanisms of thermal instability. For the same configuration, when eccentricity is large, nonlinear heating and thermal expansion can create a second component wave on the bearing surface, with two peaks and two troughs. Thus, extreme eccentricity, under a large radial load, can lead to ellipticity. If the elliptical configuration grows, irrespective of its cause, it can lead to a loss of clearance at both peaks. This two-lobe wave can cause a kind of seizure similar to that caused by uniform radial expansion. Ellipticity of the journal can cause a similar kind of failure. Imbalance can cause a rotating pattern of heat input, which may affect journal ellipticity. Waves may form on both the journal and bearing, and each may grow as though the mating body were smooth.

Development of the Film: Unwrapping

Reynolds (1886) showed that lubricant films can be unwrapped from the cylindrical element, causing the nominal cylindrical surfaces to develop into flat planes. This is convenient for the analysis of surface thermal expansion and for treating the fluid film. The bearings in Fig. 1-6 transform into the diagrams of Fig. 1-7. The same diagrams may represent the seal, which is unwrapped from around the shaft to form a geometry of two parallel bars.

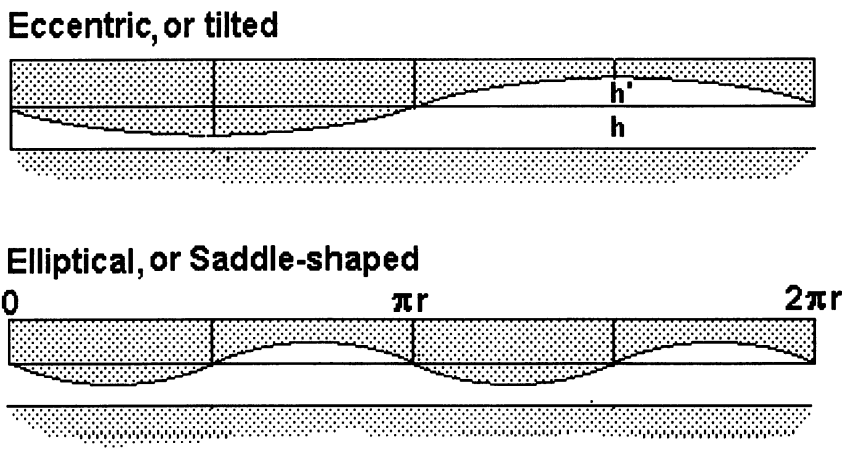

FIGURE 1-7. Journal bearing or seal developed from polar to rectangular coordinates. In both cases one circumference is shown. The single-lobe wave represents eccentricity in the bearing and tilt in the seal. The two-lobe configuration represents ellipticity in the bearing and a saddle shape for the seal with two peaks opposite each other, separated by two troughs.

In general, primed quantities, such as the h' in Fig. 1-7, designate a departure from the nominal surface. When this is supplemented by a further excursion, as the result of thermal expansion, the quantity will be designated by a double prime, such as h''. The waves will be spoken of as *perturbations* on the nominal geometry.

Partial Bearings

Many practical applications lie between the seal and full bearing configurations, with segmented or partial enclosure of the journal. Figure 1-8 shows schematically the bearing on a railroad car. The flanged wheels ride on rails and are joined by a solid axle. The weight of the car is transferred to a journal that extends outward from each wheel. Historically, the bearing was a bronze block that enclosed only half of the circumference of the journal. A small sump below this was filled with oil and cotton linters, which served to wick the fluid from the sump to the unshielded surface of the journal. A system of this general type led to the modern theory of hydrodynamic lubrication, when Tower (1885) showed a liquid film did indeed separate the surfaces and support the load, with high hydrodynamic pressure. When developed or unwrapped into a straight line, the system would be as in Fig. 1-7, with the wavy surface truncated so that fluid enters into a converging film and passes through a minimum of clearance before leaving the confined region.

Other partial bearings are shown in Fig. 1-9, which applies equally well to either annular thrust bearings or special journal bearings. The fixed inclined pad derives

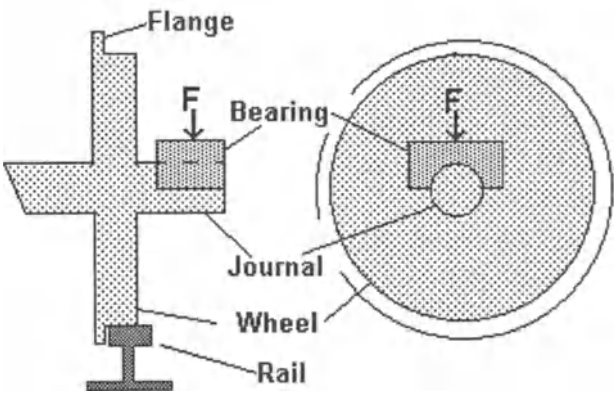

FIGURE 1-8. Schematic diagram of a bearing block that transfers load from a railway car to an extended journal. Not shown is a sump below the journal, which is attached to the stationary bearing structure, and supports a cotton wick that transfers a thin film of oil to the journal. Modern cars use tapered roller bearings.

its lift by the moving journal surface (top, in each case) dragging fluid into a converging film. Such pads may be machined into the face of a thrust bearing, or may be cut in the surface of a journal bering. Such a configuration is less sensitive to dynamic effects than is a smooth bearing. The stepped pad functions in much the same way, but is easy to make by laser etching, chemical etching, or plating, when very small step height is desired.

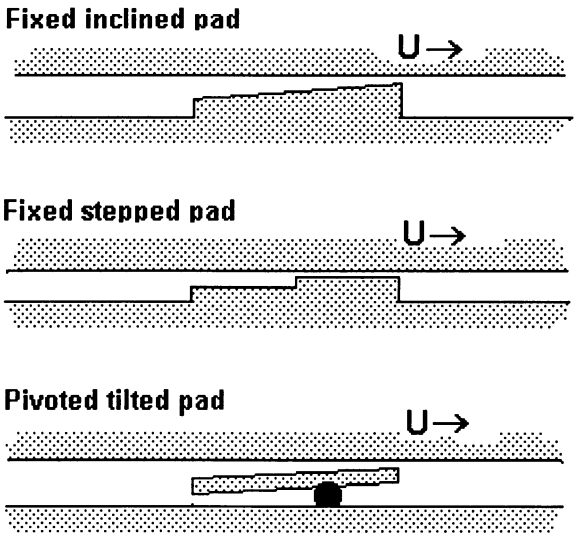

FIGURE 1-9. Partial-bearing configurations that may be used separately or in clusters on both axial and radial surfaces.

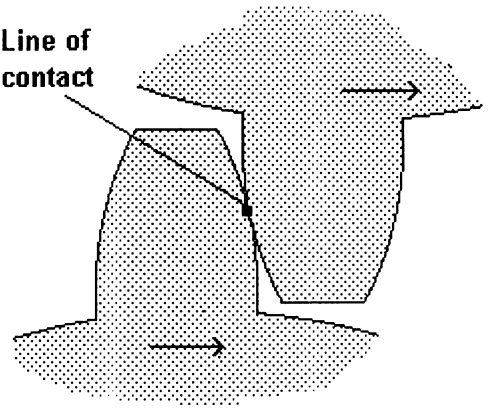

FIGURE 1-10. Gear teeth moving to the right with the lower tooth driving the upper one. Contact begins near the root of the lower tooth and progresses upward to the tip of that tooth.

Counterformal Contact

In all of the above examples, the nominal surfaces of the rotor and stator conform to one another. A different kind of conformance is found in the engagement of gear teeth pressing convex surfaces into contact along a line or band of highly stressed material. Engagement begins with the tip of one tooth meeting near the root of the other; then, as they turn, the contact band moves away from this position until the root of the first tooth meets the tip of the other at the point of disengagement.

Figure 1-10 shows an intermediate point of engagement. The relative motion of the teeth has components of rolling and of sliding. Local surface temperature (called "flash temperature") can be estimated for full engagement on the band of contact. This is multiplied when instabilities cause the band of contact to contract to a point. Then, if the temperature or stress becomes high enough, serious surface distress results. This kind of damage may be called scuffing or scoring. A similar phenomenon occurs on the face of a cam-follower, where a rounded surface slides while supporting a large load.

Vanes

Figure 1-11 shows a configuration used in vacuum pumps, refrigeration machinery, air compressors, and air motors. As the rotor turns, a "chamber" (bounded by the stator, the rotor, and a pair of vanes) increases in volume as it moves away from the top, and fluid is drawn in. Similarly, fluid is forced from the decreasing volume of the chambers converging near the exit port. The vanes wear to a rounded tip configuration, making line contact with the stator. Lubricant may cover that surface with a light film, or the contact may be dry. In either case small waviness along the vane length (into the plane of the figure) may be amplified and concentrate the load on a hot spot. Experimental simulation of this phenomenon is accomplished

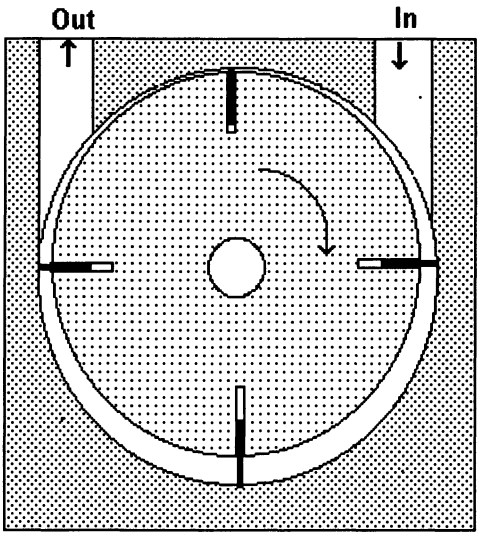

FIGURE 1-11. A vane compressor, consisting of a stator with a cylindrical bore around an eccentric rotor. The vanes (black) are moved outward in their slots by springs. Flat end-plates seal the ends of the vanes and cylinders. Typical compressors have more than four vanes.

with a single vane pressed against the exterior of a turning drum, a configuration that opens the line of nominal contact to observation.

Categories of Interactions between a Fluid Film and Its Boundaries

Thermally induced effects may be separated into nine major interactions, each with its own dynamics, and each of which is largely independent of the others.

1. A cylindrical journal in a cylindrical bearing that encounters radially outward heat flow will have a temperature difference between the journal and bearing. This can cause relative expansion of the journal and reduction of film thickness. In some cases a steady-state solution can cease to exist, the system will lose clearance, and seizure will result. (See chapters 5, 8, and 20.)
2. When thermal constraints make the radial temperature gradient small, the overall temperature rise can cause different materials in the journal and bearing to expand differentially. Steady operation will become impossible beyond a clearly defined threshold for seizure. (See chapter 7.)
3. When the choice of materials is favorable and thermal constraints are favorable, a time-dependent change of clearance can feed transient heating, which may also lead to seizure. A similar phenomenon can lead to clearance loss during start-up. In either case the controlling effect is the lag of bearing temperature relative to the journal when the overall temperatures are rising. (See chapters 6, 9, 17, 18, and 19.)

4. For wavy boundaries on the lubricant film, thermoelastic effects may lead to growth of the initial waviness. Viscous heating is enhanced where the film is thinnest, and this leads to increased heat flow into the intruding peak of the surface wave. This feedback can cause the wave peak to grow to a new amplitude, or it can lead to an instability with runaway growth until contact between journal and bearing is concentrated at hot, highly stressed patches on the peaks of the waves. (See chapters 14, 15, 17, 18, 19, and 20.)

5. When the boundaries approach geometrically perfect cylinders or flats, the feedback phenomenon may cause exponential growth of an infinitesimal surface wave in a process of "theromoelastic instability." (See chapters 14 and 15.)

6. Governing equations of surface deformation may yield multiple solutions. For example, one solution would represent moderate deformation and one would represent catastrophic deformation. This condition may be characterized as "metastable," and the system can be driven from safe operation to failure. (See chapter 21.)

7. The geometry of the bearing may be far from symmetric, and external cooling may be localized. These effects can lead to distortion even when the initial film and viscous heating are symmetric. This condition may feed the wave-growth phenomena listed in 5, above. (See chapter 20.)

8. Nonlinear effects may couple axisymmetric clearance changes with wave growth. For a large surface wave, the film is thinned in some regions and thickened in others. The increase of dissipation in the thin-film regions can exceed the reduction in the thick-film regions, and a net radial flow of heat will supplement the zero-average radial flow from the wavy displacement. Correspondingly, a change of clearance can contribute to the process of growth of surface waviness. (See chapters 18 and 19.)

9. Counterformal systems such as gear-teeth and cam-followers may experience contact instability. This can lead to transition from line contact to point contact at the interface, and can contribute to fatigue and scuffing of the surfaces. (See chapter 21.)

2
Viscous Heating in Laminar Couette Flow

Shear flow in a thin film between concentric cylinders is an idealization of practical bearing flows, and is called Couette flow. The resistance to shearing causes viscous heating, and the temperature of the film is determined by thermal resistance to the passage of the heat outward to the environment. Ranges are given for the thermal resistance when the cylinders are cooled by external fluids.

Background

In a simple hydrodynamic journal bearing, a cylindrical shaft (the journal) is separated from a cylindrical bore (the bearing) by a thin film of lubricant. When the journal turns, the lubricant film is sheared and the viscous heating of the lubricant elevates the journal temperature. This heating can cause relative thermal expansion and a reduction of clearance between the elements. The resulting temperature rise and clearance change can become destructive for fluids and speeds used in modern machinery.

M. Couette (1890) published a pivotal study of this geometry in which he measured the torque required to shear several fluids. He also ran the same fluids through capillary tubes, and he showed that the same viscosity could be used to calculate fluid motion in both geometries when he applied the equations of Navier to each. The equations of Navier are now called the Navier-Stokes equations, and their generality is so fully accepted that the need for Couette's study is forgotten, although his name is still used to designate the bearing-like shear flow in an annular space.

Couette reported accurate measurements of the transition to turbulent flow between cylinders, and the resistance of the turbulent flow to sliding. This flow is characterized by rapid, small-scale velocity fluctuations in the fluid film, and a significant increase of turning resistance.

Couette chose to hold the inner cylinder stationary and allowed the outer one to turn, and he thereby missed the discovery of vortex flow, which occurs when the inner cylinder turns in a stationary outer one and when the film thickness is large. The vortices cause increased turning resistance similar to that caused by turbulence. Vortex flow was later investigated by G. I. Taylor (1960), who gave

R. A. Burton, *Heat, Bearings, and Lubrication*

the first theoretical explanation of an instability that could cause transition from simple laminar flow to vortex flow. His annuli were found to contain orderly rows of ring vortices around the inner cylinder.

Taylor reworked Couette's data, showing that the simple turbulent transition occurred at a critical Reynolds number. For his own geometry, Taylor pointed out that when the film thickness is a small fraction of the radius, the vortex transition may be largely hidden by the turbulent transition to more chaotic flow. Taylor's plots of his and Couette's data remain accurate predictors of turning resistance. The present chapter is restricted to the laminar flow, and questions involving turbulence are treated in chapters 8 and 9.

Schlichting (1968) has summarized the development of a theory of viscous heating in annular flows, and Vogelpohl (1949) has shown that high temperatures could develop in the liquid film. Nahme (1940) and de Groff (1956) have treated thermoviscous fluids for which the temperature rise determines the viscosity of the fluid and the energy dissipation in the film.

The search for an understanding of these interactions necessitates a fresh look at thin-film flows to clarify the relationship of fluid behavior to the physical properties of the fluid and to the particulars of heat removal and boundary deformations. Subsequent chapters treat these interactions, first in simple axisymmetric flow and then in the same flows with wavy boundaries.

Plane Couette Flow

The limiting case of Couette flow for a very thin fluid film between large cylinders approaches the condition of flow between parallel flat plates and is called "plane Couette flow." In the absence of turbulence or vortices, the fluid velocity is parallel to the surfaces.

Figure 2-1 shows the geometry of plane Couette flow, in which a Cartesian coordinate system is placed a distance, d, from one wall. The x-coordinate is

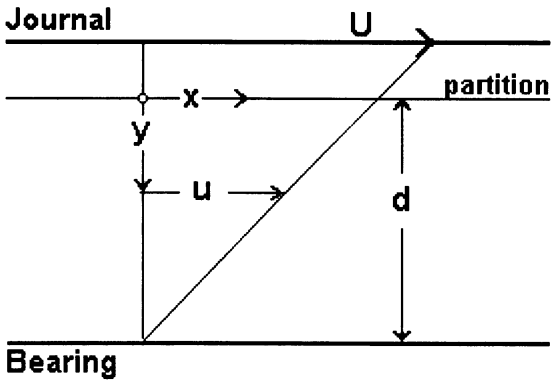

FIGURE 2-1. Schematic diagram for plane Couette flow, where U is the velocity of the moving surface. The local fluid velocity varies linearly out from the stationary wall.

parallel to the walls and in the direction of sliding, and the y-coordinate is normal to the walls. The velocity, u, is measured in the direction of sliding, and U is the sliding speed of the moving surface. For two-dimensional plane Couette flow, the equation of equilibrium reduces to:

$$\frac{d\sigma_{xy}}{dy} = \frac{dp}{dx}, \tag{2-1}$$

where σ_{xy} is shear stress and p is pressure. For axial symmetry and single-valued pressure:

$$\frac{dp}{dx} = 0. \tag{2-2}$$

The shear stress is uniform throughout the flow and may be designated σ without subscripts. Couette showed that:

$$\sigma = \mu \frac{du}{dy} \tag{2-3}$$

The rate of viscous heating per unit of volume of fluid is:

$$w = \mu \left(\frac{du}{dy}\right)^2 = \frac{\sigma^2}{\mu} \tag{2-4}$$

This is dependent only upon the local value of the viscosity and remains valid when μ varies with temperature across the film. For axial symmetry, heat transfer is restricted to conduction in the y-direction. When conductivity is constant, the Fourier heat-transfer equation reduces to:

$$K \frac{d^2T}{dy^2} = -w = -\frac{\sigma^2}{\mu} \tag{2-5}$$

Table 2-1 shows that the fluid properties K and μ spread over a large range. Conductivity is lowest for a gas and has intermediate values for organic lubricants. It is extremely high for liquid metals, but it is not strongly sensitive to temperature. On the other hand, viscosity is markedly sensitive to temperature in oils, dropping when temperature is increased. Viscosity may vary as much as 10-fold for the temperature range within a conventional machine. The practical importance of oils makes the combination of a constant K and variable μ a reasonable model for the thermoviscous fluid film.

Isoviscous Flow

Isoviscous flow not only serves as a useful reference condition, but often is a valid model for the thin film, even when the entire system is not isothermal. Returning to eq. (2-5), when K and μ are constant, temperature will vary parabolically from

TABLE 2-1. Representative Fluid Properties

Fluid	T (°C)	C_P Specific heat (kJ/kg-°C)	K Thermal conductivity (N/s-°C)	$k \times 10^6$ Thermal diffusivity (m^2/s)	$\mu \times 10^2$ Absolute viscosity (N-s/m^2)	$\mu\nu \times 10^6$ Kinematic viscosity (m^2/s)	μ/K (°C-s^2/m^2)
Water	20	4.18	0.60	0.14	0.10	1.00	0.0017
	60	4.19	0.65	0.16	0.047	0.48	0.00072
	100	4.2	0.68	0.17	0.028	0.29	0.0004
Mercury	20	0.14	9.3	5	0.15	0.12	0.00017
Oil	20	1.84	0.145	0.088	79.6	892	5.49
	40	1.92	0.143	0.084	20.4	231	1.43
	60	2.00	0.141	0.081	7.1	82	0.51
	80	2.10	0.140	0.078	3.15	37	0.23
Air	0	1.006	0.024	19.2	0.0017	13.6	0.0007
	50	1.006	0.028	26.2	0.0019	18.6	0.0008
	100	1.009	0.031	33.6	0.0021	23.8	0.0007

a maximum, T_M.

$$T = T_M - \frac{\sigma^2 y^2}{2K\mu} \tag{2-6}$$

This is illustrated in Fig. 2-2, where the temperature maximum, T_M, is at a distance d from a solid wall. The plane of maximum temperature is called the "partition plane" because heat does not flow across it. For symmetric cooling the partition

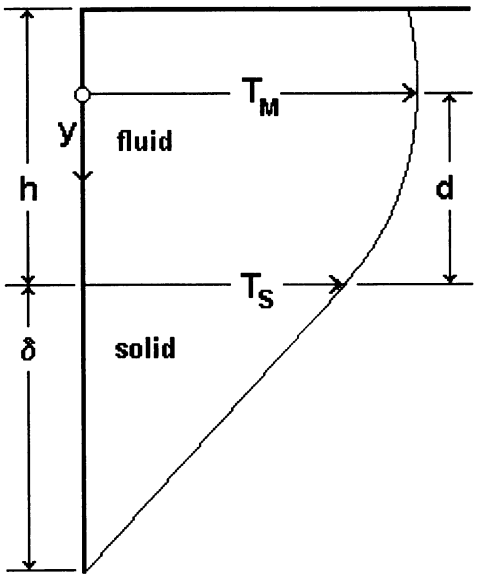

FIGURE 2-2. Temperature profile in fluid film, dropping parabolically from a maximum, T_M, at the partition surface to T_S at the solid wall, and then dropping linearly to the ambient across the thermal resistance, δ.

plane is in midfilm. When heat flow to one surface is blocked, the partition plane lies against that surface. When viscous dissipation is the only source of heat, the partition lies a distance d from a reference wall, where $d/h < 1$.

As illustrated in Fig. 2-2, the temperature follows its parabolic trajectory out to the solid surface. It then drops across the external thermal resistance, down to the ambient temperature, T_A. The drop from the partition to the solid boundary is:

$$T_M - T_S = \frac{\sigma^2 d^2}{2K\mu} \tag{2-7}$$

When U is the sliding speed, and T_S is the temperature of the solid-fluid interface, eq. (2-3) requires that $\sigma = \mu U/h$, and it follows that:

$$T_M - T_S = \frac{\mu U^2}{2K}\left[\frac{d}{h}\right]^2 \tag{2-8}$$

Fluid properties from Table 2-1 permit numerical estimates of the temperature drop, which is independent of film thickness. These data are adapted from Schlichting (1968, p. 256). For the oil at 20°C, $\mu/K = 5.49°C(s/m)^2$. If sliding speed is typical of household machinery, $U = 10$ m/s, and if $h/d = 2$, eq. (2-8) gives $T_M - T_S = 68°C$. On the other hand, when the film temperature is raised to 80°C, and $\mu/K = 0.225$, then $T_M - T_S = 2.8°C$ for the chosen sliding speed. These two calculations show that the temperature drop can range from significant to negligible, depending upon the temperature of the film. In Table 2-1, μ = Kg/m-s = N-s/m^2 $\approx$ centipoise $\times 10^{-3}$.

Cooling of the Solid Walls

For steady turning, the dissipated heat must flow through the journal and bearing surfaces to the environment. In either case, it must be conducted through the solid and then may pass into a liquid or gaseous medium. The combined thermal resistances may be lumped into an equivalent thickness, δ, of stagnant working fluid. Sometimes it is also convenient to define a corresponding quantity, δ_A, which is an equivalent thickness of *coolant* fluid on the exterior of the solid. The working fluid may be oil and the coolant may be air or water in a typical application.

When the external heat transfer coefficient, h, is known, the equivalent thicknesses are given by:

$$h = \frac{K_A}{\delta_A} \tag{2-9}$$

where K_A is the thermal conductivity of the ambient coolant. Table 2-2 is adapted from Burton (1991), and shows ranges of h and δ, for typical coolants such as water or air. The quantity δ/d has been computed for a representative film thickness, and is large.

Extended surfaces reduce the thermal resistance by several fold. In seals and bearings, flow may be confined to a narrow band, as shown in Fig. 2-3, while

TABLE 2-2. Typical Values of Thermal Resistance

	K Heat transfer coefficient (J/m^2-s-°C)	δ Equivalent oil film (mm)	δ/d (for $d = 10\ \mu m$)
Natural convection			
to liquid	40–80	3–1.5	150–300
to gas	4–8	30–15	1500–3000
Forced convection			
to liquid	80–240	1.5–0.5	50–150
to gas	8–40	15–3	300–1500
Boiling liquid	160–400	0.75–0.3	30–75
Conduction			
1 cm of carbon	0.089	8.9	
1 cm of silicon carbide	0.067	6.7	
1 cm of cast iron	0.024	2.4	
1 cm of aluminum	0.0052	0.52	

cooling occurs over a large surface. Because thermal resistance drops inversely with area,

$$\delta_1 = \delta_2\left(\frac{A_1}{A_2}\right) \tag{2-10}$$

where δ_2 is the resistance on the exterior of the ring. The area ratio of the wetted band to the cooled exterior surface could be as small as 0.1. The ratio δ/d in Table 2-2 would be a tenth of the value shown, but would remain much larger than film thickness. Boiling liquid gives the smallest equivalent δ, and with extended surfaces could give $\delta/d = 1$.

Solid material must bridge between the Couette flow and the outer surface, and it will account for several film thicknesses of thermal resistance, as shown for the

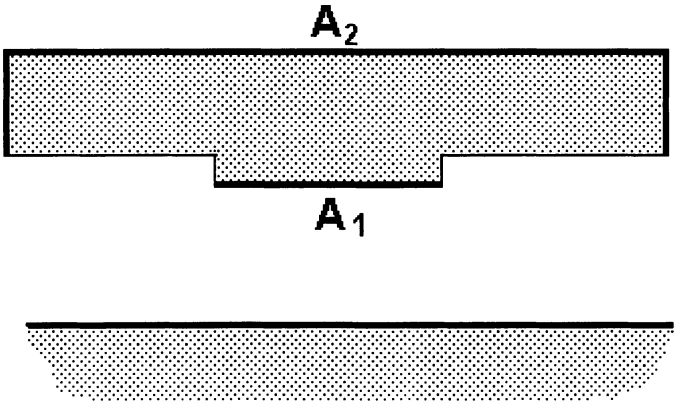

FIGURE 2-3. Cross section of a face seal in which heat enters through a narrow band of area A_1, and exits from an external area A_2.

layers of solids listed in Table 2-2. The sum of the solid resistance and the reduced external resistance would typically raise the effective δ up to several multiples of d.

Heat Transfer from a Rotating Cylinder

Heat transfer from a rotating cylinder to ambient air is a relevant example of forced convection. Typical data are plotted in Fig. 2-4, where the heat transfer coefficient is incorporated into the dimensionless Nusselt number, *Nu*, as defined by:

$$Nu = \frac{hD}{K_A} \tag{2-11}$$

Here the subscript A designates properties of the external coolant. When eq. (2-9) is applied to the coolant:

$$h = \frac{K_A}{\delta_A} \tag{2-12}$$

Combining eqs. (2-11) and (2-12),

$$Nu = \frac{D}{\delta_A} \tag{2-13}$$

Referring again to eq. (2-9), δ may be found as a thickness of the *internal* fluid:

$$\delta = \left(\frac{D}{Nu}\right)\left(\frac{K}{K_A}\right) \tag{2-14}$$

Here D is a characteristic dimension of the body, the diameter of the cylinder in this example. The unscripted K is conductivity of the lubricant fluid.

Referring to Fig. 2-4, *Nu* varies from 40 to 100 over the range of the tests. If the external coolant is the same as the fluid in the film, then $0.01 < \delta/D < 0.025$, and for a diameter $D = 10$ cm, δ will range from 1 to 2.5 mm. If $d = 0.01$ mm,

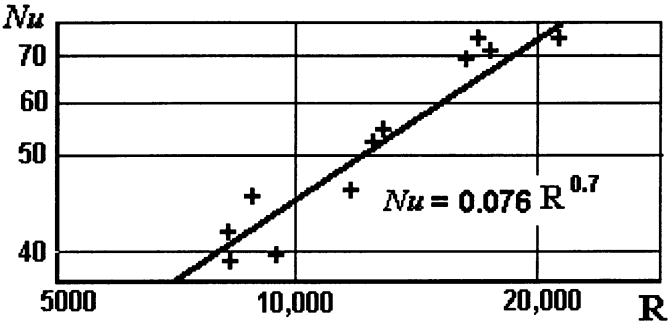

FIGURE 2-4. Dimensionless plot of heat transfer from a horizontal, rotating cylinder in an open space. Nusselt number, *Nu*, varies as the 0.7 power of Reynolds number, *R*.

then $100 < \delta/d < 250$. This range is close to that listed in Table 2-2 for forced convection with a liquid coolant.

Turning to the extreme case of liquid metal coolant, mercury serves as the external fluid and the internal fluid is oil, and $K_C/K = 64$. This would bring the equivalent film thickness down to $1.6 < \delta/d < 3.9$.

If there were also a 10-fold extended surface, this would be reduced further to $0.16 < \delta/d < 0.39$. When one centimeter of a conductive metal, such as aluminum, copper, or silver, is required to create the extended surface, the combined thermal resistance from the solid and the film would make $\delta/d \approx 1$. This is an extreme example, which does not undermine the contention that, in general, $\delta/d \gg 1$.

Film Temperatures with External Cooling

Figure 2-2 illustrates the variation of temperature with distance, y, measured from the partition plane. The surface temperature is T_S, and the drop across the equivalent stagnant fluid, δ, is linear. The drop across the sheared film is parabolic, and the gradient at the surface is

$$\frac{dT}{dy} = \frac{2(T_M - T_S)}{d}$$

For the geometry of Fig. 2-2, the temperature drop to the ambient is:

$$\frac{T_S - T_A}{\delta} = \frac{2(T_M - T_S)}{d} \tag{2-15}$$

Substituting from eq. (2-8),

$$T_S - T_A = \frac{\mu U^2}{2K}\frac{2\delta}{d}\left[\frac{d}{h}\right]^2 \tag{2-16}$$

Returning to eq. (2-15),

$$T_M - T_A = \frac{\mu U^2}{K}\frac{\delta d}{h^2}\left[1 + \frac{d}{2\delta}\right] \tag{2-17}$$

Although the extreme viscosity range of oils requires a special approach to solving eq. (2-17), working fluids such as air and mercury have nearly constant μ/K and are easily accommodated. For the special case of partially blocked heat transfer, where $d/h = 1$, and for large δ/d, where $(1 + d/2\delta) \approx 1$, eq. (2-17) becomes:

$$T_M - T_A = \frac{\mu U^2}{K}\frac{\delta}{h} \tag{2-18}$$

Summary

Viscous heating in thin-film bearings is significant under ordinary mechanical operating conditions. When the dissipative heat divides and flows to each of the solid surfaces, there is a fictitious surface in the fluid, across which the temperature gradient is zero. This is the *partition* surface. When viscosity is constant throughout, the temperature drop from the partition to the wall is independent of film thickness (see eq. (2-7)). Of the fluids in Table 2-1, only the oil experiences an exceptionally large drop.

The viscosity and temperature in the fluid film are primarily dependent upon the mode of external cooling of the solid boundaries of the cylinders. This resistance may be expressed as an equivalent thickness of stagnant fluid, δ, and this is typically many multiples of the internal film thickness, h, even for exceptionally good cooling by boiling liquids or convection to liquid metals.

3
Thermoviscous Fluids

Use of the reciprocal of viscosity, called fluidity, facilitates the interpretation of thermoviscous thin-film flows. The rapid drop-off of fluidity near the maximum temperature is linearized in this chapter and incorporated into a thermoviscous analysis. Closed-form equations are found for the performance measures of such flows.

Background

The large range of viscosity for a modest range of temperature puts into question the concept of the isoviscous oil film. Yet such films are central to the theory of hydrodynamic lubrication, as derived from the models of Reynolds and Stokes. Even the elastohydrodynamic analyses of gear teeth and ball bearings may be based on an isoviscous model from surface to surface, with allowance for viscosity changes along the film.

The paragraphs that follow set the bounds of validity for the isothermal model by introducing a lineraized treatment of the viscosity drop-off near the maximum temperature (Burton, 1989). Figure 3-1 shows the influence of temperature on the fluidity, ϕ, where the tangent at the maximum temperature is extended to the abscissa at T^*.

Under constant shear stress, σ, viscous heating is proportional to fluidity, as in eq. (2-4). Below T^*, where ϕ is small, heating is also small. Above T^*, the most important feature of the curve is the rapid rise of fluidity up to the maximum temperature. A linearized solution above T^* models fluidity that follows the slope, S, up to T_M. It takes into account the most important effects, and gives manageable equations for the temperature and velocity profiles. An interesting treatment of film temperature is also given by Sadeghi and Dow (1987).

Models of Thermoviscous Fluids

A comprehensive survey of fluid models is given by Dakshina-Murthy (1985). Only the power law and exponential law will be considered here.

R. A. Burton, *Heat, Bearings, and Lubrication*

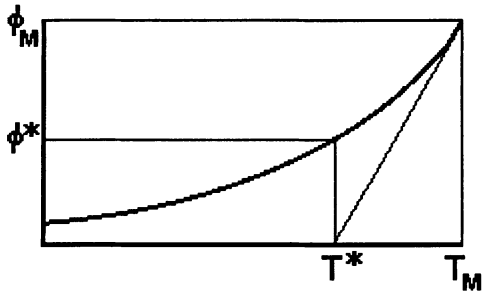

FIGURE 3-1. Fluidity of an oil plotted against temperature, where $\phi = 1/\mu$. At a selected T_M fluidity is ϕ_M. The slope from the maximum extrapolates to T^*, where the fluidity is ϕ^*.

Power Law Fluid

An adaptation of the equation of Slotte (1881) can be written:

$$\phi = a(T - T_0)^n \tag{3-1}$$

where T is Celsius temperature, and T_0 is the hypothetical temperature at which fluidity goes to zero—the "natural zero" of the fluid. Evaluating this numerically for the oil in Table 2-1:

$$\phi = (3.1 \times 10^{-6})(T + 20)^{3.5} \tag{3-2}$$

Table 3-1 shows that the data from Table 2-1 and eq. (3-2) track one another over the entire range. They differ by 5.9% at 40°C, and agree within 2% elsewhere. The intersection, T^*, is found by differentiating eq. (3-1), giving the slope, S.

$$S = \left[\frac{d\phi}{dT}\right]_M = \frac{\phi_M}{T_M - T^*} = \frac{n\phi_M}{T_M - T_0} \tag{3-3}$$

which becomes:

$$\frac{T_M - T^*}{T_M - T_0} = \frac{1}{n} \tag{3-4}$$

TABLE 3-1. Comparison of Power-Law and Exponential Equations for Viscosity (when $\mu = 1/\phi$)

	μ		
T (°C)	Experiment (Table 1-1)	Power law (eq. (3.2))	Exponential (eq. (3-9))
20	0.796	0.797	0.171
40	0.204	0.193	0.098
60	0.071	0.070	0.0548
80	0.0315	0.0315	0.0306
100	—	0.0170	0.0170
120	—	0.0099	0.0095

For a numerical check, let $T = 80°C$, and $T_0 = -20°C$:

$$T_M - T^* = \frac{100}{3.5} = 28.5°C \tag{3-5}$$

Exponential Fluid

Sadeghi et al. (1983) found the interior film temperature in rolling-sliding elasto-hydrodynamic contact for a fluid where, at constant pressure:

$$\phi = \beta e^{\alpha T} \tag{3-6}$$

For this model:

$$T_M - T^* = \frac{1}{\alpha} \tag{3-7}$$

The coefficients β and α may be evaluated at a selected T_M, where the magnitude of ϕ and $d\phi/dT$ are made to agree with the reference data. Applying eqs. (3-5) and (3-7) to the oil of Table 1-1, and letting $T_M = 100°C$:

$$\alpha = \frac{n}{T_M - T_0} = \frac{3.5}{100 + 20} = 0.029 \tag{3-8}$$

Letting $\beta = 3.17$:

$$\phi = 3.17e^{0.029T} \tag{3-9}$$

Viscosities from Table 1-1, eq. (3-2), and eq. (3-9) are compared in Table 3-1. Because the exponential law is only a three-parameter fit, agreement is not good over the entire range, but is not bad close to 100°C. An additional measure of the agreement is ϕ^*, evaluated at T^*. For the exponential fluid:

$$\frac{\phi^*}{\phi_M} = \frac{1}{e} = 0.368 \tag{3-10}$$

For the power-law, with $n = 3.5$:

$$\frac{\phi^*}{\phi_M} = \left[\frac{n-1}{n}\right]^n = 0.30 \tag{3-11}$$

Changes of n do not change this greatly. For example, when $n = 2.5$, $\phi^*/\phi_M = 0.27$.

Linearized Thermoviscous Fluid

Most of the fluidity drop-off near the peak can be accounted for by replacing the true fluidity curve with the linear slope. This line bridges between T_M and T^*, below which $\phi = 0$. The fluid is a stagnant layer below T^*, where negligible heat is generated. Across the layer, conduction occurs with a linear temperature drop (for constant K). Because of the large external resistance to heat flow, it is difficult to bring film temperature below T^*, so the nearly stagnant layer is seldom found.

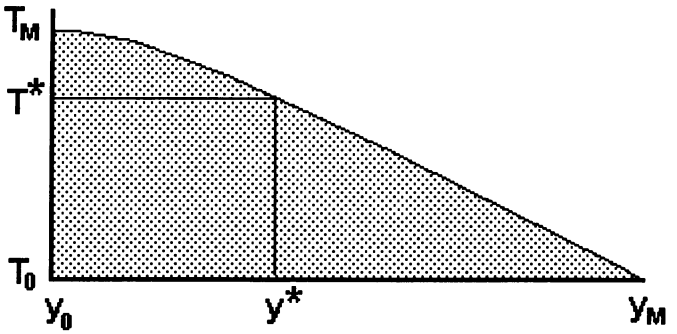

FIGURE 3-2. Temperature against distance from the partition surface, dropping from T_M to T^* in a quarter sine wave, then dropping almost linearly to T_0.

Returning to the heat transfer equation, eq. (2-5), and letting $\phi = S(T - T^*)$:

$$\frac{K}{\sigma^2}\frac{d^2T}{dy^2} = -\phi = -S(T - T^*) \tag{3-12}$$

This is analogous to the equation for vibration with a linear spring, where S is the spring rate, T is displacement, and y corresponds to time. A solution for y measured from the partition plane is:

$$T - T^* = (T_M - T^*)\cos(\beta y) \tag{3-13}$$

where

$$\beta^2 = \frac{S\sigma^2}{K} \tag{3-14}$$

Evaluating S for the power-law fluid gives

$$\beta^2 = \frac{\phi_M \sigma^2}{K(T_M - T^*)} \tag{3-15}$$

This solution is valid down to T^* where $T = 0$, $y = y^*$, and $\beta y = \pi/2$.

Figure 3-2 illustrates the entire temperature function, or profile, measured from $y = 0$ at the partition plane. The linear temperature gradient below T^* joins the cosine curve without change of slope. Letting the natural zero of temperature occur at y_M:

$$\frac{y_M}{y^*} = 1 + \frac{2(n+1)}{\pi} \tag{3-16}$$

Comparison with the Isoviscous Case

When the temperature profile near T_M is expanded in a power series, the first two terms correspond to those for isoviscous flow. Even when the linearized solution is

TABLE 3-2. Thermoviscous and Isoviscous Temperature Profiles for Dimensionless Distance from the Partition Plane (evaluated for $n = 3$)

	βy	Isoviscous $(\beta y)^2/2n$	Linearized $[\cos(\beta y) - 1]/n$	Ratio (isoviscous/linearized)
$\pi/6$	0.52	0.046	0.045	1.02
$\pi/4$	0.79	0.103	0.098	1.05
$\pi/3$	1.04	0.183	0.167	1.10
$\pi/2$	1.57	0.411	0.333	1.23

carried to $y/y^* \approx 2/3$, it does not depart far from the isoviscous one. For small y:

$$\cos(\beta y) = 1 - \frac{\beta y^2}{2} \tag{3-17}$$

Equation (3-15) becomes:

$$T - T^* = (T_M - T^*)\left[1 - \frac{\beta y^2}{2n}\right] \tag{3-18}$$

Substituting for β,

$$T = T_M - \frac{\phi_M \sigma^2 y^2}{2K} \tag{3-19}$$

This agrees with the isoviscous solution in eq. (1-6). The agreement between the linearized, cosine solution and the parabolic, isoviscous solution is shown in Table 3-2.

Velocity Profile in the Film

In Couette flow, when σ is constant throughout:

$$\frac{du}{dy} = \phi\sigma \tag{3-20}$$

Burton (1989) has shown that for the linear variation of fluidity, using eq. (3-13) for temperature:

$$\frac{u}{u^*} = \sin(\beta y) \tag{3-21}$$

The quantity u^* is a property of the fluid, and is given by

$$u^* = (\phi_M T_M K)^{1/2} = \left[\phi_M \frac{(T_M - T_0)K}{n}\right]^{1/2} \tag{3-22}$$

Something seems to be wrong with this, since the the limit of sliding speed is $u = u^*$. However, when the entire problem is considered in appropriate boundary

TABLE 3-3. Derived Thermoviscous Properties of Oils, for $T_M = 100°C$ (for $K = 0.14$, $n = 3.5$, $T_0 = -20$)

Oil	μ (N-s/m^2)	u^* (m/s)	μu^* (N/m)	S (m^2/Ns°C)
SAE-10	0.004	34.6	0.13	8.10
SAE-20	0.006	28.3	0.17	4.86
SAE-30	0.010	21.9	0.22	2.91
SAE-40	0.013	19.2	0.25	2.24
SAE-50	0.017	16.8	0.29	1.71

conditions (as in chapter 4), the temperature sensitivity of u^* eliminates this problem. Table 3-3 shows the range of u^* for several oils. For convenience, S is included in Table 3-3 along with μu^* or u^*/ϕ_M. Returning to eq. (3-15):

$$\beta = \frac{\sigma \phi_M}{u^*} \tag{3-23}$$

With this, eq. (3-21) may be rearranged to read:

$$\sigma = \frac{u^*}{y\phi_M \arcsin(u/u^*)} \tag{3-24}$$

From this, the shear stress can be calculated when maximum temperature and fluidity are known along with the sliding speed at a known distance from the partition plane. In eq. (3-21) the velocity is almost linear out to $y/y^* \approx \frac{2}{3}$, and isoviscous flow remains a useful approximation.

The SAE numbers are a familiar classification that specifies bounds on kinematic viscosity near 100°C (e.g., for SAE-30, $9.6 < \mu v < 12.9$ m^2/s). A midrange value has been selected here for each oil, and converted by an assumed specific volume. A common engine lubricant would be SAE-30, whereas a light oil for winter use might be SAE-10. The oil for Table 1-1 is SAE-50.

Summary

When the viscosity of an oil is strongly dependent upon temperature, the fluidity, $1/\mu$, may be expressed as a power of temperature. The principal feature of the fluidity curve is a steep slope near the maximum temperature. An approximate treatment is based on fluidity, which drops linearly from T_M to T^*. Below T^*, viscous heating is assumed to be negligible, and the fluid acts as a simple conductive layer.

For extremely high sliding speed with fixed surface temperature, fluid deformation is restricted to a band of thickness y^* on either side of the partition plane. This band does not collapse to a slip plane but approaches a fixed fraction of the film thickness at high sliding speed. Such a condition is not to likely to be found in engineering applications, however, because of the difficulty of removing the heat. More important, there is a broad operating range at which the temperature in the film is close to the parabolic distribution of isoviscous flow. This is true when $y < 0.67y^*$.

4
The Thermal Boundary Condition

Power-law equations for thermoviscous fluids are combined with both the linearized analysis of chapter 3 and a numerical analysis. When thermal resistance at the solid boundaries is included, these results provide easily accessible insights into fluid film behavior. They also support the accuracy of the isoviscous film model, and aid in writing a family of equations for use in analyses of expanded scope.

Background

The linearized solution of chapter 3 gives a useful representation of the temperature distribution in thermoviscous Couette flow. It is difficult, however, to interpret when the thermal boundary condition is expressed as a temperature. The remedy is to incorporate the boundary condition into a thermal resistance between the fluid and the environment. This approach, as outlined by Burton (1991, 1965), treats the combined resistance between the bearing surface and the ambient temperature as δ, the equivalent thickness of a layer of stagnant fluid. Estimates of δ are offered in Table 2-2 for different modes of heat transfer. Operating temperature, energy dissipation, and shear stress in the film can be calculated from these.

In chapter 3, a power-law equation for fluidity is offered, with the origin of temperature at the "natural zero" of an SAE-50 oil and at $-20°C$. Even if accuracy is reduced, there is considerable advantage in using a power-law expression with the origin shifted to the ambient temperature, T_A. This can preserve the slope, S, and the magnitude, ϕ_M, where both are evaluated near the maximum temperature in the fluid film. Two simple rules are derived in this chapter to shift the origin from the natural zero, while preserving the slope and magnitude at the selected temperature. A change of symbols warns of this transformation in the simplified equation. At any point in the analysis, the rules may be reapplied to shift the ambient temperature back to the original power-law equation.

Thermoviscous solutions for the transformed fluid with realistic boundary conditions show that the limiting case of isoviscous film is not just a convenience,

R. A. Burton, *Heat, Bearings, and Lubrication*

but is dictated by these conditions. This is fortunate in that a set of simple, useful performance equations may be written with this assumption, and these may be carried into the more intricate analyses of succeeding chapters. This approach was developed in an effort to find a simple way to look at problems presented by Blok (1948).

Nomenclature

Figure 4-1 shows the velocity distribution in a thermoviscous Couette flow, where the y-coordinate is measured from the partition plane. Because the external thermal resistances may differ, the partition plane is not necessarily halfway between the solid boundaries. Figure 4-2 shows the temperature distribution, with T_M at the partition plane, and with temperature dropping off to either side until a point of tangency, T_S, is reached at the solid boundary, where:

$$\frac{T_S - T_A}{\delta} = -s = -\frac{dT}{dy} \tag{4-1}$$

The temperature drop across the equivalent stagnant film is linear, as explained in chapter 3. In general, the ambient temperature is above the Celsius zero as well as the natural zero of the fluid. This temperature is easily defined when a bearing, shaft, or seal element transfers heat to ambient air. In a thermostat-controlled system such as an internal combustion engine, the appropriate "ambient" temperature is the "control temperature." For example, if the surroundings are at 20°C, but the lubricant sump is held at 100°C, then the natural or forced convection between the triboelement and the oil will transfer heat to the sump. This is no different from operation of a machine in an air-conditioned room with controlled temperature, where the temperature rise from dissipative heating is measured from room temperature, without regard to outdoor temperature. A similar argument may be made for heat transfer to melting ice or boiling liquid, where the coolant fluid is maintained at a fixed temperature.

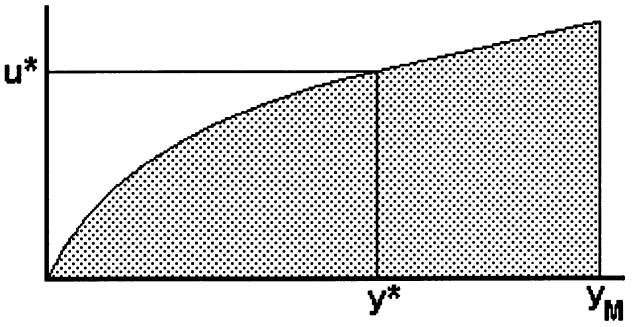

FIGURE 4-1. Velocity in thermoviscous Couette flow, rising from zero on the partition surface to y^*, and then almost constant to y_M.

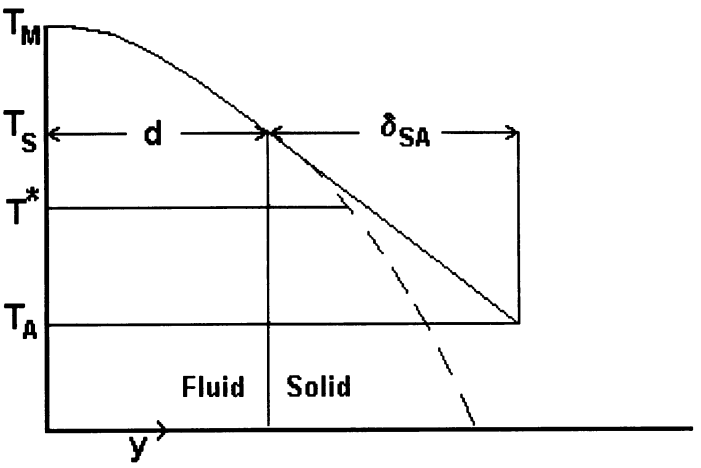

FIGURE 4-2. Temperature drop across a thin film and into a solid wall. Here y represents physical distance out to d, the interface, and then a hypothetical distance where the solid is replaced by thermally equivalent stagnant fluid. The broken line shows how the film would continue if still liquid, and the tangent represents the linear drop in the solid; δ_{SA} is the thermal resistance between the interface and the ambient, expressed as an equivalent liquid thickness.

Shift of the Origin of Temperature

The power-law expression for fluidity, eq. (3-1), is repeated here for reference

$$\phi = a(T - T_0)^n \tag{4-2}$$

When the temperature zero is shifted to the ambient, new symbols will be used as a reminder. The temperature will be lower case, such that $t = (T - T_A)$, and the parameters a and n will be replaced by b and m, respectively

$$\phi = b(T - T_A)^m = b\,t^m \tag{4-3}$$

The slope and magnitude of the fluidity function are preserved at a given T_M or t_M when

$$\frac{m}{n} = \frac{T_M - T_A}{T_M - T_0} \quad \text{and} \quad \frac{b}{a} = \frac{(T_M - T_0)^n}{(T_M - T_A)^m} \tag{4-4}$$

For the SAE-50 oil in eq. (3-2), $T_0 = -20$,

$$a = 3.1 \times 10^{-6} \quad \text{and} \quad n = 3.5.$$

For $T_A = 20$, and $T_M = 100$, the new parameters are

$$b = 0.00213 \quad \text{and} \quad m = 2.333 \tag{4-5}$$

Equations (4-2) and (4-3) are evaluated for a broad range of fluidity in Table 4-1.

TABLE 4-1. The Effect of Shifting Reference Temperature on Power-Law Fluidity Prediction ($T_A = 20°C$)

T	t	ϕ Eq. (3-2)	$\phi_{approx.}$ Eq. (4-3)	$\phi_{approx.}$ Forced exponent
		$a = 3.1 \times 10^{-6}$	$b = 0.00213$	$b = 0.0092$
SAE-50 Oil ($T_0 = -20$)		$n = 3.5$	$m = 2.333$	$m = 2$
60	40	14.2	11.6	15
80	60	31.0	30.0	33
100	80	58.7	58.7	58.7
120	100	100.6	98.7	92
140	120	160.6	151.0	132
		$a = 1.4 \times 10^{-4}$	$b = 0.061$	$b = 0.032$
SAE-30 Oil ($T_0 = -10$)		$n = 3.0104$	$m = 1.85$	$m = 2$
60	40	67.3	56.1	51
80	60	123.2	118.8	115
100	80	203.7	202.3	205
120	100	313.3	305.7	320
140	120	456.7	428.4	461

The two equations track one another closely both above and below $T_M = 100$, where correspondence is forced on them. In the last column of Table 4-1, the exponent is forced to be $m = 2$. For each fluid, a temperature of correspondence has been selected, and the data from this approximation draw away from the more exact data as temperature departs from the reference. For many numerical tests this agreement is good enough to represent the fluid, with considerable simplification in the analysis.

The Linearized Thermoviscous Equation with External Resistance

Figure 4-3 shows the temperature profile for a fluid where T_A is made the zero of t. Starting at t_M the temperature drops off in a cosine function to the arbitrary point of tangency where it follows a linear drop across the resistance δ. For the linearized treatment of chapter 3, the temperature curve becomes:

$$t = \frac{t_M}{m}[m - 1 + \cos(\beta y)] \tag{4-6}$$

At the arbitrary point of tangency, eq. (4-1) calls for:

$$\frac{dt}{dy} = \frac{\beta t_M}{m}\sin(\beta y) = \frac{t}{\delta} \tag{4-7}$$

Rearranging, and letting d be the magnitude of y at the surface:

$$\frac{\delta}{d} = \frac{[m - 1 + \cos(\beta d)]}{\beta d \sin(\beta d)} \tag{4-8}$$

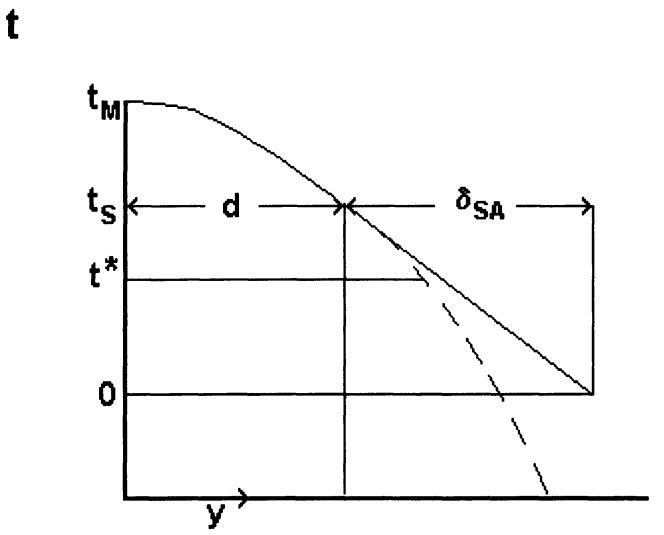

FIGURE 4-3. Redefined temperature, t, measured from the ambient.

The velocity relative to the partition surface is:

$$u = u^* \sin(\beta d) \tag{4-9}$$

The departure from the isoviscous case may be displayed as:

$$\frac{u}{u_{\text{isovis}}} = \frac{\sin(\beta d)}{\beta d} \tag{4-10}$$

Table 4-2 lists solutions for a range of δ/d and the corresponding βd for a physically realistic range of the thermal resistance. It shows that for $\delta/d > 10$, $\beta d \approx 0.45$, which is well within the limits of good accuracy for the isoviscous equation as shown in Table 3-2. Comparisons of the isovisous and linearized-thermoviscous solutions support the isoviscous film as an excellent model for the thermoviscous solution of chapter 2, and for solutions in succeeding chapters.

TABLE 4-2. Solutions for the Linearized Thermoviscous Film with External Cooling ($m = 2.333$)

δ/d	βy	$\sin(\beta d)/\beta d$	$\beta d/(\pi/2)$
933	0.05	0.999	0.032
233	0.1	0.998	0.063
103	0.15	0.996	0.095
58.2	0.2	0.993	0.127
37.2	0.25	0.989	0.159
25.8	0.3	0.985	0.190
18.9	0.35	0.980	0.223
14.5	0.4	0.973	0.255
11.4	0.45	0.966	0.286
9.22	0.5	0.959	0.318

The third column of Table 4-2 compares the velocity with a linear profile, and is seen to remain near unity over the entire range. The fourth column is included for convenience, setting βy in ratio to $\pi/2$, the limit of the selected functions.

Numerical Solution of the Heat Transfer Equation

The heat transfer equation, eq. (2-5), may be integrated for any fluidity function, by a simple algorithm. As written in Table 4-3 this mimics a program in BASIC, with the exception that the variables represented by Greek letters, as well as subscripted and superscripted quantities, are retained as such in the program listing for clarity. The variable S represents the slope dt/dy, and $1/\phi = \mu$.

The algorithm of Table 4-3 allows integration of eq. (2-5), beginning with temperature t_M at the partition plane, and proceeding outward. At each y-position the tangent s is taken, and the magnitude of δ is calculated as though the wall was located at that position, or $y = d$, in accord with eq. (4-1). In this way a sequence of operating conditions is generated, along with the thermal resistance that is required for each to exist. Because δ/d is an externally imposed condition on the physical system, this quantity is placed in the first column when the calculated results are tabulated. Typical results are listed in Table 4-4 for the transformed thermoviscous equation, eq. (4-8), in step 30, and with surface temperature measured from $t_M = 100$. Although a set of operating variables was required for the calculation, these variables do not appear in the dimensionless presentation of the table.

The extreme right-hand column of Table 4-4 is calculated by the same algorithm, but for a linear drop-off of fluidity with dropping temperature as y moves away from the partition plane (the origin). Ideally, this would correspond to the results for the linear analysis, as in Table 4-2. This provides a test of the effectiveness of the numerical analysis. To two significant figures the numerical and linearized-analytical results track one another. The numerical analysis is not restricted to the transformed thermoviscous equation, but can accommodate any empirical law or even a data table in step 30 of Table 4-3. It can be written in T rather than t, and can accommodate the fact that the thermal resistance spans a temperature drop other than to $t = 0$. Step 80 can be replaced by $\delta = (T - T_A)/s$.

TABLE 4-3. Algorithm for Solution of Eq. (2-5)

10	Input dy: Input t_M: Input b: Input K: Input σ: Input m
20	$y = 0$: $s = 0$: $t = t_M$
30	$\phi = b\,t^m$
40	$ds = (-\sigma^2/K)\phi\ dy$
50	$s = s + ds/2$
60	$dt = s\ dy$
70	$t = t + dt$: $y = y + dy$: $s = s + ds/2$
80	$\delta = (t/s)$
90	$u = (K/\sigma)\ s$
100	Print y, t, ϕ, δ, u
110	Go to 30

TABLE 4-4. Numerical Solution for the Thermoviscous Film with External Cooling ($m = 2.333$)

Thermoviscous Eq. (4-8) δ/d	βy	$T - T_A$	Linearized (numerical) δ/d
907	0.05	99.94	972
236	0.10	99.79	223
103	0.15	99.51	102
59	0.2	99.15	58
38	0.25	98.69	38
26.1	0.3	98.10	25
19.2	0.35	97.42	19
14.6	0.4	96.65	14.5
11.6	0.45	95.8	11.5
9.3	0.5	94.8	9.1

Approximate Solutions

The quantities entering into β may be evaluated in a somewhat tedious process. t_M may be adjusted, and explicit solutions can be had in physical variables. On the other hand, one may go directly to the isothermal-film solutions, which are more than justified by the above discussions. Even so, it is desirable to continue with the transformed thermoviscosity equation, as this permits a simple writing of the major film equations and presents the variables in easily interpreted powers. When the simplified equation of state was introduced, it seemed to be flying in the face of all of the efforts of physical chemists to produce good and accurate predictors of fluid behavior. However, for the present kind of analyses the more general equations do not add much accuracy, yet they complicate the display of the design and operating variables.

Another approach would be to use an iterative method, where a guessed t_M provides a trial ϕ, which enters into the heat balance to produce an improved t_M. The process can then be repeated with an improved ϕ. To some extent the transformation of the thermoviscosity equation in this chapter may seem to be a similar step, using a trial t_M to set the point of correspondence between the best power-law fit and the one with the shifted origin. However, the two curves track one another for a sizable range, and a near-miss in the trial t_M gives a suitable model in the range of interest. The model shows increasing error as operation is carried to low temperatures; but typically the thermoviscous model is really of interest only when temperature is elevated.

For the isoviscous fluid, shear stress is given by:

$$\sigma = \frac{\mu U}{h} = \frac{U}{\phi h} \tag{4-11}$$

Dissipation per unit of film surface area is:

$$W = \sigma U = \frac{\mu U^2}{h} = \frac{U^2}{\phi h} \tag{4-12}$$

Heat flux into a wall a distance d from the partition is:

$$W_S = W\frac{d}{h} = \frac{U^2 d}{\phi h^2} \tag{4-13}$$

Dissipation per unit of fluid volume is:

$$w = \frac{W}{h} \tag{4-14}$$

The maximum temperature is:

$$t_M = W_S\frac{\delta}{K} \tag{4-15}$$

Here δ includes all of the thermal resistances including that of the film itself. It can be expanded as $\delta = \delta_C + \delta_S + (d/2)$, and is consistent with the treatment in chapter 2. Equation (4-3) may be used to evaluate the fluidity in the above equations, giving:

$$t_M = \left(\frac{\delta}{h}\frac{d}{h}\frac{U^2}{Kb}\right)^{1/(m+1)} \tag{4-16}$$

$$W = \frac{1}{h}\left(\frac{h}{\delta}\frac{h}{d}K\right)^{m/(m+1)}\left(\frac{U^2}{b}\right)^{1/(m+1)} \tag{4-17}$$

$$\sigma = \left(\frac{h}{\delta}\frac{h}{d}K\right)^{m/(m+1)}\left(\frac{U^{(1-m)/(m+1)}}{hb^{1/(m+1)}}\right) \tag{4-18}$$

$$w = \frac{1}{h^2}\left(\frac{h}{\delta}\frac{h}{d}K\right)^{m/(m+1)}\left(\frac{U^2}{b}\right)^{1/(m+1)} \tag{4-19}$$

$$W_S = \left(\frac{d}{h}\frac{U^2}{hb}\right)^{1/(m+1)}\left(\frac{K}{\delta}\right)^{m/(m+1)} \tag{4-20}$$

Interpretation of the Equations

The variables are broken into dimensionless groups, which reflect design or operating conditions. For example, d/h is determined by the relative thermal resistances on the shaft and bearing. When heat flow to the shaft is blocked, $d/h = 1$; when heat transfer to the two elements is symmetric, $d/h = 0.5$. The exponent $1/(m+1)$ is 0.3 for the SAE-50 oil, and 0.35 for the SAE-30 oil. Hence the doubling of d/h leads to a change of 23% or 27% for the two oils, respectively.

The quantity δ/h reflects design conditions, and would have a fixed value, except in the analyses of relative thermal expansion, where the change of h is significant. Although δ/h varies broadly, Table 2-2 would support a value about $\delta = 100h$.

When considering a film cooled from both surfaces, let d_1 and δ_1 refer to one side of the partition, and d_2 and δ_2 refer to the other. If the maximum temperature

at the partition is shared by both sides, eq. (4-16) is satisfied when:

$$\frac{d_1}{d_2} = \frac{\delta_2}{\delta_1} \tag{4-21}$$

In eq. (4-17) for shear stress, the sliding speed carries the exponent $(-m + 1)/(m + 1)$; for $m > 1$ this exponent is negative. This means that an increase of speed causes a drop in shear stress. On the other hand, when heating is small, viscosity is nearly constant and σ rises linearly with speed. This is consistent with eq. (4-4), where $m \to 0$ as $T_M \to T_A$. Thus we learn that as speed increases from zero the shear stress initially rises, passes through a maximum, and then begins to drop as U is further increased. The maximum occurs at the temperature T_σ where $m = 1$, and shear stress becomes independent of speed. This condition can be found by application of eq. (4-4), letting $T_M = T_\sigma$:

$$(n - 1)T_\sigma = nT_A - T_0 \tag{4-22}$$

For the SAE-50 oil, $n = 3.50$, $T_A = 20$, $T_0 = -20$, and:

$$T_\sigma = 36$$

For the SAE-30 oil, $n = 3.01$, $T_A = 20$, $T_0 = -30$, and:

$$T_\sigma = 74$$

Because viscosity enters through the coefficients b and m, its effect can best be evaluated by comparing two fluids in a sample calculation. Returning to eq. (4-18), and letting $d/h = 1, \delta/h = 100$, $K = 0.14$, $h = 2 \times 10^{-5}$, and $U = 10$ gives:

$$t_M = 180.7 \quad \text{for SAE-50 and}$$
$$t_M = 133 \quad \text{for SAE-30}$$

Summary

The dominant theme of this chapter is that the resistance between the bearing film and the environment is typically large relative to the resistance inside the film. This leads to a small temperature drop across the film and supports the limiting approximations of linear velocity and constant viscosity across the film. These conditions are implicit in the useful set of equations (4-16) through (4-20). Confidence in these equations is provided by comparison with the linearized thermoviscous equation and with the numerically integrated equation. In several recent papers, Etsion (1992, 1996; Etsion and Pascovici, 1993) independently arrive at similar conclusions.

Considerable simplification results from writing the power-law viscosity equation with "zero" at the ambient temperature. Rules are given in eq. (4-4) to tie this to a more accurate representation at a selected elevated temperature. Numerical

comparisons show that the two equations track one another over a broad range on either side of the temperature selected for correspondence.

Considering the accuracy to which the system parameters and operating variables can be specified, the least well known is δ. Equally uncertain are oil properties, unless measured for the specific oil to be used. A broad classification such as SAE grade covers a range of viscosity, although it may be treated in the literature as a single entity. On the other hand, any errors in these quantities tend to be suppressed because their exponents in the principal equations tend to be small.

5
Steady-State Clearance in Bearings with Thermal Expansion

Relative expansion between journal and bearing is considered in this chapter, and conditions are found when stable steady-state solutions become impossible for Couette flow with a viscous lubricant.

Background

There is no phenomenon in tribology as unequivocal and distressing as the seizure of a bearing. In a free-running machine, a change in lubricant flow or turning speed can throw the system into a condition in which the fluid film thins rapidly, dry contact occurs, and a bearing locks up. For some bearings the materials can survive seizure. After cooldown, the system may be restarted and operated on the safe side of the threshold of failure. Burton (1965) offered an early treatment of these interactions. When the bearing is thick and cooled externally, an increase of turning speed will lead to relative expansion of the inner parts of the system and will reduce the lubricant film thickness. When this is carried far enough, a condition is reached at which no static solution can exist. The clearance then shrinks in a dynamic process that ends in seizure. The process is not one of steadily rising temperature and steadily dropping clearance; rather, it is the crossing of a threshold with little warning. Horace Staph (Staph and Burton, 1967) has shown that similar phenomena can occur in ball bearings.

There are other processes that can lead to seizure, including start-up with a sudden increase of viscous heating, where the massive bearing does not expand as fast as the journal. This condition is treated in chapter 17. In other geometries, steady-state solutions may be possible; yet, a transient disturbance of the viscous heating can be self-accelerated until the clearance disappears. This condition is treated in chapter 6. In the present chapter, the phenomenon is viewed in its simplest form, where both bearing and journal are axially symmetric and made of the same material. The small temperature drop across the lubricant film is neglected here, although it is treated in some detail in chapter 10. As a realistic but severe operating condition, cooling of the journal will be neglected, in which case the mean

R. A. Burton, *Heat, Bearings, and Lubrication*

temperature of the journal, t_J, and the inner surface temperature of the bearing, t_S, will be the same.

Isoviscous Couette Flow in an Axisymmetric Bearing

Figure 5-1 shows the geometry for analysis, where viscous heating in the thin film leads to radial heat transfer out through the bearing. The sliding speed is U, the film thickness is h, the outer radius of the journal is r_J, and that of the bearing is r_B. The viscosity, μ, is constant. When the fluid film is thin, the rate of heat generation per unit of surface area on the journal or on the bearing interior approaches

$$W = \frac{\mu U^2}{h} \tag{5-1}$$

A rule for thermal expansion with an axially symmetric temperature distribution is:

$$\frac{dr}{r} = \varepsilon dt_{\text{mean}} \tag{5-2}$$

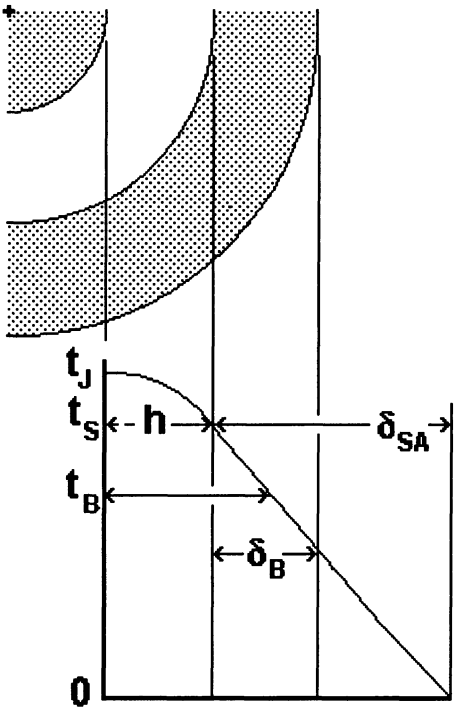

FIGURE 5-1. Temperature drop from journal, t_J, across the film to t_S, through the mean bearing temperature, t_B, across the external resistance and to the ambient, $t = 0$. The symbolic drawing of the journal, film, and bearing are in false dimensions, where each is represented as an equivalent thickness of lubricant.

The change of either inner or outer radius of a cylinder is determined by the change of mean temperature in the cross section. This is true for either plane stress or plane strain with zero end-load. This rule will be examined further in succeeding chapters for steady, transient, and nonsymmetric heating.

When the fluid film is very thin, the inner temperature of the bearing is close to the outer temperature on the journal; and when the mean temperature of the bearing is below the inner temperature, the solid material will encroach into the clearance. The temperature gradient at the inner surface of the bearing is:

$$\left(\frac{dt}{dr}\right)_S = -\frac{W_S}{K_S} \tag{5-3}$$

When the inner temperature is shared with the journal, t_J, the mean temperature of the bearing, t_B, can be found by extrapolating this gradient. The resulting equation includes a dimensionless correction, Φ_L, to account for the small departure from the actual logarithmic temperature function (see the section "The Logarithmic Correction" in this chapter).

$$t_J - t_B = \Phi_L \left(-\frac{dt}{dr}\right)_S \frac{(r_B - r_J)}{2} \tag{5-4}$$

The clearance change is given by:

$$h_0 - h = \varepsilon_J r_J t_J - \varepsilon_B (r_J + h) t_B \tag{5-5}$$

Since $h/r_J \approx 0.001$, h may be dropped from the right-hand term without significant error. When the journal and bearing are of the same material, a single ε replaces the two expansion coefficients. Combining eqs. (5-3), (5-4), and (5-5),

$$(h_0 - h) = \varepsilon r_J \Phi_L \left(\frac{W(r_B - r_J)}{2K_S}\right) \tag{5-6}$$

Substituting from eq. (5-1),

$$(h_0 - h) = \varepsilon r_J (r_B - r_J) \Phi_L \left(\frac{\mu U^2}{2K_S h}\right) \tag{5-7}$$

Letting $h/h_0 = H$,

$$(1 - H) = \frac{G}{H} \tag{5-8}$$

where the dimensionless G is defined as:

$$G = \varepsilon r_J (r_B - r_J) \Phi_L \left(\frac{\mu U^2}{2K_S h_0^2}\right) \tag{5-9}$$

Equation (5-8) is quadratic in H. For small G there are two real solutions, and when G is sufficiently large these move to a single point. For larger G the solution becomes complex. This critical condition occurs for:

$$G = 0.25; \qquad H = 0.5 \tag{5-10}$$

TABLE 5-1. Representative Design and Operating Parameters for a Journal Bearing

Parameter	Magnitude	Units
R_J	500	—
R_{JB}	500	—
ε/K_S	2×10^{-7}	s/N
ε	10^{-5}	1/°C
δ_{SA}/h_0	100	—
b, SAE-50	0.0092	$m^2/(N\text{-}s)°Cm$
b, SAE-20	0.031	$m^2/(N\text{-}s)°Cm$
K (oil)	0.14	N/s-°C
m	2	—
Φ_L	1	—
G	0.25	—

This is the limit for steady-state operation with an isoviscous fluid. It is the threshold of failure.

Numerical Estimates for Isoviscous Flow

It is instructive to regroup the variables in eq. (5-8) by introducing two dimensionless ratios:

$$R_J = \frac{r_J}{h_0}; \qquad R_{JB} = \frac{r_B - r_J}{h_0} \tag{5-11}$$

These ratios reflect the fact that bearing size determines film thickness. Their product could lie near 250,000, at the choice of the designer. Typical magnitudes for the variables are listed in Table 5-1.

The dimensional group ε/K_S takes account of the material properties (see Table 6-1). It is not a strong variable, and ranges from 10^{-7} for copper or aluminum to 3×10^{-7} for carbon and silicon carbide. Iron is in midrange at 2×10^{-7}. Representative values of viscosity can be taken from Table 2-1 for water, mercury, and air; but oils should be reserved for a thermoviscous analysis in view of their extreme variation of viscosity. With the new variables, eqs. (5-9) and (5-10) may be combined to give the limit of operation. The revised equation becomes:

$$G = 0.25 = \left(\frac{\varepsilon}{K_S}\right) R_J R_{JB} \mu U^2 \tag{5-12}$$

For cast iron, with $\Phi_L = 1$:

$$\mu U^2 = 5 \tag{5-13}$$

Evaluating this for water, mercury, and air as working fluids yields

Water:	$\mu = 0.001$,	$U = 70$ m/s
Mercury:	$\mu = 0.0015$,	$U = 58$ m/s
Air:	$\mu = 0.00002$,	$U = 500$ m/s

(5-14)

For $r_J = 2$ cm, 70 m/s would call for 30,000 rpm. A turbine turning 3600 rpm must have a bearing radius of 0.2 m (8 in.) to bring the sliding speed to 70 m/s. The result for the air may be changed when it is recalled that designers tend to use extremely thin films in precise applications such as gyroscopes and small turbomachines. Such a change could bring the turning speed into the same range as for the other fluids. In any case, the most sensitive design variable is initial film thickness.

Thermoviscous Flow

For thermoviscous fluids, the preceding equations may be rederived, letting $1/\mu = \phi = b\,t^m$. Measurement of t from the ambient is appropriate because heat is transferred to the ambient and because the rest-clearance, h_0, would prevail at $t = 0$. This may be incorporated into eq. (5-6) upon substitution of W from eq. (4-17), giving:

$$(h_0 - h) = \varepsilon r_J (r_B - r_J)\Phi_L \frac{\left(\dfrac{K}{\delta_{SA}}\right)^m \dfrac{U^2}{bh^{1/(1+m)}}}{2K_J} \tag{5-15}$$

This can be nondimensionalized, as in eq. (5-6).

$$(1 - H) = \frac{G}{H^{1/(1+m)}} \tag{5-16}$$

where:

$$G = \frac{\varepsilon r_j (r_B - r_J)\Phi_L}{2h_0 K_J} \left[\frac{(K/\delta_{SA})^m U^2}{bh_0}\right]^{1/(1+m)} \tag{5-17}$$

This may be nondimensionalized in analogy to eq. (5-12):

$$G = \frac{\varepsilon R_J R_{JB}\Phi_L}{2K_J} \left[\frac{(Kh_0/\delta_{SA})^m U^2}{b}\right]^{1/(1+m)} \tag{5-18}$$

The relative importance of the design variables and operating variables is best shown by substituting a typical m. Table 5-1 suggests that $m = 2$, is reasonable for substitution into eq. (5-18):

$$G = \frac{\varepsilon R_J R_{JB}\Phi_L}{2K_J} \left[\frac{(Kh_0/\delta_{SA})^2 U^2}{b}\right]^{1/3} \tag{5-19}$$

The exponents in eq. (5-19) may be compared with those of eq. (5-12) for the isoviscous model (see Table 5-2). The power-law equation does not present μ directly; but $1/b$ varies linearly with μ when m is fixed. By this measure, the thermoviscous model is relatively insensitive to viscosity. The effect of film thickness alone is suppressed by the nondimensionalization, in that the designer tends to vary clearance and bearing size together. Similarly, δ_{SA} tends to vary with size, and therefore with h_0. On the other hand, eqs. (5-9) and (5-17) display δ_{SA} and h_0

TABLE 5-2. Exponents of Operating Variables for Two Fluid Models

	Isoviscous (eq. (5-12))	Thermoviscous (eq. (5-19))
U	2	$\frac{2}{3}$
h_0	−2	$-\frac{4}{3}$
μ or $1/b$	1	$\frac{1}{3}$
δ_{SA}	—	$-\frac{2}{3}$
ε/K_S	1	1

independently, and this is reflected in the table. Contrary to the intuitive feeling that improved cooling will help control thermal effects, eq. (5-18) shows that an increase of external resistance, δ_{SA}, will allow increased sliding speed.

Equation (5-16) is solved numerically by substituting the full range of values for H and calculating G. As with the quadratic equation, there are two real solutions up to a maximum G, above which the solutions do not exist. Typical magnitudes for G and H at the point of instability for several fluid viscosity exponents are listed in Table 5-3. Data for the isoviscous fluid are taken from eq. (5-10). The numerical magnitude for G is seen not to vary greatly. For the fluid with $m = 2$, it is the same as for the isoviscous fluid. The two fluids of Table 5-1 are also included in Table 5-3.

The Logarithmic Correction

Temperature does not drop off linearly from the bearing surface, but follows a logarithmic function. In the preceding equations the linear form is kept with a multiplier, Φ_L, to correct it. This is workable because the corrector is close to unity for reasonable dimensions. In a hollow cylinder, the temperature drops from the bore according to:

$$t_J - t = AW\left(\frac{\ln\left(\frac{r}{r_J}\right)}{K}\right) \tag{5-20}$$

TABLE 5-3. Effect of Viscosity Exponent on the Stability Parameter G and the Critical Dimensionless Film Thickness H

	m	H	G
	3	0.5349	0.2
	2	0.4725	0.25
	1	0.3849	0.335
Isoviscous	0	0.5	0.25
SAE-50	2.33	0.4955	0.23
SAE-20	1.85	0.4618	0.26

TABLE 5-4. Correction of Equation (5-4) for Thick Bearings

r_B/r_J	$(r_B - r_J)/r_J$	Φ_L $(t_S - t_B)/[W\delta_B/2K]$	Approx. Φ_L (eq. (5-23))
1.3	0.3	0.95	0.96
1.4	0.4	0.93	0.93
1.5	0.5	0.92	0.92
1.6	0.6	0.90	0.90
1.7	0.7	0.89	0.89
1.8	0.8	0.88	0.88
1.9	0.9	0.86	0.87
2	1.0	0.85	0.85

The drop from surface temperature to mean temperature, t_B, of the cylinder can be found by letting $R = r_B/r_J$:

$$t_J - t_B = \frac{\left[\left(\frac{AW}{K}\right) R^2 \ln(R) - \frac{R^2}{2} + 0.25\right]}{(R^2 - 1)} \tag{5-21}$$

The linearized approximation with the corrector is:

$$t_J - t_B = \frac{\Phi_L \left(\frac{AW}{K}\right)(R - 1)}{2} \tag{5-22}$$

Equations (5-21) and (5-22) may be solved for Φ_L. The results are listed in Table 5-4. Therefore, Φ_L may be accurately represented by the linear equation:

$$\Phi_L = \frac{1 - 0.15(r_B - r_J)}{r_J} \tag{5-23}$$

From Table 5-4, it is clear that $\Phi_L = 1$ is a good approximation.

Calculated Limit of Stability for the Thermoviscous Fluid

A review of the derivation of eq. (5-12) suggests that it is correct for isoviscous and thermoviscous fluids as long as the appropriate viscosity is substituted. Equation (5-12) can also give an estimate of operating temperature at the point of instability. Recall that:

$$t_M = \frac{W\delta_{SA}}{K} = \frac{\mu U^2(\delta_{SA}/h)}{K} \tag{5-24}$$

Drawing upon eq. (5-13):

$$t_M = \frac{5(100)}{0.14} = 3571°C \tag{5-25}$$

This operating condition is far removed from typical practice.

Equation (5-19) is repeated here for easy reference. It may be solved for critical speed using properties and design parameters from Table 5-1.

$$G = 0.25 = \frac{\varepsilon R_J R_{JB} \Phi_L}{2K_J} \left(\frac{(Kh_0/\delta_{SA})^2 U^2}{b} \right)^{1/3} \tag{5-26}$$

Of the variables in the table, the dimensionless radii; the viscosity parameter, b; the fluid velocity, U; and the thermal resistance to the environment are strong variables. In this trial calculation, the dimensionless radii will be retained because they are close to practice. The fluid viscosity parameter is not too influential because it appears to a small power. The resistance, δ_{SA}, is important because it appears to a reasonably high power, and it can be varied greatly. For the calculation, $\delta_{SA}/h_0 = 100$; SAE-20 oil is used; and U is calculated. In Table 5-1 the oils have been forced to the exponent $m = 2$ with appropriate values for b. The resulting function tracks the accurate function both below and above $t = 80°C$. For these conditions:

$$U = 4037 \text{ m/s} \tag{5-27}$$

This is much higher than the isoviscous predictions for low-viscosity fluids; but when the excessively high temperature is taken into account, the oil viscosity must be extremely low, whether physically possible or not.

Summary

The thermoviscous analyses from the previous chapters are incorporated into a two-dimensional cylindrical system with a solid journal in a concentric bearing. Both cylinders are of the same material, and operation is assumed to be at steady state. The lubricant film is isoviscous, with viscosity determined by the overall heat balance. Heat is conducted outward through the bearing, and a difference in mean temperatures of journal and bearing arises.

For these conditions, real solutions for steady operation can disappear and seizure would be predicted. Sample calculations suggest that this is expected at temperatures well above physically reasonable operating conditions, and other kinds of distress might be expected before the instability is realized, under the restrictions of the analysis.

6
A Transient Mechanism of Seizure

Even when the conditions of stable static operation are satisfied, a self-actuated dynamic process of clearance loss can cause bearing seizure. A small decrease in film thickness causes heating to increase, and this leads to relative thermal expansion with further decreases in film thickness. This chapter explores the conditions necessary for this process for the journal–bearing system of a single material. The analysis postulates an exponentially growing temperature perturbation in the film. Heat transfer to the journal and bearing is found, and relative expansion is derived from the heat inputs. The result is the combination of geometric and operating variables necessary for the transient process to be sustained. The solution requires that the heat input be concentrated in thin thermal boundary layers beneath the surfaces of the journal and bearing. This condition cannot be satisfied at low sliding speeds when the thermal boundary layer grows to the characteristic dimension of one of the bodies, a fuzzily defined event that sets a lower bound for the dynamic instability phenomenon.

The Finite Perturbation in Temperature

The self-feeding seizure mechanism causes an exponentially growing encroachment of the surfaces into the clearance space, along with the incrementation of viscous heating. When the growth exponent is large, the thermal boundary layer in the solid material is thin. Consequently, the partitioning of heat as well as the dynamics of heat transfer are locally determined and are independent of the geometry of the journal and bearing. For a thin thermal boundary layer, the heat transfer into a cylindrical body is not greatly different from the heat flow directly into the flat face of a straight bar or the surface of a slab. When both bodies are made of the same material, heat flow divides equally between them, and the surface temperature increment is the same for each.

The thermal resistance, δ', for the transient conduction into the solid is much smaller than the overall resistance, δ_{SA}; consequently the temperature perturbation is small, and the fluid film may be treated as isothermal and isoviscous in the initial stages of the process. The temperature may, of course, be elevated above ambient

R. A. Burton, *Heat, Bearings, and Lubrication*

TABLE 6-1. Response Time for Boundary Layer Growth across a Viscous Lubricant Film

Fluid	t (°C)	$\mu v \times 10^6$ (m^2/s)	$\tau \times 10^6$ (s)
Water	20	1.00	6.25
	100	0.29	21.5
Mercury	20	0.12	52.1
Oil	20	892	0.007
	40	231	0.027
	60	82	0.076
	80	37	0.168
Air	0	13.6	0.459
	50	18.6	0.336

by the steady, parent Couette flow. To be consistent with the usage in chapter 2, the thermal resistance, δ', is an equivalent thickness of oil. Where there is an advantage in replacing this by an equivalent thickness of solid material, the thermal resistance will be designated δ'_S.

Thermal Response Time for Viscous Heating

Chapter 5 stated that the viscous heating in the film is determined instantaneously by sliding speed and fluid viscosity, whereas thermal equilibration in solids occurs over an extended period of time. Stated more carefully, the viscous heating will approach the steady-state value in a fraction of a second, whereas the process of heat transfer in the solid may require several minutes. A guide to the time response of a viscous film is offered by Schlichting (1968, p. 83), in treating the growth of the viscous boundary layer on a suddenly accelerated plate. The boundary layer thickness, δ_{BL} is:

$$\delta_{BL} \gg 2(\mu v \tau)^{1/2} \tag{6-1}$$

Assuming an analogous process, a characteristic time required for the layer to grow to the film thickness in the Couette flow might be written:

$$\tau = \frac{h^2}{\mu v} \tag{6-2}$$

Table 6-1 shows this characteristic time for fluid properties from Table 2-1 for $h = 0.0025$ cm. At its greatest, the response time is only a few milliseconds.

Thermal Expansion of Solid Elastic Cylinders

Timoshenko and Goodier (1970, p. 448), give equations for thermal stress in a cylinder of radius r_2 with a concentric bore of radius r_1 for the condition of

"zero end-load," but not necessarily without local axial stress. If there is no radial component of normal stress (pressure) acting on the internal or external cylindrical surfaces, then the radial displacement must be, for combined elastic and thermal strain:

$$\frac{\delta r}{r} = \varepsilon t + \frac{\sigma_{\theta\theta} - \upsilon\sigma_{zz}}{E} \tag{6-3}$$

Evaluating the stress equations at the inner radius:

$$\sigma_{\theta\theta} = \left[\frac{\varepsilon E}{1-\upsilon}\frac{2}{r_2^2 - r_1^2}\right]\int_{r_1}^{r_2} tr\,dr - t \tag{6-4}$$

$$\sigma_{zz} = \sigma_{\theta\theta} \tag{6-5}$$

Irrespective of the temperature distribution (changing or steady):

$$t_{\text{mean}} = \frac{2}{r_2^2 - r_1^2}\int_{r_1}^{r_2} tr\,dr \tag{6-6}$$

Therefore, the expansion of the bore for a rise in temperature from the ambient is:

$$\frac{dr_1}{r_1} = \varepsilon t + \frac{\sigma_{\theta\theta} - \upsilon\sigma_{zz}}{E} = \varepsilon t_{\text{mean}} \tag{6-7}$$

The same result is obtained for the exterior of a solid cylinder or journal of radius r_J.

Rate of Expansion of a Journal

When the heat flux per unit of surface area, W'_J, into the journal is known, then the time rate of change of the mean temperature will be:

$$\frac{dt'_{\text{mean}}}{d\tau} = \frac{2\pi W' r}{m_J C_P} \tag{6-8}$$

where C_P is specific heat, and m is the mass per unit of length of the cylinder. For a journal of radius r_J:

$$m_J = \frac{\pi r_J^2}{v} \tag{6-9}$$

where v is specific volume of the solid. When the expansion of the solid is small relative to the original dimension, it is customary to apply the theory of small displacements, and r_J on the right-hand side of eq. (6-7) is treated as a constant parameter of the system. Differentiating eq. (6-7) in time:

$$\left(\frac{dr}{d\tau}\right)_J = \varepsilon r_J \frac{dt'_{\text{mean}}}{d\tau} \tag{6-10}$$

Combining this with eqs. (6-8) and (6-9):

$$\left(\frac{dr}{d\tau}\right)_J = \frac{2\varepsilon W_J' v}{C_P} \tag{6-11}$$

When the bearing bore is r_S and the outer radius is r_B, a similar derivation gives:

$$\left(\frac{dr}{d\tau}\right)_B = \frac{2\varepsilon W_B' v}{C_P[(r_B/r_S)^2 - 1]} \tag{6-12}$$

Although the heat flow is transient in the thermal sense, the stress field and thermal expansion that go with it may be thought of as instantaneous. Neglect of axial heat transfer is consistent with the thin thermal boundary layer, where the radial temperature gradient is dominant.

Exponential Growth of Surface Temperature

The Fourier heat transfer equation reduces to the following form for transient heat conduction normal to a flat surface:

$$k_S \frac{\partial^2 t'}{\partial y^2} = \frac{\partial t'}{\partial \tau} \tag{6-13}$$

where k_S is the thermal diffusivity of the solid. For the thin thermal boundary layer, this serves as a valid asymptotic limit for heat transfer. When the surface temperature, t_S', rises exponentially,

$$t_S' = A' e^{\beta' \tau} \tag{6-14}$$

Equation (6-9) is satisfied in the solid when:

$$t' = t_S' e^{\beta' y} \tag{6-15}$$

where

$$\beta' = \left(\frac{\alpha'}{k_S}\right)^{1/2} \tag{6-16}$$

We have discarded the positive solution as inconsistent with a thin heated layer in an initially equilibrated body. The temperature gradient at the surface is:

$$\left(\frac{\partial t'}{\partial y}\right)_S = \beta' t_S' \tag{6-17}$$

The thermal boundary layer may be defined as illustrated in Fig. 6-1, where the thickness, δ_S', is such that:

$$\frac{t_S'}{\delta'} = \left(\frac{\partial t'}{\partial y}\right)_S \tag{6-18}$$

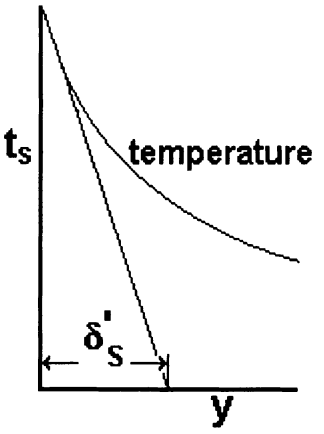

FIGURE 6-1. Thermal boundary layer thickness, δ'_S in a solid, determined by the temperature gradient at the interface.

It follows that:

$$\delta'_S = \frac{1}{\beta'} = \left(\frac{k}{\alpha'}\right)^{1/2} \tag{6-19}$$

The thermal boundary layer is designated "thin" when $\delta'_S \ll r_J$. For the thin thermal boundary layer, and for the same material in the bearing and journal, the perturbation on viscous dissipation, W', would see the same resistance in both bodies and would divide evenly, and therefore, $W'_J = W'_B = W'/2$. This would be independent of the quasi-static temperature distribution upon which the perturbation is superposed, where all heat flow might be blocked from one of the solids to the environment, for example.

Transient Expansion of the Journal and Bearing

For a single material in the bearing and journal, when half of the transient heat perturbation goes to the journal, eq. (6-11) calls for:

$$\left(\frac{dr'}{d\tau}\right)_J = \frac{W'\varepsilon v}{C_P} \tag{6-20}$$

Similarly, the expansion of the bearing bore is given by eq. (6-12):

$$\left[\frac{dr'}{d\tau}\right]_B = \frac{W'\varepsilon v}{C_P[(r_B/r_S)^2 - 1]} \tag{6-21}$$

where ε is the coefficient of expansion for both bodies. The net rate of decrease of the clearance, $-dh'/dt$, can be found as the difference between the expansion

of the journal and the bearing:

$$\frac{dh'}{d\tau} = -\frac{W'\varepsilon v\Gamma}{C_P} = -\frac{W'\varepsilon k\Gamma}{K} \tag{6-22}$$

where $r_S = r_J + h \approx r_J$, for small film thickness, and

$$\Gamma = \frac{(r_B/r_S)^2 - 2}{(r_B/r_S)^2 - 1} \tag{6-23}$$

This equation is interesting in that the denominator must always be greater than unity. The numerator becomes negative when: $(r_B/r_S) < \sqrt{2}$. If the bearing is a tube thinner than this, the film thickness will increase with increasing viscous heating, and this would quench any feedback effect. Because there are sometimes design considerations that call for a thick bearing, there may be conditions where dh/dt will be negative, and the film will thin.

The Increment of Viscous Heating

For steady-state operation of a bearing, the viscosity is strongly influenced by the frictional heating because of the temperature rise needed to drive the heat through the resistance δ_{SA}. For the perturbation considered here, the effect of heating on temperature is much smaller because the resistance δ' may be equivalent to a millimeter or less of solid, whereas δ_{SA} is typically several centimeters. Consequently, the perturbation in temperature, t'/t, is at least an order smaller than the perturbation in heating, W'/W. The isoviscous approximation is therefore appropriate when viscosity is based upon the steady-state temperature.

For isoviscous flow, where h is the fixed initial clearance and W is the initial rate of dissipation:

$$W = \frac{\mu U^2}{h} \tag{6-24}$$

When the perturbation is superposed upon this flow, both heating and film thickness may be incremented appropriately:

$$W + W' = \frac{\mu U^2}{h + h'} \tag{6-25}$$

For the small-perturbation condition, where $h' \ll h$, and $W' \ll W$:

$$W' = -\frac{Wh'}{h} \tag{6-26}$$

Substituting eq. (6-26) into eq. (6-22) yields:

$$\frac{dh'}{d\tau} = \frac{W\Gamma h'}{h^2}\left(\frac{\varepsilon k}{K}\right)_S \tag{6-27}$$

where the nonprime quantities W and h are taken from steady-state operation. Substituting eq. (6-24) into eq. (6-27) gives:

$$\frac{dh'}{d\tau} = \left(\frac{U}{h}\right)^2 \left(\frac{\mu\varepsilon k}{K}\right) \Gamma h' \tag{6-28}$$

When h' is the sole variable in time, the equation is satisfied by:

$$h' = h'_0 e^{\alpha' \tau} \tag{6-29}$$

where $dh'/dt = \alpha h'$, and

$$\alpha' = \left(\frac{U}{h}\right)^2 \left(\frac{\mu\varepsilon k}{K}\right) \Gamma \tag{6-30}$$

For a thin bearing cylinder, Γ and α would be negative, and the perturbation would decay. For for a thicker cylinder, the perturbation would grow. Depending upon the sign of h'_0, the perturbation could represent a thickening or a thinning of the film. If the latter is possible, then it should be expected to occur sooner or later. The point is that a self-sustained dynamic thinning of the film is possible, and this can constitute a mode of failure.

Limit of Validity for Thin-Thermal-Boundary-Layer Approximation

As the exponent of growth is made lower by the choice of relative mass of the journal and bearing, the thermal boundary layer is thickened. When the calculated thermal boundary layer thickness is several times the dimension r_J, the problem becomes one of quasi-static heat transfer, and the above derivation becomes invalid. To set an arbitrary upper limit for the thin boundary layer, let $\delta' = r_J$ in eq. (6-19):

$$\alpha' = \frac{k_J}{\delta'^2_J} = \frac{k_J}{r_J^2} \tag{6-31}$$

Substituting from eq. (6-30), and recognizing that $(kC_P/v)_J = K_J$:

$$\left(\frac{U}{h}\right)^2 = \frac{K_J}{\Gamma\varepsilon\mu r_J^2} \tag{6-32}$$

or

$$U^2 = \frac{K_J}{\Gamma\varepsilon\mu R_J^2} \tag{6-33}$$

where $R_J = r_J/h$, and h is not a variable but the steady-state magnitude upon which h' is imposed. If the size, fluid, and material of the system are specified, then the lower limit for the "thin thermal boundary layer" is a sliding speed. Representative design and operating parameters for a journal bearing are shown in Table 6-2.

TABLE 6-2. Representative Design and Operating Parameters for a Journal Bearing

Parameter	Magnitude	Units
R_J	500	—
ε	10^{-5}	1/°C
μ	0.017	N-s/m^2 (at 100°C)
Γ	0.7	—
K	50	N/s-°C

A Numerical Calculation of the Limit of Stability

As in chapter 4, let the material be iron for the bearing and journal, and let the fluid be the SAE-50 oil at 100°C. The bearing thickness will be such that $r_B = 2r_S$. Using eq. (6-33):

$$U = 41 \text{ m/s} \tag{6-34}$$

This is a high sliding speed, outside the range of operation of ordinary machinery. It is likely that turbulence will occur in the film at a lower speed, however, and alter the heating in subtle ways. This situation is treated in chapter 9. Furthermore, when the bearing and journal are of different materials, as discussed in chapter 7, this number can be changed by several orders of magnitude.

Summary

A dynamic process of bearing seizure may occur when relative expansion of the journal in the bearing leads to an increase in viscous heating. For a single material in both the journal and bearing, the geometric condition for positive feedback is that $\Gamma > 0$, or $r_B/r_S > 1.414$.

The postulated instability mechanism is valid only when the thermal boundary layer is thin relative to the dimensions of the system. An approximate limit of this condition is given by eq. (6-33). A numerical calculation shows that this condition lies outside ordinary operating conditions. The mechanism may take place when a cold bearing is suddenly started, and the film is highly viscous. If the viscosity in the example is raised nine-fold, for example, the critical speed U would drop to 13 m/s, which might be found in commonplace machinery.

Probing further, one may ask how sharply the lower boundary of thin-film operation can be defined. Figure 6-2 shows a thermal boundary layer extending from one side of a slab to the other, with thickness defined as the intercept of the maximum slope. When the remote surface rises in temperature, some of the heat stored in the body may be bled to the surroundings. The significance of this loss would depend upon the magnitude of δ_{SA}. If the resistance is large, the tail of the boundary layer would be reflected. This would influence the partitioning of heat only when it returns to the wetted surface in sufficient strength to affect the

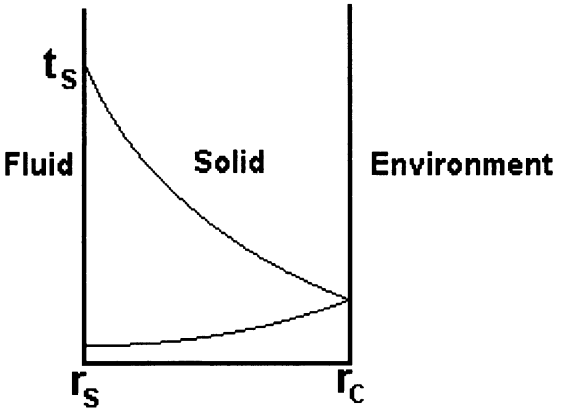

FIGURE 6-2. Thermal boundary layer for exponentially rising t_S in a thin slab with high resistance on the outer surface. The profile is reflected back from the exterior boundary to the slab.

surface temperature perturbation. Would a "fuzzy" criterion of the significance of the reflected tail occur when $\delta'_S = 2r_J$? If so, this would halve the critical sliding speed. Fuzzy or not, the analysis provides two insights: (1) there is a mechanism for an exponential thinning of the film, and (2) an estimate of the lower speed limit shows which parameters control the phenomenon. For these estimates, see eqs. (6-31) through (6-33).

7
Different Materials in the Journal and Bearing

Requirements other than thermoelastic stability may dictate the materials of a journal and bearing. This choice can greatly modify the conditions for quasi-static and dynamic seizure. Partitioning of heat, expansion, and especially the resistance to external cooling all play significant roles in quasi-static seizure. On the other hand, external cooling is of marginal importance in the dynamic seizure mechanism.

The derivations in this chapter are tied closely to the single-material presentation, and the effects of material differences are lumped into coefficients that bias system behavior that is already defined. For quasi-static operation, the principal effects are incorporated into Φ_E, which replaces Φ_L of the analyses in chapter 5. For the dynamic seizure process, the material effects are incorporated into a modified Γ_E, which replaces Γ of chapter 6.

Quasi-Static Operation with Differing Materials

Although the coefficient of thermal expansion, ε, is the most obvious material variable, diffusivity, k, and conductivity, K, also play important roles. Table 7-1 lists these properties, along with elastic modulus, E, for a range of metallic and nonmetallic materials.

When the coefficient of expansion differs for the journal and bearing, and when $h \ll r_J$, the equivalent of eq. (5-5) becomes:

$$h_0 - h = r_J[(\varepsilon t)_J - (\varepsilon t)_B] \tag{7-1}$$

Recall that the temperatures, t_J and t_B, are the "mean" temperatures of the cross sections of the journal and bearing, and are measured from the ambient, or rest, condition, at which the clearance is h_0. When heat flow to the journal and shaft is blocked, the bearing temperature can be found from the geometry of the temperature diagram in Fig. 4-1, where the small temperature drop across the liquid film is neglected.

$$\delta_B = (r_B - r_J)\left(\frac{K}{K_B}\right) \tag{7-2}$$

R. A. Burton, *Heat, Bearings, and Lubrication*

TABLE 7-1. Thermal Properties of Bearing Materials

Material	$\varepsilon \times 10^6$ (1/°C)	$k \times 10^2$ (cm^2/s)	K (N/s-°C)	E (MPa)
Copper	16.6	43.6	130	1×10^5
Aluminum	17	83	227	6.8×10^4
Cast iron	11	11	50.4	2×10^5
Silicon carbide	4.7	6	18	8.8×10^4
Graphite	4.7	8	13.5	6.8×10^3
Polyethylene	100	0.31	0.5	9.00×10^2

Here δ_B is *not* the physical thickness of the bearing, but the equivalent thickness of oil that would have the same thermal resistance as the bearing cylinder. This requires reinterpretation of the logarithmic correction if it is retained. Let $\Phi_L = 1$, which is strictly correct as the limit for thin bearing cylinders but not seriously in error for typical thickness ratios, and the bearing temperature is the journal temperature less half the drop across the bearing cylinder:

$$t_B = t_J\left(\frac{1 - \delta_B}{2\delta_{SA}}\right) \tag{7-3}$$

Equation (7-1) then becomes, upon substitution:

$$h_0 - h = r_J t_J\left[\varepsilon_J - \varepsilon_B\left(\frac{1 - \delta_B}{2\delta_{SA}}\right)\right] \tag{7-4}$$

Recalling that $t_J = W\delta_{SA}/K$, the equivalent of eq. (5-6), may be written, where the expansion differences are incorporated into a multiplier, Φ_E:

$$h_0 - h = r_J\varepsilon_J\left(\frac{W(r_B - r_J)\Phi_E}{2K_J}\right) \tag{7-5}$$

where Φ_E is defined by:

$$\Phi_E = \left[\left(\frac{\varepsilon_B}{\varepsilon_J}\right) + \left(\frac{2\delta_{SA}}{\delta_B}\right)\left(1 - \frac{\varepsilon_B}{\varepsilon_J}\right)\right]\left(\frac{K_J}{K_B}\right) \tag{7-6}$$

This corrector may be carried through the derivations of chapter 4 as a coefficient similar to Φ_L, and would appear in the same position in the final equations. As shown in Table 7-2, for an iron journal in a graphite bearing, Φ_E is most strongly influenced by the thermal resistance to the environment, δ_{SA}, and almost equally

TABLE 7-2. Stability Parameters for an Iron Journal in a Graphite Bearing

Mode of cooling	δ_{SA}/h	δ_{SA}/δ_B	Φ_E	$1/\Phi_E^{1/2}$	$1/\Phi_E^{3/2}$
Natural convection to a gas, NCG	2000	800	3401	0.017	5.0×10^{-6}
Forced convection to a liquid, FCL	150	50	216	0.068	3.2×10^{-4}
Boiling liquid, B	30	10	44	0.15	3.4×10^{-3}

by the expansion and conductivity ratios. The two right-hand columns of Table 7-2 anticipate needs that appear farther along in the analysis.

Stability Limit for an Isoviscous Fluid

In eq. (7-5), the dissipative heating, W, may be substituted by $\mu U^2/h$ for the isoviscous case, or evaluated by eq. (4-17) for the thermoviscous case. With either substitution, the method of solution is an in chapter 5, leading to a dimensionless group, G, which defines the threshold of stability, where $G = 0.25$ for both the isoviscous fluid and the thermoviscous fluid when the power-law exponent is $m = 2$. For other values of the exponent, G does not wander far from 0.25, as shown in Table 5-2. In the present nomenclature, for isoviscous flow:

$$G = \varepsilon_J r_J \frac{(r_B - r_J)\Phi_E \mu U^2}{2K_J h_0^2} \tag{7-7}$$

If all of the other variables are fixed, the critical sliding speed varies as $1/\Phi_E^{1/2}$. Data from eq. (5-14) and from Table 7-2 may be combined to give estimates of the limit of performance for selected fluids and modes of heat removal. Table 7-3 compares two material choices: the iron journal in an iron bearing and the same journal in a graphite bearing. The modes of cooling are by *natural convection to a gas* (NCG), *forced convection to a liquid* (FCL), and *boiling* (B). The fluids, water, air, and mercury are treated as isoviscous. The extremely low critical speed for high external thermal resistance (NCG) indicates that the overall expansion of the system from the high temperature rise is the dominant effect, irrespective of the temperature gradient in the bearing. The carbon might have been chosen for good performance under lubricant starvation; however, it can lead to severely reduced operating speeds for the full film condition. These speeds might be increased by opening up the clearance, since U varies directly with h_0. On the other hand, a small clearance may be dictated by the need for stiffness in hydrodynamic operation. The temperature might be lowered by cooling the journal, if that is feasible.

The dominant variable, δ_{SA}, is difficult to predict in the design phase. Nevertheless, the calculated results serve as a warning, and the equations allow assessment of the effects of changes of other design variables.

TABLE 7-3. Critical Sliding Speed for an Iron Journal with Isoviscous Fluids

			Sliding Speed (m/s)		
Bearing	Fluid	μ	NCG	FCL	B
Iron	Water	0.001	70	70	70
	Mercury	0.0015	58	58	58
	Air	0.00002	500	500	500
Graphite	Water	0.001	1.4	4.8	10.6
	Mercury	0.0015	1	4	8.8
	Air	0.00002	8.6	34.2	75.8

TABLE 7-4. Quasi-Static Stability Threshold for a Cast Iron Journal and Carbon Bearing

Fluid	b ($m=2$)	Sliding Speed (m/s) NCG	FCL	B
SAE-10	0.052	0.51	2.47	8.75
SAE-20	0.032	0.40	1.93	6.87
SAE-30	0.016	0.29	1.37	4.85
SAE-40	0.012	0.25	1.18	4.20
SAE-50	0.009	0.22	1.03	3.66

Stability Limit for a Thermoviscous Fluid

In eqs. (5-15) through (5-18) the limit of quasi-static operation is found, and it is expressed in the dimensionless variable G, which becomes, for a power-law thermoviscous fluid:

$$G = \frac{\varepsilon_J r_J (r_B - r_J)\Phi_E \left[\dfrac{(K/\delta_{SA})^m U^2}{bh_0}\right]^{1/(1+m)}}{2h_0 K_J} \tag{7-8}$$

This group will lie at the limit of stability when $G = 0.25$ (for $m = 2$). In present nomenclature, this criterion of instability is:

$$G = \frac{\varepsilon_J r_J (r_B - r_J) \left[\dfrac{\left(\Phi_E^{3/2} K U/\delta_{SA} h_0^2\right)^2}{b}\right]^{1/3}}{2K_J} = 0.25 \tag{7-9}$$

Table 7-4 shows the effects of different oils on stability with a cast iron journal in a carbon bearing, for which $R_J = R_{JB} = 500$, with properties from Table 7-1 and operating conditions from Table 7-2. These numbers may be compared with eq. (5-27), where the stability threshold is much higher when the journal and bearing are of the same material.

The mode of cooling has far more influence than the entire range of viscosities. The mode of cooling causes a 17-fold change in U, whereas the viscosity range causes only a twofold change. Unlike the earlier examples, the better the cooling the higher the limit of stability. *Internal* cooling by forced lubricant flow is also effective in this mode of operation; this topic is treated in chapter 13, Laminated bearings of two materials are treated in chapter 16.

Effect of Material Differences on Dynamic Seizure

Let the subscripts J and B designate all quantities associated with the journal and the bearing, respectively. Heat flow into either body will be controlled by the thermal boundary layer thicknesses, δ'_J and δ'_B, expressed as actual thicknesses in the solid material and not as an equivalent oil film. As shown in chapter 6, for conduction straight into a solid, and where t' is the transient component of surface

temperature, heat flow to the journal is:

$$W'_J = \left(\frac{Kt'}{\delta'}\right)_J = \left[Kt'\left(\frac{\alpha'}{k}\right)^{1/2}\right]_J \tag{7-10}$$

A similar equation may be written for the bearing. If resistance in the fluid film is negligible, the two surfaces will share the temperature t', and:

$$W' = W'_J + W'_B = t'\left[K\left(\frac{\alpha'}{k}\right)^{1/2}\right]_J + t'\left[K\left(\frac{\alpha'}{k}\right)^{1/2}\right]_B \tag{7-11}$$

It follows that:

$$\frac{W'_J}{W'} = \frac{1}{1 + (K_J/K_B)(k_B/k_J)^{1/2}} \tag{7-12}$$

The same equation may be made to apply to the bearing upon interchanging subscripts. The net rate of encroachment of the journal and bearing into the clearance may be accounted for in the equivalent of eq. (6-11), where $v/C_P = k/K$:

$$\left(\frac{dr}{d\tau}\right)_J = 2\left(\frac{W'\varepsilon k}{K}\right)_J \tag{7-13}$$

The equivalent of eq. (6-12) may be written similarly for the rate of expansion of the bore of the bearing.

$$\left[\frac{dr}{d\tau}\right]_B = \frac{2(W\varepsilon k/K)_B}{(r_B/r_S)^2 - 1} \tag{7-14}$$

Subtracting the encroachment by the journal from the expansion of the bearing, the net rate of change of film thickness may be found upon substitution from eq. (7-9) and its equivalent for the bearing:

$$-\frac{dh'/d\tau}{W'(\varepsilon k/K)_J} = \Gamma_E \tag{7-15}$$

and

$$\Gamma_E = \left[\frac{2}{1 + (K_B/K_J)(k_J/k_B)^{1/2}}\right] - \left[\frac{2(\varepsilon_B/\varepsilon_J)(k_B/k_J)(K_J/K_B)}{[(r_B/r_J)^2 - 1][1 + (K_J/K_B)(k_B/k_J)]^{1/2}}\right] \tag{7-16}$$

When Γ_E is evaluated for identical properties in the bearing and the journal, this quantity reduces to Γ, as defined in eq. (6-23). It serves, therefore, as a generalized coefficient in the equations of expansion.

Numerical Comparisons of Bearing Materials

To evaluate Γ_E, property data are taken from Table 7-1. For an iron journal, and for bearings made of polyethylene, iron, aluminum, and carbon, the appropriate ratios are listed in Table 7-5.

TABLE 7-5. The Parameter Γ_E for Cast-Iron Journal Material and Four Bearing Materials

	Bearing Material			
	Polyethylene	Aluminum	Iron	Graphite
$\varepsilon_B/\varepsilon_J$	11	1.54	1	0.42
k_B/k_J	0.0036	7.55	1	0.72
K_B/K_J	0.01	4.5	1	0.26
r_B/r_J	2	2	2	2
Γ_E	1.34	−0.31	0.66	1.35

Table 7.5 shows that $\Gamma_E = \frac{2}{3}$ when the journal and bearing are made of the same material. An aluminum bearing around an iron journal would perform well, as expected. In view of its low expansion, its resistance to heat input, and its poor performance in quasistatic seizure, the graphite bearing shows a tendency toward seizure.

Summary

When a journal operates in a bearing of different material, the relevant properties may be grouped into a multiplier, Φ_E, which is defined in eq. (7-6). Worked examples show that for different materials the critical speed for stable operation may be reduced far below that for a single material. The effect of external cooling is strong.

In the equations for dynamic seizure of a two-material system, the variables may be grouped into a dimensionless parameter, Γ_E, defined in eq. (7-16). This coefficient replaces Γ of the prior derivations. For example, it may appear in the fuzzy criterion for the lower speed limit of dynamic seizure,

$$\left(\frac{U}{h_0}\right)^2 = \frac{K}{\varepsilon\mu\Gamma_E r_J^2} \tag{7-17}$$

When Γ_E is made small, the permissible speed is raised. Table 7-5 shows that the choice of materials can alter this significantly. More important, when $\Gamma_E = 0$ dynamic seizure is quenched. For a single material, this occurs when $r_B/r_J = \sqrt{2}$. Table 7-6 shows when this occurs for several material combinations. The values of R_B/R_J can be used as design criteria to assure that dynamic seizure does not take place.

TABLE 7-6. Radius Ratio That Makes $\Gamma_E = 0$ for Several Material Combinations

Journal	Bearing	R_B/R_J
Iron	Polyethylene	1.3
Iron	Graphite	1.16
Iron	Aluminum	2.3
Iron	Iron	1.414
Graphite	Iron	2
Aluminum	Iron	1.12

8
Steady Turbulent Couette Flow

Dissipative heating in turbulent Couette flow is determined by a dimensionless fluid-friction coefficient, C_F, which is itself determined by wall roughness and Reynolds number. Turbulent heating can be related to film thickness by a simple equation, which may then be incorporated into the equations for relative expansion and seizure. A critical Reynolds number determines the transition from laminar to turbulent flow. This is strongly affected by thermal boundary conditions and the sensitivity of viscosity to temperature. These effects also dominate the process of bearing seizure at high turning speeds.

Wall Shear Stress in Couette Flow

Wall shear stress and energy dissipation in smooth-wall turbulent Couette flow can be characterized accurately by a simple power law for the friction coefficient, C_F, as shown in Fig. 8-1. There the crosses represent a rework of the data of Couette (1890) by Taylor (1960), for the case where the outer cylinder is turning and the inner cylinder is stationary. Taylor showed that for the ratio $h/r_J < 0.04$, the transition to turbulence and the friction law are not greatly different, whether the outer or inner cylinder turns. Robertson (1959) offers detailed data on turbulent plane Couette flow.

For a large clearance ratio and the inner cylinder turning, the transition from simple laminar flow occurs at a reduced Reynolds number, owing to an instability that imposes a pattern of large vortices upon the flow. Most bearings of interest have thin fluid films and do not show this effect. Perhaps an exception, however, the bearing data of Smith and Fuller (1956) are for a relatively thick fluid film and lie in the vortex flow regime. Figure 8-1 shows that the data of Smith and Fuller blend smoothly into the resistance data of Couette, where turbulence dominates at elevated Reynolds number. Similar results were found by Burton and Carper (1967).

Sneck (1969) offers a broad analysis of thermoviscous and thermoturbulent flow in seals. The present treatment is based on an analysis by Burton (1994a), directed specifically to the heating problems.

R. A. Burton, *Heat, Bearings, and Lubrication*

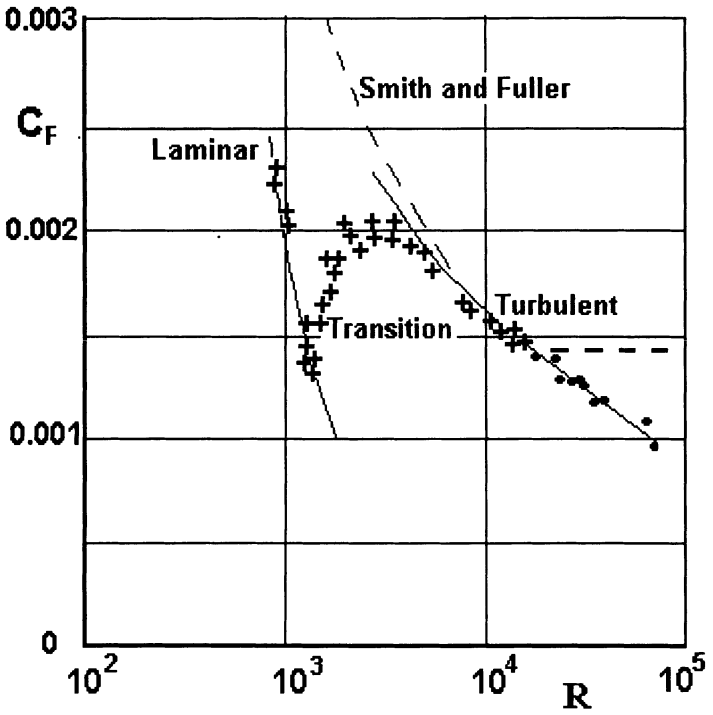

FIGURE 8-1. Friction coefficient, C_F, for Couette flow, ranging from laminar (left), through transition, and turbulent (right). The broken horizontal line is an idealization of the effect of roughness. The links above the laminar flow are data from Smith and Fuller (1956).

Heat Generation

The dimensionless friction coefficient for the Couette flow is defined such that:

$$\sigma = \frac{C_F U^2}{2v} \tag{8-1}$$

where σ is the wall shear stress, U is the relative sliding speed of the surfaces, and v is specific volume of the fluid. The power dissipated per unit of boundary-surface area is

$$W = \sigma U$$

or

$$W = \frac{C_F U^3}{2v} \tag{8-2}$$

As in the preceding chapters, the resistance to heat flow from the wetted surfaces to the environment is δ, an equivalent thickness of fluid, for which typical values are listed in Table 2-2. This thickness is large relative to the actual lubricant film thickness, which typically is $h \approx 25$ μm. The relatively large resistances both

dominate and simplify the thermal analysis. Chapter 3 shows that for large δ/h the flow is almost isothermal across the thickness of the film, in which case:

$$t = \frac{W\delta}{K} \tag{8-3}$$

where t is film temperature measured from the ambient, $\delta = 1/(1/\delta_{JA}+1/\delta_{SA})$, and K is the thermal conductivity of the lubricant. As before, thermoviscous behavior of typical oils can be modeled as a simple power law:

$$\frac{1}{\mu} = bt^m \tag{8-4}$$

Reynolds Number

The Reynolds number is defined here as:

$$\mathbf{R} = \frac{Uh}{\mu v} \tag{8-5}$$

Typically the specific volume, v, is a weak variable and will be treated as constant, whereas U, h, and μ may range over several orders of magnitude. Friction coefficient may be approximated as:

$$C_F = \frac{A}{\mathbf{R}^\alpha} \tag{8-6}$$

where magnitudes for A and α may be taken from Table 8-1 for laminar and for smooth-wall turbulent Couette flow. The rough-wall flow is idealized as having a constant friction coefficient, above a Reynolds number based upon roughness height. For lower speeds, C_F may behave as for smooth-wall flow. Combining eqs. (8-1) through (8-6) leads to a single equation for the Reynolds number in smooth wall flow, where the parameters are given in Table 8-1.

$$\mathbf{R}^{1+m\alpha} = \frac{hbU^{1+3m}}{v^{1+m}}\left[\frac{A\delta}{2K}\right]^m \tag{8-7}$$

TABLE 8-1. Parameters for Equation (8-6) for Friction Coefficient

Class of Flow	A	α
Laminar	2	1
Turbulent (smooth wall)	0.016	$\frac{1}{4}$
Turbulent (rough wall)	—	≈ 0

Discussion of the Parameters of Equation (8-7)

Table 4-1 presents two idealized oils with the exponent $m = 2$ and widely differing viscosities. Although this simplicity has been forced on the fluids, each falls within the indicated SAE viscosity grade at 100°C. These aid in the simplification of eq. (8-7) as well as those that follow.

For laminar flow. ($\alpha = 1$, $A = 2$):

$$\mathbf{R}_{\mathrm{L}}^{1+m} = \frac{hbU^{1+3m}}{v^{1+m}} \left[\frac{\delta}{K}\right]^{m} \tag{8-8}$$

Letting $m = 2$,

$$\mathbf{R}_{\mathrm{L}} = \frac{(hb)^{0.33}\, U^{2.33}}{v} \left[\frac{\delta}{K}\right]^{0.67} \tag{8-9}$$

The most sensitive variable is the speed, U, which has exponent 2.33.

For smooth-wall turbulent flow. ($\alpha = \frac{1}{4}$, $A = 0.016$):

$$\mathbf{R}_{\mathrm{T}}^{1+m/4} = \frac{hbU^{1+3m}}{2^m v^{1+m}} \left[0.016\frac{\delta}{K}\right]^{m} \tag{8-10}$$

Letting $m = 2$,

$$\mathbf{R}_{\mathrm{T}} = 1.6 \times 10^{-3} \frac{(hb)^{0.66}}{v^2} U^{4.66} \left[\frac{\delta}{K}\right]^{1.33} \tag{8-11}$$

Doubling of b or h will raise the Reynolds number by 25% in laminar flow and by 58% in turbulent flow. The most striking effect is the strong power of U, which is 4.66 for the turbulent flow. The resistance to external cooling, δ/K, is a stronger factor than film thickness in determining $\mathbf{R}$.

Transition

In Figure 8-1 the slope changes sign in the transition range. When replotted on log-log (Fig. 8-2), the slope α_{LT} is about -0.3 in the transition zone. Returning to eq. (8-7), the exponent on U is $(1 + 3m)/(1 + m\alpha)$, and for $m = 2$ this is 17.5, so that for all else held constant:

$$\mathbf{R} = \text{const}\, U^{17.5} \tag{8-12}$$

It is unusual to apply the power law to the transition, and α may not be precisely evaluated. Irrespective of the numbers chosen, speed appears to a very large power. Hence, thermoviscous flow experiences a much sharper transition than does isoviscous flow.

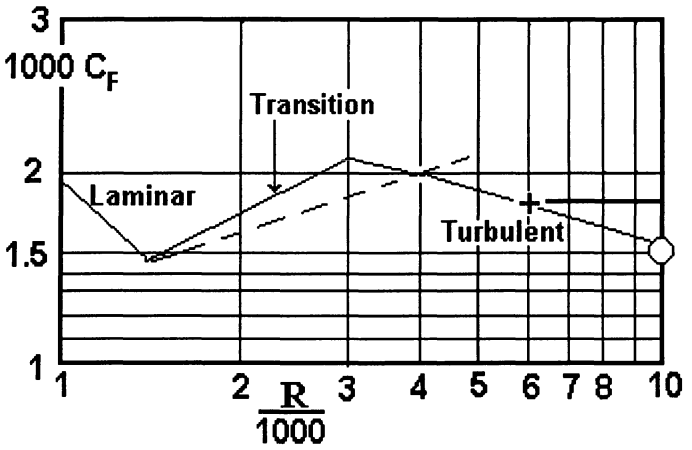

FIGURE 8-2. Friction coefficient C_F, for thermoviscous flow on log-log coordinates, showing the rise in R at transition, and the idealized leveling for rough-wall flow at the +.

Reynolds Number for Selected Values of C_F

Returning to eq. (8-7) and letting $\alpha = 0$, in which case $A = C_F$:

$$\mathbf{R} = \frac{hbU^{1+3m}}{2^m \upsilon^{1+m}} \left[\frac{\delta}{C_F K}\right]^m \tag{8-13}$$

For transition, where only C_F changes in going from laminar to turbulent flow:

$$\frac{\mathbf{R}_T}{\mathbf{R}_L} = \left[\frac{C_{FT}}{C_{FL}}\right]^m \tag{8-14}$$

Because the friction coefficient of the transitioned flow is larger than that of the laminar flow, when $m = 2$ there will be a large increase of R. Figure 8-2 shows a broken line running from a point near the lower limit of laminar flow with the exponent $1/m$, in accordance with eq. (8-14). This indicates that transition could occur with a jump in Reynolds number from around 1500 to 3000 without a change in speed or film thickness. This also suggests that reduction of operating speed may find a thermoviscous fluid remaining turbulent below the isothermal transition speed.

Roughness-Limited C_F

The turbulent velocity profile may be visualized as a turbulent core spanning most of the film, with large *apparent viscosity* or *eddy viscosity*, and with small velocity gradient. Near the solid surfaces, or "walls," the turbulence is damped and a thin layer of nearly laminar fluid experiences a large velocity gradient. For present arguments the sublayer thickness, δ_{SL}, may be defined such that $\sigma = (U/2)/\delta_{SL}$ as illustrated in Fig. 8-3.

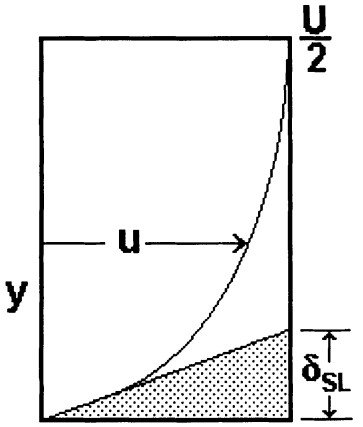

FIGURE 8-3. Velocity profile for turbulent Couette flow, with y measured from the wall (bottom). Sublayer thickness is defined by the slope at the wall.

Early in the study of turbulence, Nikuradse (1933) demonstrated that when the laminar sublayer was thinned by increasing Reynolds number, C_F would tend to level out at a nearly constant magnitude (see the "cross" (+) in Fig. 8-2). Specifically, this would happen when the thickness of the sublayer was of the same general magnitude as the roughness height. The boundary of "fully rough" operation converted to present nomenclature is:

$$\frac{\delta_{SL}}{h} = \frac{10}{\mathbf{R}C_F^{0.5}} \tag{8-15}$$

To provide a scale for viewing these quantities, take an arbitrary point on the turbulent portion of the curve in Fig. 8-2, indicated by the circle where $C_F = 0.00155$, and $\mathbf{R} = 10{,}000$. Equation (8-15) calls for:

$$\frac{\delta_{SL}}{h} = 0.025 \tag{8-16}$$

To set this into perspective, let $h = 0.0025$ cm, then $\delta_{SL} = 0.0000625$ cm $= 0.625\ \mu$m $\approx 24\ \mu$in. This would fall within the range of roughness expected on surfaces formed by grinding. Hence rough-wall flow would be expected in reasonable bearing applications.

Dissipative Heat Flux Density and Thermal Expansion

The heat flux per unit of surface area is given by eq. (8-2), upon substitution from eqs. (8-6) and (8-7).

$$W^{1+m\alpha} = \frac{A}{z}\left(\frac{K}{\delta}\right)^{m\alpha} \frac{U^{3-\alpha}}{(hb)^{\alpha}\nu^{1-\alpha}} \tag{8-17}$$

For $\alpha = \frac{1}{4}$, $A = 0.016$, and $m = 2$ this simplifies to:

$$W = (0.04)\left[\frac{K}{\delta}\right]^{0.333} \frac{U^{1.83}}{(hb)^{0.16}\upsilon^{0.5}} \tag{8-18}$$

This may be substituted into eq. (7-5), the equation for film thickness where the shaft and bearing are the same material, where all cooling is through the external surface of the bearing. This is repeated here for quick reference.

$$h_0 - h = \varepsilon r_S \Phi_E \left(\frac{W(r_B - r_J)}{2K_J}\right) \tag{8-19}$$

When W is substituted and the equation is nondimensionalized in h, as was eq. (5-7), letting $H = h/h_0$,

$$1 - H = \frac{G}{H^{\alpha/(1+m\alpha)}} \tag{8-20}$$

For $a = \frac{1}{4}$ and $m = 2$, the exponent of H on the right-hand side is $\frac{1}{6}$. Solution of the equation for maximum G gives:

$$H = 0.143; \qquad G = 0.62 \tag{8-21}$$

When the film is reduced to a small value of H, relaminarization may occur, which would break the fluid away from the turbulent power law. The condition for this can be found by returning to eq. (8-11). If the transition is impending when $H = 0.146$, and if $\mathbf{R} = 1500$ at transition, then the nominal operating R will be given by:

$$\mathbf{R} = 1500\left(\frac{h_0}{h}\right)^{0.66} = 10{,}489 \tag{8-22}$$

This means that if $\mathbf{R}$ is calculated for the nominal film thickness, and if it is above 10,489, then relaminarization would not be expected to occur in the range of real solutions to eq. (8-20).

Additional insight into the seizure mechanism can be had by returning to eq. (7-5), and substituting for the heat flux, W, from eq. (8-2):

$$h_0 - h = 0.857h_0 = \varepsilon^2 r_J (r_B - r_J)\Phi_E \left(\frac{C_F U^3}{4\upsilon K_J}\right) \tag{8-23}$$

Equation (8-23) has been used to remove h. Since Figure 8-1 shows only a small variation of C_F over the expected range of operation in the turbulent regime, eq. (8-20) allows a quick test for critical sliding speed. Properties and dimensions for a numerical estimate are: $r_J = (r_B - r_J) = 0.01$ m; $h_0 = 2.5 \times 10^{-5}$ m; $\upsilon = 0.001$ m^3/Kg; $C_F = 0.001$; $\varepsilon = 10^{-5}$/°C ; $K_J = 50$ N/s-°C; $\Phi_E = 1$, and the bearing and journal are cast iron.

$$U = 158 \text{ m/s} \tag{8-24}$$

For the chosen r_J, this would be 150,000 rpm. This is extremely high; however, Table 7-2 shows that Φ_E may rise quite high when the journal and bearing are of different materials, and could be 3400 for cooling by natural convection to a gas. For this application, $U = 10.5$ m/s, and the turning speed would be 10,000 rpm, which falls in the range of common systems. Judicious choice of materials and mode of cooling will raise the critical speed to a safe level.

Summary

Although the onset of turbulence raises the friction coefficient, this effect does not tremendously alter the critical sliding speed for quasi-static seizure. This is because the friction coefficient is relatively insensitive to temperature, and the film thickness must be reduced to a very small value before the stable solutions disappear. All of the materials effects in previous chapters carry over to turbulent operation, and the role of thermal resistance, δ_{SA}, remains dominant. The critical Reynolds number for transition is given by eqs. (8-9) and (8-11). No longer is it a simple function of speed, film thickness, and viscosity; and no longer is it the same on the viscous and turbulent sides of the transition.

9
Transient Seizure with Turbulent Flow

The dynamic seizure mechanism developed in chapters 6 and 7 involves a coupling between changes of film thickness and the rate of dissipative heating. This coupling of heating and thickness is explored in this chapter for smooth-wall and rough-wall turbulent flow as well as laminar flow. The results are incorporated into the equations for exponential growth of a disturbance.

Background

Exponential growth of a small change in film thickness is treated in chapters 6 and 7 for laminar flow, where the sign of the exponent is determined by the geometry and materials of the bearing and journal. The combined effect of these is incorporated into Γ_E, which is defined by eq. (7-16). When this coefficient is negative, the seizure mechanism is precluded. When it is positive, seizure is possible if the thermal boundary layer is thin. The onset of turbulence, or any other change that increases viscous heating, alters the magnitude of the exponent, but does not change its sign. The transition to turbulence not only changes the rate of heating in the film but also changes the sensitivity of this to changes of film thickness. The first of these effects can be estimated as in chapter 7 for steady or quasi-equilibrium operation. The second effect can be bracketed by two conditions: quasi-equilibrium changes of film thickness and isoviscous changes. The latter is thought to be the more accurate approximation for rapid growth rate and the thin thermal boundary layer. This has been discussed by Burton (1994a).

Sensitivity of Turbulent Heating to Film Thickness Changes

The dissipative heating per unit of surface area may be expressed in terms of a friction coefficient, as defined in eq. (8-2) and repeated here:

$$W = \frac{C_F U^3}{2v} \tag{9-1}$$

R. A. Burton, *Heat, Bearings, and Lubrication*

Typical values of the friction coefficient, C_F, are plotted in Fig. 8-1. In the turbulent range of Reynolds number expected for bearing films, C_F drops from 0.002 to 0.001, which is a small change in view of the 16-fold change of Reynolds number. The laminar flow in the vicinity of transition shows a similar range of friction coefficient, except when elevated by the vortex-flow transition, as exemplified by the data of Smith and Fuller (1956) for a thick film and inner-cylinder turning. This does not mean that energy dissipation is the same for laminar and turbulent flow. In a typical experiment, the Reynolds number would rise as sliding speed is increased, and this would lead to a large increase of heating. For example, for the 16-fold increase in speed in the turbulent regime, eq. (9-1) would predict an increase of heating by a multiple of 2048. Obviously, this must strongly affect the stability of steady operation. In chapter 8 friction coefficient is expressed as a power law in Reynolds number, fluidity is expressed as a power law in temperature, and temperature is related to dissipative heating and to thermal resistance between the film and the environment. This has led to eq. (8-17), which is repeated here for easy reference.

$$W = \left\{ A \left(\frac{K}{\delta} \right)^{m\alpha} \frac{U^{3-\alpha}}{2(bh)^{\alpha} v^{(1-\alpha)}} \right\}^{1/(1+m\alpha)} \tag{9-2}$$

This shows a strong dependence of energy dissipation on sliding speed, U, although weaker than the cubic relationship of eq. (9-1). The exponent of film thickness is $-\alpha/(1 + m\alpha)$, and for quasi-equilibrium changes of film thickness,

$$\frac{dW}{dh} = -\left(\frac{\alpha}{1 + m\alpha} \right) \left(\frac{W}{h} \right) \tag{9-3}$$

Recall that for laminar flow, $\alpha = 1$; for turbulent flow, $\alpha = \frac{1}{4}$; and for rough wall turbulent flow (with constant C_F), $\alpha = 0$. Table 9-1 shows the dependence of heating on clearance in the bearing. The three classes of flow are represented for three reasonable values of the viscosity exponent, m. In all cases the numerical multiplier is small, indicating insensitivity of the dissipation to changes of film thickness. Also, this quantity for smooth-wall turbulent flow is about half its value for laminar flow. For rough-wall turbulent flow, there is no coupling.

TABLE 9-1. Sensitivity of Dissipative Heating to Film Thickness Changes for Thermoviscous Fluids and Steady Operating Conditions

	$m = 1$	$m = 2$	$m = 3$
$\left(\frac{dW}{dh}\right)_T =$	$-\frac{1}{5}\frac{W}{h}$	$-\frac{1}{6}\frac{W}{h}$	$-\frac{1}{7}\frac{W}{h}$
$\left(\frac{dW}{dh}\right)_L =$	$-\frac{1}{2}\frac{W}{h}$	$-\frac{1}{3}\frac{W}{h}$	$-\frac{1}{4}\frac{W}{h}$
$\left(\frac{dW}{dh}\right)_R =$	-0	-0	-0

Effect of Sudden Changes of Film Thickness

Recall that eq. (9-2) represents equilibrium flow. In typical bearings and seals, the thermal time constant of the solid parts is several seconds, and often minutes. Hence, transient changes of h may occur without significant change of film temperature or viscosity, for example, with dynamic oscillations, transient expansions under sudden changes of turning speed, and the exponential collapse of film thickness. In each case, the principal condition of the analysis is that the thermal resistance associated with the surface displacement, δ', is much smaller than the δ_{SA} associated with overall cooling of the system. This is also consistent with the condition of a thin thermal boundary layer. For these conditions the assumption may be made that viscosity remains at the value set by the steady operating conditions of the parent Couette flow. Returning to eq. (9-2), the isoviscous derivative is found, where $m = 0$, b is constant, and $\mu = 1/b$.

$$\frac{dW}{dh} \approx -\alpha \left(\frac{W}{h}\right) \tag{9-3}$$

For the three classes of isoviscous flow:

$$\begin{aligned} \left(\frac{dW}{dh}\right)_{\mu,T} &= -\frac{1}{4}\left(\frac{W}{h}\right) \\ \left(\frac{dW}{dh}\right)_{\mu,L} &= -\frac{W}{h} \\ \left(\frac{dW}{dh}\right)_{\mu,R} &= 0 \end{aligned} \tag{9-4}$$

For small perturbations on h, designated h', there is a corresponding W'.

$$\frac{dW}{dh} \approx \frac{W'}{h'} \tag{9-5}$$

When the data of Table 9-1 and eq. (9-4) are compared for the smooth-wall turbulent flow with $m = 2$, the W'/h' for the isothermal case is 50% greater than for equilibrium.

Effect of Transition on the Heating Increment

The comparative effects in eq. (9-4) are difficult to interpret because the transition to turbulent flow increases the heating, W, while lowering the ratio W'/W. However, at transition at test can be made for the ratio W'_T/W'_L. For either laminar or turbulent flow, $W' = \alpha W$, since transition occurs with little change in turning speed, for the same h'/h:

$$\frac{W'_T}{W'_L} = \frac{(\alpha W)_T}{(\alpha W)_L} = 0.25\frac{W_T}{W_L} \tag{9-6}$$

With the appropriate C_F, for either class of flow, $W = C_F U^3/2v$. Although there is scatter in the data of Fig. 8-1, $C_{F,T} = 2C_{F,L}$, and:

$$\frac{W'_T}{W'_L} = (0.25)(2) = 0.5 \tag{9-7}$$

This may be a surprising result for those who think turbulence increases turning resistance and heating. The moderating effect derives from the small sensitivity of C_F to changes of R in the turbulent regime. For the rough-wall case, $\alpha = 0$, and the perturbation in heating disappears. Even if the constant C_F is a coarse idealization of the rough-wall behavior, it reflects the basic truth that changes in R, through changes in h, will cause only a very small change of heating—if any.

For the smooth-wall flow, the rise of **R** well above transition calls for W well above that for the fictitious extrapolation of laminar flow. Consequently, when the derivations of chapters 5 and 6 are carried formally to high sliding speeds before instability occurs, the onset of turbulence can still multiply the dissipative heating several fold and lower the transition sliding speed.

The Limit of Thin Thermal-Boundary-Layer Operation

Equation (6-22) relates the time rate of growth of h' to the steady-state operating condition for laminar flow. It may be rewritten in properties of the journal, with bearing properties lumped into Γ_E as appropriate. In the present nomenclature, this equation becomes:

$$\frac{dh'}{d\tau} = -\alpha \left(\frac{W}{h}\right)\left(\frac{\varepsilon v}{h}\right)_J \Gamma_E h' \tag{9-8}$$

This is consistent with exponential growth, as in eq. (6-29), with the exponent $\alpha'\tau$, where:

$$\alpha' = \alpha \Gamma_E \left(\frac{W}{h}\right)\left(\frac{\varepsilon v}{C_P}\right)_J \tag{9-9}$$

Using $\alpha = \frac{1}{4}$ for turbulent flow

$$\alpha' = 0.25 \Gamma_E \left(\frac{W}{h}\right)\left(\frac{\varepsilon v}{C_P}\right)_J \tag{9-10}$$

This will permit the runaway growth of h' when α' is positive, with the sign being determined by Γ_E. In eq. (6-31) an estimate of the limit of thin-thermal-boundary-layer operation is proposed:

$$\alpha' = \left(\frac{k}{r^2}\right)_J \tag{9-11}$$

Combining eqs. (9-10) and (9-11), and recalling that $k = Kv/C_P$:

$$W = 4\left(\frac{h}{\Gamma_E r_J^2}\right)\left(\frac{K}{\varepsilon}\right)_J \tag{9-12}$$

Substituting from eq. (9-1):

$$U^3 = 8\left(\frac{h}{C_F \Gamma_E r_j^2}\right)\left(\frac{vK}{\varepsilon}\right)_J \tag{9-13}$$

This gives the sliding speed below which the thermal boundary layer thickness would become the same size as the shaft radius. Recall that C_F lies between 0.001 and 0.002 over most of the expected range of **R**.

Summary

Equation (9-9) applies equally well to laminar or turbulent flow, when the appropriate values of α and C_F are employed. Although C_F ranges widely in laminar flow, Fig. 8-1 shows it to vary only about twofold over the expected range of operation in turbulent flow. This entire range leads only to a 25% change in U. By far the most important factor is Γ_E, which is determined by materials properties and the relative thickness of the bearing.

10
The Temperature Drop across the Fluid Film

In the analyses of quasi-static and dynamic seizure, the temperature drop across the liquid film has been neglected, yet chapter 2 showed it to be significant. In this chapter, the relative thermal resistances are reviewed, and their roles are explored in (1) quasi-static seizure with constant viscosity, (2) quasi-static seizure with a thermoviscous fluid, (3) dynamic seizure, (4) turbulent flow, and (5) operation with forced heat flow through the film.

The viscosity is treated as constant across the film, and its magnitude is determined by the overall heat balance for the system. This calls for a parabolic temperature distribution in the film. Power laws are used for thermoviscosity and for the turbulent friction coefficient.

Temperature Drop between the Partition Plane and a Wall

Since t_M resides on the partition plane, the distance to the solid wall is d, and the fluid temperature at the wall is t_S, eq. (2-6) requires that:

$$t_M - t_S = \frac{\sigma^2 d^2}{2K\mu} \tag{10-1}$$

For laminar flow

$$\sigma = \frac{\mu U}{h} \tag{10-2}$$

and

$$t_M - t_S = \left(\frac{\mu U^2}{2K}\right)\left(\frac{d}{h}\right)^2 \tag{10-3}$$

The temperature drop is independent of film thickness, and was shown in chapter 1 to range from a few degrees up to 60°C, where it could contribute significantly to the temperature drop between the shaft and bearing. To set this into scale, the temperature drop between the journal and the bearing may be calculated for the

R. A. Burton, *Heat, Bearings, and Lubrication*

TABLE 10-1. Thermal Resistance of Several Materials Expressed as an Equivalent Oil-Film Thickness

Material	$r_B - r_J$ (mm)	δ_B (mm oil)	h_0/δ_B ($h_0 = 0.01$ mm)
Carbon	10	0.089	0.11
Silicon carbide	10	0.067	0.14
Cast iron	10	0.024	0.41
Aluminum	10	0.0052	1.9

condition in which clearance is closed by thermal expansion. For a journal radius of 1 cm and clearance of 0.001 cm, the temperature drop $t_J - t_B = 0.001/\varepsilon$ would close the clearance. For cast iron, this is $t_J - t_B = 100°C$. The drop across the film alone could therefore be a significant part of the temperature difference, but would be insufficient to cause seizure without some additional drop in the bearing material. Furthermore, that 60°C drop was calculated for an unusually viscous fluid at room temperature.

In eq. (10-3), the property μ/K accounts for the thermal contribution of the fluid. Table 2-1 shows that this property is extremely small for water, air, or mercury, and is much greater for an oil. For this reason, improved estimates of film effects will be restricted mainly to oils.

Thermal Resistance as an Equivalent Thickness of Fluid

To combine the thermal resistance of the film with that of solids in the heat-flow path, these must be converted to the same basis. Specifically, the thermal resistance of the bearing can be expressed as an equivalent oil film thickness, δ_B, and for $\Phi_L = 1$:

$$\frac{(r_B - r_J)K}{K_S} = \delta_B \tag{10-4}$$

The oil-film equivalents for several materials are listed in Table 10-1 for an arbitrary 1-cm thickness. Where this is set in ratio to a typical lubricant film, different film thicknesses might have been chosen for h_0. However, a much larger clearance will both lower heating and enlarge the permissible clearance change. An extremely small clearance would virtually ensure seizure for any reasonable operating speed. The selected clearance is in a range used by designers.

Thermal Resistance in Turbulent Flow

The temperature equation for dissipation in a Couette flow, eq. (2-5), may be written with modified symbols for turbulent flow.

$$K_T \frac{\partial^2 t}{\partial y^2} = \frac{\sigma^2}{\mu_T} \tag{10-5}$$

Here the conductivity and viscosity of the fluid are replaced by K_T and μ_T, their eddy-enhanced equivalents. These approach the viscous flow quantities K and μ in the sublayer adjacent to the interface, and rise by many multiples in the core flow. As a consequence, the dissipation (right-hand term) is principally restricted to the sublayer, where μ_T is small. The temperature is nearly constant across the core flow, dropping mainly across the sublayer, where K_T is small. The thickness of the sublayer is treated in chapter 8, and the following equation is derived:

$$\frac{\delta_{SL}}{h} = \frac{1}{C_F \mathbf{R}} \tag{10-6}$$

This is consistent with "Reynolds' analogy" as proposed by Osburn Reynolds in 1874, and reviewed by Schlichting (1968, pp. 268–270). From Fig. 8-2, for $R = 10{,}000$, $C_F = 0.00155$, and this calls for:

$$\frac{\delta_{SL}}{h} = 0.065 \tag{10-7}$$

In laminar flow the equivalent thickness for the temperature drop is $h/4$; hence the turbulent film resistance is about one-fourth that for laminar flow. In the analyses that follow, the role of film resistance in seizure is found to be small for laminar flow, and would be much smaller for turbulent flow.

Film Resistance in Quasi-Static Seizure with Isoviscous Flow

Figure 10-1 shows the temperature drop across the film and bearing, where both are expressed as equivalent oil films. The heat flux to the journal is blocked, and the

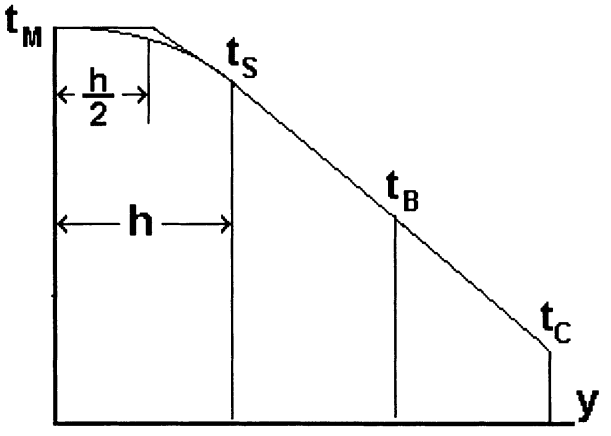

FIGURE 10-1. Temperature drop from the partition surface, across the film, and through a hypothetical solid with the conductivity K to the outer surface of the bearing. The film has a parabolic profile, and is equivalent to a solid thickness $h/2$, as shown schematically.

journal temperature is t_M, measured above ambient. Because of the parabolic temperature distribution in the film, the temperature drop is like conduction through the thickness $h/2$. Following chapter 4, the mean bearing temperature is approximated as that halfway between the inner and outer radii, and the appropriate resistance is $\delta_B/2$. For a single material in the bearing and journal, using eq. (10-1) to replace $(r_B - r_J)/K_S$, and including the film resistance in eq. (5-6):

$$h_0 - h = \frac{\delta r_J W(\delta_B + h)}{2K} \tag{10-8}$$

This may also be written:

$$h_0 - h = \left(\frac{\varepsilon r_J (r_B - r_J)\mu U^2}{2K_S h}\right)\left(\frac{1+h}{\delta_B}\right) \tag{10-9}$$

Defining G as in eq. (5-9), and letting $h/h_0 = H$,

$$1 - H = \left(\frac{G}{H}\right)\left(\frac{1 + Hh_0}{\delta_B}\right) = \frac{G}{H} + \frac{Gh_0}{\delta_B} \tag{10-10}$$

This may be expanded as the quadratic equation:

$$H^2 + \left(\frac{-1 + Gh_0}{\delta_B}\right) H + G = 0 \tag{10-11}$$

Real solutions disappear when:

$$\left(\frac{-1 + Gh_0}{\delta_B}\right)^2 = 4G \tag{10-12}$$

Table 10-2 shows typical solutions, where decreasing G decreases the permissible sliding speed. However, the downward trend is not large.

TABLE 10-2. Effect of Film Resistance on the Threshold of Failure in Quasistatic Operation with Isoviscous Flow

Resistance (h_0/δ_B)	Operating Parameter (G)
0	0.25
0.1	0.238
0.2	0.228
0.4	0.209
0.6	0.202
0.8	0.182
1.0	0.171
1.5	0.150
2.0	0.134

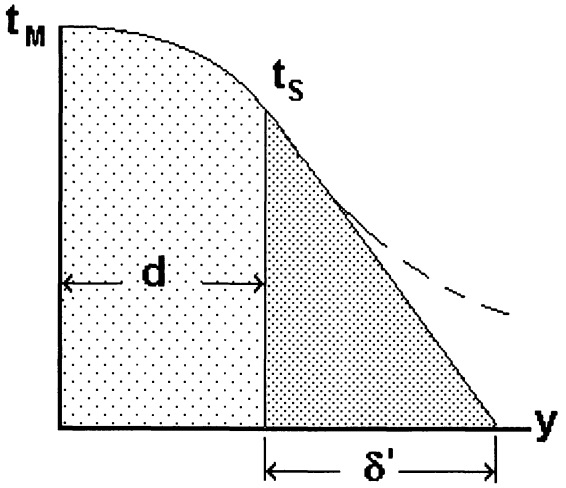

FIGURE 10-2. Schematic temperature profile with a thin thermal boundary layer, δ', in the solid, which is represented as an equivalent of stagnant liquid.

Partitioning of Heat for Walls of Differing Materials

In the dynamic process of seizure, the film temperature rises exponentially and heat is transferred into thin thermal boundary layers below the bearing and journal surfaces. The partitioning of heat is determined by the solid materials and moderated by conduction in the fluid. Figure 10-2 shows schematically the temperature drop from the partition surface, across a fluid thickness, d, and through a thermal boundary layer thickness, δ. When the journal and bearing are arbitrarily designated 1 and 2 respectively, the following equations are consistent with the parabolic temperature distribution in the film, for the journal:

$$W_1 = \frac{K t_M}{\delta_1 + (d_1/2)} \tag{10-13}$$

A corresponding equation can be written for W_2 into the bearing. Setting these heat-flux components into ratio:

$$\frac{W_1}{W_2} = \frac{d_2 + 2\delta_2}{d_1 + 2\delta_1} \tag{10-14}$$

Since heat is generated uniformly across the film:

$$\frac{d_1}{h} = \frac{W_1}{W} \tag{10-15}$$

Defining dimensionless variables, let $\mathbf{d_1} = d_1/h$, $\boldsymbol{\delta_1} = \delta_1/h$, $\mathbf{W_1} = W_1/W$, with corresponding terms for the second body. Equation (10-14) now becomes:

$$\frac{\mathbf{W_1}}{\mathbf{W_2}} = \frac{W_1}{W_2} = (\mathbf{W_2} + 2\delta_2)/(\mathbf{W_1} + 2\delta_1) \tag{10-16}$$

TABLE 10-3. Partitioning of Dissipative Heat W_1/W in the Presence of Significant Film Resistance

		δ_2/δ_1			
δ_1/h		1	2	3	4
0	$W_1/W =$	0.5	0.5	0.5	0.5
0.5		0.5	0.6	0.67	0.71
1		0.5	0.63	0.7	0.75
2		0.5	0.64	0.72	0.77
4		0.5	0.66	0.74	0.78
∞		0.5	0.67	0.75	0.8

In Table 10-3, W_1/W, is listed for selected values of δ_1/h, where the body designated 1 is arbitrarily the one with the thinner thermal boundary layer. In practice it could be either the journal or bearing, depending upon the materials chosen.

The upper row represents the equal partitioning of heat when the resistance in the solids is negligible. The bottom row satisfies:

$$\frac{W_1}{W} = \frac{1/\delta_1}{1/\delta_1 + 1/\delta_2} \tag{10-17}$$

This is valid when the film resistance is negligible. Even with the lesser solid resistance, $\delta_1/h = 1$, the partitioning is close to that for the bottom row. Although the equivalent film thicknesses for the solids are the same order as h, inclusion of film resistance does not change the conclusions made in its absence.

Quasi-Static Failure for Thermoviscous Flow

The results for isoviscous flow may be extended to thermoviscous flow upon review of the derivation of eq. (5-15). There the resistance $(r_B - r_J)/K_J$ is unaltered by the temperature effects on viscosity, and may be replaced as in eq. (10-8) with $(\delta_B + h)/K$, all referenced on the fluid. This leads to replacement of G in eq. (5-16) with $G[1 + H(h_0/\delta_B)]$, and the thermoviscous equivalent of eq. (10-8) when evaluated for $m = 2$ becomes:

$$(1 - H) = \frac{G[1 + H(h_0/\delta_B)]}{H^{1/3}} \tag{10-18}$$

where $H = h/h_0$, and for $m = 2$:

$$G = \frac{\varepsilon r_J \delta_B \left[\left(\frac{K}{\delta_{SA}}\right)^2 \frac{U^2}{bh_0}\right]^{0.333}}{2K} \tag{10-19}$$

As before, numerical solutions may be found by running through the range of H and determining the maximum value of G, for selected values of h_0/δ_B. Solutions are listed in Table 10-4.

TABLE 10-4. Limiting Operating Conditions for a Single Material in Bearing and Journal with Thermoviscous Flow

δ_B/h_0	h/h_0	G	$G(1+h/\delta_B)$
∞	0.5	0.25	0.25
10	0.46	0.24	0.25
5	0.45	0.22	0.25
2	0.43	0.21	0.25
1	0.39	0.16	0.22
0.5	0.35	0.12	0.20
0.25	0.30	0.08	0.18

The operating parameter G is dropped only 36% when the thermal boundary layer is made equal to the start-up clearance. This suggests that the temperature drop in the film does not greatly change the perceived physics of seizure.

Forced Heat Transfer through the Journal Bearing

In practice, the viscous heating in the bearing may be small relative to the forced heat transfer from the shaft through the film and to the environment. This heat may derive from the immersion of a turbine rotor in combustion gases, from the eddy currents in the rotor of an electric motor, or from the adiabatic heating in a compressor. Review of the results in chapter 7 finds that seizure is most likely to occur when the bearing is a different material from the journal, and the reasonable combination of carbon bearing and iron journal provides an example that can be subject to failure from relative expansion in a reasonable range of operation. Running out of clearance would occur at a limiting value of the dimensionless performance parameter, G, which may be written to include the expanded materials parameter, Φ_E:

$$G = \left(\frac{W\varepsilon_J r_J}{K h_0}\right)\left[\frac{\varepsilon_B}{\varepsilon_J} + 2\left(\frac{\delta_{SA}}{\delta_B}\right)\left(1 - \frac{\varepsilon_B}{\varepsilon_J}\right)\right] \tag{10-20}$$

For a carbon bearing and an iron journal, $\varepsilon_B/\varepsilon_J = 0.42$, and $\delta_{SA}/\delta_B \approx 100$. This means that running out of clearance is caused by the overall expansion of the system (second term in the brackets) rather than the gradients from heat flow (first term in the brackets). The clearance would disappear if the system were put in an oven and raised to a temperature, t_+, where the subscript + is used to denote the absence of clearance; hence, there is also a W_+ associated with this condition. In the bearing the overall heating comes from the forced component, W_F, and the frictional component, W_μ. The forced heating can be scaled conveniently by:

$$\frac{W_F}{W_+} = \mathbf{n} \tag{10-21}$$

In eq. (10-21), W_+ is equal to the forced heat flow when the clearance goes to zero. The condition $\mathbf{n} = 1$ specifies the condition for failure when there is no frictional heating, and all relative expansion is due to the forced heat transfer. When forced heat transfer is accompanied by frictional heating,

$$h_0 - h = \frac{(\varepsilon_J - \varepsilon_B)(\mathbf{n}W_+ + W_\mu)\delta_{SA}}{K} \tag{10-22}$$

Here W_μ may be written:

$$\frac{\mu U^2}{h} = \left(\frac{\mu_+ U^2}{h_0}\right)\left[\left(\frac{t_+}{t}\right)^m \left(\frac{h_0}{h}\right)\right] \tag{10-23}$$

The viscosity μ_+ is evaluated at the failure temperature t_+, and the power law of chapter 3 is incorporated into the terms in the brackets. Note that the relative expansion serves as a thermometer:

$$\frac{t}{t_+} = \frac{h_0 - h}{h_0} \tag{10-24}$$

In eq. (10-23), the quantity in parentheses is designated W_0, the film thickness is nondimensionalized as in eq. (10-10), and eq. (10-22) becomes:

$$1 - H = \mathbf{n} + \left(\frac{W_0}{W_+}\right)\left(\frac{1}{H}\right)\left(\frac{1}{1-H}\right)^m \tag{10-25}$$

Here the W_0/W_+ stands in place of the G of the prior derivations, and

$$(1-H)^2 H(1 - H - \mathbf{n}) = \frac{W_0}{W_+} \tag{10-26}$$

This may be solved as before by selecting $\mathbf{n}$ and running through values for H until the maximum W_0/W_+ is found. Results of this calculation are compiled in Table 10-5, where the column of $\mathbf{n}$ presents the forced heat flow as a fraction of that which could cause clearance to disappear. The dimensionless H is the operating film thickness below which quasi-static operation becomes impossible, and W_0/W_+ is a measure of the severity of the permissible viscous heating load. Since U^2 is the only operating variable in this quantity, U/U_0, the ratio of the critical sliding speed to that in the absence of forced heat flow, can be calculated and is listed in the right-hand column. These speeds can be compared with those of chapter 7.

TABLE 10-5. The Influence of Forced Heat Transfer, W_F, on W_0/W_+

$W_F/W_+ = n$	H	W_0/W_+	U/U_0
0	0.25	0.106	1
0.1	0.25	0.105	0.995
0.2	0.23	0.078	0.86
0.4	0.20	0.051	0.69
0.6	0.16	0.027	0.50
0.8	0.09	0.008	0.27
1.0	0	0	0

Summary

Although the temperature drop across the film does not change the physics of thermoelastic-Couette flow, there are significant effects that can be cataloged and estimated. When the thermal resistance of the bearing cylinder is expressed as an equivalent thickness of fluid, as in Table 10-1, it is seen to be about 10 times the film thickness. The exception is aluminum, which experiences little temperature drop and is not subject to quasi-static seizure in the typical range of operation. This is clarified in Table 10-2 for isoviscous flow, where the operating parameter G is displaced only 20% from the value for zero resistance, even when the film resistance is 60% of the bearing resistance.

When the temperature grows exponentially in time, the thermal boundary layer in the solid may be, say, one-tenth of the film thickness of the bearing. Even so, the partitioning of energy to the two surfaces is not far from that determined by the solids alone, even down to the condition in which the solid resistance is equivalent to half of a film thickness. Thermoviscosity affects the transient seizure process only through setting the overall level of viscosity in the film. The perturbation is charcterized by small resistances into the solids and is itself close to isothermal.

Returning to quasi-static seizure, thermoviscosity complicates the analysis, but, as shown in Table 10-4, it has a strong effect on the performance parameter G only when the fluid-equivalent of bearing resistance is equal to or smaller than the film thickness. For turbulent flow, arguments consistent with the Reynolds analogy hold that the sublayer is the principal thermal resistance in the fluid film, and it is small relative to the film component of resistance in laminar flow. Hence fluid-film effects are even smaller than in laminar flow.

Forced heat transfer outward from the journal may dominate the thermal behavior of real bearings. In single material systems, the forced heat transfer adds almost linearly to the frictional heat in its effects on thermal expansion. Yet these systems are not typically sensitive to quasi-static seizure under reasonable conditions. Two-material systems show their effects when there is a marked difference in thermal properties of journal and bearing, and their seizure is determined principally by the temperature rise. This is determined primarily by forcing heat through the external resistance on the exterior of the bearing. The magnitude of forced heat transfer that would lead to seizure when acting alone is given by eq. (10-22) when $\mathbf{n} = 1$ and frictional heat is $W_\mu = 0$.

$$W_+ = \frac{K h_0}{\delta_{SA}(\varepsilon_J - \varepsilon_B)} \tag{10-27}$$

Table 10-5 shows that the forced heat must be six-tenths of the limiting value to cut permissible sliding speed in half. In general, accounting for film resistance does not change the general ideas of the causes of seizure or the permissible ranges of operation. The biggest factor, and most difficult to pin down, is the resistance to external cooling. This dominates the seizure of two-material systems and figures heavily in determining the operating level of viscosity in others.

11
Viscous Heating in Pressure Gradients

A nominally cylindrical bearing in Couette flow may have a small surface waviness. Heat generation will vary from the peak to the trough of the wave. Two cases bracket most real applications: (a) the *long* bearing with zero end leakage, and (b) the *short* bearing, for which the axial pressure gradient is orders of magnitude greater than tangential pressure gradient. When the amplitude of the circumferential wave is small compared to the film thickness, there is a linear relationship between the film-thickness perturbation and the heat-flux perturbation.

Background

There are no tangential pressure gradients in axisymmetric Couette flow. Pressure arises from steps in the film, eccentricity of the cylinders, and surface waviness. Pressure-driven flow between stationary parallel walls is called plane Poiseuille flow in honor of J. L. M. Poiseuille (1840), who conducted early experiments on liquids in capillary tubes. In lubrication theory, relative motions of the boundary surfaces and the effects of pressure gradients act together to produce Reynolds flow, named for Osborne Reynolds (1886), who formalized the analysis of thin-film flows with negligible inertia over nearly parallel surfaces. Both the sliding of the surfaces and the pressure gradients contribute to viscous heating in Reynolds flows. These effects are reviewed here for isoviscous and thermoviscous fluids, with special attention to the condition in which the pressure gradient makes a small but significant contribution.

Pascovici (1969) published an exhaustive study of viscous heating in a thermoviscous lubricant, giving a complete analysis of a bearing configuration and comparing the isoviscous and thermoviscous conditions. Sneck (1969) has treated thermal phenomena for both laminar and turbulent thermoviscous flow in seals. The analysis presented here is principally concerned with the relative magnitudes of the contributions to heat generation that arise from the Couette and Poiseuille components in Reynolds flows.

R. A. Burton, *Heat, Bearings, and Lubrication*

Viscous Heating in Plane Reynolds Flow (Long Bearing)

In plane Reynolds flow the fluid pressure is constant on y, the coordinate normal to the wall. For isoviscous flow, with fluid movement restricted to the x-direction, pressure is a function of x alone, and is related to local shear stress by the equation for equilibrium (2-1).

$$\frac{\partial \sigma_{xy}}{\partial y} = \frac{dp}{dx} \tag{11-1}$$

For viscous flow, $\sigma_{xy} = \mu \partial u / \partial y$, and this equation becomes:

$$\mu \frac{\partial^2 u}{\partial y^2} = \frac{dp}{dx} \tag{11-2}$$

Integrating from the stationary surface (bearing) out to the second surface (journal), which moves at the speed U, the velocity profile will be as in Fig. 11-1. This shows the linear distribution of a Couette flow, supplemented by a parabolic distribution, which results from the pressure gradient. When the parabolic distribution is averaged across the channel, its mean contribution is u_P and is related to the pressure gradient by:

$$\frac{dp}{dx} = -\frac{12 \mu u_P}{h^2} \tag{11-3}$$

This relationship was first found by Stefan (1874), and is implicit in the Reynolds equation. The shear stress may also be expressed as two components, as in Fig. 11-2, where σ_C is the component produced by the relative sliding, and σ_P is the

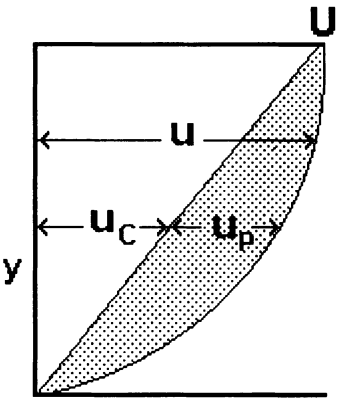

FIGURE 11-1. Velocity profile for a combined Couette flow (linear) and tangential displacement flow (parabolic). The combined local velocity is u, which is made up of Couette, u_C, and Poiseuille, u_P, components.

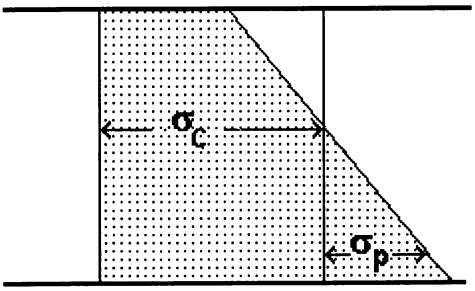

FIGURE 11-2. Shear stress across a fluid film, with the Couette component (constant) and the displacement flow or Poiseuille component (triangular).

wall stress resulting from the pressure gradient:

$$\sigma_{xy} = \sigma_C + \frac{2\sigma'_P y}{h} \tag{11-4}$$

Equation (2-4) for viscous heating now becomes:

$$w = \frac{\left(\sigma_C + \frac{2\sigma_P y}{h}\right)^2}{\mu} \tag{11-5}$$

Expanding the term in parentheses:

$$\mu w = \sigma_C^2 + \left(\frac{2\sigma_P y}{h}\right)^2 + \frac{4\sigma_C \sigma_P y}{h} \tag{11-6}$$

Heating in Isoviscous Flow

When viscosity is constant, eq. (11-5) may be integrated to give W, the total viscous heating of the combined flow per unit of surface area on the stationary wall.

$$\mu W = \sigma_C^2 h + \frac{\sigma_P^2 h}{3} \tag{11-7}$$

The odd term disappears in the integration, and the heating is reduced to two components, the first determined by the Couette flow as if acting alone, and the other determined independently by the Poiseuille flow component.

Coupling of Heating and Waviness of a Boundary

Figure 11-3 shows a stationary boundary with sinusoidal waviness, and a flat boundary moving relative to it at speed U. The average film thickness is h_C,

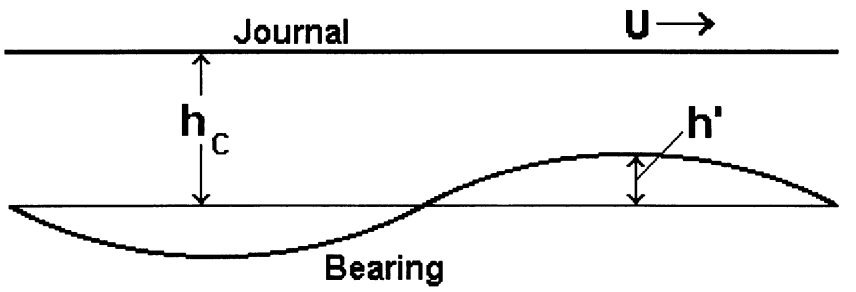

FIGURE 11-3. A stationary boundary with sinusoidal waviness and a flat boundary with relative velocity U. Mean film thickness is h_C, and wave amplitude is h'. Simple Couette flow prevails where the wave crosses the mean surface and the local thickness is h_C.

and the local amplitude of the wave is h', which is positive when it reduces film thickness, such that $h = h_C - h'$. Let the fluid be in simple Couette flow at the tangential position halfway between the peak and trough of the wave, where the local thickness is h_C. Continuity requires that the velocity components at the minimum thickness become:

$$\frac{Uh_C}{2} = \left(\frac{U}{2} + u_P\right)(h_C - h') \tag{11-8}$$

Simplifying:

$$\frac{Uh'}{2} = u_P h \tag{11-9}$$

When $h'/h \ll 1$, the term $u_P h'$ is much smaller than Uh, and:

$$u_P \approx \frac{Uh'}{2h_C} \tag{11-10}$$

Equilibrium requires that $\partial p/\partial x = 2\sigma_P/h$, which, along with eq. (11-3), renders, eq. (11-9) into:

$$\sigma_P = \frac{6\mu u_P}{h} = \frac{3\mu U h'}{h^2} \tag{11-11}$$

where σ_P is the wall shear stress contribution from the Poiseuille component of the flow. Returning to eq. (11-7):

$$W = \left(\frac{\mu U^2}{h}\right)\left[1 + 3\left(\frac{h'}{h}\right)^2\right] \tag{11-12}$$

Recall that for the Couette flow:

$$W_C = \frac{\mu U^2}{h_C} \tag{11-13}$$

TABLE 11-1. Dimensionless Heat Generation as Affected by Surface Wave Amplitude

h'/h_C	W_1/W_C (at $h = h_C - h'$)	W_2/W_C (at $h = h_C + h'$)	$(W_1 - W_2)/W_C$	$(W_1 - W_2)/W_C$ Eq. (11-15)
0	1	1	0	0
0.1	1.152	0.932	0.220	0.20
0.2	1.484	0.9028	0.5812	0.41
0.3	2.216	0.892	1.324	0.65

Setting these two measures of heating into ratio:

$$\frac{W}{W_C} = \left(\frac{h_C}{h}\right)\left[1 + 3\left(\frac{h'}{h}\right)^2\right] = 1 + \frac{h'}{h} + 3\left(\frac{h'}{h}\right)^2 + 3\left(\frac{h'}{h}\right)^3 \qquad (11\text{-}14)$$

since $h_C = h + h'$. A useful small perturbation limit is found when only the first-order term is retained:

$$\frac{W}{W_C} \approx 1 + \frac{h'}{h} \qquad (11\text{-}15)$$

Table 11-1 shows how W/W_C varies with the amplitude of the wave, evaluated at the peak and trough, and gives the difference between these. Here W_1 is heat generation at minimum film thickness and W_2 is heat generation at film thickness. The difference is compared with eq. (11-15). Good agreement is shown for $h'/h_C \approx 0.1$, which supports linear variation for small wave amplitude. For larger amplitudes the heating greatly exceeds the linear prediction.

Viscous Heating in Short Bearing Flow

The short bearing concept was introduced by Ocvirk (1952), and is based on several idealizations. Although pressure may vary in the direction of sliding, x, the pressure gradient in that direction is negligible, and the velocity profile in the x, y plane is as in Couette flow. The width of the boundary surfaces across the direction of sliding (or in the z-direction) is short relative to the wavelengh; and the pressure gradient, $\partial p/\partial z$, gives rise to a Poiseuille flow profile in the z, y plane. For isoviscous flow, the equivalent of eq. (11-3) becomes:

$$\frac{\partial p}{\partial z} = \frac{12\mu w_P}{h^2} \qquad (11\text{-}16)$$

where w_P is the mean transport velocity in the z-direction, obtained by averaging the velocity across the film. Although the symbol w is commited elsewhere to the rate of heat generation per unit of volume, the present subscripted variable is an exception, which applies here and in Fig. 11-4. Let σ_P be the magnitude of σ_{zy} at the wall, and eq. (11-4) becomes:

$$\sigma_{zy} = \sigma_P y/d \qquad (11\text{-}17)$$

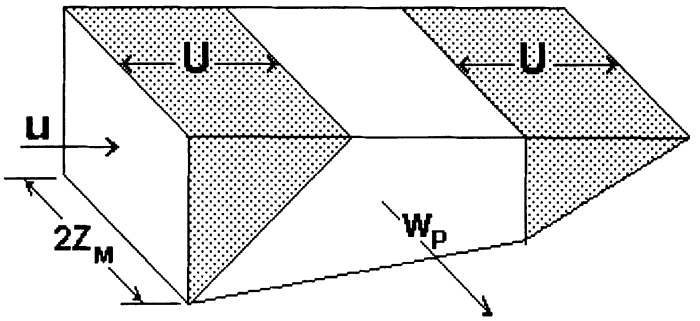

FIGURE 11-4. Schematic diagram of a control volume showing tangential Couette-flow velocity profiles and an axial flow out the side. The moving upper surface draws in more fluid in the tangential direction than it draws out, forcing the axial flow with velocity w_P.

where $d = h/2$. The intensity of viscous heating per unit of volume, w_z, is found as in eq. (11-5)

$$w_z = \frac{\partial w_P}{\partial y} = \frac{(\sigma_P y/d)^2}{\mu} \tag{11-18}$$

W_P is found by integrating from wall to wall across the film:

$$W_P = \frac{\sigma_P^2 h}{3\mu} \tag{11-19}$$

Equilibrium requires that $2\sigma_P/h = \partial p/\partial z$. This may be substituted into eq. (11-16),

$$W_P = \frac{12\mu w_P^2}{h} \tag{11-20}$$

The Coupling between a Surface Wave and the Cross-Flow Transport Velocity

Figure 11-4 shows schematically how z-direction flow must be extruded when one boundary surface is inclined relative to the other. If h varies with x alone, continuity requires:

$$\frac{\partial(Uh)}{\partial x} = 2h\frac{\partial w_P}{\partial z} \tag{11-21}$$

Sinusoidal waviness, which satisfies these conditions, is:

$$h = h_C - h' \cos(\pi x/L) \tag{11-22}$$

where L is half the wavelength, and h' here and in the following derivation serves as the amplitude. Differentiating, *evaluating at the point of maximum slope* where

$h = h_C$, and substituting into (11-21):

$$\frac{Uh'\pi}{2L} = h_C \frac{\partial w_P}{\partial z} \tag{11-23}$$

At axial midlength of the film, there is a second kind of partition surface for flow, for which the z-velocity component is zero, and from which fluid moves toward the open edge of the boundaries. When the origin for z is taken at that surface, eq. (11-23) may be integrated to give:

$$w_P = \frac{\pi z h' U}{2L h_C} \tag{11-24}$$

Returning to eq. (11-20),

$$W_P = 3\left(\frac{\pi h' z}{L h_C}\right)^2 \left(\frac{\mu U^2}{h_C}\right)^2 \tag{11-25}$$

Let W_P be the average magnitude of W_P, taken in the z-direction between the partition plane and the exit from the film at z_m.

$$W_P = 9.9\left[\left(\frac{z_m}{L}\right)\left(\frac{h}{L}\right)\left(\frac{h'}{h_C}\right)\right]^2 \left(\frac{\mu U^2}{h_C}\right) \tag{11-26}$$

The variables have been grouped to make them accessible to designers. To provide a numerical example let $L = 1$ cm, $z_m = 0.1$ cm, $h_C = 0.0025$ cm, and take the definition for W_C from eq. (11-13).

$$\frac{W_P}{W_C} = 6 \times 10^{-7}\left(\frac{h'}{h_C}\right) \tag{11-27}$$

This makes clear that the contribution of the leakage flow to heating is negligible in short bearing flow for small wave amplitudes.

Summary

Isoviscous plane Couette flow is characterized by a linear velocity profile across the film and a uniform shear stress. When a pressure-driven Poiseuille flow component is added, the velocity profile is incremented by a parabolic distribution, and the shear stress profile shows a linear variation from wall to wall. The Poiseuille flow component arises for departures from constant film thickness. The departure of most concern here is waviness of one of the solid boundaries of the film and its effect on viscous heating.

Two configurations are of special interest: (1) the *long* bearing, in which the flow is two-dimensional, and end-leakage is negligible, and (2) the *short* bearing, in which the tangential flow component, in the direction of sliding, resembles Couette flow. Viscosity varies because of changes of film thickness, with a small

correction for the axial flow that is necessary to accommodate fluid displaced by these thickness changes. Equation (11-15) gives the components of viscous heating for an isoviscous film without end-leakage. This may be written:

$$W = \frac{\mu U^2}{h_C(1 + (h'/h) + 3(h'/h)^2 + 3(h'/h)^3)} \tag{11-28}$$

At the peak and trough of the wall waviness, the mean film thickness, h_C, is incremented or decremented by h'. Results for the peak-to-trough change in heating are listed in Table 11-1. In the chapters that follow, interest is focused on the sinusoidal wave, and stability questions will be addressed where the amplitude of this wave is small relative to the mean film thickness. For small, finite wall waviness, the axial flow in the short bearing configuration typically gives rise to a very small increment on the heating from the Couette flow, and the remaining evolution will be given by:

$$W = \frac{\mu U^2}{h_C(1 + h'/h)} \tag{11-29}$$

This linear relationship corresponds to the first two terms of eq. (11-28), and will be used to explore the coupling of heating and thermal expansion in bearing and seal configurations. It will be extended by letting h' be the local wave amplitude, and W becomes the Couette component of heating based on local film thickness. This also applies to transient, axisymmetric clearance variation and seizure treated in chapter 6.

12
Coupling of Waviness and Boundary Heat Flux in Reynolds Flow

The analysis of viscous heating over a wavy bearing surface is extended by consideration of subsurface heat transfer. Special cases for the *long bearing, short bearing*, and *moving* wave are treated in this chapter. Partitioning of heat to the solid surfaces is determined.

Background

When there is circumferential waviness on the surface of a bearing, the partitioning of viscous heat is dominated by the pattern of heat conduction beneath the boundary surfaces. This phenomenon is best understood by considering three cases: (1) a stationary sinusoidal temperature distribution on the surface of a bearing, (2) a stationary sinusoidal temperature distribution along a narrow band on the surface of a bearing (as on the nose of a seal), and (3) a translating sinusoidal temperature distribution on the surface of a bearing. As in prior discussions, the bearing is developed into the flat surface of a slab, a simplification permitted by the thin film and thin thermal boundary layer concepts. By a shift in the frame of reference, the same interactions are applicable to the journal, which may also be developed into the nominally flat slab with a small waviness perturbation.

When the wave is stationary on one surface, it is moving at the sliding speed, U, relative to the other surface. This causes the thermal resistance to the wave component of heating, δ', to be different in the two surfaces even when the materials are the same. Whether moving or stationary, δ' is much smaller than the overall resistance, δ_{SA}, between the film and the environment. For this reason the surface temperature increment from the waviness, t'_S, is small except when the wave amplitude almost bridges the full thickness of the film. In this extreme case, the conditions near the minimum film thickness resemble the contact of cylinders and tend toward the "elastohydrodynamic" conditions found in gears and rolling-contact bearings. These contacts have an extensive literature of their own. Large-amplitude waves are discussed in chapter 22, and the thermoelastic/elastohydrodynamic contact is dealt with in chapter 21. Emphasis in this chapter remains focused on the film between nominally conformal surfaces and

R. A. Burton, *Heat, Bearings, and Lubrication*

the interactions that may lead to the growth of waviness as the result of thermal deformation.

As discussed in chapters 3 and 4, the viscosity of a fully thermoviscous fluid may range widely from the rest value at ambient temperature. However, the temperature drop across the film is much smaller than the drop between the film and the environment, and the change in viscosity across the film is even smaller, making the isoviscous film a valid approximation. Chapter 11 showed that changes of viscous heating from peak to trough of a surface wave are primarily determined by the Couette component of the flow. In the short bearing configuration, where a weak Poiseuille flow component acts across the parent Couette flow, the contribution of the Poiseuille component is especially weak. Because the short bearing configuration is frequently chosen for face seals and for high-speed bearings (such as automotive crankshaft bearings), omission of Poiseuille heating is appropriate for these important systems.

The Model

Couette flow is defined by a film thickness h, viscosity μ, heat flux W_C, and surface temperature t. On this will be superposed a boundary perturbation of the type $h' \cos(\pi x/L)$ with corresponding perturbations in p', t', μ', and W'. The coordinate x is measured along the sliding direction, y is measured normal to the mean surface of the Couette flow upon which the perturbation is imposed, and z is measured parallel to the mean surface and perpendicular to x, or axially. Treatment of convected heat is deferred to chapter 13. Here all heat generated in the film is assumed to flow normal to the walls. This is based on the analysis by Burton (1992).

Thermal Resistance in a Solid under a Stationary Sinusoidal Distribution of Surface Temperature

When the temperature on the flat surface of a slab varies according to $t = |t| \cos(\pi x/L)$, the Laplace equation for heat conduction is satisfied in the slab when:

$$t' = t'_S \exp\left(-\frac{\pi y}{L}\right) \cos\left(\frac{\pi x}{L}\right) \tag{12-1}$$

Here t' is the local temperature in the solid material, and y is the distance from the surface measured "into" the material. The surface heat flux is, $W_S = -K_S(\partial t/\partial y)$ evaluated at $y = 0$.

$$W'_S = K_S t'_S \left(\frac{\pi}{L}\right) \cos\left(\frac{\pi x}{L}\right) = K_S \left(\frac{\pi}{L}\right) t'_S \tag{12-2}$$

The thermal resistance expressed as an equivalent thickness of metal is:

$$\delta'_S = \left(\frac{Kt}{W}\right)'_S = \frac{L}{\pi} \tag{12-3}$$

Since L is half the wavelength, the thermal boundary layer is about one-sixth of the wavelength of the perturbation. The analysis may be repeated for bars of finite thickness or for heat flow into the surface of a cylinder. However, thickness of the thermal boundary layer does not change greatly as long as there is sufficient material to accommodate it. For example, if a bearing has a radius of 1 cm, and if the wave arises from simple eccentricity of the shaft, the length L will be $L = \pi$cm, and $\delta_S = 1$cm. For ellipticity, the thickness will be half of this.

Heat Transfer along a Narrow Band on a Bar

Figure 12-1 shows an idealized section of a seal ring of axial length $2Z_m$, with a band of quasi-Couette flow of width $2z_m$, where the dimension z_m is defined by a raised *nose* on the sealing ring. The extra material on each side of the band facilitates heat transfer from peaks to troughs in the temperature distribution, and δ'_S is reduced significantly below that for the strictly two-dimensional wave treated above. In Fig. 12-2, the strong variable is z_m/Z_m. On the semilogarithmic plot, halving the fraction of surface covered by the band of contact also halves δ'_S/L. Reduction of z_m/Z_m to 0.2 reduces the thermal resistance 10-fold relative to the full-width film. This is not an unreasonable "nose" width for conventional face seals, and it means that the thermal boundary layer is restricted to a very thin region.

Heat Transfer from a Moving Temperature Wave

When heat flows from a moving temperature distribution, the thermal boundary layer is much reduced, and the the overall geometry of the body becomes

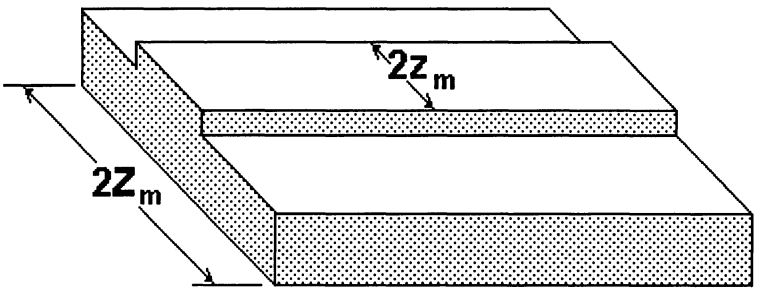

FIGURE 12-1. Cut across sealing rings showing a raised nose, $2z_m$ wide, which defines a Couette flow. The width of the ring is $2Z_m$.

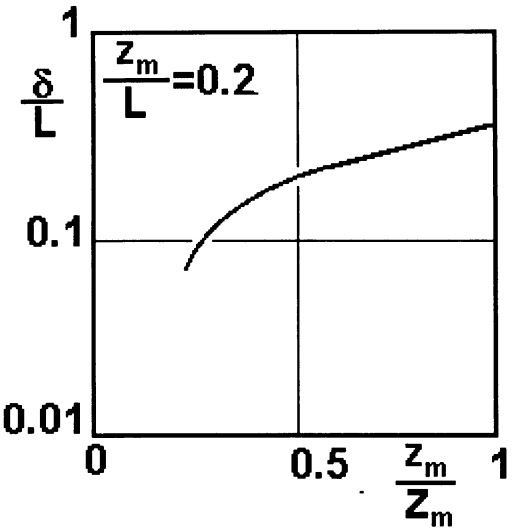

FIGURE 12-2. Thermal resistance for a narrow band of sinusoidal heat input on a wider surface. Not to precise scale.

unimportant. The full-width and narrow-band cases approach the same δ'_S. The controlling parameter is the dimensionless Peclet number, Pe. When $Pe > 1$, the thermal boundary layer becomes very thin relative to wavelength. This is based on Ling and Mow (1966), and has been adapted by Burton (1992), where Fourier's heat transfer equation is satisfied in a semi-infinite body (thick bar) with constant conductivity and heat capacity. Designating the traversal speed of the wave, c', the Peclet number is defined by:

$$Pe = \frac{c'L}{k\pi} \tag{12-4}$$

The surface temperature may be rewritten in present terminology:

$$t_S = t'_S \cos\left(\frac{\pi x}{L} - \frac{\pi c'\tau}{L}\right) = t'_S \cos\left(\frac{\pi x}{L}\right) \tag{12-5}$$

where τ is time, and $X = x - c'\tau$. The corresponding equation for heat flux into the surface is, for high Peclet number:

$$W'_S = K t'_S \left(\frac{c'\pi}{2kL}\right)^{1/2} \left[\cos\left(\frac{\pi x}{L}\right) + \sin\left(\frac{\pi x}{L}\right)\right] \tag{12-6}$$

Since the heat flux and temperature are displaced relative to one another, the definition of thermal resistance is not as simple as for the stationary wave. For general magnitude arguments, it will serve to relate maximum temperature to

TABLE 12-1. Thermal Boundary Layer Thickness, δ'_S or δ'. (for $c' = 5$ m/s, and $L = 5$ cm)

Material	k (cm^2/s)	$c'L/k\pi$ (Pe)	δ'_S (cm solid)	δ' (μm oil)
Aluminum	0.83	9.5	0.051	0.26
Iron	0.11	72.3	0.019	0.46
Silicon carbide	0.06	132.6	0.014	0.94
Carbon	0.08	99.5	0.016	1.42

maximum heat flux, or the ratio of the moduli of the waves in eqs. (12-5) and (12-6).

$$\delta'_S = \left(\frac{Kt}{W}\right)'_S = \left(\frac{kL}{c'\pi}\right)^{1/2} \tag{12-7}$$

Estimates of δ'_S are shown in Table 12-1, for four materials and for representative values of c' and L. The numerical magnitudes show that $Pe \gg 1$ for sliding speeds in the range of common applications. The thermal boundary layer thickness δ_S is thin, even for large L. This supports the idealization that the heat transfer is principally into and out of the surface directly below the source of heat input, and not greatly influenced by remote dimensions of the body. Here δ'_S is in cm of solid material and δ' is in μm of oil.

In Table 12-2, the equivalent oil film thickness, δ', is set in ratio to a relatively thin lubricant thickness. Only for the stationary wave is the resistance large relative to the film thickness. Referring to Fig. 12-1, one would expect even this resistance to be reduced considerably in band contact in seals or in bearings where a wide structure converges to a relatively thin band of confined film.

Table 12-2 justifies the boundary condition used by Hahn and Kettleborough (1967), making the perturbation temperature zero on the moving wall. When the wave is carried on the stationary surface, the temperature perturbations in the film see a very low thermal resistance on the moving surface. Table 12-2 allows comparison of a range of material combinations, of which the extreme case would be the carbon in the moving wall with $\delta'/h = 0.022$, and aluminum in the stationary wall with $\delta'/h = 0.41$. The ratio of these resistances is 18.6. For iron in both walls, the ratio of resistances is 271. Little damage is done in making the resistance zero on the moving wall in either case.

TABLE 12-2. Thermal Resistance for Temperature Waves, Expressed as Multiples of an Oil film, where $h = 40$

Material	δ'/h ($c' = 0$)	δ'/h ($c' = 5$ m/s)	δ'/h ($c' = 50$ m/s)
Aluminum	0.41	0.013	0.0041
Iron	1.9	0.023	0.007
Silicon carbide	5.3	0.047	0.014
Carbon	7.0	0.07	0.022

Effects of the Perturbation Flow on Temperature and Viscosity

Temperature at the wall must satisfy the general equation, $t = KW/\delta$. Since the resistances differ for the perturbation flow and the parent Couette flow, it follows that:

$$\frac{t'}{t} = \frac{W'\delta'}{W_C\delta} \tag{12-8}$$

Referring to Tables 2-2, 12-1, and 12-2, one must conclude that $\delta'/\delta \approx 0.01$, and may be much smaller. It follows from eq. (11-29) that $W'/W \approx -h'/h$, where both quantities are measured as positive in the direction that increases film thickness, and the temperature ratio is of second order. When viscosity satisfies the power-law equation in temperature, $1/\mu = b\,t^m$,

$$\frac{d\mu}{dt} = -m\frac{\mu}{t} \tag{12-9}$$

Replacing differentials by primed quantities, for small perturbations on temperature,

$$\frac{\mu'}{\mu} = -m\frac{t'}{t} \tag{12-10}$$

Combining the above:

$$\frac{\mu'}{\mu} = -m\frac{h'\delta'}{h\delta} \tag{12-11}$$

If $\delta'/\delta < 0.01$, $h'/h < 0.1$, and $m = 2$:

$$\frac{\mu'}{\mu} < 0.002 \tag{12-12}$$

This more than justifies the isoviscous treatment of the perturbation flow.

For viscous heating, retain only the Couette component of heating, as justified in chapter 11.

$$W_C = \frac{\mu U^2}{h} \tag{12-13}$$

Since both viscosity and film thickness vary, one may differentiate by parts and rearrange to find:

$$\frac{dW}{W} = \left(\frac{d\mu}{\mu} - \frac{dh}{h}\right) = \frac{W'}{W_C} \tag{12-14}$$

Here W_C and W' represent components of the heat generation that is uniform across the entire film. When W'_S is the fraction of the heat perturbation going to

the bearing surface:

$$W'_S = \left(\frac{d'}{h}\right) W' \tag{12-15}$$

and

$$\frac{W'_S}{W_C} = \left(\frac{\mu'}{\mu} - \frac{h'}{h}\right) \frac{d'}{h} \tag{12-16}$$

Since the viscosity ratio is much smaller than the boundary perturbation, this may be simplified to:

$$\frac{W'_S}{W_C} = \left(-\frac{h'}{h}\right) \frac{d'}{h} \tag{12-17}$$

Here d' is the distance from the wavy wall to the partition surface *of the perturbation*, a concept that will be further defined.

Partitioning of Heat

Figure 12-3 shows the temperature profile for the perturbation, with $t' = 0$ on the moving wall at the top, which satisfies the Hahn-Kettleborough condition. The resistance to the perturbation in the stationary wall is δ', an equivalent thickness

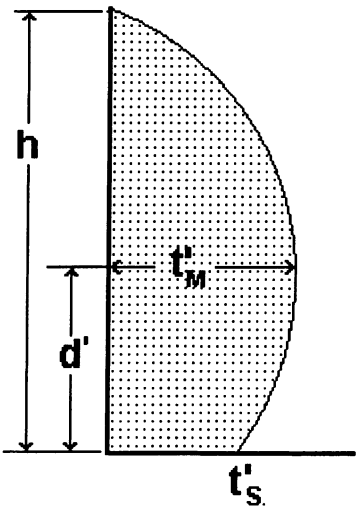

FIGURE 12-3. Temperature profile for the perturbation flow, with the Hahn-Kettleborough condition, $t' = 0$, on the moving (upper) surface and t'_S on the stationary, wavy surface. The maximum temperature identifies the partition plane, a distance d' from the stationary surface.

of oil. Under the assumptions of isoviscous heat generation uniformly across the flow, the temperature profile is parabolic, and geometry requires:

$$2\frac{d'}{h} = \frac{1}{1+\delta'/h} \tag{12-18}$$

Combining this with eq. (12-17):

$$\frac{W'_S}{W_C} = -\frac{h'/2h}{1+\delta'/h} \tag{12-19}$$

Taking the example of iron from Table 12-1, where $\delta' = 0.46\,\mu$m, and letting $h = 20\,\mu$m:

$$\frac{W'_S}{W_C} = -\frac{h'/2h}{1+0.023} = -0.49\frac{h'}{h} \tag{12-20}$$

where the sign convention for h' is positive "into" the solid.

Summary

A Couette flow with waviness imposed on a boundary is an idealization of several lubrication problems of fundamental importance. It may represent a bearing with an eccentric journal, a face seal with inclined faces, or one with saddle-shaped waviness. It may also represent a system with thermoelastic waviness on the boundaries. The result of the analysis is contained in eq. (12-19), where the perturbation of heat flux into the wavy wall, W'_S, follows the wave of amplitude h'. The magnitude is set by the heat flux intensity of the parent Couette flow, W_C, and an easily calculated thermal resistance, δ', expressed as an equivalent thickness of fluid. Typical magnitudes of δ'/h are listed in Table 12-2. Equation (12-19) may be expanded to read:

$$W'_S = \frac{\mu U^2 d'}{h^2} = \frac{\mu U^2(-h'/2h^2)}{1+\delta'/h} \tag{12-21}$$

When $d'/h = 1/2$, eq. (12-19) may also be written:

$$W'_S = -\frac{W_C h'}{2h} \tag{12-22}$$

The analysis is not restricted to vanishingly small perturbations of h'/h, but will serve for $h'/h \approx 0.5$, or possibly even larger when applied to a band of contact. See also chapter 22, where h'/h exceeds 0.9 or thereabouts. When the minimum gap in the film becomes small relative to the mean thickness, load and heating are concentrated on the peaks of the wave, and the analysis must ultimately proceed as a problem of elastohydrodynamics, as in chapter 21.

13
Convection

The transfer of heat by convection has a subtle influence on bearing flows. This may involve tangential convection in the flow bounded by a wavy surface, or it may involve forced, pressure-driven axial flow. The bearing film may be modeled as in steady Couette flow modified by a zero-average surface waviness. In the absence of convection, local perturbations on viscous heating are conducted straight into the boundaries, and the temperature increment is determined by a resistance, δ'_S, in the boundary wall. When tangential convection is significant, the heat flux from the parent Couette flow is unaffected, but the contribution from wall waviness is displaced circumferentially and is reduced in magnitude.

An independent kind of convection is caused by pressure-driven axial flow. This can reduce operating temperature greatly in quasi-steady operation with large external thermal resistance. In the more critical condition, start-up, axial convection causes only a small drop in temperature. When forced cooling of surface waves is analyzed, the axial flow modifies the heating perturbation by only a small amount.

Background

Banerjee and Burton (1976) treated tangential or circumferential convection in their analysis of thermoelastic instability in seal flows, and found a condition for which convection precludes thermoelastic instability. They used a parabolic profile for the oil temperature in the lubricant film, and treated both the short bearing and the long bearing. They avoided the problem of partitioning of energy by blocking heat to one surface. They assumed that a low-conductivity ceramic surface would serve as an insulating boundary on the film. Chapter 12 shows that the insulating-boundary assumption is valid only when the material is a solid of remarkably low conductivity. That condition may have been met by the glass used in Banerjee and Burton's experiments, but would not be met for carbon or silicon carbide. Georgopoulos (1980) offered a careful treatment of tangential convection with wall waviness, and found an accurate temperature profile in the film. This analysis is difficult to apply, and a parabolic temperature profile is a justifiable approximation.

R. A. Burton, *Heat, Bearings, and Lubrication*

A Favored Control Volume

The coordinate system in the fluid is that used in prior chapters, with y measured normal to the solid wall, from an origin in the partition surface. As discussed in chapter 12, linearity of the isoviscous film permits separate treatment of the Couette flow and the perturbation flow caused by wall waviness. Each will have its own partition surface, determined by external thermal resistances. For the perturbation flow, the distance from the partition surface to the wall is d', as in Fig. 12-3, with or without tangential convection. The temperature profile must also go to zero at the moving wall, pass through a maximum, t_M, and drop to the stationary wall, where temperature is t_S and the slope is $\partial t/\partial y = t_S/\delta'$. Here δ' is the thermal resistance of the solid expressed as *an equivalent thickness of oil* for the wave component of heat flux. When there is no convection, the curve is parabolic, and the critical dimension d' is given by:

$$d' = \frac{h}{2(1 + \delta'/h)} \tag{13-1}$$

When convection is incorporated, the curvature of the profile is no longer fully determined by the local intensity of dissipative heating, and higher-order terms appear. Burton (1994b) accounts for these, and shows them to be small. Consequently, d' does not stray far from the value in eq. (13-1).

The favored volume for the heat balance is illustrated in Fig. 13-1, where the footprint on the wall is the small rectangular surface area A and the height is d'. The quantity W'_U is the net heat (per unit of surface area) convected from the volume in the x-direction; W'_S is the heat conducted into the surface (per unit of area); and $d'W'/h$ is the viscous heat generation within the volume (per unit of surface area).

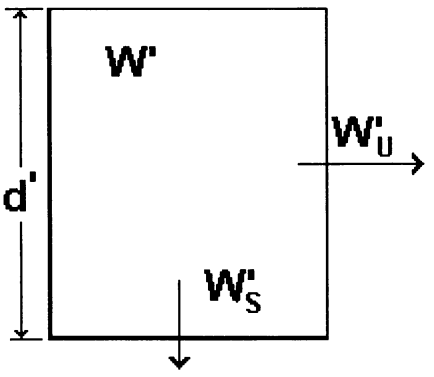

FIGURE 13-1. Control volume for heat convection, with height d' and arbitrary area on the stationary wall. Dissipated heat in the volume is W'. Conducted heat per unit of wall area is W'_S. Heat flow across the plane of the paper is not considered.

Conduction into the Wall

For simple cross-film conduction, the temperature profile must be parabolic and must satisfy the Hahn-Kettleborough condition (1968), where temperature approaches zero on the moving wall. This condition is approached even when the moving wall is of nonmetallic material, such as carbon or silicon carbide, as long as the Peclet number is high. This is supported by Dowson et al. (1966–67).

The principal features that affect heat transfer to the stationary wall are the maximum, t'_M, the distance d' from the stationary wall to the partition surface, and the temperature drop between the maximum and the stationary wall. Here the stationary wall is the one that carries the surface wave; it is also called the bearing surface. A similar analysis can be made where the journal carries the wave and the bearing is in relative motion.

The parabolic temperature profile is exact for pure conduction and will be retained. In the region between the partition surface and the wall, the temperature may be represented by the equation:

$$t = t'_M\left[1 - \alpha'\left(\frac{y}{d'}\right)^2\right] \tag{13-2}$$

where the parameter α' can be adjusted to satisfy boundary conditions. When t'_S is temperature on the stationary wall:

$$\frac{t'_S}{t'_M} = 1 - \alpha' \tag{13-3}$$

The heat passing into the stationary surface is given by:

$$W'_S = K\left(\frac{\partial t}{\partial y}\right)_S = 2K\alpha'\left(\frac{t'_M}{d'}\right) \tag{13-4}$$

External to the film, the thermal resistance δ' controls the heat transfer:

$$W'_S = K\left(\frac{t'_S}{\delta'}\right) = K(1-\alpha')\left(\frac{t'_M}{\delta'}\right) \tag{13-5}$$

Combining eqs. (13-4) and (13-5),

$$\alpha' = \frac{1}{1 + (2\delta'/d')} \tag{13-6}$$

For the limiting case of simple conduction, eq. (13-1) requires:

$$\frac{d'}{h} = \frac{1}{2(1 + \delta'/h)} \tag{13-7}$$

As an example, if $\delta'/h = 2$, then $d'/h = 1/6$, $\alpha' = 1/13$, and $t'_S/t'_M = 0.916$. The

TABLE 13-1. Typical Magnitudes t'_S/t'_M ($L = 1$ cm, $h = 10$ μm)

Material	δ'/h	t'_S/t'_M
Aluminum	0.104	0.31
Iron	0.48	0.74
Silicon carbide	1.34	0.88
Graphite	1.78	0.95

temperature is almost constant between the partition surface and the wall. Data from Tables 12-2, for δ'/h allow the temperature drop to be evaluated as in Table 13-1.

Estimation of Convected Heat

The predominant convection term for heat flux density in a Reynolds flow is:

$$w_U = \rho C_P u \frac{\partial t}{\partial x} \tag{13-8}$$

This function must go to zero at the stationary wall because $u = 0$ there. It will also go to zero on the moving wall because of the Hahn-Kettleborough condition. Figure 13-2 illustrates the variation of temperature and velocity in the volume defined by d', adjacent to the stationary wall.

Over a unit of surface area, on the stationary surface, the net heat convected from a volume defined by d' is:

$$W'_U = \frac{d}{dx}\int_0^{d'} \rho C_P t u \, dy \tag{13-9}$$

Making $u = 0$ at the wall where $y = d'$, the velocity distribution of the Couette parent flow becomes:

$$u = \frac{u(d' - y)}{h} \tag{13-10}$$

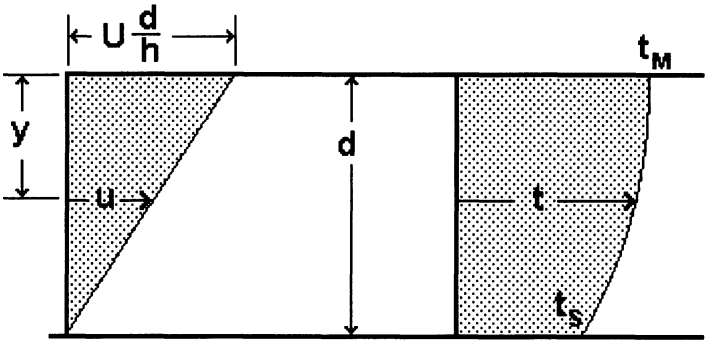

FIGURE 13-2. Velocity and temperature profiles near the wavy stationary wall.

TABLE 13-2. Typical Magnitudes for the Convection Function

δ'/h	Θ_C	$\Theta_C\delta'/h$
0.1	0.32	0.032
0.2	0.18	0.035
0.4	0.096	0.039
0.6	0.066	0.039
0.8	0.049	0.039
1.0	0.038	0.038
1.5	0.023	0.034
1.8	0.018	0.032

For the temperature distribution of eq. (13-2):

$$W'_U = \rho C_P \frac{dt'_M}{dx} \frac{Ud'^2}{h} \int_0^1 \left(1 - \frac{y}{d'}\right)\left[1 - \alpha'\left(\frac{y}{d'}\right)^2\right] d\left(\frac{y}{d'}\right) \tag{13-11}$$

For convenience, let the integral be H, and use eq. (13-3) to replace t'_M:

$$W'_U = \rho C_P \frac{dt'_S}{dx} Uh \left[\frac{H(d'/h)^2}{(1-\alpha')}\right] \tag{13-12}$$

The dimensionless quantity in brackets is a function of δ'/h, and may be evaluated from eqs. (13-6) and (13-7). It is designated Θ_C, and called the "convection function," for which numerical values are given in Table 13-2. Table 13-2 also includes the useful product $\Theta_C\delta'/h$, and shows it to be insensitive to the thermal resistance δ'. Using the convection function, the simplified version of eq. (13-12) is:

$$W'_U = \rho C_P \frac{dt'_S}{dx} Uh\Theta_C \tag{13-13}$$

Ratio of Convected to Conducted Heat

Sinusoidal waves may account for eccentricity, ellipticity, and multilobed waves on the surface of the bearing. These surface waves cause sinusoidal waves of temperature and heat flux density. When x is the tangential coordinate on a bearing or seal surface, and when it is "developed" into a straight line for the analysis, a sinusoidal wave of temperature can be represented by:

$$t = t' \cos\left(\frac{Nx}{R}\right) \tag{13-14}$$

Here t' is the modulus of t, N is the number of cycles of the wave on the circumference of the ring (or wave number), and R is the radius of the ring. This radius would be measured from the center of the ring to the midline of the nose of a seal,

TABLE 13-3. Oil Film Thickness for Equal Convected and Conducted Heat, $|W'_U|/|W'_S| = 1$, $N = 2$

rad/s	rpm	h (mm)	h (in.)
100	955	0.11	0.004
1000	9550	0.03	0.001
10000	95500	0.01	0.0004
20000	191000	0.007	0.0003

or could be the journal radius for a bearing. Differentiating:

$$\frac{dt'}{dx} = -\frac{N|t|}{R}\sin\left(\frac{Nx}{R}\right) \tag{13-15}$$

Fluid shearing can be expressed in terms of sliding speed or rotational speed, where $Ud'/h = R\omega d'/h$. Recalling that $W'_S = t'K/\delta'$, then

$$\frac{|W'_U|}{|W'_S|} = \frac{N\delta'\omega h\Theta_C}{k} \tag{13-16}$$

or:

$$\frac{|W'_U|}{|W'_S|} = \left[\frac{\Theta_C\delta'}{h}\right]N\left(\frac{h^2\omega}{k}\right) \tag{13-17}$$

The quantity in brackets is displayed in Table 13-2, where it is found to be almost constant. For a numerical example, take k for oil at 80°C from Table 2-1, where $k = 7.8 \times 10^{-4}$ cm^2/s, and take a representative midrange value of $\Theta_C d'/h = 0.039$ from Table 13-2. Equation (13-17) becomes:

$$\frac{|W'_U|}{|W'_S|} = 50Nh^2\omega \tag{13-18}$$

To measure the importance of tangential convection, the operating condition is found where the convected and conducted heat flow components are equal. Table 13-3 shows the film thickness for this condition for an elliptical bore ($N = 2$). At speeds of household devices ($\omega < 360$ rad/s) a large film thickness would be required for convection to equal conduction. At high speeds such as found in machine tools, turbomachinery, and aerospace systems, very thin films may be subject to significant convective effects. The data in Table 13-3 show that convection is significant within a reasonable range of turning speeds and film thicknesses when oil is the lubricant.

Cross-Flow Convection

In journal bearings, cooling is forced by pumped fluid that exits in the axial direction. The influence is greatest when a reasonable pressure drop can drive a significant lubricant flow. In the present analysis, the lubricant is supplied at

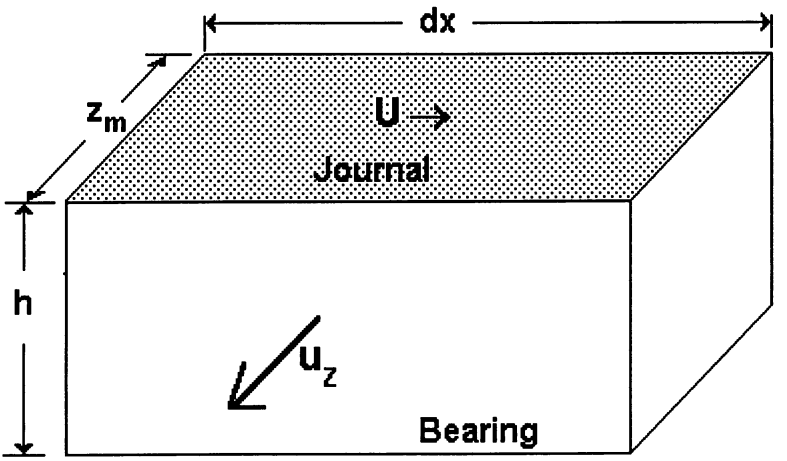

FIGURE 13-3. Control volume for deriving the heat balance. The curved bearing film is developed onto rectangular coordinates.

ambient temperature, and the fluid is assumed to rise to the temperature, t, at exit. This same temperature is assumed to drive conduction into the solid bearing. The control volume in Fig. 13-3 facilitates a heat balance involving generation, conduction, and axial convection. To remove consideration of tangential convection, the analysis is restricted to Couette flow. The control volume encloses a segment of film with tangential dimension, dx, and axial length, z_m. The film thickness is h, and the sliding speed is U. The mean axial velocity of the fluid leaving the film is u_z, and the heat carried out by the forced flow is W_z. The volume flow carried by the axial velocity is:

$$Q = u_z h\, dx \tag{13-19}$$

When temperature variation across the film is small, and the efflux carries the surface temperature, t, the heat flow out the end-face is:

$$W_z = u_z h C_P \rho t\, dx \tag{13-20}$$

The heat generated inside the volume is:

$$W = \left(\frac{\mu U^2 z_m}{h}\right) dx \tag{13-21}$$

W_S, which represents the heat conducted into the bearing surface, is determined by the conductivity of the solid bearing material, K_S, and a thermal resistance expressed as an *equivalent thickness of surface material*, δ_S. For steady operation, this resistance might be very high and determined by natural convection to air on the exterior of the bearing. For the steady-state case, data in Table 2-2 may be converted to an equivalent thickness of metal, and would range around $\delta_S = 10$ m of iron. At the other extreme, start-up may find $\delta_S = 0.01$ m. In either case, this

may be accounted for in:

$$W_S = \left(\frac{K_S z_m}{\delta_S}\right) t\, dx \tag{13-22}$$

If axial convection and surface conduction are the only means of heat removal, and if the partition plane lies against the journal surface,

$$W = \left[u_z h C_P \rho + \frac{K_S z_m}{\delta}\right] t\, dx \tag{13-23}$$

Solving eq. (13-23) for t,

$$t = \frac{\mu U^2 z_m h}{u_z h C_P \rho + \dfrac{K_S z_m}{\delta}} \tag{13-24}$$

The effectiveness of cooling is found by comparing t with $t_{Q=0}$, the film temperature without forced cooling, when $u_z = 0$.

$$\frac{t_{Q=0}}{t} = 1 + \left[\frac{u_z h \delta_S C_P \rho}{K_S z_m}\right] = 1 + \zeta_Q \tag{13-25}$$

The group in brackets is dimensionless and is designated ζ_Q, the "cooling parameter." Cross-flow cooling will halve the bearing temperature when ζ_Q goes to unity. Let the fluid be SAE-30 oil at 100°C, where $C_P\rho = 2 \times 10^6$ J/m-°C, and $\mu = 0.005$ N-s/m^2. Let the bearing material be iron alloy with $K_S = 50$ W/m-°C; and let $\delta_S = 10$ m of iron. Reasonable values of the design parameters for a small bearing are: $h = 2 \times 10^{-5}$ m; $z_M = 0.01$ m. For steady operation, the cooling parameter now becomes:

$$\zeta_Q = \frac{u_z h \delta_S C_P \rho}{K_S z_m} = 800 u_z \tag{13-26}$$

Halving the surface temperature occurs then when $u_z = 0.00125$ m/s. The axial pressure drop required to produce this flow is:

$$p = 12 \frac{\mu z_m u_z}{h^2} \tag{13-27}$$

Substituting the selected parameters:

$$p = 1.87 \times 10^3 \text{ Pa}, \quad \text{or} \quad 0.18 \text{ bar} \tag{13-28}$$

This is a reasonably small pressure requirement; in many systems, a pressure of 2 bar is available and would assure a significant temperature reduction. Recall that this represents steady or quasi-steady operation. On the other hand, during start-up the equivalent δ_S is less than the thickness of the bearing and may be as low as 0.01 m, or even smaller. To achieve a 50% temperature drop in start-up would now require a thousand-fold multiplication of u_z to 1.25 m/s, and the required pressure

TABLE 13-4. Cooling of a Thermal Wave in a Bearing

ζ_Q	$t'/t'_{Q=0}$
1	$\frac{3}{4}$
2	$\frac{5}{9}$
3	$\frac{7}{16}$
4	$\frac{9}{25}$

drop would be 180 bar, which is excessively large; in this case, forced-flow cooling would be of little importance during start-up.

Cross-Flow Cooling of a Wave

A small-amplitude surface wave is represented by $h' \cos(Nx/R)$. It will cause a surface-temperature perturbation of $t' \cos(Nx/R)$. When the film is in the short bearing regime, dissipative heating will be given by eq. (13-22) if h is identified as the local film thickness. For this condition, eq. (13-24) gives the local temperature produced by the combined effects of dissipation, conduction, and convection. For the isoviscous fluid, sensitivity of temperature to changes of film thickness is found by differentiation:

$$\frac{dt}{dh} = \frac{-\mu \delta_S U^2 z h}{K_S} \left[\frac{2\zeta_Q + 1}{(\zeta_Q + 1)^2} \right] \tag{13-29}$$

Chapter 12 argued that for small wave amplitude the perturbation quantities may replace the differentials, or $(t'/h') \rightarrow (dt/dh)$. Equation (13-29) may now be nondimensionalized upon dividing the temperature by that for zero cooling:

$$\frac{t'}{t'_{Q=0}} = \left[\frac{2\zeta_Q + 1}{(\zeta_Q + 1)^2} \right] \tag{13-30}$$

Table 13-4 shows how this varies with the cooling parameter. The temperature is halved for $\zeta_Q = 2.41$. Since a wave δ_S is of the order of half the wavelength, on a small bearing or seal this would be similar to the value for start-up, around 0.01 m. This means that forced cooling has little effect on wave growth. It is especially ineffective for short wavelengths.

Equivalent Thickness of Oil for Cross-Flow Cooling

Equation (13-20) gives the heat flow to the oil, and eq. (13-22) gives the heat flow to the solid surface. This may be rewritten to express the heat flow to the oil as equivalent to conduction through an oil film of thickness, δ_z. Combining these,

and letting $k = K_S/C_P\rho$:

$$\delta_z = \frac{z_m k}{u_z h} \tag{13-31}$$

For example, when $z_m/h = 1000$, and $k = 8.8$ m^2/s:

$$\delta_z = \frac{8800}{u_z} \tag{13-32}$$

The resistance is in meters of oil. Substitution of eq. (13-31) into eq. (13-27) gives a useful expression containing lubricant-supply pressure, p.

$$\delta_z = 12\left(\frac{\mu k}{ph}\right)\left(\frac{z_m}{h}\right)^2 \tag{13-33}$$

Discussion of the Results

Axial Convection

The results for axial convection are simple: When the thermal resistance of the solid material is low, convection has little effect on surface temperatures. When the system is passing through transient start-up, the surface resistance is that offered by the solid bearing to heat flow to its interior. It is the resistance of 1 cm or less of material in typical geometries and is so small that the heat in the film is stolen by conduction. Surface waves on the bearing also offer a small resistance into the solid, and they are almost unaffected by forced cooling. On the other hand, when the system is at steady state, the external resistance becomes similar to that for internal cooling. A very significant and useful temperature reduction can be had for modest pumping effort.

Tangential Convection

The principal finding is displayed in eq. (13-17), which may be rewritten in terms of sliding speed since $R_\omega = U$, and $\pi R/N = L$:

$$\frac{|W'_U|}{|W'_S|} = 0.038\frac{\pi h^2 U}{kL} \tag{13-34}$$

Oil was chosen for this example because of its general use in machinery, and because it has a low diffusivity, k, which emphasizes the effect of convection. Table 2-1 shows that the diffusivity of air is about 250 times that of oil, mercury is about 55 times and even water is about 1.8 times. This means that for the same geometry and operating conditions, convection plays a much smaller role for those fluids than for oil. It also means that eq. (13-34) is more than a special case for an arbitrary fluid. It is a very simple equation, which applies to the most important fluid.

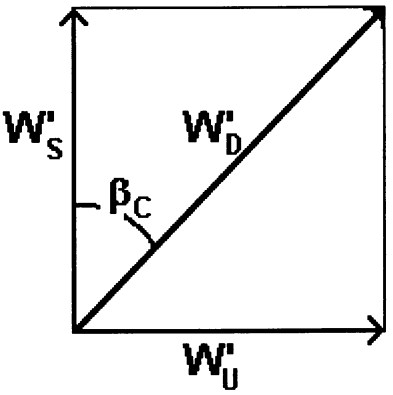

FIGURE 13-4. Conducted, convected, and dissipated heat represented as vectors.

Vector representation of the sinusoidal components of heat transfer allows the three components shown in Fig. 13-1 to be related, as in Fig. 13-4. The vectors W'_S and W'_U are orthogonal legs of a triangle, and W' serves as the hypotenuse. The orthogonality results because the maximum of W'_U is located were dt_S/dx is maximal, whereas W'_S must be in phase with t_S. The included angle satisfies the condition:

$$\beta_C = \arctan(W'_U/W'_S) \tag{13-35}$$

Information from this diagram is applied directly to wave growth in chapter 14.

14
Thermal Growth of a Surface Wave

In this chapter, viscous heating is coupled with film thickness so that a surface protrusion into the film will increase local heating. This heating increment can cause the protrusion to grow. The phenomenon can cause a strong amplification of a surface wave, and can lead ultimately to contact of the boundary surfaces at the peaks of the waves. The thermal coupling is influenced by convection and by the effects of turbulence.

Surface Deformation for a Sinusoidal Heat Input

Simple systems in bearings and seals, where surface deformation is directly proportional to heat flux, include:

1. axial heat flow into a ring, as in a face seal
2. radial heat flow into a cylinder or journal
3. radial heat flow into a cylindrical bore or bearing
4. heat flow into the straight edge of a plate or bar

The relationship between heat flow and curvature change is almost the same for all of these. The last system is the simplest to visualize and will be used for the discussions of thermoelastic interactions.

The analytical treatment of moving and stationary surface waves derives from the work of Ling and Mow (1966). Many of the ideas are presented in Ling's book *Surface Mechanics* (1973). Analysis of a journal bearing with stationary waves was undertaken by Hsu and Burton (1967) and Barber (1972). Banerjee and Burton (1976b) offer an analysis of the liquid film interacting with moving and stationary waves.

A complex body may be idealized as cut from a plate, with flat sides and a perimeter or "edge" that may be significantly thick. Heat is visualized as transferring into and out of the perimeter, but not from the sides. For such a simply connected, two-dimensional linearly thermoelastic body in "plane stress," imposition of *steady* heat transfer on the edges does not produce internal stress. Internal

R. A. Burton, *Heat, Bearings, and Lubrication*

elements expand freely, and heat flow into an edge facet gives rise to local surface curvature. This simple relationship between heat flux and surface curvature was hidden in an earlier derivation by Burton et al. (1973) for thermoelastic expansion along the edge of a plate. It was then developed and rationalized by Dundurs (1974), and has become known as Dundurs rule. The broad implications of this concept are explained in chapter 16. For a steady heat input of the type

$$W_S = W'_S \cos\left(\frac{\pi x}{L}\right) \tag{14-1}$$

the thermal displacement is:

$$h = h'' \cos\left(\frac{\pi x}{L}\right) \tag{14-2}$$

where:

$$h'' = \left(\frac{L}{\pi}\right)^2 \frac{\varepsilon W'_S}{K_S} \tag{14-3}$$

Thus a wave of surface heat input gives rise to a wave of surface displacement. The single- and double-primed quantities are used here as amplitudes or moduli for the waves. This is illustrated in Fig. 14-1, where the x-axis lies in the mean surface, h is measured outward from the solid, and W_S is positive for heat flux into the solid.

Dunders rule may be assumed to apply to a curved plate, if thin, and for axial heat transfer into a ring. However, uniform heat flux into the flat end-face of a ring leaves the surface without curvature along a circumferential coordinate, although there may be coning that raises the surface at the inner radius of the ring. Independently, a circumferential sinusoidal axial heat input will give rise to a sinusoidal axial displacement, as in eq. (14-2). Similarly, if a ring is subjected to uniform radial heat flux, it may expand uniformly, as discussed in chapter 5. A sinusoidal distribution of radial heat flux around the inner or outer surface of the ring will give rise to surface waviness in the radial direction, also in accord with eq. (14-2). This is explained further in chapter 16.

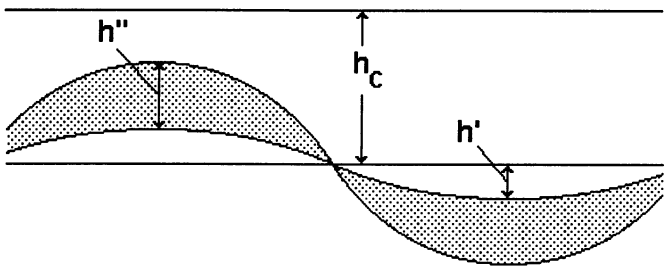

FIGURE 14-1. Geometry for the analysis of thermoviscous flow over a wavy wall. The original wave is h', the increment from thermal expansion is h'', and the amplitude of the combined wave is $h' + h''$.

Thermal Deformation and Viscous Heating in the Absence of Convection

Equation (12-17) gives the increment of surface heat flux that arises from a surface waviness of amplitude h', imposed on a stationary boundary of a Couette flow. It neglects convection and is based on the parabolic temperature profile in Fig. 12-3. It is repeated here in modified form:

$$W'_S = W_C\left(\frac{h'}{h_C}\right)\left(\frac{d'}{h_C}\right) \tag{14-4}$$

Here W_C is the heat generation per unit of wall area by the parent Couette flow, which for laminar flow is:

$$W_C = \frac{\mu U^2}{h_C} \tag{14-5}$$

The wave amplitude in present nomenclature is *positive* for displacement *into* the film. It is the sum of an initial wave, h', and the thermoelastic contribution from surface heat flux, h'', or

$$h_{wave} = h' + h'' \tag{14-6}$$

Here the h' of the previous chapter is replaced by, h_{wave}, a thermally augmented wave. This is illustrated in Fig. 14-1. When the combined wave replaces h' of Eq. (14-4):

$$W'_S = \frac{W_C d'}{h^2}(h' + h'') \tag{14-7}$$

Returning to Eq. (14-3)

$$h'' = \frac{L^2\varepsilon}{\pi^2 K_S}\frac{W_C d''}{h^2}(h' + h'') \tag{14-8}$$

Solving for h'',

$$\frac{h''}{h'} = \frac{1}{G' - 1} \tag{14-9}$$

Where the dimensionless group G' is defined by:

$$G' = \left(\frac{\pi h_C}{L}\right)^2 \frac{K_S}{\varepsilon W_C d'} \tag{14-10}$$

For low sliding speed, W_C is small and G' is large, hence h''/h' is small. When operating conditions approach $G' = 1$, however, h'' becomes a large multiple of h'. The sliding speed associated with this condition is called the "critical sliding speed," U^*. Using Eq. (14-5) to evaluate W_C, and letting $G = 1$, the critical speed is found to be:

$$U^*2 = \left(\frac{\pi h_C}{L}\right)^2 \frac{K_S}{\mu\varepsilon}\frac{h}{d'} \tag{14-11}$$

For low sliding speed, W_C is small and G' is large, hence h''/h' is small. When operating conditions approach $G' = 1$, however, h'' becomes a large multiple of h'. The sliding speed associated with this condition is called the *critical sliding*

speed, U^*. Using Eq. (14-5) to evaluate W_C, and letting $G = 1$, the critical speed is found to be:

$$U^*2 = \left(\frac{h_C \pi}{L}\right)^2 \frac{K_S h_C}{\mu \varepsilon d'} \tag{14-11}$$

Factors Influencing d'

The quantity d' is the distance from the wavy wall to the partition surface. For the parabolic temperature profile, with the Hahn-Kettleborough condition on the moving surface, it satisfies Eq. (12-18), which may be written:

$$\frac{d'}{h_C} = \frac{1}{2(1 + \delta'/h_C)} \tag{14-12}$$

Table 12-2 gives values for δ', for typical materials, and for the stationary wave where $c' = 0$. For iron, if $h_C = 20\ \mu$m, $\delta'/h_C = 1.9$ and:

$$\frac{d'}{h_C} = 0.17 \tag{14-13}$$

If δ' is extremely thin, as for a narrow band of heat transfer along a large bar, $d'/h_C \to 0.5$. The important observation is that it does not vary greatly. It is controlled by the material of the stationary surface, and for metallic material may rise as high as 0.5.

Banerjee and Burton (1976a) demonstrated experimentally that thermoelastic instability in hydrodynamic lubrication does, indeed, take place for a metal ring on a glass plate. For their operating conditions, the partition plane lay against the glass surface, and $d' = h_C$. For the materials considered in the present study, $d' < h/2$. Dow and Stockwell (1977) presented an independent experimental study of similar phenomena for a scraper on a drum, giving temperatures as well as thermal distortion. Banerjee and Burton (1979) extended experiments to a comparison with theoretical predictions and included measurements of stabilization temperature and of film thickness for several seal-nose widths.

Numerical Estimates of the Critical Sliding Speed, U^*

To estimate the critical sliding speed, U^*, one may substitute W_C from eq. (14-5), and the condition $G' = 1$, to get

$$U^* = \frac{\pi h_C}{L}\left[\frac{K_S}{\varepsilon \mu}\frac{h_C}{d'}\right]^{0.5} \tag{14-14}$$

Drawing upon eq. (13-7), d' may be expressed in terms of the externally determined δ'.

$$U^* = \frac{\pi h_C}{L}\left[\frac{2K_S}{\varepsilon \mu}\left(1 + \frac{\delta'}{h}\right)\right]^{0.5} \tag{14-15}$$

For the simple two-dimensional body (plate sliding along its edge), eq. (12-3) allows δ' to be expressed in terms of wavelength and the ratio of material conductivity

TABLE 14-1. Critical Sliding Speed for Four Materials

	U^*(m/s)			
L/h_C	Iron	Aluminum	Silicon carbide	Carbon
1000	54.6	93.6	49.9	43.4
2000	27.3	46.8	24.9	21.7
3000	18.2	31.2	16.6	14.4
4000	13.6	23.4	12.4	10.9
K_S/ε (N/s)	4.54×10^6	13.35×10^6	3.8×10^6	2.87×10^6

to that of the fluid:

$$U^* = \frac{\pi h_C}{L}\left[\frac{2K_S}{\varepsilon\mu}\left(1 + \frac{LK}{\pi K_S h_C}\right)\right]^{0.5} \tag{14-16}$$

Taking the conservative limit, $d'/h = 0.5$, for small wall resistance, this asymptotic condition applied to eq. (14-14) gives:

$$U^* = \frac{\pi h_C}{L}\left(\frac{2K_S}{\varepsilon\mu}\right)^{0.5} \tag{14-17}$$

This permits a safe estimate of the critical sliding speed, as compiled in Table 14-1. The viscosity of SAE-50 oil at 80°C (see Table 2-1), is $\mu = 3 \times 10^{-2}$ N-s/m^2; the solid properties come from Table 7-1.

The critical speed falls in the "high range" of typical sliding speeds but may be encountered in turbomachinery. For example, if a shaft turns at 20,000 rpm, and the seal diameter is 10 cm, the sliding speed is 105 m/s, and is well above the listed speeds. Banerjee's apparatus was capable of about one-fourth of this speed, but showed criticality.

Effect of Convection on Thermoelastic Growth of a Surface Wave

In Figure 13-4, the conducted heat, W'_S, and the convected heat, W'_U, are represented as orthogonal vectors, for a sinusoidal distribution of surface heating. The sum of these is the viscous dissipation, W'. A similar diagram may be constructed for the components of the surface displacement wave, where:

1. The thermoelastic componenent, h'', is produced by W'_S and is in phase with it.
2. The heat generation, W', is produced by the combined wave, and h_{wave} is in phase with it.
3. The amplitude h' is fixed in length, and h_{wave} is the vector sum of h' and h''.

When frictional heating is small, $h'' \to 0$, and $h' \to h_{wave}$. As sliding speed is increased, W' must increase, and the diagram becomes as in Fig. 14-2. Further increases of speed increase the angle β, as well as W' and W_S, until the limiting condition shown in Fig. 14-3 is reached, where β has opened up as far as is allowed by the fixed length of h'. At this condition, the ratio of h''/h' is maximal. This

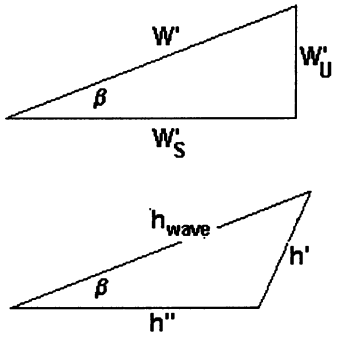

FIGURE 14-2. Vector diagram for surface and heating perturbations on a sine-wave wall, and the corresponding components of wave amplitude. Here h'' parallels W'_S, h_{wave} parallels W', and h' is the original waviness created when the surface was fabricated.

occurs when:

$$\frac{h''}{h} = \frac{1}{\sin\beta} \tag{14-18}$$

Returning to eq. (13-17), and letting the W' quantities represent the moduli of the appropriate components of heating:

$$\frac{W'_U}{W'_S} = \tan(\beta) = \frac{\Theta_C \delta' N h^2 \omega}{h_C k} \tag{14-19}$$

As has been demonstrated in chapter 13, this tends to be less than unity, and is usually much smaller. If this is unity, then $h'' = 1.4h'$, a significant but not runaway amplification. When convection is small, $\sin(\beta) \to \tan(\beta)$, and h'' may grow large. This makes $h_{wave} \to h''$, which is also the condition for instability without convection.

When b is small, $\sin(\beta) \to \tan(\beta)$, and:

$$\frac{h'}{h''} = \tan(\beta) = \frac{\Theta_C \delta' N h^2 \omega}{h_C k} \tag{14-20}$$

Although this appears to reduce the amplification as speed, N, is increased, it is consistent with the above arguments, because small convection is associated with small Θ_C and small β.

The Effect of Turbulence on Critical Sliding Speed

Chapter 8 treats the effects of turbulence in an instability that involves radial expansion into the fluid film. The principal concepts may be retained, when it is

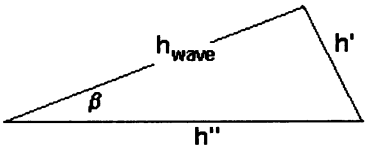

FIGURE 14-3. Limiting case for the largest β that can be accommodated by a given h'.

assumed, as previously, that the displacement flow components contribute only a small amount to viscous heating. Equation (9-4) shows a sensitivity of the heating increment to changes of film thickness to be negligible for limiting rough-wall turbulence. For smooth-wall turbulence, it would be:

$$W'_S = \frac{1}{4} W_{CT} \left(\frac{h'}{h} \right) \tag{14-21}$$

For laminar, isoviscous flow, the multiplier, $\frac{1}{4}$ would be replaced by unity. Correspondingly, eq. (8-2) replaces eq. (14-5) to estimate of the heat generation, where $W_{CT} = C_F U^3 / 2v$. Combining these effects, the conditions for $G \approx 1$ for smooth-wall turbulence would be:

$$G' = 1 = \left(\frac{h\pi}{L} \right)^2 \left(\frac{K_S}{\varepsilon W_{CT} d'} \right) = \left(\frac{h\pi}{L} \right)^2 \left(\frac{2K_S v}{d' C_F U^3} \right) \tag{14-22}$$

This is useful in itself as a predictor of critical speed. As in chapter 8, the comparisons with laminar flow are not simple, particularly near transition.

Summary

The third class of thermoelastic instability involves thermally enhanced surface waves on the boundary of a Couette flow. When sliding speed is increased, the waves will grow, increasing without limit at critical speed U^*. This is derived for laminar flow in eq. (14-11), and displayed in several forms in eqs. (14-14) through (14-17). For smooth-wall, turbulent flow a similar effect is predicted, as in eq. (14-22). This condition has been demonstrated experimentally by Banerjee and Burton (1976a) and shown to lift the mating surface on the expanded peaks of waves that were small at the outset. The critical speed is given by:

$$U^{*2} = \left(\frac{\pi h_C}{L} \right)^2 \frac{K_S}{\mu \varepsilon} \frac{h_C}{d'} \tag{14-23}$$

Here h_C/L is a design choice, being a dimensionless film thickness, and h_C/d' is determined by thermal constraints on the wavy surface, ranging from 2 to 5. The remaining properties are those of the wavy surface or of the fluid, and U^* is independent of the mating material as long as the Hahn-Kettleborough boundary condition is satisfied. When circumferential convection is taken into account, the critical condition becomes better defined, and the necessary conditions for quasi-static waviness disappear at the critical speed U^*. This is similar to the quasi-static axisymmetric instability of prior chapters.

The critical speed, U^*, is shown to lie in the high-speed range of realistic applications. It is not so high as to lie outside the range of interest in turbomachines, machine tool spindles, and similar high-performance systems. Equation (14-9) gives amplification of the initial surface wave, and can be converted by the definitions of G' and U^* to read:

$$\frac{h''}{h'} = \frac{1}{(U^*/U)^2 - 1} \tag{14-24}$$

15
Transient Growth of a Surface Wave

Time-dependent surface displacement is found for an exponentially growing sinusoidal temperature distribution on the surface of a solid. This surface is treated as one boundary of a Couette flow, and the increment of viscous heating is found, along with the heat flux to the boundary. This determines the condition when the increment of boundary heating is exactly that required to maintain the growing wave. The finding is that operation at a sliding speed above U^* is accompanied by the exponential growth of wall waviness. Experimental verification of the stability threshold is reviewed along with verification of the thermoviscous stabilization temperature.

Background

Both Dow and Burton (1972) and Banerjee and Burton (1997b) have treated exponentially growing waves on the solid boundaries of sliding systems. Although Dow and Burton's interest was in sliding systems heated by dry friction, their treatment of surface deformation is applicable to the present geometry. Bannerjee and Burton treated the coupling of the surface wave with viscous heating in the liquid film. The derivations of both sources are truncated here, and drawn into the nomenclature of the preceding chapters. The objective is to find what happens when the sliding system is forced above the limiting sliding speed, U^*.

There is an analogy between this condition of exponential growth and the transient seizure mechanism of chapter 9. However, the threshold for exponentially growing *radial* expansion is not tied to the condition for quasi-static seizure. In the present instance there is a close relationship between the static and dynamic solutions for the stability threshold of surface waviness.

Temperature Field and Surface Displacement for an Exponentially Growing Surface Temperature Wave

A semi-infinite body in plane strain will be considered, where the x-coordinate is stationary on the surface, and y is measured into the solid, along with its associated

R. A. Burton, *Heat, Bearings, and Lubrication*

temperature field. This field is required to satisfy the Fourier heat transfer equation. Letting τ represent time, this condition is represented by:

$$t = |t|e^{(-b''y+\beta''\tau)}\cos\left(\frac{\pi x}{L}\right) = t_S e^{-b''y} \tag{15-1}$$

Here $|t|$ is the amplitude of an initial surface temperature wave, β'' is real and positive when the wave is growing in time, and t_S is the instantaneous surface-temperature distribution. When b'' is restricted to positive values, the perturbation decays with distance into the solid. For this condition the chosen temperature distribution satisfies the Fourier heat transfer equation when:

$$b'^2 = \left(\frac{\pi x}{L}\right)^2 + \frac{\beta''}{k} \tag{15-2}$$

Dow and Burton (1972) have shown that for the chosen temperature field, the thermoelastic equation is satisfied by a sinusoidal distribution of normal stress, p, *if the surface is held flat.*

$$p = \frac{E\varepsilon t_S}{1 + b''L/\pi} \tag{15-3}$$

This stress may be removed, giving the displacement, h'', for an unloaded surface by superposing the elastic displacement of the surface that would occur for a sinusoidal surface loading, $-p$. This is accomplished when $h'' = 2pL/\pi E$, and the sign is adjusted to make the displacement positive away from the surface:

$$h'' = \frac{2\varepsilon t_S L/\pi}{(1 + b''L/\pi)} \tag{15-4}$$

Heat Balance at the Solid Surface

For the chosen temperature distribution, heat flux through the surface, W_S, may be found from the temperature gradient normal to the surface.

$$W_S = K_S\left(\frac{\partial t}{\partial y}\right)_{y=0} = K_S b'' t_S \tag{15-5}$$

In the absence of convection, the viscous heat generation in the control volume of height d'' is W' and is given by:

$$W' = W_C\left(\frac{h''}{h_C}\right)\left(\frac{d''}{h_C}\right) \tag{15-6}$$

Here d'' is the distance from the solid surface to the partition surface in the film for the exponentially growing wave, and W_C is the heat dissipated per unit of area by the parent Couette flow. The resistance to heat flux for such a transient disturbance is shown in chapter 8 to be small, and the simplification $d''/h = 0.5$

may be justified by the arguments surrounding eqs. (14-12) through (14-13), in which case:

$$W' = \frac{W_C h''}{2h_C} \tag{15-7}$$

For the condition discussed above, where dissipation in the control volume is equal to heat conducted into the surface, this may be combined with eq. (15-5) to give:

$$t_S = \frac{W_C h''}{2h_C b'' K_S} \tag{15-8}$$

This temperature may be substituted into eq. (15-4), to give the relationship between the frictional heating W_C and the remaining variables for the condition where frictional heating feeds the exponentially growing wave:

$$b''\left(1 + \frac{b''L}{\pi}\right) = \frac{\varepsilon W_C L/\pi}{h_C K_S} \tag{15-9}$$

Let W^* represent the critical heat flux associated with U^*. For this condition, $b'' = \pi/L$, as in eq. (15-2) when restricted to the condition $\beta'' = 0$. Under these conditions eq. (14-26) becomes:

$$2\left(\frac{\pi}{L}\right)^2 = \frac{\varepsilon W^*}{K_S h_C} \tag{15-10}$$

The Condition for Positive Exponential Growth

Combining eqs. (15-9) and (15-10),

$$\frac{2W_S}{W^*} = \left(\frac{b''L}{\pi}\right)\left(1 + \frac{b''L}{\pi}\right) \tag{15-11}$$

This is quadratic in $b''L/\pi$, and may be solved to give:

$$\frac{2b''L}{\pi} = -1 + \left(1 + 8\frac{W_S}{W^*}\right)^{1/2} \tag{15-12}$$

Here only the positive sign is retained before the radical, because interest has been restricted to positive b'' from the outset. Recall that this condition corresponds to a temperature distribution that decays with distance into the solid, whereas a negative b'' would correspond to a temperature distribution that grows with depth into the solid.

Returning to eq. (15-2), the condition for positive β'', and positive growth of the disturbance in time would be:

$$k\left[b''^2 - \left(\frac{\pi}{L}\right)^2\right] = \beta'' \tag{15-13}$$

It follows that β'' is positive when $b''L/\pi > 1$. Inspection of eq. (15-12) shows that this is indeed the case when $W_S/W^* > 1$. This does not mean that the stability limit for a quasi-static wave is exactly the threshold for transient growth. These two correspond exactly when the heat partitioning is the same for both cases. In the present instance, it is equal to half the heat generated in the film as a result of the wave.

Experimental Results

The above analysis differs from that of Banerjee and Burton (1976b) in that a small finite stationary surface wave is postulated, and the condition is found where it will grow without limit. Banerjee and Burton tackled a somewhat different problem: "When would a thermally induced surface wave be self-sustaining on a geometrically flat face of a seal?" Whereas the wave in chapter 14 is anchored, Banerjee and Burton's wave is required to translate slowly along the surface at a speed determined by convection. When convection is small, the condition for their wave to expand and the stability criterion of chapter 14 are the same.

To test their analysis, Banerjee and Burton (1976a) constructed the apparatus shown in Fig. 15-1, where an inverted, cylindrical metal cup was pressed against a self-aligning plate of low-conductivity glass. A proximity detector mounted in the glass displayed a much-magnified representation of the cup surface as it passed over the probe. A second probe read the displacement of the center of the cup to verify the absence of bouncing or axial vibration. A typical oscillogram is shown in Fig. 15-2, taken at a sliding speed just above that necessary for hot-spot formation. The upper line is the output of the bounce probe and shows the absence of vertical

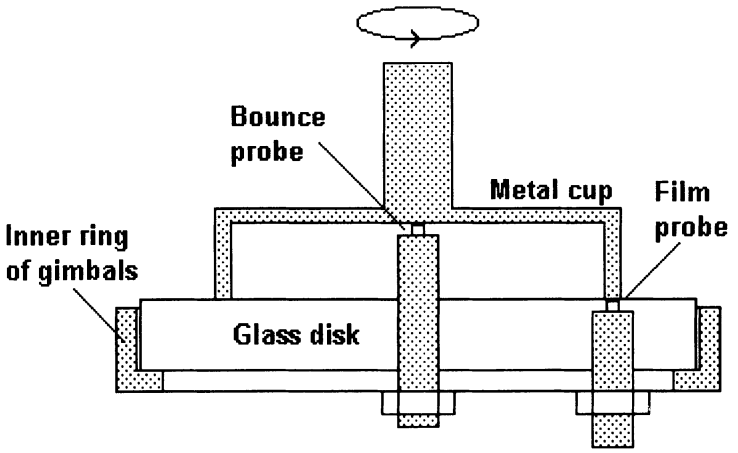

FIGURE 15-1. Diagram of Banerjee and Burton's (1976) apparatus, showing a proximity probe in the "nonconductive" glass plate, reading on the surface of the rotating cup. A central probe detects bouncing of the entire cup, to assure that measured clearance changes are truly profile effects and not bouncing.

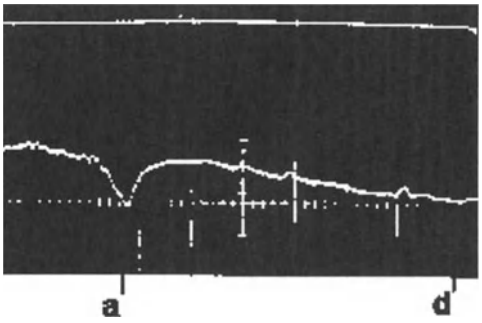

FIGURE 15-2. Typical oscillogram of the cup rim, with a hot spot at **a**, the sharp waviness peak. The rounded lobe, **d**, is the edge of the tipped cup opposite the peak. The upper line is the output of the bounce probe.

travel. The peak toward the left end of the lower line was associated with a red glow in the darkened laboratory. The peak causes a lifting away of the surfaces of the cup; the undeformed surface near the right end of the line owing to tilt of the ring appears as a rounded lobe.

Some mechanicists are troubled by the fact that the rings rest on a peak and a lobe. They intuit that three points of contact are required for stability. One should, however, recall that a rocking chair can rest stably on two points when the center of curvature of the rockers is above the center of gravity of the supported body. This is easily met for the contact of a tilted ring against a second ring. Figure 15-3

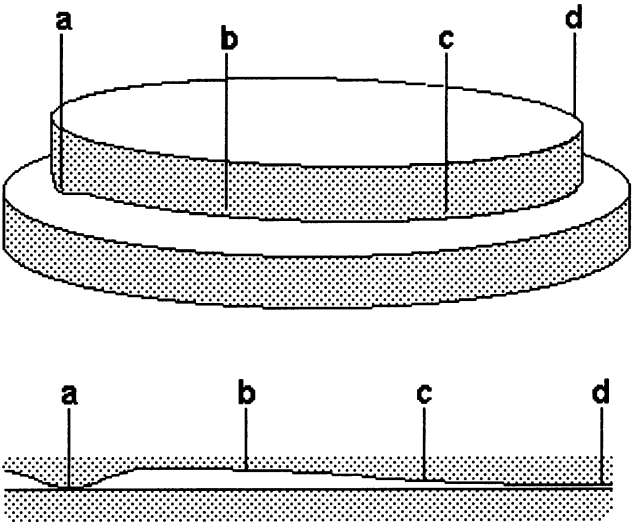

FIGURE 15-3. Schematic representation of a thermal asperity, **a**, supporting a rigid ring. The plot above the diagram shows how a proximity probe would represent film thickness, with corresponding points indicated as a, b, c, and d.

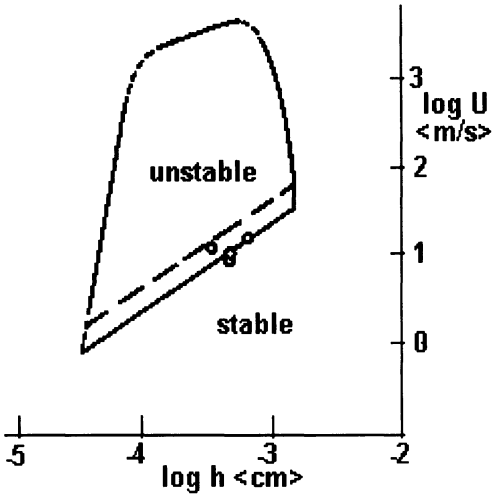

FIGURE 15-4. Film thickness and sliding speed at transition, compared with theory.

illustrates an idealized proximity trace for a rigid ring resting on a single protrusion and an opposite lobe.

Figure 15-4 compares observed points of instability with the theoretical threshold, displaying a reassuring consistency. A question arises because the natural operating condition lies close to the stability threshold, yet does not cross over it. This is because the wavy surface generates a hydrodynamic force that floats the cup away from the disk. This question disappears in a journal bearing, where the mean clearance is fixed. It also disappears in those seals for which the operating clearance is determined by hydrostatic force, as discussed in chapter 22. These questions do not prejudice the interpretation of the instability; however, they do suggest that more work on the "bearing" effect of the wavy surface would be of value.

Wu and Burton (1981) undertook a full dynamic and thermoelastic modeling of the ring and cup. They found a dynamic instability, which seems to be one discovered earlier by Etsion and Dan (1981). Etsion demonstrated it under thick-film, low-heating conditions, using the same apparatus that Bannerjee and Burton (1976a) used.

Kennedy et al. (1985) used thermocouples near the surface and running on the surface of the opposite face of a seal. These did not reveal the spectacular effects shown by the proximity probes because the temperature waves are mainly weak when compared with displacement waves—except for point contact. See also Doust and Parmer (1991).

Operating Temperature

Banerjee and Burton (1979) reported on stabilization temperature for the experimental seal as in Fig. 15-5. Their data include film thickness measurements, and

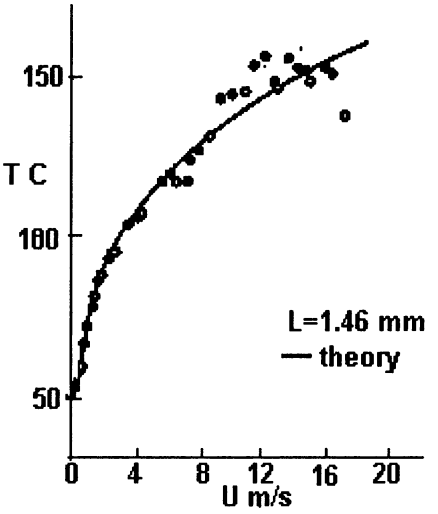

FIGURE 15-5. Stabilization temperature for an experimental seal, as determined by sliding speed. Nose width (radial) is L.

they provided an empirical equation for the viscosity of their oil. For present purposes, the temperature origin is shifted to 25°C, and the power-law coefficients become:

$$b = 0.303; \quad m = 2. \tag{15-14}$$

The operating temperature is given by eq. (4-16). Because of the high thermal resistance of the glass counterface $d/h = 1$. Equation (4-16) then becomes:

$$T = 25 + 6.71\left[\left(\frac{\delta}{h}\right)U^2\right]^{0.333} \tag{15-15}$$

Table 15-1 shows computed values of δ/h, using the temperature data from Fig. 15-4; δ is found using h values from Fig. 15-6. The two left-hand columns are taken directly from the figure. The Reynolds number is $UD/\mu v$, where μ and v are for air and D is cup diameter.

TABLE 15-1. Thermal Stabilization Data for an Experimental Seal.

U (m/s)	T (°C)	R ($UD/\mu v$)	δ/h	δ (mm oil)
4	100	16600	85	0.425
8	125	33300	53	0.265
12	143	49990	38	0.19
16	145	66656	22	0.11

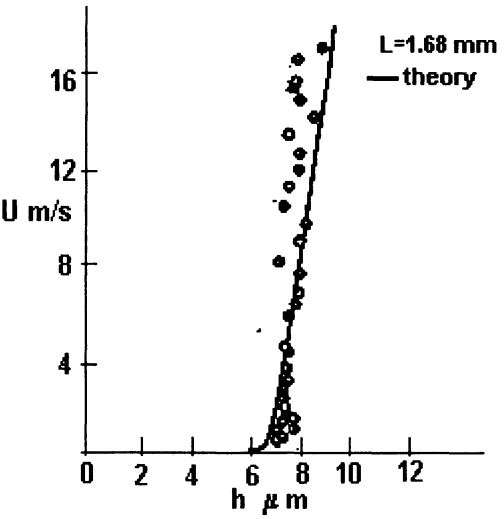

FIGURE 15-6. Experimental values of film thickness as determined by sliding speed, compared with theoretical curve.

Comparison with Predicted Heat Transfer Parameters

The data of Etemad (1955) for cooling of a rotating cylinder are represented by the empirical equation in Fig. 2-4. Equation (2-14), relates δ to the Nusselt number, Nu, for a rotating cylinder. Here δ_B is the thermal resistance to convective cooling on the exterior of the cylinder, expressed as an equivalent oil film thickness. This can be converted to effective coolant thickness in the present nomenclature:

$$\delta = \frac{DK}{Nu\, K_B} \tag{15-16}$$

where K_B is for air as coolant. From the empirical equation and the curve in Fig. 2-4, $Nu = 111$ at $R = 33{,}300$. From Table 2-1, $K/K_B = 5.9$, and $D = 76.2$ mm. The prediction is that:

$$\delta = 4.04 \text{ mm oil at } \mathbf{R} = 33{,}300 \tag{15-17}$$

This is 15.2 times the δ in Table 15-1 at the same Reynolds number. The thermal resistance on the cylinder is a large multipler of that needed for the stabilization temperature to be achieved. This discrepancy is accounted for by eq. (3-10), which corrects for the influence of extended surfaces, where heat goes to the environment through A_B, yet passes out of the film through the smaller area, A:

$$\frac{\delta_B}{\delta} = \frac{A_B}{A} \tag{15-18}$$

One must conclude that the effective heat transfer area of the cup exterior, A_B, is 15.2 times the area, A, of the small band of Couette flow. Although this seems

reasonable, the search for agreement should not be pushed too far. After all, the data for Fig. 2-4 were taken for a long horizontal cylinder, and the test seal is a short vertical cylinder.

Summary

The conditions for an exponentially growing surface waviness are set and tested. It is shown that the critical sliding speed, U^*, determines the threshold between steady-state operation and exponentially growing waviness.

Experimental determinations of thermoelastic instability show transition to occur in the vicinity of the predicted threshold. Thermal stabilization of the same system also verifies the general order of magnitude of the resistance δ, as summarized in Table 2-2, and displays the extended-surface effect, which is also treated in chapter 2.

This exercise of data analysis supports the ideas of the simplified power law, the thermoviscous equations of chapters 3 and 4, along with the general magnitude and importance of the δ measures of thermal resistance.

16
Constraints

Factors that may modify the thermal expansion of the bearing include shape, the effects of surrounding material, and thermal resistances, which alter the direction of heat flow. These exert different influences on the quasi-static expansion, exponential expansion, and distortion by time-dependent waviness. Of particular interest are those instances for which these constraints do not change thermoelastic behavior of the bearing bore from that of the axisymmetric system.

Quasistatic Expansion

In chapter 7 the axisymmetric problem of relative expansion is treated for different materials in the bearing and journal. The difference between rest clearance and operating clearance is given by eqs. (7-5) and (7-6), which are repeated here:

$$h_0 - h = r_J \varepsilon_J \left(\frac{W(r_B - r_J)\Phi_E}{2K_J} \right) \tag{16-1}$$

where the dimensionless group is defined as:

$$\Phi_E = \left[\left(\frac{\varepsilon_B}{\varepsilon_J} \right) + \left(\frac{2\delta_{SA}}{\delta_B} \right) \left(1 - \frac{\varepsilon_B}{\varepsilon_J} \right) \right] \left(\frac{K_J}{K_B} \right) \tag{16-2}$$

The quantity Φ_E is made up of two parts in the square brackets, and the second part is dominant because of the typically large thermal resistance δ_{SA}. It represents the effect of a general temperature rise of the elements, and the smaller term accounts for internal thermal gradients. As far as relative expansion is concerned, it is as if the components were heated uniformly and the small gradients associated with local heat transfer were insignificant. This has several important ramifications:

1. *The shape of the bearing has little effect.* A square block with a hole in it will expand uniformly in a uniform field of temperature, and the hole will remain round.

R. A. Burton, *Heat, Bearings, and Lubrication*

2. *The temperature drop across the film disappears.* Once the resistances of the components and the film are small relative to δ_{SA}, each of these resistances becomes unimportant.
3. *The path of heat flow has little effect.* It does not matter if the heat is transferred out from one side or is uniformly distributed; blockages determine only the internal gradients and not the drop to ambient. Of course, extreme blockages will increase δ_{SA}.
4. *The logarithmic correction becomes unimportant.* Because the logarithmic correction is applied to an internal temperature gradient, it is not necessary when the gradient is small.
5. *Outward or inward heat flow has the same effect.* Only the stabilization temperature is important. Consequently the blockage of flow to the journal (as was forced on the prior derivations) becomes unimportant. Cooling may be through the journal or through the bearing or through both.

Constrained Expansion of the Bearing Cylinder

Nica (1965) treated both free expansion of an axisymmertric bearing and constrained expansion where the housing holds the outer radius rigid. Hahn and Kettleborough (1968) treated free expansion while emphasizing that constraints have been disregarded, and thereby raise a big question. Since the true expansion must lie between the free and the fully constrained, it is informative to examine the constraint on a bearing cylinder embedded in a cylindrical housing of another material.

The condition for free expansion of a uniform cylinder is:

$$\frac{\delta r}{r} = \varepsilon \delta t_{\text{mean}} \tag{16-3}$$

applied on either the inner or outer radius. This is introduced in chapter 5 and discussed in chapter 6. This result may seem to be counterintuitive because there is a widespread belief that the hollow cylinder will expand inward as well as outward. This is not the case for the free-expanding single-material cylinder, where all dimensions expand proportionally. On the other hand, if the bearing is pressed into a second cylinder with small expansion coefficient and large Young's modulus, the inner cylinder can actually be constrained to expand inward, although a reasonable choice of engineering materials would call for the housing to modify only the expansion of the bearing. Such a system is illustrated in Fig. 16-1, in which the two cylinders share the temperature, t, Poisson's ratio, $\nu = 0.25$, and the common radius at the interface. The bore radius of the inner cylinder is r.

The analysis allows each of the cylinders to expand independently according to eq. (16-3). Boussinesq's solution for the thick-walled pressure vessel (Timoshenko and Goodier, 1970, p. 70) is applied to each tube to determine the change of interface radius of each when the pressure p is applied on the interface. The

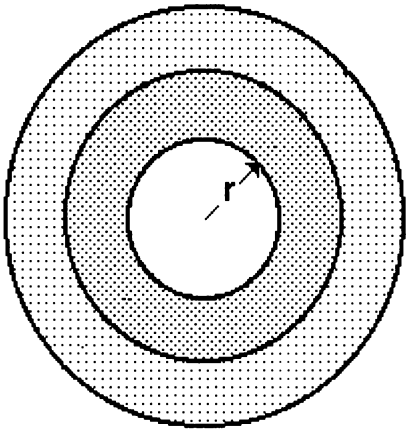

FIGURE 16-1. Schematic diagram of an outer cylinder constraining the bearing cylinder.

expansion of the inside of the inner cylinder is then found under the combined effects of temperature and pressure:

$$\frac{dr}{r} = \frac{\varepsilon_1 t - 2p}{(1 - A_1^2)E_1} \tag{16-4}$$

and

$$p = \frac{(\varepsilon_1 - \varepsilon_2)t}{\left[\dfrac{(Z_2 + \nu)}{E_2} + \dfrac{(Z_1 - \nu)}{E_1}\right]} \quad \text{and} \quad Z = \frac{1 - A}{1 + A} \tag{16-5}$$

where A is the ratio of inner radius to outer radius for the designated cylinder. For numerical calculations, the results are presented such that:

$$\frac{\left(\dfrac{dr}{r}\right)}{\varepsilon_1 t} = 1 - \zeta \tag{16-6}$$

Here ζ represents a dimensionless expansion deficit, and calls for zero expansion of the bore when $\zeta = 1$. In convenient form:

$$\zeta = \frac{2\left(1 - \dfrac{\varepsilon_2}{\varepsilon_1}\right) \Big/ (1 - A_1^2)}{\left[\left(\dfrac{E_1}{E_2}\right)(Z_2 + \nu) + (Z_1 - \nu)\right]} \tag{16-7}$$

Since $A < 1$ by definition, the denominator must always be positive, and z will be positive if $\varepsilon_2 < \varepsilon_1$. This condition calls for a reduction in expansion of the bore.

TABLE 16-1. Coefficient of Expansion and Elastic Modulus

Material	$\varepsilon \times 10^6$ 1/°C	$E \times 10^5$ MPa
Copper	16.6	1
Aluminum	17	0.7
Iron	11	2
Silicon carbide	4.7	0.88
Carbon	3–4.7	0.2

A rigid housing would call for $E_1/E_2 = 0$, and $\varepsilon_2/\varepsilon_1 = 0$, in which case:

$$\zeta = \frac{2}{(1 - A_1^2)(Z_1 - \nu)} \tag{16-8}$$

Taking $A_1 = 0.5$ as an example, $Z_1 = 3$ and $\zeta = 0.97$, which is a neutral expansion of the bore, without encroachment into the film. A more realistic estimate may be made for real materials, such as listed in Table 16-1. All of these quantities are altered in a small way by temperature and state of heat treatment or method of formation; but this does not change their general range. The carbon is most variable, with significant changes from the ratio of graphite to other carbons, and the degree of consolidation before firing.

Table 16-2 summarizes solutions for eq. (16-7) for three combinations of materials. The somewhat unlikely combination of an iron bearing in a silicon carbide housing shows a large expansion deficit. The more likely silicon carbide bearing in an iron housing shows negative deficit or "enhanced" thermal expansion. This can be possible when the cylinders are press-fitted in the initial assembly, and will continue until the negative p exceeds the positive p of the press fit. The carbon shows maximally enhanced expansion, although this is a little deceptive because the dimensionless ζ is based on the bearing properties. If the journal is

TABLE 16-2. Quasi-Static Expansion Deficit ζ for Selected Materials

Bearing	Housing	A_1	A_2	ζ
Iron	Silicon carbide	0.707	0.5	0.51
		0.707	0.707	0.44
		0.5	0.5	0.35
		0.5	0.707	0.28
Silicon carbide	Iron	0.707	0.5	−3.9
		0.707	0.707	−2.6
		0.5	0.5	−2.15
		0.5	0.707	−1.3
Carbon	Iron	0.707	0.5	−14
		0.707	0.707	−7.6
		0.5	0.5	−6.26
		0.5	0.707	−3.3

iron, then the expansion surplus may be referenced on the expansion of iron, and $\zeta_{Fe} = \zeta \varepsilon_C / \varepsilon_{Fe}$. The enormous value of -6.26 becomes the moderated, but still favorable, -2.2 for $\varepsilon_C = 4 \times 10^{-6}$.

Housing Restraint of Transient Expansion of the Journal and Bearing

The above derivations can be adapted to shed light on the transient expansion behavior of a constrained bearing, where the thermal boundary layer is thin and contained within the bearing cylinder. In this case the housing does not expand at all, a condition that can be accommodated by letting $\varepsilon_2 = 0$. The temperature t is the mean temperature of the bearing cylinder, and is the same temperature as used in chapters 5, 6, and 8. Equation (16-7) becomes:

$$\zeta = \frac{\left[\dfrac{2}{(1 - A_1^2)}\right]}{\left[\left(\dfrac{E_1}{E_2}\right)(Z_2 + \nu) + (Z_1 - \nu)\right]} \tag{16-9}$$

One example is displayed in Table 16-3. For all of the relative thicknesses, A, chosen there, the deficit is positive and large, indicating that the cabon expands inward and exacerbates any instability phenomena where a positive shaft expansion must be accommodated.

In the initial analysis of transient expansion, it was pointed out that runaway clearance change is to be expected whenever the heat flow to the walls leads to a relative decrease of clearance. Only the change from a thin to a thick thermal boundary layer served to set a lower limit for the instability. The results in Table 16-3 do not address this complex phenomenon. They provide only a measure of the modification the expansion of the bearing by its housing. As in the preceding paragraphs, the expansion deficit is converted to an "iron" basis so that it may be compared with the expansion of an iron journal. Except for the most extreme case, $\zeta_{Fe} < 1$, and in one instance it would account for only one-third as much expansion as would be expected from the journal. Hence it only modifies but does not totally alter the expected changes of film thickness.

TABLE 16-3. Transient Expansion Deficit ζ for Carbon in Iron

Bearing	Housing	A_1	A_2	ζ	ζ_{Fe}
Carbon	Iron	0.707	0.5	5.3	1.41
		0.707	0.707	2.8	0.74
		0.5	0.5	2.3	0.61
		0.5	0.707	1.2	0.33

Constraints That Distort the Temperature Field in the Bearing

Dundurs rule (1974) may be applied to the single-material bearing, giving insights into the effects of thermal blockages that distort the temperature field. This rule is introduced in chapter 14 and applied to sinusoidal temperature distributions. Here it is reviewed in a more general context and applied to the changes of curvature of internal surfaces of a two-dimensional body when heat is conducted through these surfaces. As extended by Barber (1975), this may be made to apply to either plane-strain or plane-stress bodies with a modification of the coefficient. A component formed from a plate with heat flow restricted to the edges will find on any straight surface that:

$$\frac{d^2h'}{dx^2} = \frac{\varepsilon W_y}{K} \tag{16-10}$$

Here the x-axis defines the surface, w_y is heat flux intensity (W/m^2) normal to the surface, h' is the material displacement of the surface, and the coefficients ε and K are constant throughout the body. When heat flow is *into* one of the bodies bounded by the surface, the curvature is concave downward into that body. That is, a patch of ingoing heat flux gives rise to a bump. This equation is valid for any line in a simply connected body in plane stress. This is true because such bodies, with constant conductivity throughout, have no stress changes when steady heat flow passes through them. Obviously, the stresses and displacements around a hole do not follow this law when the hole surrounds a source of heat. However, as shown below, sinusoidal input around the periphery of the hole does satisfy Dundurs's conditions.

Barber's correction (Barber, 1975) replaces ε with $\varepsilon(1 + \nu)$ for distributions of heat input into the surface of thick plates or slabs. This correction is only a 25% change, and is not of critical importance in ambiguous geometries. For example, a circular plate may have a thickness that is small relative to the diameter. If there is a sinusoidal temperature distribution on the periphery, and the thermal boundary layer is much thinner than the plate thickness, that boundary layer is in a condition close to plane strain. On the other hand, if the distribution has a long wavelength, the thermal boundary is large relative to the plate thickness, and the condition is close to plane stress. Nevertheless, Dundurs's or Barber's versions both serve as good estimates of curvature change.

Returning to the plate in plane stress, refer to Fig. 16-2, where a square plate with a hole is divided into simply connected bodies with a "hypothetical" cut on a line of symmetry. For any heat transfer distribution without flux across the cut, there will be no change of curvature on the cut line. Heat may pass through the outer boundaries in any pattern (provided inflow equals outflow), and the unchanged cut can be rejoined without creating internal stresses, The exterior boundaries will be curved in accord with Dundurs rule, however.

As a second case, consider the cut body without external heat flow, but with a zero-average sinusoidal distribution of heat input on the periphery of the hole. Because the cut body is simply connected, Dundurs rule applies on the hole boundary;

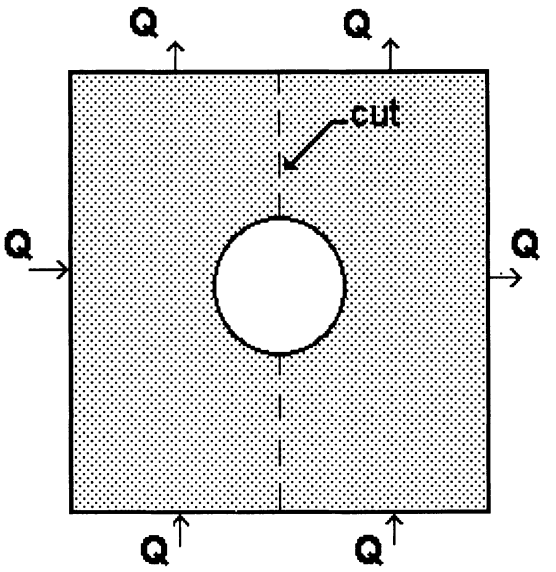

FIGURE 16-2. Cylindrical bore in a square plate, with hypothetical cut on broken line. Arbitrary set of heat inputs must sum to a net zero.

if symmertry requires that the straight boundaries of the cut have no heat flux across them, they may be rejoined without stresses.

A third case sees heat pass into one of the two bodies produced by the cut, then move through the cut boundary and out the other side. No heat flow passes through the boundary of the hole. In this case the hole remains unchanged, the body losing heat finds its cut surface concave, and the second body finds a corresponding convexity, which permits rejoining the cut surfaces without stresses. Such demonstrations show that this is a very powerful rule and applies to internal as well as external surfaces of a plane body, as long as sources or sinks are absent. Returning to the sinusoidal distribution on the interior or exterior of the disk, note that no distortion of the external boundary is called for; consequently, the housing is not required to react as a restraint on the boundary.

The Juncture of Large and Small Bodies

In machines, the bearings are generally attached to larger structures, which serve as fins and heat sinks and offer boundary constraints at the connecting seam. The general effect is as shown in Fig. 16-3, where a square bearing and housing join either a plate or a large block. Heat input in the bearing is of two types: source flow and zero-average periodic input. The latter has already been shown to leave the boundaries of the system undeformed; hence bonds to the larger body remain.

For the conditions of quasi-static clearance change, a heat source resides in the bore and gives rise to radius changes for the axisymmetric body. Considering

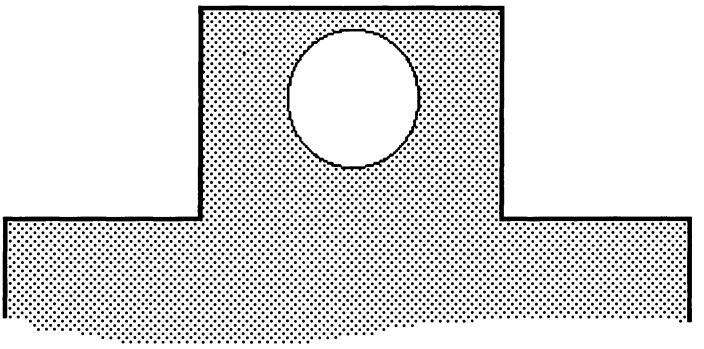

FIGURE 16-3. Bearing as square plate attached to a larger plate.

the geometry of Fig. 16-4, a phantom circular boundary is shown by the broken line. The cylinder above it, when unconstrained, would experience a radius change according to eq. (16-3). If, in addition, all of the heat flows through the phantom boundary, the effect is as if heat is forced back in through the open surface of the cylinder, and the entire heat output from the source crosses the phantom boundary. This second component of heat flow would cause a reduction of curvature of the cylinder on the phantom boundary and an equal protrusion of the remaining bearing structure below the phantom line.

If the large structure below the bearing is a plate, any further heat flow is without stress. The question remaining is: "How much does the bending of the lower structure resist the bending caused by the initial axisymmetric change of curvature of the cylinder as a result of the heat source?" This then becomes a clearly defined elasticity problem. In practice, the attachment of the bearing may occur only at smaller contact points, as shown in Fig. 16-5. This is done to avoid having to fit two imperfect surfaces together along their full length. If this is the case, the axisymmetric deformation of the bearing is virtually unconstrained.

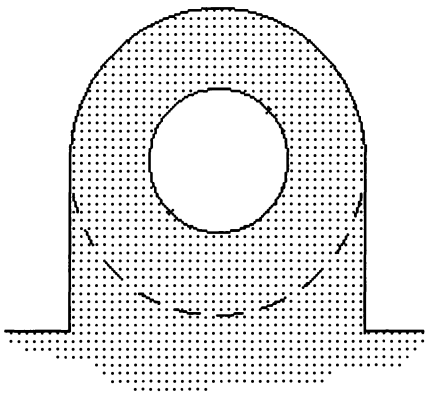

FIGURE 16-4. Partly cylindrical bearing attached to a large plate, with phantom surface continuing the cylinder.

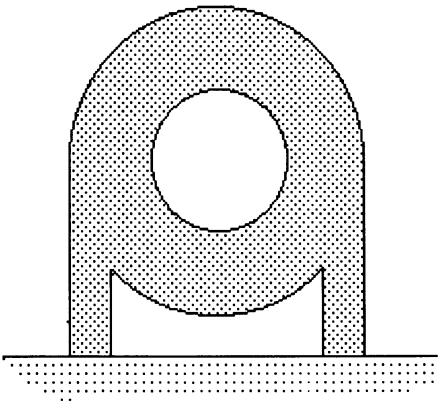

FIGURE 16-5. Schematic representation of a bearing with feet, attached to a larger plate.

Is the Two-Dimensional Body a Realistic Model?

If the bearing and housing are cut from a plate, the physical body may appear to be two-dimensional, but it will not be in plane heat flow when significant heat flows from the face planes. The constraints on heat flow are different for the two cases of source flow and zero-average input.

Heat Flow from a Source

For this problem, we are returned to the first examples in this chapter, where the resistance between the bore and the environment controls the temperature and expansion of the bore. In general, this resistance is large and the components expand as in a uniform temperature field. In the special case of attachment to a heat sink, as in Fig. 16-3, the resistance to the environment is reduced by the shunting of heat through the solid junction, at an edge of the plate. The thermal resistance remains high on the flat faces of the plate, and the small thermal gradients that are left are largely in-plane. The two-dimensional model remains reasonable.

Zero-Average Heat Flow

Sinusoidal heat input around the bore tends to stay in-plane because the heated ends of the thermal boundary layer are thin. Even when the plate is subjectively judged to be thick, and when the wave is judged to follow Barber's rule, heat flow from the ends tends to be a minor effect.

Summary

In the previous chapters, many constraints have been imposed to bring out the essential features of the thermal and thermoelastic interactions. These are listed here with comments.

1. Power-law fluidity or viscosity equations. These equations have been shown to represent the thermoviscous behavior of oils, which show the largest changes of fluidity with temperature. Because fluid behavior is of maximum interest at elevated temperatures, little damage is done to the accuracy of the thermoviscosity equation when the origin of zero fluidity is moved to the ambient temperature. With this simplification, the equations for heat generation, maximum temperature, and thermal deformation are formed around a simple two-parameter representation of the fluid. The sensitivity of system behavior to thermoviscosity parameters is displayed in an accessible form. In a few examples, the power-law exponent is forced to the form $\phi = bt^2$. If this simple representation did not mimic the true function in the vicinity of the maximum temperature, it would be an inexcusable simplification. But it does reasonably well for the examples tested. It also permits the generation of a family of SAE oils that fit into the prescribed ranges. When one actually tests oils of the same SAE number from independent sources, one finds that they differ tremendously over the range of interest. Those here with the forced exponent would be at home among such partners, and provide a convenient one-parameter scheme for comparing the general effects in the full SAE range.

2. The Hahn-Kettleborough condition. When a conductive boundary slides past a surface wave fixed on a parallel boundary, the temperature perturbation caused by the wave shows a maximum in the stream above the wave and goes to zero on the opposite surface. Supporting calculations show that this effect is a valid approximation even when the moving surface is much reduced in thermal conductivity relative to the wavy surface. A corresponding rule applies to waves on the moving surface, which carry a temperature perturbation that goes to zero on the stationary surface. This rule decouples the wave-growth problem of thermoelastic instability, making it dependent only on the temperature of the wall that carries the wave. When the wave is itself propagating on the stationary wall, thermal resistance into the surface reduces. And when the wave reaches a high Peclet number relative to both walls, the perturbation temperature approaches zero on each, and the maximum t' moves to midfilm, or $d = h/2$.

3. Plane Couette flow. The assumptions that disregard curvature of the film are consistent with Reynolds's definitions of bearing flows. For the fluid mechanicist seeking generality, thick films can be included as well as Taylor's vortices. But large thermal deformation relative to film thickness occurs only when the film is thin relative to the radius. This is fairly represented by the asymptotic condition in which the ratio h/r is vanishingly small.

4. Fixation on cylindrical bearings. Many of the important thermoelastic interactions are exhibitied in cylindrical systems. We have shown repeatedly that when the external thermal resistance is high, shape does not matter because the bodies rise in temperature together with only small internal gradients. For those conditions for which internal gradients are large enough to matter, a cylindrical bore in a square rod, for example, will expand much as a cylinder in a cylinder. A little effort can establish the appropriate external "equivalent radius". There is a second effect, and that is the formation of a surface wave with four lobes. This

wave may become the "seed" for the growth of the thermoelastic waves, which are supported by their own zero-average heat input waves.

5. *Plane strain and plane stress.* The thermal expansion differences for these two idealizations are small. Arguments presented in this chapter support the ideal of plane stress in large-scale temperature distributions and plane strain for those where the thermal boundary layer is of the same scale as the plate thickness. Actually, both concepts are troublesome to elasticians, but are convenient at the level where we must approach the problems of deformation.

6. *In-plane heat flow.* Arguments have been given in this chapter that show the assumption of in-plane heat flow to be reasonable. At one extreme, where thermal gradients are small, the errors of this assumption are hidden in the overall temperature rise. At the other extreme of a thin thermal boundary layer, the thinner it is the less the heat flows out the ends.

17
Start-Up

In this chapter, the temperature history of a journal bearing is followed from start-up, passing through a condition for which film thickness may disappear. An approximate analysis relates the phenomenon to the operating variables. A numerical model of the evolving temperature profile gives insights into the timescale for this mode of seizure. The history of film thickness is calculated for a thin-wall journal in a thick bearing with an SAE-30 fluid, and the effects of operating speed and the rate of angular acceleration are determined.

Background

In an attempt to explain nondestructive seizures of a 100,000 rpm test bearing, Burton (1965) was able to identify two possible modes of failure in an approximate theoretical treatment of an axisymmetric hydrodynamic bearing. One is the quasi-static mode of chapter 6. The second is transient clearance loss caused by a time lag in the expansion of the bearing during start-up.

The transient seizure mechanism is investigated here in an axisymmetric journal bearing made of a single material (iron alloy). The analysis is simplified by giving the thermal resistances in equivalent thicknesses of *metal* rather than *oil*. Based on the discussions of chapter 10, the thermal resistance of the oil film is assumed to be small, and the journal is allowed to share the temperature of the inner surface of the solid bearing. Nomenclature for the thermal resistances is listed in Table 17-1. Other symbols are listed in Table 17-2, where magnitudes are given and where modifications from prior practice allow more direct writing of the approximate and numerical equations. These symbols are carried over into chapter 18.

A Graphical Construction

Figure 17-1 displays the development of the temperature profile in the bearing during start-up. The initial heat input is contained in a thin thermal boundary layer, δ'_B, which is small relative to the overall thickness of the bearing, δ_{BE}. Thermal

R. A. Burton, *Heat, Bearings, and Lubrication*

TABLE 17-1. Nomenclature of Thermal Resistances

	Units	
	Millimeters of Oil	Millimeters of Metal
Resistance from outer surface to ambient	δ_{CA}	δ_{CE}
Thermal boundary layer in bearing	δ_S	δ'_B
Journal radius		r_0, or r_J
Thickness of the bearing ($r_B - r_J$)		δ_{BE}
Dimensionless ratio (r_J/h_C)		R

TABLE 17-2. Selected Properties and Operating Conditions, Hollow Journal

Expansion coefficient	ε	10^{-5}	1/°C
Initial film thickness	h_C	5×10^{-5}	m
Mean bearing temperature	t_{BE}		°C
Mean journal temperature	t_C		°C
Film temperature	t_C		°C
Diffusivity of iron	k	1.1×10^{-7}	m^2/s
Conductivity of iron	K	50	N/s-°C
Journal radius	r_0	0.02	m
Bearing thickness	δ_{BE}	0.02	m
Sliding speed	U	$1 \rightarrow 50$	m/s
External convection	δ_{CE}	0.2	m, iron
Time increment	$d\tau$	18	s
Viscosity, SAE-30	μ	$7143/(t + 30)^{3.0104}$	$N\text{-}s/m^2$
Viscosity, SAE-30	μ	$1/bt^m$; $m = 1.85, b = 0.061$	$N\text{-}s/m^2$
Viscosity, SAE-50	μ	$3.2 \times 10^5/(t - 40)^{3.5}$	$N\text{-}s/m^2$
Viscosity, SAE-50	μ	$1/bt^m$; $m = 2.33, b = 0.0021$	$N\text{-}s/m^2$

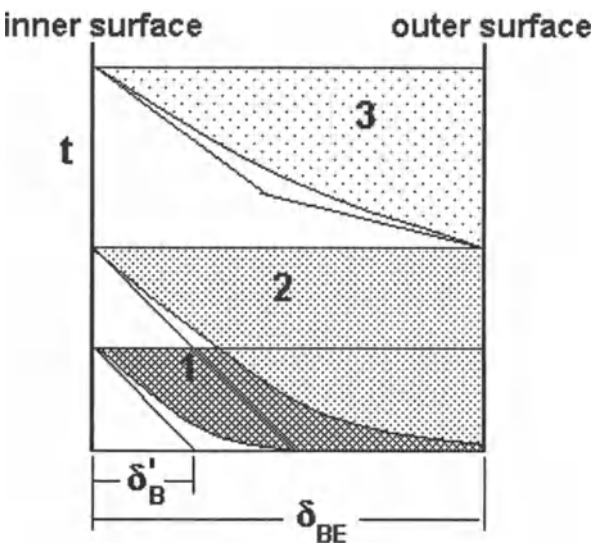

FIGURE 17-1. Successive temperature profiles in a bearing during start-up. The "temperature deficit" is shaded, and its area reflects the difference between the film temperature and the mean temperature in the solid material.

expansion is similar to that for the thin thermal-boundary layer in the treatment of dynamic seizure of chapter 6. When the journal is thin-walled and follows the film temperature without significant lag, the shaded region in each profile represents a temperature deficit in the bearing and would cause a corresponding expansion deficit relative to the journal.

The shaded region designated 1 in Figure 17-1 is for the initial heating; that designated 2 is near the maximum deficit for the start-up sequence. As temperature rises, δ'_B grows until significant heat begins to flow from the outer surface of the bearing. With continued operation, temperature rises to stabilization, and the steady-state temperature deficit of the nearly triangular profile, 3, may exceed any deficit during the start-up sequence. If it is sufficiently large, it will bring about seizure in the quasi-static mode of chapter 4. As shown, however, it is smaller than for condition 2, where the tip of the curved profile just reaches the outer surface.

An Estimate of Seizure during Start-Up

A closed-form expression that displays the important parameters can be set down conveniently when the temperature profile in condition 2 is approximated at the instant when it first bridges the thickness of the bearing. For a parabolic temperature profile, the mean temperature of the bearing is $t_{BE} = 0.33t_0$, if the body is treated as a slab of thickness δ_{BE}. If the bearing is a cylinder with $\delta_{BE} = r_0 - r_J$, then $t_{BE} = 0.27t_0$. This differs from the slab by only 10%, and supports the validity of the slab or thin-bearing model in chapter 6, as illustrated in Fig. 6-1. Throughout the start-up process, the viscous heating over a unit of bearing surface area is:

$$W = \frac{\mu U^2}{h_C - h'} \tag{17-1}$$

The thermal boundary layer thickness is $\delta_{BE}/2$ when the toe of the parabola is at the outer surface. If all of the heat from the film passes into the bearing.

$$W_B = W = \frac{2Kt_0}{\delta_{BE}} \tag{17-2}$$

where t_0 is the bore temperature of the bearing. Returning to the thin bearing case, the encroachment or relative expansion is:

$$h' = r_0\varepsilon(t_0 - t_{BE}) = \frac{2r_0\varepsilon t_0}{3} \tag{17-3}$$

Use of the simple power-law fluid, letting $1/\mu = bt^m$, yields a closed form expression:

$$h'^{m+1} = \frac{(2r_0\varepsilon/3)^{m+1}(\delta_{BE}U^2)}{2Kb(h_0 - h')} \tag{17-4}$$

Letting $H = h'/h_C$:

$$H^{m+2} - H^{m+1} + G_{SU} = 0 \tag{17-5}$$

The only variable that influences the limiting value of H is the viscosity exponent, m. The general level of viscosity, size of the system, and expansion coefficient are incorporated into the dimensionless G_{SU}, where

$$G_{SU} = \left(\frac{U^2\delta_{BE}}{2Kbh_C}\right)\left(\frac{2r_0\varepsilon}{3h_C}\right)^{m+1} \tag{17-6}$$

and

$$\begin{aligned} &\text{if } m = 1.85, \quad G_{SU} = 0.11023 \\ &\text{if } m = 2, \quad G_{SU} = 0.10547 \\ &\text{if } m = 2.333, \quad G_{SU} = 0.10157 \end{aligned} \tag{17-7}$$

The quantity G_{SU} now has two meanings: (1) It is a dimensionless coefficient with a magnitude near 0.1, and is modified by choice of the dimensionless viscosity exponent, m. (2) It is a group of design and operating variables. To aid in interpretation, let $R_J = r_J/h_C$, and let $\delta_{BE} = r_0$. Rearranging the variables:

$$R^{m+2}U^2 = (bG_{SU})\left(\frac{K}{\varepsilon^{m+1}}\right)\eta \tag{17-8}$$

The variables to the left of the equality are design parameters. Those in the first set of parentheses constitute a fluid property, where G_{SU} is a numerical value as in eq. (17-7). Those in the second set of parentheses are materials properties, and η represents the numerical contribution of the selected temperature profile. Since this derivation is based on the viscosity equation eminating from ambient temperature, for an SAE-30 fluid where $m = 1.85$ and $b = 0.061$, and for cast iron:

$$\begin{aligned} &bG_{SU} = (0.067)(0.11023) = 0.00739 \\ &\frac{K}{\varepsilon^{m+1}} = 6.83 \times 10^{15} \\ &\eta = 0.13236, \text{ for a parabolic profile (or } 0.1574381 \text{ for a quartic profile)} \end{aligned} \tag{17-9}$$

The following dimensional equation results, for the hollow-journal and parabolic temperature profile:

$$R_J^{3.85}U^2 = 3.26 \times 10^{14} \tag{17-10}$$

Seemingly, the most arbitrary assumption in the analysis is the parabolic temperature profile; however, when it is replaced with the quartic, $t = t_0(r_B - r)^4$, the change of η is small. As a test of eq. (17-10), when $U = 30$ m/s, $h = 1.99 \times 10^{-5}$. The following numerical calculations give a result close to this.

Finite Difference Representation of Bearing Temperature

A finite difference treatment of temperature in the bearing allows the simulation of the thermal history without losing sight of the physics. Fourier's equation for

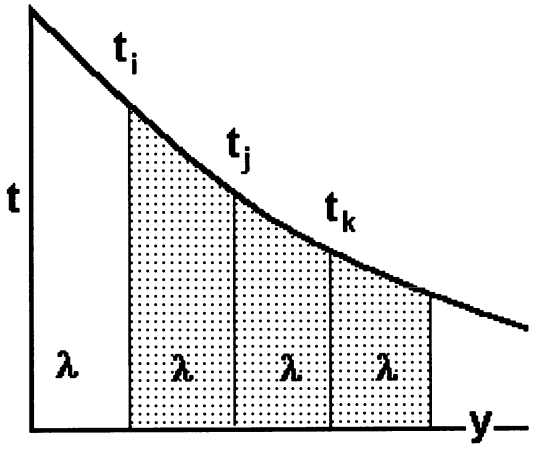

FIGURE 17-2. The temperature profile in the bearing is divided into narrow bands, with interfaces indicated by letter subscripts.

time-dependent axisymmetric heat transfer in a cylindrical solid is:

$$\frac{\partial t}{\partial \tau} = k\left[\frac{\partial^2 t}{\partial r^2} + \frac{1}{r}\frac{\partial t}{\partial r}\right] \tag{17-11}$$

To replace this by a finite difference equation, the radial y-coordinate is subdivided into bands of equal thickness, λ, between the bore and the outer surface, and their faces may be numbered from 1 to $(n-1)$. The temperature at the junction of an arbitrary pair of bands is designated t_j, and the finite difference equivalents of the first and second partial derivatives become:

$$\left(\frac{1}{r_j}\right)\left(\frac{\partial t}{\partial r}\right)_j \cong \frac{\left(\frac{\lambda}{I_J}\right)(t_k - t_j)}{2\lambda^2} \tag{17-12}$$

$$\left(\frac{\partial^2 t}{\partial r^2}\right)_j \cong \frac{t_i + t_k - 2t_j}{\lambda^2} \tag{17-13}$$

where i and k designate immediately adjacent interfaces, as illustrated in Fig. 17-2. Equality is approached as the limit when λ is made very small. To avoid confusion with the subscript $(\,)_J$, which refers to the journal, the temperature at the film interface is designated t_0.

The rate of temperature rise is:

$$\left(\frac{\partial t}{\partial \tau}\right)_j \cong \frac{k(t_{j,\text{new}} - t_{j,\text{old}})}{\delta t} \tag{17-14}$$

where the subscripts *old* and *new* indicate, respectively, the values before and after a step in time, δ_τ. The inner and outer surfaces of the bearing may be subscripted $()_0$ and $()_n$, respectively, and their temperatures are determined by external considerations. For the inner surface, the temperature gradient is forced by the heat

flux density, W_B, such that:

$$t_C = \frac{W_B \lambda}{K} + t_1 \tag{17-15}$$

At the outer surface, the gradient must be $\delta t/\delta r = (t_{n-1} - t_n)/\lambda = t_n/\delta_{CE}$, or:

$$t_n = \frac{t_{n-1}}{1 + \dfrac{\lambda}{\delta_{CE}}} \tag{17-16}$$

The mean temperature of the bearing, t_{BE}, is:

$$t_{BE} = \frac{2\lambda\left[\dfrac{t_C r_0}{2} + t_1 r_1 + t_2 r_2 + \cdots + t_{n-1} r_{n-1} + \dfrac{t_n r_B}{2}\right]}{r_B{}^2 - r_0{}^2} \tag{17-17}$$

The encroachment into the film is:

$$h' = r_J \varepsilon (t_C - t_{BE}) \tag{17-18}$$

The rate of viscous heating is W, and this is equal to W_B in the present model, where there is no heat loss to the lubricant or the journal:

$$W = \frac{\mu U^2}{h_C - h'} \tag{17-19}$$

The viscosity is a function of temperature, t_0.

Ernst Schmidt (1924) showed that there is a preferred time increment for the difference equations:

$$\delta\tau = \frac{\lambda^2}{2k} \tag{17-20}$$

When there is an existing *old* temperature distribution, the *new* temperature between each pair of elements, after a time interval $\delta\tau$, will be:

$$t_{j,new} = \frac{(t_i + t_k)_{old} + \left(\dfrac{\lambda}{2r_j}\right)(t_k - t_i)_{old}}{2} \tag{17-21}$$

To calculate successive temperature profiles, an initial set of temperatures is installed at each *internal* interface, designated 1 through $(n-1)$, with the option that this initial value may be zero throughout. The initial temperatures at the endpoints, t_0 and t_n, may be calculated by eq. (17-12) and installed. With this complete set of of *old* temperatures, eq. (17-21) is applied at each point to produce the *new* set of temperatures. From these and the original end temperatures, the encroachment, h', can be evaluated by eq. (17-18). At this point a new W_B may be calculated using eq. (17-2), and new end temperatures can be evaluated. The *new* temperatures become the *old* temperatures for the next iteration, and the process may be continued.

Start-Up and Stabilization

Three calculations are summarized in Table 17-3, showing the elapsed time, τ_H, in *hours*, the inner surface temperature, t_0, and the encroachment into the film, h'/h_0. The system is kept simple by restricting interest to the thin-walled journal, which tracks the inner surface temperature of the bearing, with minimal energy storage. This is not an unrealistic model in that hollow shafts are used in many systems to reduce weight with small sacrifice of bending stiffness. The solid journal is treated in subsequent paragraphs. The bearing is divided into 10 segments, so that $\lambda = 0.002$ m.

Under conditions for which there is no total collapse of clearance, the outer surface temperature, t_C, continues to rise for a long time (as much as six hours),

TABLE 17-3. Temperature History for a Bearing with Hollow Journal [SAE-30 oil, $h_C = 0.00002$ m, $r_J = 0.02$ m, $\delta_{BE} = 0.02$ m.]

$U = 30$ m/s		
τ_H h_r	t_J (°C)	h'/h_C
0.07	89	0.733
0.08	92	0.737
0.09	93	0.736
0.10	94	0.735
0.06	87	0.74 Max. encroachment
0.08	91	0.72
0.1	90	0.7
$U = 31$ m/s		
τ_H (h_r)	t_J (°C)	h'/h_C
0.02	73	0.68
0.03	78	0.71
0.04	86	0.76
0.05	94	0.82
0.06	110	0.95
0.065	179	1.61 Seizure
$U = 31$ m/s, 5.4 min acceleration ramp		
τ_H (h_r)	t_J (°C)	h'/h_C
0.08	78	0.68
0.09	85	0.73 End of ramp
0.10	89	0.75
0.11	93	0.77
0.12	96	0.78 Max. encroachment
0.13	98	0.78
0.14	99	0.77
0.15	98	0.74

TABLE 17-4. Stabilization of the bearing exterior for $U = 30$ m/s

τ_H (hr)	t_B (°C)
0.5	36
2.0	83
5.0	102

although the encroachment passes through its maximum value and settles down in a few minutes. Two power-law equations are listed for each oil in Table 17-2. The simpler one is used in the analytical approximation. The more accurate one is required for the numerical calculation in order to avoid zero fluidity at the ambient temperature. It is referenced on the natural zero of the fluid, yet temperature is measured from ambient, for which 20°C has been arbitrarily chosen. Hence t represents a rise from the residual temperature.

The three examples in Table 17-3 are near the threshold of instability. In the first two cases, the speed is achieved in approximately one minute and remains steady after that. In each example, the peak of encroachment is highlighted. In the upper two examples, the transient peak occurs within the first five minutes of operation, during which time little heat has transferred even as far as the middle of the bearing. Nevertheless, the inner-surface and film temperature is 90°C above ambient, with a reduction of viscosity to 0.0033 from the room-temperature value of 0.25.

The third data set in Table 17-3 shows the effect of slow ramping of the speed from rest. For operation that would be unstable for rapid acceleration, the long acceleration time serves to carry the system past the start-up instability and allow it to operate at steady state. The maximum encroachment is $h'/h_0 = 0.78$, when the film temperature reaches $t_0 = 96$°C. The retreat from this maximum shows that it is not a condition for seizure, but is an instantaneous phenomenon in a continuously changing system. This slow start-up is unreasonable for most applications, although it might apply to a large turbine.

The computation for $U = 30$ m/s was allowed to continue for several hours to determine the time required for stabilization of the system. The history of the outer-surface temperature is summarized in Table 17-4. In the last hour of operation the rise in t_n was 3 degrees, although it rose 23 degrees in the second hour,

Summary

The graphical construction shown in Fig. 17-1 suggests that a journal bearing will pass through two conditions where the film temperature exceeds the mean bearing temperature by a significant amount. The shortfall of bearing temperature is called a *temperature deficit*, and the bearing is said to have an *expansion deficit* relative to the journal. This deficit passes through a maximum when the thermal

boundary layer reaches midthickness in the bearing. This condition is exacerbated by rapid start-up of the system and can be controlled to allow operation at higher temperatures if the speed is brought up slowly. An analytical estimate of the deficit suggests an instability similar to the quasi-static failure phenomenon.

The treatment of film thickness in journal bearings is dominated by two ideas:

1. For radial heat flow, the expansion of either the bore or the exterior of a cylinder is determined by the mean temperature of the body, and independent of the temperature distribution. This is true of a cylinder in plane stress or in plane strain with zero end-load.

2. The temperature profile at maximum deficit can be approximated, and a dimensionless equation for expansion of the bearing and the journal may be derived. The analysis is forgiving as to details of the profile and can be used as expressed in eqs. (17-6) and (17-10). This is validated by a finite difference analysis of the system. In more general form, it is:

$$\left(\frac{r_J}{h_C}\right)^{m+2} U^2 = 0.01459 \left(\frac{bK}{\varepsilon^{m+1}}\right) \tag{17-22}$$

The *analytical* model exploits simplified power-law thermoviscosity, a parabolic temperature profile, and a slab model for heat transfer into the solid. The *numerical* model uses an accurate equation for thermoviscosity, and a calculated temperature profile that accounts for the cylindrical shape. Both predict almost the same critical speed. The analytical model permits a parametric study of the importance of the design and operating variables. The numerical model provides information on the critical time scale.

18
Diversion of Heat to the Journal

The analysis of start-up is continued in this chapter for the solid-journal system. In this common geometry, much of the viscous heat is diverted to the journal, which reduces the film temperature below that of the hollow-journal system. Both the bearing and journal have mean temperatures below that of the film. When the relative masses of these machine elements are similar, there is no net encroachment of solid surfaces into the film. For reasonable dimensions, however, the conditions for clearance loss and seizure can occur. A numerical model of the system provides an estimate of the critical operating conditions, and a modification of the analytical model of chapter 17 is recommended for seizure with a solid journal. Two viscosity equations are used in the analyses, one being an accurate power-law statement for which the natural zero of the fluid is removed 30 degrees from ambient. This is used in the numerical simulation. The other is a power law expanded from zero fluidity at ambient. Both agree at the elevated temperature of seizure, and the simpler law permits a convenient writing of an equation for critical operation.

Background

In chapters 6, 9, and 10, a transient heat input into the journal and bearing is treated for isoviscous flow. When the journal and bearing are of the same material, heat is initially divided equally between them, and the expansion of each component is determined by the heat stored in the component. Hence the component with the lower mass will experience the higher mean temperature and the higher thermal expansion. For example, when bearing thickness is equal to the journal radius, or $\delta_{BE} = r_J$, the bearing has three times the mass of the journal, and initially expands only a third as much. For reasonable operating speeds, the accumulated energy storage will lead to a loss of film thickness similar to that in the hollow-journal example. Heat loss to the environment is small in the time required.

There are additional resemblances between start-up and dynamic seizure. When the bearing thickness is selected to make the journal and bearing masses equal, both the journal and the bearing bore will expand almost equally, and seizure is avoided. This occurs when $\delta_{BE} = r_J/\sqrt{2}$, for a single material and equal partitioning of

R. A. Burton, *Heat, Bearings, and Lubrication*

heat. The choice of different materials and accounting for significant lubricant film resistance are discussed in chapters 9 and 10. When the bearing is beyond the critical thickness and the thermal boundary layer remains thin, and if the partitioning of heat remains unchanged, then encroachment will advance steadily with time, and the system will eventually seize. The feedback loop is broken when the calculated thermal boundary layer is a multiple of the journal diameter, and stored energy alters the partitioning of heat flow to the journal.

External cooling has little to do with the initial stabilization process. If the system begins to lose significant heat from the exterior of the bearing, the bearing temperature will lag journal temperature even further, and seizure will be hastened. Only axial heat flow to the shaft system or convection to a forced lubricant flow may quench the process. However, the estimate of δ_{oil} in chapter 13 shows that heat transfer to the lubricant is not a major factor in thin-film bearings. Similarly, the end-flow of heat from the thin thermal boundary layer will encounter a large resistance for axial heat flow down the shaft. At some state far removed from the transient events, the system will come to thermal equilibrium and all of the heat from the film will pass to these three modes of cooling.

Numerical Simulation

The analysis here closely follows the numerical treatment of Chapter 17. The list of special definitions is extended in Table 18-1. The equation set for heat storage in the bearing alone is given by eqs. (17-15) through (17-19). These may be modified to accommodate heat flow to the journal by subdividing it into elements, numbered from r_0 and designated by a $(\,)_J$, whereas the bearing quantities are designated by a $(\,)_B$. The new set of equations becomes:

$$t_C = \frac{W\lambda}{2K} + \frac{(t_{1,B} + t_{1,J})}{2} \tag{18-1}$$

TABLE 18-1. Selected Properties and Operating Conditions

Expansion coefficient	ε	10^{-5}	1/°C
Initial film thickness	h_C	5×10^{-5}	m
Mean bearing temperature	t_{BE}		°C
Mean journal temperature	t_{JE}		°C
Film temperature	t_C		°C
Diffusivity of iron	k	1.1×10^{-7}	m^2/s
Conductivity of iron	K	50	N/s-°C
Journal radius	r_J or r_0	0.02	m
Bearing thickness	δ_{BE}	0.02	m
Sliding speed	U	1→50	m/s
External convection	δ_{CE}	0.2	m, iron
Time increment	$d\tau$	18	s
Viscosity, SAE-30	μ	$7143/(t + 30)^{3.0104}$	N-s/m^2
Viscosity, SAE-30	μ	$m = 1.85, b = 0.061$	N-s/m^2
Fraction of heat to bearing	W_B		N/m-s
Fraction of heat to journal	W_J		N/m-s

At the center of the journal the temperature gradient must be zero:

$$\left(\frac{\delta t}{\delta r}\right)_{r=0} = \frac{(t_{n-1} + t_n)_J}{\lambda} = 0 \tag{18-2}$$

The mean temperature of the journal is:

$$t_{JE} = \frac{2\lambda\left[\dfrac{t_C r_j}{2} + t_1 r_1 + t_2 r_2 + \cdots + \dfrac{t_{n-1} r_{n-1}}{2}\right]}{r_0^2} \tag{18-3}$$

The encroachment into the film is:

$$h' = r_0 \varepsilon (t_{JE} - t_{BE}) \tag{18-4}$$

The rate of viscous heating is W, and the heat flux to the journal and bearing are given by:

$$W_J = \frac{K(t_C - t_{1,J})}{\lambda};\ W_B = \frac{K(t_C - t_{1,B})}{\lambda} \tag{18-5}$$

The viscosity remains a function of temperature, t_C, and the time step remains as in chapter 17.

Table 18-2 shows an example of the start-up history of a solid journal in the bearing, where $r_B/r_J = 2$, or $\delta_{BE}/r_J = 1$. Encroachment rises slowly because the journal mean temperature partially tracks the bearing mean temperature, and does not respond to the rapidly changing local t_C. Nevertheless, when operation continues, the temperature differential grows enough to reduce film thickness to zero. In the first events of start-up, the thermal boundary layer remains thin and near the film. Approximately half of the viscous heat initially passes to the journal.

TABLE 18-2. Temperature History for a Bearing with Solid Journal (SAE-30 oil, $U = 30$ m/s, $r_J = 0.02$ m, $\delta_{BE} = 0.02$ m, $r_B/r_J = 2$)

$h_C = 0.00000521$ m			
Time	Film Temperature		
τ_H	t_J	Encroachment	Temperature Ratio
(hr)	(°C)	h'/h_C	t_{SE}/t_{BE}
0.11	128	0.84	2.5
0.12	137	0.88	2.5
0.13	155	0.96	2.5
0.135	209	>1	Seizure
$h_C = 0.0000053$ m			
τ_H	t_J		
(hr)	(°C)	h'/h_C	t_{SE}/t_{BE}
0.09	109	0.73	2.56
0.10	113	0.75	2.54
0.11	116	0.76	Max. Encroachment
0.12	118	0.75	2.4

By way of reference, eq. (17-10) gives the seizure condition for the asymptotic thin, hollow journal in a bearing for which $r_B/r_J = 2$:

$$R_J^{3.85}U^2 = 3.26 \times 10^{14} \tag{18-6}$$

Using the data from Table 18-2, the numerical constant can be changed to apply to the solid journal.

$$R_J^{3.85}U^2 = 5.305 \times 10^{17} \tag{18-7}$$

For the present problem, the critical film thickness is less than the hollow-journal example, running about 0.0000053 m = 0.0002 in., which is an unusually small clearance. Changes of sliding speed have only a moderate effect since $h_C \approx 1/U^{0.52}$. The possibility of clearance loss should not be dismissed, however, because further investigation will show that waviness also plays a significant role. The time required for seizure varies with lubricant and bearing thickness; however, 0.135 hr, or 8 min, is typical. The film temperature is higher than for the hollow journal because the film thickness is much reduced.

Suppression of Encroachment

The previous calculations are restricted to a bearing for which $r_B/r_J = 2$. In the treatment of the dynamic seizure of chapter 6, a geometric parameter Γ was introduced to account for bearing thickness, as a multiplier of the coefficient of expansion, ε. It is defined as:

$$\Gamma = \frac{(r_B/r_J)^2 - 2}{(r_B/r_J)^2 - 1} \tag{18-8}$$

TABLE 18-3. Bearing with Solid Journal, $r_B/r_J = 1.8$ (SAE-30 oil, U = 30 m/s, $r_J = 0.02$ m, $\delta_{BE} = 0.016$ m)

$h_C = 0.0000036$ m			
Time	Film Temperature		
τ_H (hr)	t_J (°C)	Encroachment h'/h_C	Temperature Ratio t_{SE}/t_{BE}
0.04	104	0.70	1.7
0.05	119	0.79	1.6
0.06	139	0.90	1.5
0.65	166	>1	Seizure
$h_C = 0.0000037$ m			
τ_H (hr)	t_J (°C)	h'/h_C	t_{SE}/t_{BE}
0.06	120	0.77	2.94
0.07	126	0.78	Max. Encroachment
0.08	128	0.75	2.63

TABLE 18-4. Bearing with Solid Journal, $r_B/r_J = 1.7$ (SAE-30 oil, $U =$ 30 m/s, $r_J = 0.02$ m, $\delta_{BE} = 0.014$ m)

$h_C = 0.0000027$ m			
Time	Film Temperature		
τ_H (hr)	t_J (°C)	Encroachment h'/h_C	Temperature Ratio t_{SE}/t_{BE}
0.02	77	0.49	1.55
0.03	109	0.70	1.5
0.04	131	0.83	1.4
0.05	185	>1	Seizure
$h_C = 0.0000028$ m			
τ_H (hr)	t_J (°C)	h'/h_C	t_{SE}/t_{BE}
0.03	104	0.65	1.6
0.04	117	0.72	Max. Encroachment
0.06	124	0.64	1.25
0.10	102	0.01	1.00
0.12	96	−0.29	0.92
0.14	93	−0.55	0.86

In the present case, the heat stored in the bearing is approximately 1.5 times the heat stored in the journal. However, if the bearing is made thinner and if the same process limits the heat flux to both bodies, the relative thermal expansion would disappear when $r_B/r_J = \sqrt{2}$. The more complex interactions during start-up are simulated in Tables 18-3 and 18-4 for successively thinner bearings. As the bearing becomes thinner, the critical film thickness is reduced, and the ratio of bearing to journal temperature is reduced.

Table 18-4 shows another interesting phenomenon: The change from film shrinkage to film growth as operating time is continued beyond 0.01 hr. This time is short compared with that of the thick bearing of Table 18-2, and even for the thin film, seizure might be bypassed for slow spin-up (which may not be practical).

An Improved Design Equation

The critical film thickness can be normalized to unity for the thick bearing case by defining:

$$H_C = \frac{h_C}{0.0000053} \tag{18-9}$$

Data taken from the numerical simulations are plotted against a measure of bearing thickness in Fig. 18-1, and are found to lie close to a straight line. This suggests that a useful design equation for the solid-journal, single-material model can be adapted from eq. (18-6), with a modified numerical constant to account for reduction of

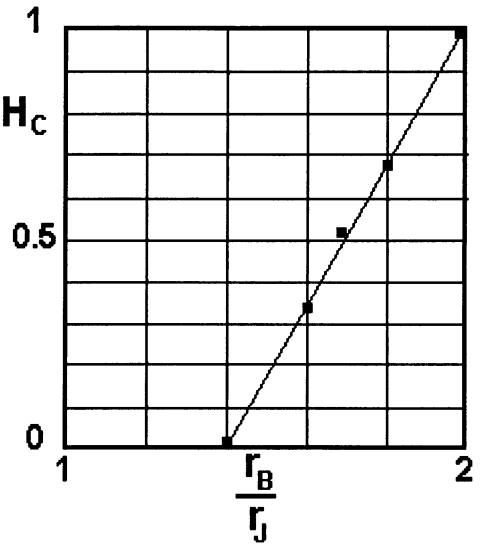

FIGURE 18-1. The effect of dimensionless bearing thickness on the dimensionless critical film thickness at seizure.

the role of the journal in the process of encroachment.

$$h_C = 7.6 \times 10^{-5} U^{2/(m+1)}(r_B - 1.4r_J) \tag{18-10}$$

The linear relationship to bearing thickness is simpler than eq. (18-8), and reflects a fortunate shift in the partitioning of heat during start-up.

A more informative equation results when eq. (17-22) is modified for the bearing-thickness effect, and the numerical constant is changed to accommodate the solid journal.

$$h_C = \frac{1.16(r_B - 1.4r_J)(u^2\varepsilon^{m+1})^{1/m+2}}{bK} \tag{18-11}$$

when $r_B/r_J \cong 1.4$. In chapter 9, this limit of safe operation is extended to different materials in the bearing and journal, and is suggested as a guide to start-up of solid-journal systems with differing materials. The disappearance of seizure from radial expansion does not mean that the bearing is free of possible trouble, however. The expansion of surface waviness proceeds independently.

The use of two equations for viscosity is dictated here by the need for accuracy extending to room temperature in the numerical simulations, which calls for the more accurate power law. Because the seizure condition typically occurs at elevated temperature, the simpler viscosity equation may be used in the design equation, and this allows eq. (18-11) to be more accessible.

When data for SAE-50 oil are introduced, $b = 0.0021, m = 2.333$, and eq. (18-11) gives:

$$h_C = 0.000091 \text{ m} \tag{18-12}$$

This much-increased critical thickness is approximately 0.0036 in., which would be considered a generous clearance in common machinery.

Summary

The graphical construction in Fig. 18-1 shows a journal bearing passing through two conditions for which the film temperature exceeds the mean bearing temperature by a significant amount. A similar diagram would apply to the journal. When the mass of journal material in the bearing length is much smaller than the corresponding bearing mass, the mean temperature of the journal will exceed that of the bearing. This difference will pass through a maximum when the temperature deficit in the bearing is near maximal. This occurs when the toe of the temperature distribution reaches the outer surface of the bearing. Numerical simulations of start-up-seizure are found to agree with the approximate analytical solution of chapter 17, but with a modified numerical coefficient. This is shown as Equations (18-10) and (18-11), which also include a linear correction for the effect of bearing thickness. The permissible film thickness becomes very small.

19
Coupling of Surface Waves and Radial Expansion

Start-up is simulated for a wavy surface on a cylindrical bearing, where thermo-viscosity and transient conduction are accounted for. The waves are sinusoidal, and growth is driven by differences in viscous heating at the trough and peak of the wave. The discussion shows how the zero-average or wave component of heat flux can be separated from the circumferentially uniform component, and how the coupling between these is taken into account. The thermal contribution to the growth of the wave is shown, numerically, to grow as a succession of quasi-static states. Rules are offered for the behavior of the waves and the uniform expansion; and a dimensionless generalization is proposed.

Background

In chapter 14, runaway growth is predicted for surface waviness on a bearing for high-speed sliding. In chapter 15, this growth is shown to be self-actuated above the threshold of instability, with the wave expanding exponentially in time. In engineering systems, the expansion of surface waviness is coupled with uniform expansion by nonlinear viscous heating. Hence, clearance change and wave growth must be re-examined in cases for which both take place together. These interactions are of particular interest in the events of start-up.

In chapter 16, a distinction is made between *uniform radial heat flow*, in the axisymmetric journal bearing, and *zero-average heat flow* into the bearing or journal surface. The zero-average heat flow is caused by surface waves and contributes to the growth of those waves. In the initial approach, the average heat flux is calculated at the peak and trough of a wave, recognizing that a numerical average over the full wavelength may provide some improvement in accuracy. The approximation is good until the minimum film thickness becomes very small. At that point additional analytical tools must be employed, as in chapter 21, where the limiting condition of patch contact at the wave peak is treated.

R. A. Burton, *Heat, Bearings, and Lubrication*

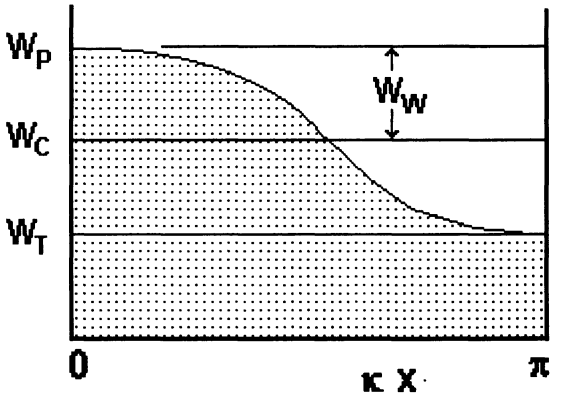

FIGURE 19-1. Components of viscous dissipation or heating in the lubricant film as produced by surface waviness on the bearing. Here W_C is the average between the peak and trough limits and W_W is the amplitude of the wave.

Nomenclature

Figure 19-1 shows the distribution of viscous heat generation in the film, with a uniform component, W_C, and a wave component with amplitude W_W. The intensity of heat generation at the peak of the wave is W_P, and that at the trough is W_T. The components of viscous heating are listed in Table 19-1. The quantity W' is the fraction of W_C that is conducted into the bearing surface, and W'' is the fraction of W_W going into that surface.

The components of film thickness may be similarly designated, where *single primed* quantities denote the uniform expansion and *double primed* ones denote expansion of the wave component. The quantity h_C is the initial mean clearance, h' is the change of mean clearance in uniform expansion, and h_W is the initial wave amplitude. The increment of amplitude caused by the wave component of heat flux is h''. When x is measured circumferentially from an origin at the wave peak, the local film thickness is:

$$h = h_C - h' - (h_W + h'')\cos\kappa x \tag{19-1}$$

where $\kappa = \pi/L$, and L is half the wavelength. Only conditions for which the wave components are in phase are treated in the present analysis.

The corresponding components of temperature are t_P and t_T, on the bearing surface at the peak and trough of the wave, respectively. The mean surface temperature is t_C, and the amplitude of the surface temperature wave is t''.

The Components of Heat Flux

The rate of heat generation in the film per unit of bearing surface area is:

$$W = \frac{\mu U^2}{h} \tag{19-2}$$

TABLE 19-1. Summary of Special Nomenclature

Film Thickness Components	
h	Local film thickness
h_C	Initial circumferentially uniform component of film thickness
h'	Circumferentially uniform reduction of clearance caused by the uniform-component of the temperature field
h''	Amplitude of waviness caused by the wave component of the temperature field
h_W	Initial waviness amplitude on the surface of a bearing
Temperatures	
t_P	Surface temperature at the wave peak
t_T	Surface temperature at the wave trough
t_C	Approximate mean temperature of bearing bore and journal surface
t_{JE}	Volume mean temperature of the journal; approaches t_C for thin, hollow journal
t_{BE}	Volume mean temperature of the bearing, see eq. (17-17)
t''	Modulus or amplitude of temperature wave
Viscous Heating	
W_P	Heat generation in the film per unit of bearing surface, at the minimum film thickness
W_T	Heat generation at the maximum film thickness
W_C	Circumferentially uniform component of heat generation
W_W	Amplitude of the wave of heat generation
W'	Mean rate of heat flux into the bearing surface
W''	Amplitude of the wave of heat flux into the bearing surface

At the peak of the wave it is:

$$W_P = \frac{\mu_P U^2}{h_P} \tag{19-3}$$

At the trough of the wave it is:

$$W_T = \frac{\mu_T U^2}{h_T} \tag{19-4}$$

The viscosity is determined by the film temperature at the specified location. The average heat flux density into the bearing surface causes the uniform component of expansion, and is:

$$W' = W_C \left(\frac{d}{h}\right) = \left(\frac{d}{h}\right)\left(\frac{W_P + W_T}{2}\right) \tag{19-5}$$

where d is the distance from the surface to the partition plane, determined by thermal constraints external to the film. The amplitude of the zero-average component of heat flux into the bearing is:

$$W'' = \left(\frac{d''}{h}\right)\left(\frac{W_P - W_T}{2}\right) \tag{19-6}$$

Here d'' is the distance from the wall to the partition plane for the wave component of heating. The important phenomena are retained when interest is restricted to systems in which all of the uniform component heat flow moves outward radially, in which case $d/h = 1$. This is in harmony with the models of chapter 17, and especially with the hollow-journal model. When the Hahn-Kettleborough condition is applied to the wave-component of heating, the material and thermal constraints on the journal do not affect the wave; and if the resistance below the bearing surface is small, $d''/h \cong 0.5$. The arguments in chapter 13 allow us to neglect the influence of circumferential convection on surface heat flux.

The Wave Component of Surface Displacement

When the thermal properties of the bearing material are constant, the temperature field may be broken into two superposed and independent fields. One is axisymmetric and determined by the uniform component of heat flux. The other varies sinusoidally around the circumference of the bearing, decays from the surface to the interior, and it is determined by the zero-average component of the surface heat flux. This wave component of the temperature field causes the surface wave to grow.

The numerical temperature fields of chapter 17 decay from a maximum at the inner surface of the bearing to small values at the outer radius. They vary smoothly between these and do not differ greatly from an exponential function. Figure 19-2 shows a semilog plot of a typical, normalized profile; the data points would lie on the straight line if it were precisely exponential. The limiting solution for steady heat transfer into a slab in chapter 12 has a thick exponential profile. The transient

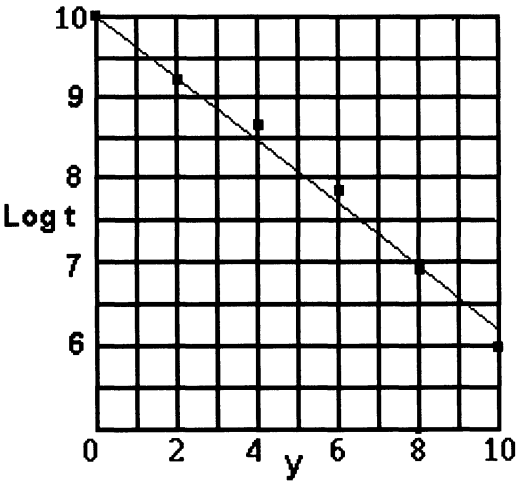

FIGURE 19-2. Semilog plot of a typical temperature profile in the wave component of the temperature field.

instability of chapter 6, and the wave of chapter 14 have thin exponential profiles. In the early stages of heating, thermal expansion is caused primarily by the amount of heat stored beneath the surface locally and is nearly independent of the wavelength or profile shape. All of these arguments suggest that an exponential temperature profile in the solid body is a good model for calculation of surface displacement. The analytical problem then becomes one of matching a calculated profile with the best exponential fit.

In chapter 15, a sinusoidal surface heat input, W, is considered where:

$$W = W'' \cos \kappa x \tag{19-7}$$

The temperature field is

$$t = t'' e^{-b''} y \cos \kappa x \tag{19-8}$$

Equation (15-4) gives surface displacement for this temperature distribution. In present nomenclature, it becomes:

$$h'' = \frac{2\varepsilon t''}{\kappa + b''} \tag{19-9}$$

For the simple two-dimensional wave, b'' is a function of time alone and may be evaluated at the surface as:

$$b'' = \frac{\left(-\dfrac{\partial t}{\partial y}\right)''}{t''} \tag{19-10}$$

Equation (19-10) corresponds to $1/\delta''$, where δ'' is the thermal boundary layer thickness for the wave component of the temperature field. The long-term or steady-state limit is $b'' = \kappa = \pi/L$, and h'' approaches the solution given by Dundurs rule. For either the asymptotic case or the rapid start-up, where $b'' \gg \kappa$, eq. (19-9) becomes:

$$h'' = 2\varepsilon t'' \delta'' \tag{19-11}$$

Here $t''\delta''$ is the "area" under the temperature profile, or "stored" heat. Should the surface wave be made of several Fourier components, and the profile of several exponential components,

$$h'' = 2\varepsilon \sum (t''d'')_1 + (t''d'')_2 + (t''d'')_3 + \cdots \tag{19-12}$$

Heat Transfer in the Solid

In chapter 17 the thin-bearing or slab-approximation of the bearing is used in the *analytical* model, and the cylindrical treatment is used in the *numerical* simulation. The overall results are closely related. For heat transfer into a two-dimensional slab, Fourier's heat flow equation may be written in x, y coordinates, where the x-coordinate is measured in the direction of sliding, lies in the surface, and originates

TABLE 19-2. Effect of Initial Waviness in a Bearing Bore on Critical Initial Film Thickness (for $r_J = r_0 = 0.02$ m, $\delta_{BE} = 0.02$ m, $U = 30$ m/s, hollow journal)

Initial Wave Amplitude h_W (m)	Thermal Boundary Layer Thickness δ' (m)	δ'' (m)	Critical Mean Thickness h_C (m)	Critical Minimum Thickness h_P (m)
0	0.012	—	0.0000198	0.0000198
0.000001	0.012	0.013	0.0000200	0.0000190
0.000005	0.012	0.012	0.0000229	0.0000179
0.00001	0.012	0.011	0.0000275	0.0000175
0.00002	0.012	0.011	0.0000370	0.0000170

at the wave peak. The y-coordinate is measured into the body from an origin at the surface.

$$\frac{\partial^2 t}{\partial x^2} + \frac{\partial^2 t}{\partial y^2} = \frac{1}{k}\frac{\partial t}{\partial \tau} \tag{19-13}$$

For temperature, $t_j \cos \kappa x$, at a position, y_j, near the surface,

$$\frac{\partial^2 t}{\partial x^2} = -\kappa^2 t_j \cos \kappa x \tag{19-14}$$

Evaluated for any t_j on the y-axis (at the origin of x), this becomes

$$\frac{\partial^2 t}{\partial x^2} = -\kappa^2 t_j \tag{19-15}$$

This may be incorporated into a finite difference expression similar to that for a slab in chapter 17.

$$\frac{-t_j(\lambda\kappa)^2}{2} + \frac{(t_j + t_\kappa)}{2} = t_{j,\text{new}} \tag{19-16}$$

where λ is the thickness of a hypothetical layer of bearing material, for computation, and $\lambda\kappa = \pi\lambda/L$. For two-lobe waviness (or an elliptical distortion of the bearing bore), $L = \pi r_0/2$, and when $\lambda = r_0/10$,

$$\frac{(\lambda\kappa)^2}{2} = \frac{1}{50} \tag{19-17}$$

This "correction" for tangential conduction is of the same general magnitude as the cylindricity correction in chapter 17. Because these may be conveniently included in a numerical simulation, they are taken into account in Tables 19-2 and 19-3.

The Uniform Component of Displacement

The uniform component of radial displacement for the bearing or journal is determined by the volume-mean temperature, as in chapter 17. Interior temperature

TABLE 19-3. Normalized Wave Amplitude and Film Thickness at the Threshold of Seizure (for $r_J = r_0 = 0.02$ m, $\delta_{BE} = 0.02$ m, $U = 30$ m/s)

	Normalized Wave Amplitude	Critical Minimum Film Thickness
Hollow journal	$h_W/h_{C,HJ}$	$h_P/h_{C,HJ}$
	0	1
	0.05	0.95
	0.25	0.904
	0.5	0.884
	1.0	0.878
Solid journal	$h_W/h_{C,SJ}$	$h_P/h_{C,SJ}$
	0	1
	1.0	1.66
	2.0	1.66
	3.33	1.66
	6.66	1.63
	3.33	0.76-Suppressed expansion of wave $h'' = 0$

profiles are found for the time-dependent surface temperature, t_C, using eq. (17-18) modified for present nomenclature.

$$h' = \varepsilon r_0 (t_{JE} - t_{BE})_C \tag{19-18}$$

For the hollow journal:

$$t_{JE} = t_C \tag{19-19}$$

and is close to the mean interface temperature of the bearing (or of the oil film).

Numerical Simulation of Start-Up

This analysis is based on operating and design variables similar to those in chapter 16. It is based on the limiting case of the hollow journal, with the SAE-30 fluid, and a single material for the journal and bearing (iron). Beginning with a film thickness h_C and the initial h_W, the film thicknesses at the peak and trough of the wave are evaluated. At both locations the dissipation, W, is calculated, and the components W_P and W_T are used in eq. (19-5) and (19-6) to find W'' and W', respectively. These new variables are inserted into the equivalent of eq. (17-18) to find the temperature profiles for the circumferentially uniform and wave fields along the y-axis. The mean of the uniform component is then determined, and h' is calculated using eq. (19-18). The wave solution is used to evaluate b'' in eq. (19-10), and h'' is then calculated using eq. (19-9) with a selected κ. The new components of displacement are then used to find new rates of viscous heating at the peak and trough, whereupon the process is repeated.

The Effects of Initial Waviness

The radial thickness of the bearing is set equal to the bore radius (0.02 m). The speed is ramped up to 30 m/s in 100. The film thickness is calculated as a function of time, and the minimum is determined. Over a succession of trials, a value of the initial h_C is found at the threshold of seizure. For a thinner film, clearance disappears in less than 0.2 hr. For a thicker film, clearance passes through a minimum and then begins to open up. Near the peak of the wave, eq. (19-1) becomes:

$$h_P = h_C - h' - h_W - h'' \tag{19-20}$$

The condition described as "seizure" occurs when $h_P = 0$.

The thermal boundary layer thickness, δ'', for the wave is close to $1/\kappa$, which would be 0.01 for two-lobe waviness. This means that the wave component grows through a succession of quasi-static states, whereas the uniform component equilibrates much more slowly, as discussed in chapter 17. This is clearly different from the exponential growth of the wave of chapters 14 and 15. During the start-up, δ'' does not differ significantly from δ'.

When initial waviness is small, the critical initial film thickness is $h_C = 0.00002$, and is the same as that determined in chapter 17 for the axisymmetric, or "smooth," bearing. For the extreme case in which $h_W = 0.00002$, the critical minimum film thickness is $h_P = 0.000018$, which is not far from 0.00002.

Dimensionless Presentation of the Effects of Initial Waviness

The critical film thickness for the smooth cylindrical bearing serves as a reference condition. Repeating eq. (17-22) for the hollow journal:

$$\left(\frac{r_J}{h_C}\right)^{m+2} U^2 = 0.01459 \left(\frac{bK}{\varepsilon^{m+1}}\right) \tag{19-21}$$

For an iron system with SAE-30 oil, this becomes:

$$h_{C,\text{hollow}} = 0.000169 r_J U^{0.519} \tag{19-22}$$

For the solid journal, this may be modified to:

$$h_{C,\text{solid}} = 0.0000456 r_J U^{0.519} \tag{19-23}$$

In any case the critical film thickness can be calculated directly from design and operating parameters. All film thicknesses in Table 19-3 are normalized, or non-dimensionalized on $h_{C,\text{solid}}$ or $h_{C,\text{hollow}}$, as appropriate. The bottom row has the thermal wave suppressed to show the importance of the initial wave. Comparison with the fourth row shows that wave expansion is significant. For the solid journal the critical film thickness at the wave peak is nearly constant. For the hollow journal

it does not range far from unity, and can be represented by:

$$\frac{h_C}{h_{C,HJ}} = 0.86 + \frac{0.14}{e^r}, \text{ where } r = \frac{4h_W}{h_{C,HJ}} \tag{19-24}$$

Summary

In the events of start-up, the bearing passes through a maximum of "temperature deficit" at which the mean temperature falls below the bore temperature by a large amount. For the small bearing in our example, the peak of the deficit occurs in about 0.15 hr after the start of rotation of the journal. When the solid material, the lubricant, and geometric similitude are maintained, the time to seizure varies as r_J^2. The axisymmetric temperature profile is far from equilibrium; on the other hand, the wave profile passes through quasi-static states. This is concluded from the thickness of the thermal boundary layer, which is close to that for a steady-state wave. Efforts to exploit these observations have not been fruitful, however, and complexity of the simplified model is worse than that of the numerical simulation. Such a model would show us little more than the normalized calculations in Tables 19-2 and 19-3. The tie to operating conditions is given by eqs. (19-22) and (19-23) for cylindrical bearings. The critical minimum film thickness for all other conditions can be expressed as a ratio to this condition, and does not range far from the reference values shown in the tables. These tables also show that journal bearings with suppressed or negative encroachment under uniform heat flow are not free from wave effects.

Two additional concepts should be remembered: (1) The journal can carry waviness, which can grow independent of the wave on the bearing. (2) The nature of touchdown of a wave peak is not necessarily as catastrophic as running out of radial clearance. Ordinarily this will lead to patch-contact around the peak, and frictional heating on the patch will determine the severity of the surface damage. It is possible for a bearing to run with localized contact patches.

20
Secondary Causes of Waviness

Primary surface waves are present at the beginning of start-up and are caused by fabrication or assembly errors. Secondary waves are caused by: (1) nonlinear heating when the journal is eccentric in the bearing; (2) departure from cylindrical symmetry in the housing, which can cause waviness even when heat flux is uniform into the bore; and (3) mechanical constraints, which distort the bearing as it attempts to expand. None of these cause remarkable effects during start-up, but when the system is allowed to equilibrate with a strong thermal gradient in the bearing, the second and third types of waves will grow and can trigger a long delayed seizure.

Background

When bearing systems are viewed intuitively, mechanical constraints and bearing geometry are the most obvious sources of distortion. These products of design choices do have their roles, principally long after start-up as the system tends toward equilibrium. They may even change in sign during the process of equilibration. Their effects are frequently small unless perversity of the designer or legitimate interests of the experimenter maximize them.

To understand nonlinear heating caused by eccentricity, it is necessary to establish an appropriate analysis, and this leads to a retrospective appraisal of the peak-and-trough analysis of chapter 19 as well as the small-perturbation approach of chapters 14 and 15. In this context, the zeroth or uniform component of heating is extracted from the distribution produced by sinusoidal surface waviness, and may, be compared with that of geometrically pure Couette flow. The wave amplitude, W_W, in chapter 19 shares the same wavelength as the surface wave that causes it. In the present context, it becomes W_1, and is the first component of the heat wave. The second component, W_2, has half the wavelength of W_1. The surface displacement it causes corresponds to ellipticity, whereas the first component represents an eccentric movement of the bearing bore.

R. A. Burton, *Heat, Bearings, and Lubrication*

The Uniform Component of Viscous Heating

In chapter 19, viscous heating at the peak and trough of the surface wave is broken into *wave* and *uniform* components in eqs. (19-5) and (19-6). A more accurate approach samples the dissipation, W, at a large number of stations along the wave, and then extracts the mean and wave components from these. The improved estimates, denoted by a subscript e, are W_{Ce}, the uniform component, corresponding to the Couette component of prior analyses, and W'_e, the wave component, which may itself be decomposed into component waves of different wavelengths. To obtain the zeroth, or Couette, component, the average for N samples is obtained directly as:

$$W_{Ce} = \frac{W_i + W_j + W_k + \cdots + W_N}{N} \tag{20-1}$$

For example, the surface wave shown in Fig. 20-1, may be expressed as:

$$h = h_C - h'' \cos\left(\frac{\pi x}{L}\right) \tag{20-2}$$

The local viscous heating associated with it is:

$$W = \frac{\mu U^2}{h} \tag{20-3}$$

When these are combined and evaluated at 100 equally spaced stations along the wave, the data may be inserted into eq. (20-1), and W_{Ce} can be calculated for different values of h''/h_C, as listed in Table 20-1.

The left-hand column of Table 20-1 is the wave amplitude, h'', expressed as a fraction of the mean film thickneses. The second column shows that the uniform component of heating never departs far from that for pure Couette flow in a smooth cylindrical bore. This is a valuable finding for simplified models, and is not restricted to flow with eccentricity, but applies to an arbitrary sine wave.

The third column compares the calculated heating component with that from peak-and-trough analysis. Clearly, the peak-and-trough calculation overcorrects for the nonlinearity. The fourth column is a simple corrector intended to mimic the

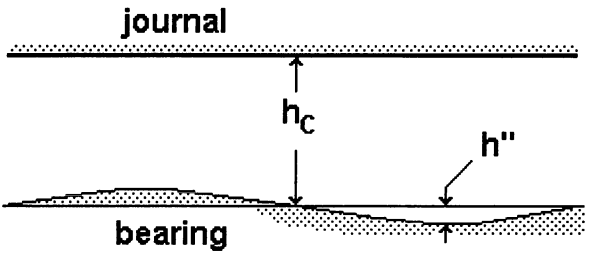

FIGURE 20-1. Simplified nomenclature for the fluid film between a smooth journal and a wavy bearing. The distance from peak to trough is L.

TABLE 20-1. The Uniform Component of Viscous Heating

Wave Amplitude h''/h_C	Uniform Heating $(W_{Ce}/W_C)_{smooth}$	Ratio to Eq. (19-5) $(W_{Ce}/W_C)_{approx}$	Corrector $1 - 0.3(h''/h_C)^3$ $(W_{Ce}/W_C)_{approx}$
0.5	1.03	0.97	0.96
0.6	1.05	0.95	0.94
0.7	1.08	0.92	0.90
0.8	1.11	0.88	0.85
0.9	1.18	0.79	0.78

third column, but in a form that is easily inserted into the calculation scheme of chapter 19. Tests of the modified calculation do not show significant changes in the results reported for start-up with an initially wavy surface because the system seems committed toward contact before it reaches a condition for which the correction is strong. A more sensitive case involves the seizure in radial expansion for a bearing with an eccentric journal. When tested, eccentricity of $h''/h_C = 0.8$ raised the critical film thickness by 2.4%, and an increase of eccentricity to 0.9 raised the thickness only by 3.9%. One must conclude that waviness does not have a strong effect on the axisymmetric seizure mode.

The Component Waves of Heat Flux

The array of samples in eq. (20-1) can be used to decompose the wave of W into components of selected wavelengths, by application of the Fourier integral, or its equivalent summation for the finite grid. This exploits the fact that for integration from $x = 0$ to $x = L$:

if $m = n$

$$a_m = \frac{2}{\pi}\int_0^L \cos\left(\frac{m\pi x}{L}\right)\cos\left(\frac{n\pi x}{L}\right)dx$$

if $m \neq n$

$$a_m = 0 \tag{20-4}$$

When a distribution, W, is made up of components of the type

$$W'' = \sum W_m \cos\left(\frac{m\pi x}{L}\right) \tag{20-5}$$

it follows that

$$\frac{W_m \pi}{2} = \int_0^L W'' \cos\left(\frac{m\pi x}{L}\right)dx \tag{20-6}$$

Thus, each component can be evaluated separately through the use of the appropriate m. This may be approximated for equally spaced data samples, δx apart.

TABLE 20-2. The First-Order Wave of Viscous Heating

Wave Amplitude h''/h_C	Normalized Heat-wave (W_1/h'')(const.)	Ratio to Eq. (19-5) $(W_{1e}/W'')_{approx}$	Corrector $1-0.3(h''/h_C)^3$ $(W_{1e}/W'')_{approx}$
0.5	1.04	0.97	0.96
0.6	1.10	0.95	0.94
0.7	1.19	0.92	0.90
0.8	1.33	0.87	0.85
0.9	1.61	0.77	0.78

Let W_m be the amplitude of the m_{th} component of the distribution, and x_j be the position of the heat-flux sample W_j. The equivalent of eq. (20-6) becomes:

$$W_m = \left(\frac{2}{\pi}\right)\sum_{j=0}^{L} W_j \cos\left(\frac{m\pi x_j}{L}\right)\delta x \qquad (20\text{-}7)$$

The sum is taken over the length L, which corresponds to half the circumference of the bearing.

Table 20-2 is based the division of the summation interval into 100 stations. Interest is restricted to the wave component with the same period as the surface wave. This would correspond to W_W in chapter 19, except that it is calculated from 100 data samples rather than two. The first column in Table 20-2 is the dimensionless amplitude of the surface wave. The second column has been normalized to unity for very small eccentricity, and may be thought of as a correction on the small amplitude solutions of chapters 14 and 15. Up to an eccentricity, $h''/h_C = 0.6$, the linear approximation is accurate. This justifies its use in those stability derivations and as a good approximation even in start-up.

The third column in Table 20-2 shows that the peak-and-trough approximation of chapter 19 is not bad, although it overcorrects for the nonlinearity when amplitude is large. The fourth column shows the same multiplier listed in Table 20-1, which serves again to correct the approximate treatment in chapter 19 to a more accurate value. Inclusion of this corrector in repeats of the numerical calculations does not change the predicted limits of operation significantly, however, and the peak-and-trough approach gives sound results.

Ellipticity Caused by Eccentricity of the Journal

Geometrically, the first component, W_1, causes only an eccentric displacement of the bore, when $2L$ is the circumference of the bore. It does not appear as a distortion of the cylindrical surface. The second component, W_2, causes an elliptical, or two-lobe, expansion when the heat is transferred into the surface. This is illustrated in Fig. 20-2, where the eccentric journal is shown in the bearing at the left. The second component of deformation of the bearing, much exaggerated, is shown at

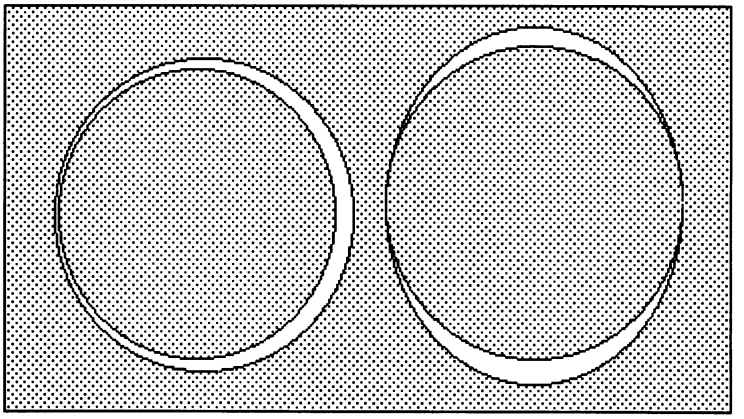

FIGURE 20-2. Illustration of eccentric journal placement (left), and second-component, or elliptical, displacement of the bearing surface (right).

the right. Numerical calculations of this effect are displayed in Table 20-3, for a range of eccentricities. Interest is displaced to the higher eccentricities where the departure from linearity is pronounced.

At the lowest eccentricity shown, the second-component wave is weak relative to the first component. At higher eccentricities, the second-component wave becomes dominant. This shows that a heavily loaded bearing operating with high eccentricity can acquire significant ellipticity, and this can be enhanced by the same mechanisms that amplify initial waviness.

Dunders rule may be applied to estimate the amplitude of the ellipticity, as in chapter 14. About half the heat is partitioned to the bearing during start-up, and almost all passes into it when steady state is approached. In either case, the arguments support the steady-state wave as a meaningful and safe approximation of the amplitude. For consistency, the wave amplitude produced by W_2 is designated h_2. When all of the heat goes to the bearing:

$$h_2 = \left(\frac{\varepsilon}{K}\right)\left(\frac{L}{\pi}\right)^2 W_2 \tag{20-8}$$

To evaluate this, let $\varepsilon = 10^{-5}$, $K = 50$, $L/\pi = r_J = 0.02$, $\mu = 0.01$ and, for

TABLE 20-3. Higher Order Heat-Waves Caused by Journal Eccentricity

Eccentricity h_1/h_C	First-Order Heat Wave W_1/W_C	Second-Order Heat Wave W_2/W_C	Third-Order Heat Wave W_3/W_C
0.5	0.182	0.034	0.0094
0.9	0.443	0.221	0.104
0.95	0.524	0.472	0.251
0.98	0.613	0.794	0.466

$h''/h_C = 0.95$, $W_2/W_C = 0.79$, all in consistent units for iron. Then:

$$W_2 = 0.79\frac{\mu U^2}{h_C} \tag{20-9}$$

Letting $U = 30$ m/s. and $h_C = 0.002r_J$:

$$W_2 = 177{,}750 \text{ W/m}^2 \tag{20-10}$$

It follows that:

$$h_2 = 2 \times 10^{-7} r_J^2 W_2 = 1.4 \times 10^{-5} \tag{20-11}$$

Since $h_C = 4 \times 10^{-5}$,

$$\frac{h_2}{h_C} = 0.35 \tag{20-12}$$

The effect of this wave component on critical film thickness can be appraised by reference to Table 19-2. In the first column, a wave amplitude of 0.01 mm is $0.36h_C$, where the critical mean thickness is $h_C = 0.0275$ mm. Without the wave the critical mean film thickness is $h_C = 0.0198$ mm, about a 30% difference.

Waviness Caused by the Uniform Component of Heat Transfer

The uniform component of heat flow may also give rise to waviness, which may then be amplified by the mechanisms of chapter 14. The source of this waviness may be subtly hidden in the bearing geometry. When the bearing is axisymmetric and governed by Dunders law, distortions of the external heat removal do not affect the curvature of the inner cylindrical bore.

Figure 20-3 shows a bearing cut from a plate, with thin sides and thick ends. Under steady uniform heat flux, the bore will become oval. However, if the bar is

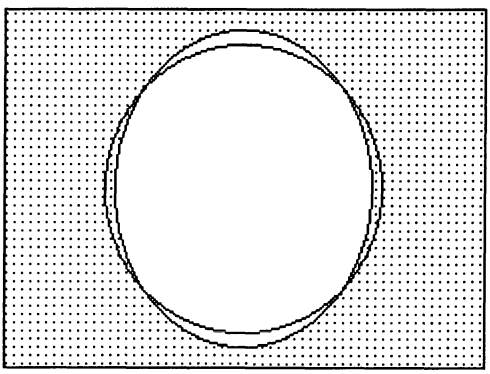

FIGURE 20-3. A simple geometry that shows elliptic deformation of the circular bore when a uniform heat flux passes radially outward.

heated uniformly with no net radial heat flux, the bore will remain cylindrical. For a sudden pulse of heating, the axes of the ellipse may be exchanged. When the ends are bolted to a large body and restrained from expanding, a uniform temperature rise will distort the bore to an oval shape with the short axis of the ellipse down the long axis of the bar.

Two kinds of distortion waves are examined here, one being proportional to the mean temperature of the bearing, and the other proportional to the uniform component of heat flux into the bearing. The temperature-controlled distortion can be scaled by a dimensionless multiplier, Z_T, on the uniform expansion component, where:

$$h_T = Z_T \varepsilon r_J t_{BE} \tag{20-13}$$

This enters the calculations like the primary wave, and may be amplified by the mechanisms of chapter 14. Because bearing temperature is not high during start-up, this wave may not be important then, but it can become a major factor as temperature rises toward equilibrium.

An independent distortion wave can be related to heat flux by Z_Δ

$$h_\Delta = Z_\Delta \varepsilon r_J (t_J - t_{BE}) \tag{20-14}$$

This has two possible maxima, one during start-up and one near quasi-static equilbration. Both of these waves may be set into the analysis of chapter 19, where:

$$h_P = h_C - h_W - h_T - h_\Delta - h'' \tag{20-15}$$

$$h_T = h_C + h_W + h_T + h_\Delta + h'' \tag{20-16}$$

These equations were introduced into the hollow-journal start-up calculation with an additional parameter to increase generality. The radial encroachment, h', is modified by a multiplier X such that:

$$h' = X \varepsilon r_J (t_J - t_{BE}) \tag{20-17}$$

When X is unity, the hollow-journal model is as in chapter 17. When X is near 0.25, encroachment is close to that for the solid journal; when X is zero, encroachment is suppressed by cooling the journal or by selecting the right journal material. These results are summarized in Table 20-4.

TABLE 20-4. Effect of Waviness Caused by Distortion of the Uniform Radial Expansion (for Modified Hollow Journal) ($r_0 = 0.02$ m, $\delta_{BE} = 0.02$ m, $U = 30$ m/s)

Normalized Expansion X	Dimensionless Distortion Z_Δ	Normalized Minimum Film Thickness $h_C/h_{C,hollow}$
1	0	1
1	1	1.5
0	1	0.85
−0.1	1	0.75

TABLE 20-5. Effect of Waviness Caused by Distortion of the Uniform Radial Expansion (for Solid Journal) ($r_0 = 0.02$ m, $\delta_{BE} = 0.02$ m, $U = 30$ m/s)

	Normalized Wave Amplitude $(h_W/h_C)_{solid}$	Dimensionless Distortion Z_Δ	Normalized Minimum Film Thickness $(h_P/h_C)_{solid}$
a	0	0	1
b	0.5	0	1.7
c	0	0.25	2.6
d	0	0.5	3.7
e	0.5	0.25	2.5
f	0.5	0.5	3.7

In each row of Table 20-4, the critical film thickness is normalized on the critical film thickness for an unsuppressed hollow-journal seizure without waviness. This corresponds to the conditions in the top row of Table 20-4. When a relatively large distortion, $Z_\Delta = 1$, is inserted, a 50% increase of clearance is required to avoid seizure. When radial expansion is then suppressed, letting $X = 0$ or $X = -0.1$, the critical film thickness is close to that for unsuppressed hollow-journal seizure. This shows that even when the radial expansion is under control, surface waves caused by the temperature gradient can cause seizure under realistic operating conditions.

Data for the solid journal are listed in Table 20-5, where row **a** shows the uniform reference condition, and **b** shows the effect of initial waviness. Rows **c** and **d** show the effect of distortion without initial waviness, and rows **e** and **f** show initial waviness has little effect in the presence of large distortion. As above, however, that minimum carries the contribution of the initial wave, since $h_P = h_C - h_W$. The most interesting finding is that even without an initial waviness and a small Z_Δ, avoidance of seizure requires a significantly enlarged film thickness.

Steady-State Wave Amplitude

The wave of most interest near equilibrium is h_T. Figure 20-3 shows how the mean temperature of the bearing is set by the large resistance δ_A,

$$h_T = \frac{Z_T \varepsilon r_J W \left(\frac{\delta_B}{2} + \delta_A\right)}{K} \cong \frac{Z_T \varepsilon r_J W \delta_A}{K} \tag{20-18}$$

Recall that the radial encroachment, h', is given by:

$$h' = \frac{\varepsilon W r_J \delta_B}{2K} \tag{20-19}$$

Without amplification of the wave, contact will occur when $h' + h_T = h_C$, or:

$$\left(\frac{h_C}{U}\right) = \left(\frac{\varepsilon r_J}{K}\right)\left(Z_T\delta_A + \frac{\delta_B}{2}\right) \tag{20-20}$$

If there is amplification, as given by eq. (14-24), then Z_T may be replaced by Z'', which is defined by:

$$Z'' = \frac{Z_T}{(U^*/U)^2 - 1} \tag{20-21}$$

Values of U^* for several materials, listed in Table 14-1, are typically large. Arguments in chapters 2 and 5 suggest that $\delta_A/\delta_B > 10$; consequently, if Z_T is greater than 0.05, it will dominate the loss of clearance.

Summary

The numerical calculations show that decoupling of the wave and uniform fields is a valid procedure. They show that Couette heating and the corresponding expansion take place whether or not the bearing surface is wavy. Similarly, the waves of surface heating and surface displacement are tied to one another and are almost independent of the uniform expansion. The general temperature level and viscosity of the fluid film is set almost exclusively by the Couette component of the flow, even when large-amplitude waves are present.

The presence of Couette heating does not necessarily lead to relative radial expansion between the bearing and the journal. This may be suppressed by vigorous cooling of the journal, or by choice of a low-expansion material for the journal. These measures do not affect the independent growth of the wave, which causes its own wave component of heating and is not influenced by external cooling—except for the influence of cooling on the viscosity. On the other hand, constraints on uniform expansion and departures from axisymmetry can cause surface waves proportional to the Couette component of heating.

In the events of start-up, the bearing passes through a maximum of "temperature deficit" where the mean temperature falls below the bore temperature by a large amount. For the small bearing in our example, the peak of the deficit occurs within about 0.15 hr after the start of rotation of the journal. When the solid material, the lubricant, and geometric similitude are maintained, the time to seizure varies as r_J^2. When operation is continued, the system approaches a second maximum in temperature deficit, which may precipitate seizure. The condition for this is given in eq. (20-15). The second and third classes of secondary waves therefore have two chances at closing the clearance in the bearing.

21
Load Concentration and Elevated Temperature on Contact Patches

When surface waves grow until they bridge the lubricant film, the solids touch on isolated spots or patches. Whether the patch is in a condition of boundary lubrication or elastohydrodynamic lubrication with a very thin liquid film, energy dissipation may be calculated by use of a friction coefficient. The concentrated heat input can lead to high contact temperature, and this can elevate the friction coefficient. Contact patches are the expected result of thermoelastic wave growth in chapters 14, 15, 18, and 19.

Background

Kenneth Johnson in *Contact Mechanics* (Johnson, 1985) devotes a section to thermoelastic contact and patch formation along with supporting material on contact temperature and heat transfer. The contact patch is affected by the materials and their geometry and is as varied in its origins as the expansion phenomena of the preceding chapters. It has been investigated in brakes in the pioneering work of Barber (1968, 1969, 1972), and in aircraft brakes by Kennedy and Ling (1974). Dow and Burton (1972, 1973) showed it to take place on a thin sliding vane, and this was followed by experimental verification by Dow and Stockwell (1977). The formation of patches in seals has been analyzed by Burton and Nerlikar (1975). This work was extended by Kilaparti and Burton (1978) to contact with wear, showing a triangular contact pressure distribution. Barber (1980) has provided a timescale for the formation or contraction of the contact patch. Johnson et al. (1988) have treated the change from line to patch-contact in gears as a possible explanation of scuffing. Supporting experiments are reported by Dow et al. (1987).

The Limit of Wave Growth and Patch Formation

Figure 21-1 shows three conditions as a surface-wave peak bridges the film and approaches the opposite surface. In segment **a** the surfaces are separated by h_P as identified in chapters 18 and 19. Because the film is thin, heat flux intensity is high.

R. A. Burton, *Heat, Bearings, and Lubrication*

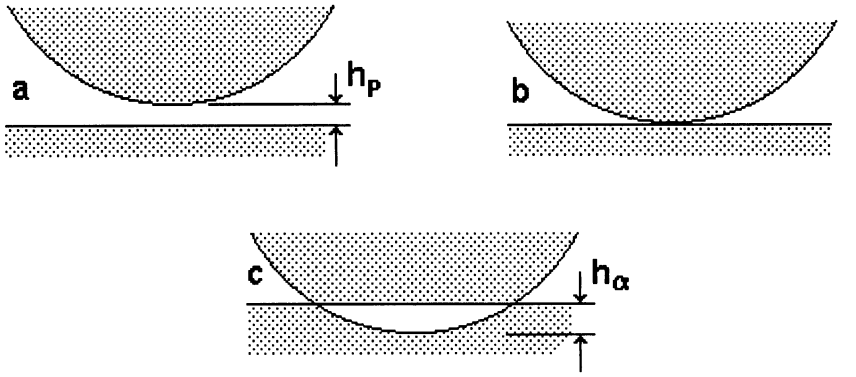

FIGURE 21-1. Idealized geometry of the wave tip as the wave grows to span the film and then continues expansion to produce a fictitious overlap.

Segment **b** represents the geometric condition of osculation, and **c** shows a fictitious overlap. In reality there is local deformation of the wave peak as osculation is approached, and overlap is prevented by elastic flattening of the surface. One may conjecture that two-dimensional waves will contact along lines or bands across the surfaces. On the other hand, even the plane-stress plates show thermal curvature along and across the edges, which would argue for initial patch contact rather than bands. Irrespective of these loosely defined transitional phases, the contact zones will contract to small patches at high sliding speed.

Figure 21-2 shows the hypothetical variation of heat flux as the point of osculation is approached. Film thickness moves from positive values at the right toward zero, where heat flux would ideally rise without limit. In reality the surfaces flatten. For typical oils, the friction coefficient levels off near $f = 0.05$. This is called elastohydrodynamic lubrication because of the interaction of hydrodynamic load support and elastic boundary deformation. The broken line in the figure symbolizes this condition. Somewhere to the left of the origin the flattened region contracts to one or more contact patches.

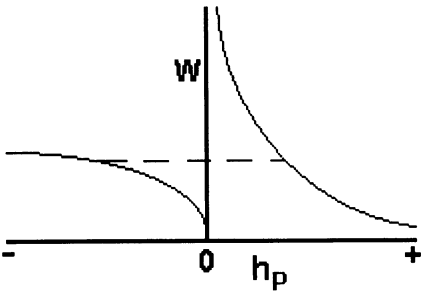

FIGURE 21-2. Heat flux, W, determined by peak clearance, h_P, which transitions from a positive value at the right to hypothetical interference at the left. The broken line symbolizes the bridging of the point of osculation by elastohydrodynamic lubrication.

The analysis of patch contact begins with the patch already formed as a disk on the interface, with radius α. Frictional heating is calculated from load and sliding speed, and the heat flux is assumed to be distributed over the patch. Surface deformation in the patch is decomposed into a thermal curvature calculated by Barber's rule, and a countercurvature caused by elastic compliance. In this way, thermoelastic "mounding" is combined with Hertzian contact theory to determine the combination of operating parameters and materials properties necessary to maintain the patch of contact. Patch temperature is estimated, using Holm's (1958) constriction resistance for passage of heat through a circular contact patch. Interest here is primarily restricted to the journal bearing near static equilibrium, where all the frictional heat passes radially outward.

Surface Curvature from Heat Flux

Figure 21-3 shows a large patch on the face of a disk. This might be the end of a bar or the face of a cam-follower, for example. Heat flux intensity, W, is distributed unformly over the patch. For steady heat transfer into a flat surface, Barber's rule relates the heat flux to the "mounding" of the surface, and is valid for zero-average conditions of heat input. The disk of heat input may be converted to such a function by subtracting a uniform flux across the entire face, leaving the input W_α on patch α, as illustrated in Fig. 21-4.

Figure 21-5 illustrates a cross section of the thermally deformed surface, with spherical rounding over the disk of heat input. Displacement decays with logarithmic and linear components outside the disk. The radius of curvature of the spherical surface is R, and is given by:

$$\frac{1}{R} = \varepsilon(1+\nu)\frac{W_\alpha}{2K} \tag{21-1}$$

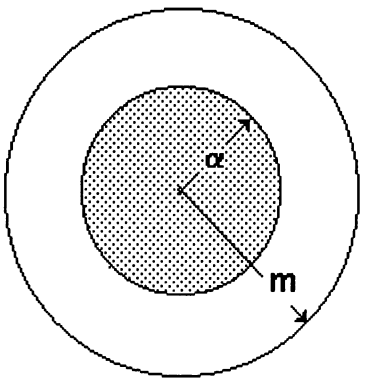

FIGURE 21-3. Schematic representation of a single patch of radius α on a circular surface of radius m.

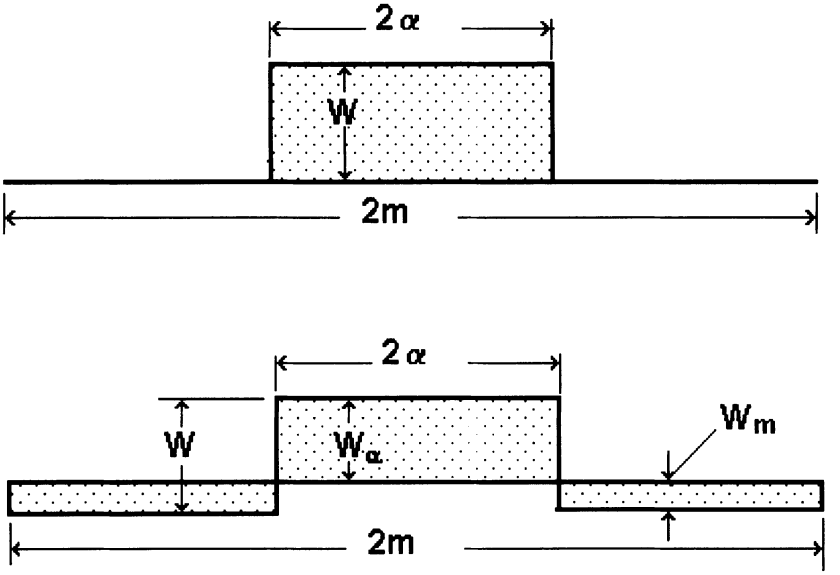

FIGURE 21-4. A uniform disk of heat flux in the upper segment is converted to a zero-average function, where W_α may be used with Barber's rule to calculate surface deformation.

When the heat flux is generated by dry friction,

$$W = \frac{fUF}{\pi\alpha^2} \tag{21-2}$$

Since $\alpha^2 W_\alpha = m^2 W_m$, it follows that $W_\alpha = fUF[1 - (\alpha/m)^2]$

$$R = \frac{2\pi K\alpha^2}{\varepsilon F[1 - (\alpha/m)^2](1 + \nu)} \tag{21-3}$$

Substituting values from Table 21-1:

$$R = \frac{2.41 \times 10^7 \alpha^2}{fUF[1 - (\alpha/m)^2]} \tag{21-4}$$

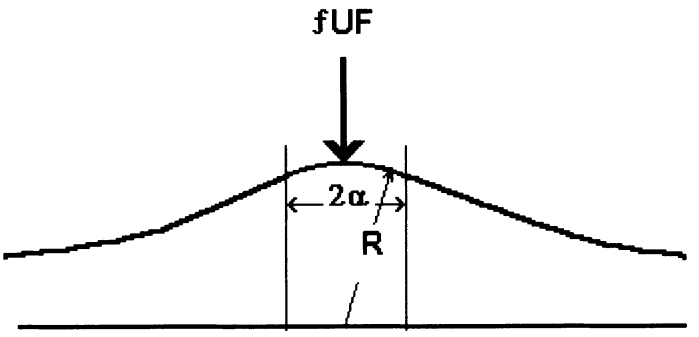

FIGURE 21-5. Schematic representation of a cross section of a surface mound caused by heat flux through a patch of radius α.

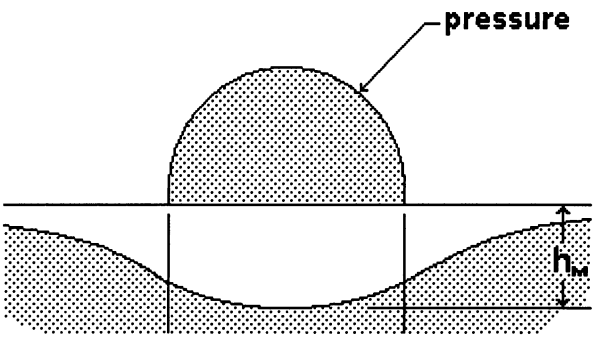

FIGURE 21-6. Pressure distribution (dark shading) on a contact patch. Below this is shown the elastically formed surface, with a maximum displacement, h_M, at midpatch.

A more precise derivation would allow for the fact that heat flux is not uniform over the surface of the contact patch, and that curvature would be greater than R at some places and consequently smaller at others. Nevertheless, uniform input gives an overall measure of the rounding of the surface on the patch.

Hertzian Contact for a Sphere Pressed against a Flat

When the rounded tip of a surface wave presses against a journal, they may meet as cylinder against cylinder at a transitional stage. However, if local heating is severe, this will contract to a small patch where $\alpha \ll r_J$. The radius of the patch is typically much smaller than r_J, and the interface is much like that of a ball of radius R pressed against a large flat surface. This is illustrated in Fig. 21-6, where an elliptical pressure profile on the circular patch leads to a concavity with spherical curvature.

When a sphere of radius R is held against the flat of the same material by a force, F, they will join on a disk of radius α such that:

$$\alpha^3 = 1.5(1 - \nu^2)\frac{FR}{E} \tag{21-5}$$

Substituting values from Table 21-1,

$$\frac{\alpha^3}{FR} = 0.68 \times 10^{-11} \tag{21-6}$$

This concept from classical contact theory applies equally well to bearing balls or thermal mounds.

Thermal and Elastic Conditions for the Same Surface Curvature

Solving eq. (21-6) for R,

$$R = 1.47 \times 10^{11}\frac{\alpha^3}{F} \tag{21-7}$$

TABLE 21-1. Symbols Used in Contact Patch Calculations

Symbol	Meaning	Units	Magnitude
f	Friction coefficient	—	0.02–0.4
U	Mean sliding speed	m/s	0–30
E	Young's modulus	$Pa = N/m^2$	2×10^{11}, for iron
F	Load on surface	N	—
k	Thermal diffusivity	mm^2/s	11, for iron
K	Thermal conductivity	W-m/°C	50, for iron
L	Wavelength	m	—
R	Radius of curvature of surface	m	—
W	Heat flux intensity	W/m^2	—
fFU	Heat flux to one body	W	—
α	Radius of contact patch	m	—
ε	Coefficient of thermal expansion	1/°C	10^{-5}, for iron
κ	Wave parameter (π/L)	1/m	—
ν	Poisson's ratio	—	0.3

Equating this radius to that of eq. (21-4),

$$1.47 \times 10^{11}\alpha^3 = \frac{2.41 \times 10^7 \alpha^2}{fU[1 - (\alpha/m)^2]} \tag{21-8}$$

Solving for α:

$$\alpha = \frac{1.64 \times 10^{-4}}{fU[1 - (\alpha/m)^2]} \tag{21-9}$$

Note that contact load, F, has disappeared. Increased force does not flatten the thermal mound but increases heating, which adds to the thermal expansion and compensates for the elastic displacement. The patch is most interesting when the radius is small, in which case the asymptotic solution is:

$$\alpha = \frac{1.64 \times 10^{-4}}{fU} \tag{21-10}$$

Typical disk radii have been calculated for selected sliding speeds and values of the friction coefficient, and these values are displayed in Table 21-2. Even for the lowest speed and smallest friction, the patch radius is small.

The Initiation of Patch Contact

Equation (21-9) can be rearranged to read:

$$fUm = \frac{1.64 \times 10^{-4}}{(\alpha/m)[1 - (\alpha/m)^2]} \tag{21-11}$$

The denominator is similar to groupings of variables found in the treatment of quasi-static seizure of bearings. Representing the group by G_α,

$$G_\alpha = \left(\frac{\alpha}{m}\right)\left[1 - \left(\frac{\alpha}{m}\right)^2\right] \tag{21-12}$$

TABLE 21-2. Radius of an Isolated Contact Patch

Friction Coefficient	Contact Patch Radius α (mm)				
f	$U = 1$	$U = 2$	$U = 4$	$U = 8$	$U = 16$ (m/s)
0.02	8.20	4.10	2.05	1.03	0.51
0.04	4.10	2.05	1.03	0.51	0.26
0.08	2.05	1.03	0.51	0.26	0.13
0.16	1.03	0.51	0.26	0.13	0.06
0.32	0.51	0.26	0.13	0.06	0.03

For exceptionally good boundary lubrication, $f \approx 0.02$
For typical boundary lubrication, $f \approx 0.05 \rightarrow 0.1$
For a deficiency of surface-active additives, $f \approx 0.3$

As before, a range of solutions can be found by scanning through values of α/m from zero to unity. A maximum value for $G_\alpha = 0.3849$, and occurs at $\alpha/m = 0.58$. To form a spot:

$$fUm > 4.28 \times 10^{-4} \tag{21-13}$$

Defining U_{critical} as the smallest U for patch formation, this may be rewritten:

$$U_{\text{critical}} = \frac{4.28 \times 10^{-4}}{fm} \tag{21-14}$$

Returning to the primary variables, this may be written:

$$U_{\text{critical}} = \frac{24.5K(1-\nu^2)}{f\varepsilon Em} \tag{21-15}$$

The behavior of solutions of eq. (21-11) is illustrated in Fig. 21-7, which shows a low-speed region that is stable and a line showing a steadily shrinking patch radius

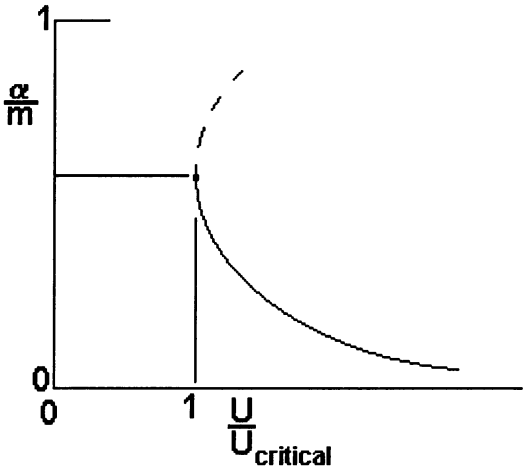

FIGURE 21-7. Solution of eq. (21-11) showing the reduction of patch size with increasing sliding speed, and a limiting speed below which patches will not form.

as speed is increased. The solution is double-valued; however, Burton (1975) has shown that the upper leg of the curve (the broken line) requires parting of the surfaces inside the contact patch. That study is not limited to the simplifications employed above, but finds solutions where there is a single contact pressure profile that controls both heating and elastic displacement.

The Definition of Face Area

The radius m is used in the preceding derivations to account for the size of the face on which the contact patch resides. It can be defined precisely in some cases, such as as the end of a cylindrical cam-follower, which is subject to rapidly repeated high-load, high-speed sweeps of the cam. In a simple bearing bored through a plate, the entire bearing may support several patches. For the bearing length, $2z_M$, and the radius, r_J, the face area is:

$$A_{total} = 4\pi r_J z_M \tag{21-16}$$

If there are N patches and the area per patch is πm^2, then

$$m = \frac{4 r_J z_M}{N} \tag{21-17}$$

This illustrates an important point, that the face area does not have to be a disk. Its role in reducing the heat input to a zero-average function is indifferent to shape.

Patch Temperature

Ragnar Holm (1965) derived an equation for electrical resistance between a surface patch and the interior of a semi-infinite body, which is given by:

$$R_{thermal} = \frac{1}{2\alpha K} \tag{21-18}$$

When the heat input to the patch is fUF, patch temperature, t, measured above the body temperature is:

$$t = \frac{fFU}{2\alpha K} \tag{21-19}$$

Using the large-m limit of eq. (21-9),

$$t = 61F(fU)^2 \tag{21-20}$$

In Table 21-3 the ratio t/F is listed for a range of sliding speed and friction coefficient. To interpret this, examples of F must be taken from practice:

- The load on a seal nose could range between 1 and 10 N.
- The load on a tappet could be in the range from 500 to 1000 N.
- The load on a thrust bearing pad can rise as high as 5000 to 10,000 N.

TABLE 21-3. Contact Patch Temperature

Friction Coefficient	Temperature/Load Ratio t/F(°C/N)				
f	$U = 1$	$U = 2$	$U = 4$	$U = 8$	$U = 16$ (m/s)
0.02	0.024	0.098	0.39	1.56	6.24
0.04	0.197	0.39	1.56	6.24	25.0
0.08	0.39	1.56	6.24	25.0	99.9
0.16	1.56	6.24	25.0	99.9	399
0.32	6.24	25.0	99.9	399	1599

For a seal, let $F = 5$ N, $U = 8$ m/s, and $f = 0.05$. Then

$$t = 125°C \tag{21-21}$$

This must be added to the bulk temperature of the body, which could be 100°C or more in the interior of a machine. Raising the friction coefficient to $f = 0.16$, and U to 16 m/s brings the patch temperature to

$$t = 1995°C \tag{21-22}$$

Recall that iron melts around 1600°C. This shows the sensitivity of contact temperature to operating conditions. When one considers that the friction coefficient is dependent upon surface films and these, in turn, are dependent upon temperature, something similar to the effects sketched in Fig. 21-8 must take place. Four different curves are sketched to represent the relationship between friction coefficient and temperature for three sliding speeds, with the highest speed at the left.

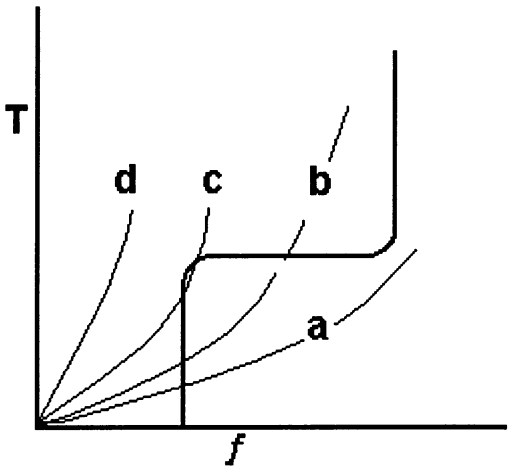

FIGURE 21-8. Four curves are shown for a range of sliding speeds. The chair-shaped curve is a simplified representation of friction coefficient as determined by surface temperature. On the low friction leg, boundary lubrication is maintained up to a critical temperature, where friction rises to a second level indicative of poor lubrication.

The chair-shaped bold curve symbolizes the variation of friction coefficient with temperature in the surface film, beginning at low temperature with a low friction coefficient, transitioning at a critical temperature, and then remaining high as temperature is increased. Two things are apparent: (1) There is a critical temperature at which the operating curve just touches the knee of the chair-shaped curve. This is the upper limit of low friction operation. (2) Once the knee is passed, friction and temperature rise as the crossing point of the curves moves to the top of the diagram. Thus a third kind of critical condition is found. The first is the critical speed for wave growth with hydrodynamic lubrication, the second is the critical speed below which patch contact cannot exist, and the third is the speed above which low-friction contact cannot survive on the patch.

Contact Load Associated with Fictitious Overlapping of the Surfaces

Consider the two-lobe wave that expands to bridge the film and continues to expand. This would lead to overlap of the surfaces if elastic accommodation did not take place. The force acting on the wave peak is determined by surface compliance and the nominal interference, and can be estimated from the relationship between surface load and patch displacement for a uniformly loaded patch. Although the surface waves reported originate and develop as two-dimensional waves, the surface is rounded even for the plane stress waves on thin plates. The reason is that under steady heat flow the interior of the plate is unstressed, and the elements are free to expand with temperature. When there is a gradient into the surface, the outer layers expand more than the layers below them, and the surface must bulge outward in accordance with Dundurs rule. The unstressed elements are free to expand across the edge of the plate as well, and the wave peak approaches a spherical surface. It follows that contact of a wave peak with the opposed surface is similar to the Hertzian contact of a sphere on a flat surface. This requires that the peak be pressed inward relative to distant points on the edge of the plate. This compliance may be estimated from the solution for the displacement of the center of a unformly loaded circular patch on a slab (see Timoshenko, 1970, p. 404). In present nomenclature:

$$h_1 = \frac{2(1-\nu^2)F}{\pi\alpha E} \tag{21-23}$$

This applies to a single body, and the net compliance for two bodies of the same material is:

$$h_M = \frac{4(1-\nu^2)F}{\pi\alpha E} \tag{21-24}$$

For the properties of iron listed in Table 21-1, this is:

$$h_{M,W} = 5.79 \times 10^{-11}\frac{F}{\alpha} \tag{21-25}$$

Returning to the surface wave in the bearing, where $y = h\cos\kappa X$, the curvature at the peak is $\kappa^2 h = \pi^2 h/L^2 = 1/R$. The patch radius may be found from eq. (21-6):

$$\alpha^3 = 0.68 \times 10^{-11} FR = 0.68 \times 10^{-11} \left(\frac{FL^2}{\pi^2 h}\right) \tag{21-26}$$

Taking an arbitrary $L = 0.02$ m, and $L/h = 500$, or $h = 4 \times 10^{-5}$ m as in previous examples,

$$\alpha = 1.9 \times 10^{-4} F^{1/3} \tag{21-27}$$

Returning to eq. (21-25),

$$h_{M,W} = 3 \times 10^{-7} F^{2/3} \tag{21-28}$$

To determine a typical load, let the wave grow to the thickness of the film, h, and then exceed this by $h/10$, in which case $h_M = 4 \times 10^{-6}$ m:

$$F = 48 \text{ N} \tag{21-29}$$

This is in the range of moderate contact loads.

A Thermal Mound on the Peak of a Surface Wave

When a surface wave makes contact and a patch forms, the supplemental friction contributes to an additional thermal mound that must be accommodated. Figure 21-9 shows the mound perched on the peak of a more lightly shaded wave. Inside the radius, α, the surface is of constant curvature with radius R, as above. Outside the patch the displacement decays logarithmically when $m/\alpha \gg 1$. Because the logarithmic function does not converge to a finite asymptote, estimation of the peak height is somewhat fuzzy, but is manageable for present purposes because the value of the logarithm is not sensitive to changes in its argument. The discussion of face area thus far sets limits on m in a reasonable

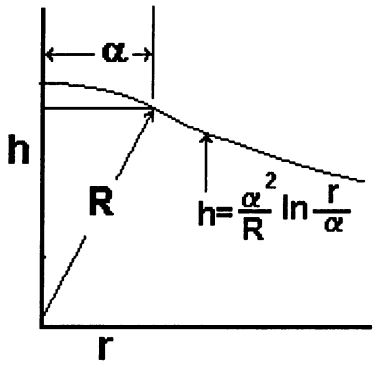

FIGURE 21-9. Schematic illustration of a bluff wave peak with an axisymmertic thermal mound that extends its nominal penetration into the mating surface.

system. The estimates of α in Table 21-1 may also serve as guides. For example if $r/\alpha = 10$, its logarithm r/α is 2.303. If r/α is increased to 20, its logarithm grows to 2.99. A reasonable value can therefore be picked to estimate the general magnitude of the patch height. The numerical contribution of the rise within the patch is 0.5. Consequently, a reasonable estimate of the patch peak is:

$$h_{M,P} = 3.5\left(\frac{\alpha^2}{R}\right) \tag{21-30}$$

Equation 21-4 allows an estimate of R, when reduced to the limit for large m/α.

$$h_{M,P} = 1.45 \times 10^{-7} fUF \tag{21-31}$$

Once a numerical value is assigned to the logarithmic term, the peak height is independent of patch radius. Using a load of 48 N, as in eq. (21-29), friction coefficient $f = 0.1$, and sliding speed 10 m/s, $fUF = 48$, and the peak height in meters is:

$$h_{M,P} = 7 \times 10^{-6} \tag{21-32}$$

Typical film thickness in prior examples is 4×10^{-5} m; hence the peak height is about 17% of film thickness. This height is therefore a major contributor to contact load and is a significant component of the process of seizure. It is tempting to iterate the process of interaction with increasing mound height; however, this becomes difficult to define when the thin, wave-peak film is opened by the expansion and reduces the viscous component of local heating. The indicators are clear as to the interpretation of $h_{M,P}$, nevertheless. If $h_{M,P}$ is small relative to h_M, then it may not be a major effect. If it is large, as in the present instance, conditions for extreme concentration of load and heating are at hand.

Time Dependence and Intermittency

The initial formation of a contact patch may begin with a large area of contact that contracts down to the steady-state value. Barber (1980) solved the time-dependent history of such a contact, and showed that a large change in size can be accommodated in the dimensionless time $k\tau/\alpha^2 \approx 10$. Taking the diffusivity from Table 21-1, this would call for formation of a patch with 1 mm radius in 0.9 s. If patch radius is reduced by half, the time increases fourfold. Barber showed that the process breaks away from rapid convergence as the asympote is approached; nevertheless, his results provide a time scale. Machine cycles range around 60 cps with higher frequencies occurring in turbomachinery, and lower ones in domestic applications. Surface heat flux for intermittent contact may be broken into a steady component and a high-frequency zero-average component, which has only a small effect on patch size.

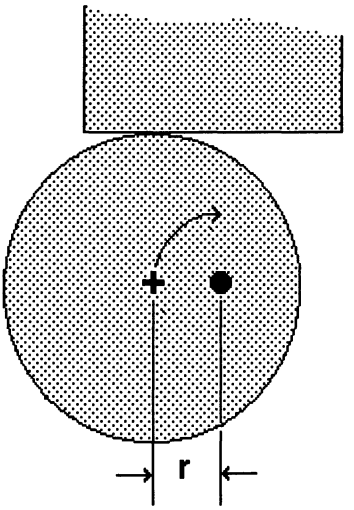

FIGURE 21-10. A flat-faced follower in contact with an eccentric cam. The center of curvature of the cam (cross) rotates about the dark circle, causing the follower to rise and fall while engaged in sliding contact.

A practical example of intermittent contact is the cam and follower shown in Fig. 21-10, where an eccentric cam produces a sliding contact on the face of the follower as it moves it vertically, up and down. If the follower is loaded by a spring or, say, pneumatic pressure, the simplest case is uniform load, F. The steady component of the local heat rate is $W = f P_{\text{mean}} U$. This reaches a maximum when the eccentricity is vertical, at the middle of the contact face. If the width of the swept area is $2Z$, and the length of the sweep is $2r$, then $p_{\text{mean}} = F/4Zr$. The maximum heat flux intensity becomes:

$$W = \frac{fUF}{4Zr} \tag{21-33}$$

This can cause a mounding of the surface and the interaction with elastic compliance as above. If it leads to full-time support of the load on a central patch, $P_{\text{mean}} = F/\pi\alpha^2$, and the severity is exacerbated. Following the path from the initial smooth contact to the small-patch condition is not easy. However, one can postulate the metastable condition, where smooth contact and patch contact represent two possible conditions of the system. When patch contact is itself stable, the system will remain in that condition once it is driven there. On a separate timescale, the patch, once formed, may indent plastically under heat, may melt, and may wear away.

In this discussion, a major question has been avoided, that of the partitioning of the steady component of heating to the bucket and the cam. This is a somewhat different problem from the elastohydrodyamic contact of freshly cooled surfaces, and is controlled by remote applications of coolant or blockages with heat dams. It

can be addressed only in the context of the full system; however, it may be simply determined in that context.

Summary

The distressed contact treated in this chapter may be considered as the result of the expansion phenomena associated with viscous heating in liquid films. Those are brought into focus beginning in chapter 16. During the transient events of start-up, the mean film thickness may change with time and even collapse to bring about seizure. Waves on the bearing surface may be amplified and ultimately bridge the film and contact the journal. Once the wave peak closes the film thickness to a small value, elastic deformation will flatten the surface, and elastohydrodynamic lubrication will provide a thin residual film. Although an elaborate series of phenomena affect the liquid in the film, including an immense increase in viscosity as the result of contact pressure, heat generation may be estimated as if the surfaces were in dry contact, and characterized by a friction coefficient near 0.05. Further loading may raise temperature and increase friction.

When contact is reduced to a small patch at the peak of a surface wave, heat flux gives rise to thermal mounding, which may further reduce the patch size. The flat geometry of a face seal or a thrust bearing allows the mounds to rise and support most of the applied load, providing a condition by which temperature and contact pressure may be estimated. When the waves are on the surface of a journal bearing, ellipticity, for example, will produce a condition in which the surfaces would overlap, if undeformed. This hypothetical overlap is accommodated by elastic deformation, which determines the loading of the wave peak. Again, this loading can lead to thermal mounding and an accelerated concentration of stress.

Even when relative radial expansion is controlled by selection of bearing material or blockage of the net heat flow, surface waves may grow independently, and can lead to failure. These waves may be the amplified result of imperfections in the machined bearing bore, or they may be caused by secondary effects such as constraints on expansion of the bearing. Ellipticity may be produced by a Fourier component of the heat flux distribution in a loaded bearing with eccentric shaft placement.

The examples chosen above represent realistic problems in which the partitioning of heat is easily specified. The formation of patches is predicted at modest speeds. In his early work, Dow examined a thin vane sliding on a cylinder or slab, with a large fraction of the heat flux moving to the slab. Despite this "cooling effect," the vane was found to distort and form intermittent contact on patches. When wear was taken into account, it was shown to control patch formation in the low speed range; but ultimately patches formed. Kilaparti and Burton (1978) showed that there is a wear rate that removes material so fast that no patches will form. Of course, this is not especially gratifying, because the surface recedes

from simple wear rather than wear compounded with high temperature and high stress.

In addressing problems such as the cam-follower, Johnson et al. (1988) investigated the condition in which line contact might break into patch contact. Their results seem to provide a reasonable explanation of the failure of such junctions. In this chapter an additional possibility is included, and that is the quasi-static bowing upward of the surface as a result of the time–mean heat input. A complete analysis must include both phenomena.

22
Load Support near Touchdown

Solutions are found for hydrodynamic support of a wavy bearing segment as the film thickness is made small over the wave peak. Short bearing and long bearing models are compared, and the latter is found to be appropriate in the thin film as contact is approached.

For either model, there is a region in which pressure in the film drops below atmospheric. The simplest treatment replaces the negative pressure by zero or atmospheric pressure. Reynolds (1886) proposed that the pressure gradient and pressure both go to zero at the same point, and this becomes the end of the continuous film. This condition is applied to long bearing flow.

The long bearing model follows a simple force-displacement equation, which may be coupled with an estimate of local heating to predict a condition for which surface curvature increases without limit.

Background

Banerjee's initial analysis (1976) and the treatment of chapter 14 have left a troublesome gap in the understanding of transition from a hydrodynamic load-bearing film to solid contact at the peaks of thermal asperities. This problem appears in seals and thrust bearings where thermal waviness can be the principal source of the fluid-dynamic lift that holds the surfaces apart. Yet, there is no question that a transition does take place where the surfaces are engaged at the wave peaks. Although the experiments show that the transition occurs close to the predicted threshold, a difficulty of interpretation arises because the steady-state operating condition for the film is also close to the threshold of instability. A puzzle exists as to how the system can cross that barrier.

The present chapter addresses the force and displacement in an open seal-like fluid film. This is done through application of the Reynolds equation to bearing geometry to answer two principal questions:

- What determines the minimum film thickness when a wavy surface slides over a flat surface, as in a seal or thrust bearing?
- When does film thickness degenerate and allow contact with the bearing surface?

R. A. Burton, *Heat, Bearings, and Lubrication*

These questions are approached by both the short bearing and long bearing models, each of which gives useful information. In the short bearing model, pressure is controlled by side leakage, a realistic condition for the geometries of high-speed bearings and seals when surface wave height is small relative to film thickness. The long bearing model, without end leakage, is more appropriate near the minimum film thickness where pressures are largely confined to a narrow band that spans the film and large pressure gradients appear in the direction of sliding.

Short Bearing Model

Osborne Reynolds (1886) derived the basic equation for flow in thin films with nearly parallel boundary surfaces. For simple sliding, constant viscosity, and constant fluid density, this equation may be written:

$$\frac{\partial}{\partial x}\left[h^3\frac{\partial p}{\partial x}\right]+\frac{\partial}{\partial z}\left[h^3\frac{\partial p}{\partial z}\right]=6\mu U\frac{\partial h}{\partial x} \tag{22-1}$$

Ocvirk (1952) showed that when the axial length of the bearing is small relative to radius, the circumferential pressure gradient becomes small, and the first term may be dropped from the equation. Additional simplification follows when the film thickness varies with x alone.

$$\frac{\partial^2 p}{\partial z^2}=\frac{6\mu U}{h^3}\frac{\partial h}{\partial x} \tag{22-2}$$

Figure 22-1 illustrates the geometry, with a stationary bearing surface, and the slider moving in the x-direction with speed U. The pressure in eq. (22-2) must vary parabolically in the z-direction from a maximum, p_{max}, at the axial centerline of the bearing, dropping to zero at the open ends. When the bearing length

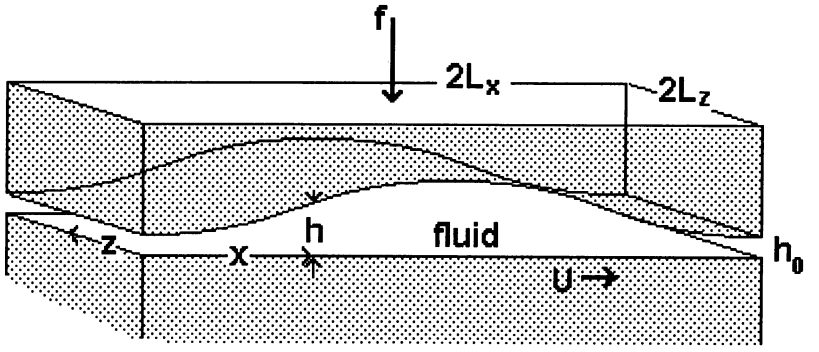

FIGURE 22-1. A segment of a wavy surface with a flat surface sliding past it. Normal load on the segment is f_{BL}, width is $2L_z$, and length is $2L_x$. Film thickness, h, varies in the direction of sliding. The minimum film thickness is h_0.

is $2L_z$,

$$\frac{\partial^2 p}{\partial z^2} = -\frac{2p_{max}}{L_z^2} = -\frac{3p_{mean}}{L_z^2} \tag{22-3}$$

The mean pressure is the more meaningful measure of load support.

Returning to eq. (22-1):

$$-\frac{p_{mean}}{L_z^2} = \frac{2\mu U}{h^3}\frac{\partial h}{\partial x} \tag{22-4}$$

This equation may be used to determine the pressure in a Couette flow modified by surface waviness on the bearing. This condition will occur when the journal operates eccentrically in a cylindrical bearing or operates concentrically in an elliptical bearing. A change to moving coordinates can transform this to an elliptical journal in a cylindrical bearing. When wave amplitude is h' and minimum clearance is h_0, at the peak of the wave:

$$h = h'\left[1 - \cos\frac{\pi x}{L_x} + \frac{h_0}{h'}\right] \tag{22-5}$$

and,

$$\frac{dh}{dx} = -h'\frac{\pi}{L_x}\sin\frac{\pi x}{L} \tag{22-6}$$

Returning to eq. (22-4), letting $\theta = \pi x/L$:

$$p_{mean} = \frac{2\pi\mu U L_z^2}{L_x h'^2}\frac{\sin\theta}{(1 - \cos\theta + h_0/h')^3} \tag{22-7}$$

The pressure force on an increment of bearing surface is:

$$dF = 2p_{mean}L_z\,dx = 2p_{mean}L_z L_x\frac{d\theta}{\pi} \tag{22-8}$$

Combining eqs. (22-7) and (22-8) and integrating over the length of the wave, $2L_x$, gives f_{BL}, the bearing load on the segment.

Figure 22-2 illustrates the short-bearing pressure distribution. Pressures less than ambient are encountered in the film, and, following the precedent of Sommerfeld (1904), these regions are assigned zero pressure. Knight and Ghademi (1992) have shown that the fluid film breaks into filaments in such regions, and although these filaments do not support load, they contribute to frictional heating as they are sheared between the surfaces. The Sommerfeld condition is achieved when pressure is positive in the limits $0 < x < \pi$. Dimensionless force, **F**, may be defined as follows:

$$\mathbf{F} = \frac{F}{4\mu h' U}\left[\frac{h'}{L_z}\right]^3 = \int_{-\pi}^{0}\frac{\sin\theta}{(1 - \cos\theta + h_0/h')^3}\,d\theta \tag{22-9}$$

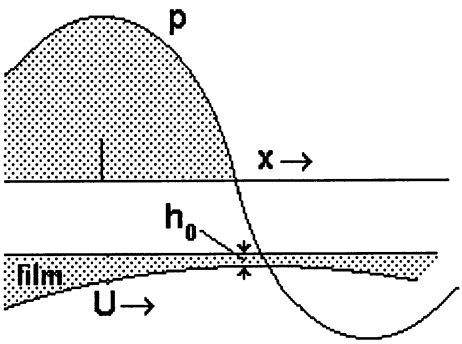

FIGURE 22-2. Schematic diagram of pressure distrubution overlaid on the bearing film. The minimum spacing is h_0; L is a truncated length of the pressure zone. The positive pressure is shaded, and the negative pressure is traced, although it is made zero in the calculation.

This function can be represented by two useful equations, at the extremes of h_0/h'. The most important limit in the present discussion is F_A, for operation near to touchdown for the short bearing model. The validity of these is demonstrated in Table 21-1.

$$\mathbf{F}_A = \frac{1}{2}\left[\frac{h'}{h_0}\right]^2 \tag{22-10}$$

At the other extreme, F_B, the wave amplitude is small, $h'/h_0 \ll 1$,

$$\mathbf{F}_B = 2\left[\frac{h'}{h_0}\right]^3 \tag{22-11}$$

The near-contact approximation, F_A, is accurate over a broad range, extending up to $h_0/h' = 1$, where the wave bridges half of the film. Combining eqs. (22-10) and (22-11), the dimensional load is given by:

$$F_A = \frac{2\mu U L_z^3}{h_0^2} \tag{22-12}$$

Neither the amplitude of the surface wave nor its length appear in eq. (22-12). The minimum film thickness is determined by the dimensional parameters: viscosity, load, and speed. It is completely decoupled from the thermoelastic curvature.

TABLE 22-1. Approximation of the Dimensionless Force

h_0/h'	F	F_A/F	F_B/F
0.001	493,590	1.012	—
0.01	4,993	1.001	—
0.1	49.88	1.002	—
1	0.444	1.125	—
10	0.0015	—	1.3
100	2×10^{-6}	—	1.02

At the other extreme, small wave amplitude, the force is proportional to h'. However, there is a significant range of operation for which the negative pressure in the film does not drop below atmospheric, and the lift would be zero for a simple viscous fluid. This problem does not affect the arguments in prior chapters on the coupling of waves and heating in the film.

Load Support of a Cylindrical Bearing

The force in eq. (22-12) applies to a flat slider, which might be the surface of a seal or thrust bearing. When the flat surfaces are wrapped around a cylinder, the lower one becomes the journal and the upper one becomes the bearing. For journal eccentricity, without additional waviness, the length $2L$ corresponds to the circumference, and $2L_z$ is the axial length of the bearing. The force produced by the pressure on an increment of the journal surface has two components. The force component in the direction of displacement is:

$$dF_y = dF \cos\theta \tag{22-13}$$

The force component perpendicular to this is:

$$dF_x = df \sin\theta \tag{22-14}$$

Each of these components may be integrated separately around the journal, giving f_x and f_y. The resultant of these forces is:

$$F_{CL} = \sqrt{F_x^2 + F_y^2} \tag{22-15}$$

Numerical integration of this force is shown in Table 22-2 along with the result for the flat slider and the power approximation, F_A, for large eccentricity or near contacts. Although not as precise as Table 22-1, this table remains useful. The reason this approximation works is that the main pressure effects are distributed over a nearly parabolic region adjacent to the point of nearest approach. Numerical experiments show that essentially the same results are found for a parabolic curve, when the maximum film thickness sets the limits of integration, and is $h_{max} > 4h_0$. More than 80% of the load is supported on the region where $h < 2h_0$.

TABLE 22-2. Load, f_{CL}, on a Cylindrical Journal

h_0/h'	F_A/F_{CL}
0.05	1.02
0.1	1.04
0.2	1.07
0.4	1.14
0.8	1.27

Long Bearing Model

Although eq. (22-13) is independent of the curvature of the surface wave, the validity of the short bearing model remains sensitive to this factor. When heat flow into the surface reduces the radius of curvature, the extent of the region of hydrodynamic support shrinks in the x-direction. This region of closest approach develops a significant pressure gradient in the circumferential direction, and local end-leakage is small. Insight into this condition comes from the Reynolds equation by dropping the axial pressure gradient and retaining tangential gradient. This is the long bearing model, for which eq. (22-1) becomes:

$$\frac{dp}{dx} = \frac{6\mu U(h - h_m)}{h^3} \tag{22-16}$$

Here h_m is the film thickness where pressure is maximum. It serves as a constant that may be adjusted to satisfy end conditions. This need does not arise in the short bearing model, for which end conditions are contained in the pressure calculation inside the continuous film. The lobe of the surface wave may be treated as a parabola with radius of curvature, r', at the point of nearest approach. The film thickness is represented by:

$$h = h_0 + \frac{x^2}{2r'} \tag{22-17}$$

When film thickness satisfies eq. (22-6), the radius, r', is given by:

$$r' = \frac{1}{h'}\left[\frac{L_x}{\pi}\right]^2 \tag{22-18}$$

Equation (22-17) may be nondimensionalized on r' by defining: $H = h/r'$; $H_m = h_m/r'$; $X = x/r'$; $X_L = L/r'$; $P = pr'/\mu U$. Then,

$$\frac{dP}{dX} = \frac{6(H - H_m)}{H^3} \tag{22-19}$$

Equation (22-18) becomes:

$$H = H_0 + \left(\frac{X^2}{2}\right) \tag{22-20}$$

Figure 22-3 illustrates the pressure distribution for the parabolic lobe, showing the parameters that satisfy the Reynolds end condition. Numerical calculations show that this is satisfied when the ratio of film thicknesses is $h_m/h_0 = 1.226$, and the dimensionless distance from the minimum thickness to the zero pressure point is $X_R = 0.0672H_0^{1/2}$. The same distance lies between the minimum film thickness and the pressure peak.

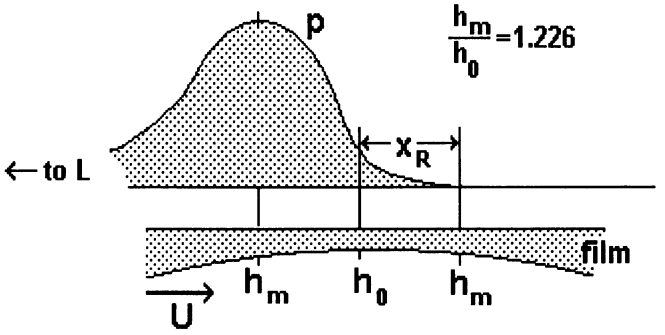

FIGURE 22-3. Pressure distribution near a parabolic wave peak, with Reynolds boundary condition. The pressurized film extends a distance, L, to the left. Beyond the minimum pressure, to the right, the pressure is assumed to be zero (ambient), although fluid may remain between the surfaces and may contribute to viscous heating as it is sheared.

To find the local pressure in the film, eq. (22-19) may be integrated from zero pressure at the position $x = -L$, or in dimensionless terms, $X = -X_L$:

$$p = \frac{6\mu U}{r'} \int_{-x_L}^{x} \frac{(H - H_m)}{H^3}\, dX \tag{22-21}$$

The force increment supported by the pressure is:

$$dF = 2L_z p\, dx \tag{22-22}$$

To find the total load, pressure may be integrated over the entire continuous film. The result may be written so as to define the dimensionless force, $\mathbf{F}$:

$$\mathbf{F} = \frac{F}{\mu U L_z} = 12 \int_{-x_L}^{x_R} P\, dX \tag{22-23}$$

The integrals are dimensionless, and when done numerically and for large L/h_0 they are accurately represented by

$$\mathbf{F} = \frac{0.4}{H_0} \tag{22-24}$$

For this calculation, $-L$ was evaluated where $h/h_0 = 10$. Numerical experimentation found $h_m = 1.226h_0$ and the distance to the end of the film, $x_R = 0.672(h_0/r')^{1/2}$. Returning to the physical variables:

$$\frac{F}{\mu U L_z} = \frac{0.4r'}{h_0} \tag{22-25}$$

The important difference from the short bearing equation is that the radius of curvature is retained. An insight into the conditions for film collapse is found when

account is taken for the influence of heating on r'. It may appear that wavelength has been lost; however, it is indirectly accounted for in r'. For journal bearings where both surfaces are curved, $1/r' = 1/r_J - 1/r_B$, and $L_x = \pi r_B$.

Viscous Heating near Touchdown

Chapter 11 shows that for Couette flow and small wave amplitude, the primary source of viscous heating is accounted for by:

$$W_C = \frac{\mu U^2}{h} \tag{22-26}$$

This will be called the local Couette component of viscous heating, and it is the heat per unit of surface area on the bearing. Although pressure-driven Poiseuille flow was shown to contribute a small amount to heating, it was omitted from the prior derivations. However, such flow must be considered here in this extreme departure from simple Couette flow. In long bearing flow, this is given by:

$$W_P = h\bar{u}\frac{dp}{dx} \tag{22-27}$$

Here $\bar{u}$ is the mean transport velocity of the Poiseuille component of the flow, is given by:

$$\bar{u} = \frac{U}{2}\left[\frac{h_m}{h} - 1\right] \tag{22-28}$$

It follows that

$$W_P = 3W_C\left[\frac{h_m}{h} - 1\right]^2 \tag{22-29}$$

For the film with the Reynolds end condition, this becomes:

$$W_P = 3W_C\left[\frac{1.226h_0}{h} - 1\right]^2 \tag{22-30}$$

And at the point of nearest approach, where $h = h_0$,

$$W_P = 0.15W_C \tag{22-31}$$

This supports the argument that the Couette component of heating is dominant, even in an extreme example. Drawing upon eqs. (22-25) and (22-31), and combining with eq. (22-26):

$$W = \frac{2.9UF}{L_z r'} \tag{22-32}$$

This is valid for long bearing flow, evaluated at the minimum film thickness.

Effect of Heating on Surface Curvature near Touchdown

The thermal contribution to surface curvature may be approximated by Dundurs rule for steady operation. Under the Hahn-Kettleborough boundary conditions in the film, and very small thermal resistance into the bearing as a consequence of the narrow zone of heat input, heat flux to the bearing is close to $W/2$, where W represents the combined Poiseuille and Couette components of heating. Letting the thermoelastic contribution of curvature be $1/r''$, Dundurs rule gives:

$$\frac{1}{r''} = \frac{\varepsilon W}{2K} \tag{22-33}$$

Drawing upon eq. (22-33) and combining this curvature with the geometric curvature, $1/r'$, eq. (22-32) becomes:

$$W = \frac{2.9Uf}{L_z}\left[\frac{1}{r'} + \frac{1}{r''}\right] \tag{22-34}$$

Drawing upon eqs. (22-34) and (22-33) to eliminate W,

$$\frac{2K}{\varepsilon r''} = W = \frac{2.9Uf}{L_z}\left[\frac{1}{r'} + \frac{1}{r''}\right] \tag{22-35}$$

Rearranging the terms:

$$\frac{r''}{r'} = \frac{0.69L_zK}{\varepsilon Uf} - 1 \tag{22-36}$$

Here r'' remains finite as long as:

$$0.69L_zK > \varepsilon UF \tag{22-37}$$

This is a *criterion for transition*, and is different from what might be expected from other models. For example, it is different from the patch model of chapter 21. When there is such a difference between criteria, the least severe operating condition is the reasonable design guide.

Viscous Heating near Touchdown

Estimates of the circumferential mean rate of viscous heating were made along with the numerical estimates of load support. The most accurate calculation incorporates the Reynolds end condition, and an estimate of local heating of the streamers, is given by:

$$W = \frac{\mu U^2}{h}\left[\frac{h_m}{h}\right] \tag{22-38}$$

This treats the streamer as beginning at h_m and continuing without a Poiseuille component of heating in the diverging film. The quotient in brackets allows for

TABLE 22-3. Mean Heating Rate on Bearing Surface Compared with Estimates

h_0/h'	h'/h_C	W/W_A	W/W_C
0.01	0.99	0.996	—
0.04	0.96	0.978	—
0.16	0.86	0.915	—
0.64	0.61	0.747	1.41
2.56	0.28	—	1.06
10	0.09	—	1.07

conservation of matter in the partially separated flow, and accounts for the necking-down of streamers as the film thickness increases beyond h_m.

Table 22-3 summarizes the results for mean heat generated per unit of bearing surface for the near-contact condition. The data are accuratedly represented by the following approximations:

$$W_A = 0.919\frac{\mu U^2}{h'}\left[\frac{h'}{h_0}\right]^{1/2} = 0.919\frac{\mu U^2}{(h'h_0)^{1/2}} \tag{22-39}$$

At the other extreme condition, where the wave height is small relative to film thickness, the data are represented by:

$$W_C = \frac{\mu U^2}{(h_0 + h')} = \frac{\mu U^2}{h_C} \tag{22-40}$$

In viewing Table 22-3, recall that h_C is the mean film thickness and W is the heat generated per unit of bearing-surface, averaged over the complete area of Fig. 22-1. The approximation of eq. (22-39) is seen to apply with fair accuracy even when the minimum film thickness is raised to half the wave amplitude, h'. The heating rate for simple Couette flow applies with fair accuracy at that limit and with increasing accuracy as wave amplitude is reduced. Additional calculations show:

- When the Poiseuille component of heating is removed, the estimated heating falls by 21%.
- When the separated region is treated as unbroken, full film flow, heating increases by only 3% above the streamer model.

In reviewing these calculations, the distinction between short bearing and long bearing flow becomes blurred as to the modeling of heating and turning resistance. The Poiseuille component is important only near the point of closest approach, and because the long bearing model applies there, this model may be extended to the entire film without raising the question of when the short bearing model should take over as far as heating is concerned. Heating in the Couette flow without a wave is not affected by the Poiseuille component. Table 22-3 therefore serves as a general guide to the overall viscous heating, with or without waves.

A Kind of Friction Coefficient

In the present instance, band loading is formed when a large-radius wave finds its peak very close to a second surface. Band loading can also occur in applications such as gear teeth or cams when the contacting members are strongly curved. Band loading may occur for contact with a vane when the vane is rounded on its narrow dimension. It is of interest to estimate the resistance to sliding under such a condition. The shear stress that opposes sliding of the journal can be incorporated into an equation for heat dissipation:

$$W = U\sigma_{xy} \tag{22-41}$$

Combining this with eq. (22-39):

$$\sigma_{xy} = 0.919\frac{\mu U}{(h'h_0)^{1/2}} \tag{22-42}$$

Equation (22-12) may be rewritten to give the normal stress on the moving surface:

$$\sigma_{yy} = \frac{\mu U L_z^2}{2L_x h_0^2} \tag{22-43}$$

The ratio of tangential stress to normal stress may be defined as a friction coefficient, f, which is given by:

$$f = 0.919\left(\frac{2L_x h_0^{3/2}}{h'^{1/2}L_z^0}\right) \tag{22-44}$$

This is not a convenient expression, but it does provide some guidance in interpreting experimental data. For example, the friction coefficient drops as the minimum film thickness is reduced. One would expect a bearing to turn more easily if it is wavy, in which case h' is large and h_0 is small.

A Static Mechanism of Lift

In some seals a small leakage is allowed, and this gives rise to a pressure gradient in the groove as lubricant flows across the step presented by the seal nose. Even when the shaft is not turning, this hydrostatic force maintains separation of the surfaces. This is illustrated in Figure 22-4, where a cross section is shown. Since the gradient varies as $1/h^3$, and the overall drop is fixed, the pressure distribution is "humped," and the height of the hump increases as h_2/h_1 is reduced. A small displacement of the upper ring changes the thin film by a larger fraction than it does the thick film. Thus mean pressure rises as the surfaces are displaced toward one another. This causes a spring-like restoring force that becomes greater as the surfaces are forced toward one another. Considerable effort in seal design is expended in balancing this pressure force with other forces acting on the seal rings, and can lead to noncontacting, machanically stable seals. In the present context, this effect can

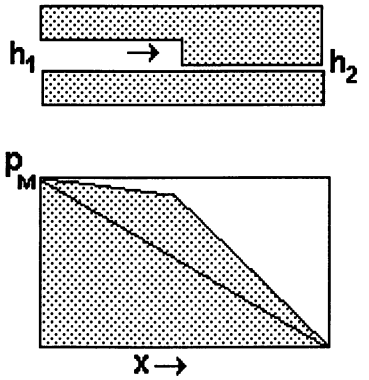

FIGURE 22-4. Seal cross section above pressure distribution (shaded). Flow is to the right, and the gradient is higher in thin-film region. Diagonal line across the pressure diagram is the condition for uniform film thickness. As the upper ring descends, the pressure-hump rises, and the mean pressure rises.

maintain a fixed spacing between the elements somewhat like the clearance in a journal bearing, and the surface waves are free to begin growth without altering film thickness. Otherwise, the film thickness is determined by load, as discussed previously.

Summary

In typical seals, the circumferential length of the fluid film may be several centimeters, whereas the width of the seal nose is one or two millimeters. Ordinarily this would be considered a short bearing. Similar arguments apply to high-speed journal bearings such as the big-end connecting rod bearings in an internal combustion engine. Nevertheless, when the mean film thickness is 0.01 cm or less, and when the minimum thickness under a wave peak may be one-tenth of this, the region of significant fluid pressure will have a circumferential extent of 100 times the minimum thickness, or ≈0.1 cm. This region is properly treated as a film in the long bearing mode. At the other extreme, where wave amplitude is small relative to the film thickness and wavelength is long, the short bearing model is appropriate. That limiting case is treated in chapter 12.

For the long bearing model, the relationship between film thickness and load is given by eq. (22-25). For a rigid journal forced into extreme eccentricity, $r' \cong L_x^2/\pi^2 h'$, where h' is the journal displacement. For an elliptical journal or bearing, h' would be the amplitude of the wave that generates the ellipticity. Equation (22-25) may be rewritten:

$$\frac{F}{\mu U L_z} = \frac{0.4 L_x^2}{\pi^2 h' h_0} \tag{22-45}$$

and h' will be close to h_C, the mean film thickness. This relationship is illustrated in Figure 22-5.

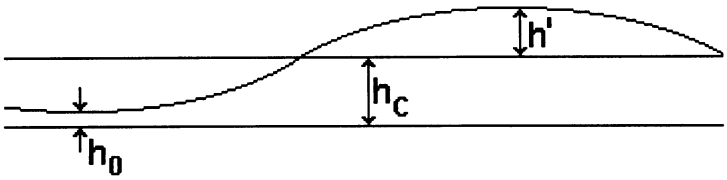

FIGURE 22-5. How the wave amplitude approaches the mean film thickness when the minimum film thickness becomes small.

The heat generated in the region of the minimum film thickness is given by eq. (22-32). As above, when the r' is replaced by wave parameters:

$$W = \frac{2.9\pi^2 h' U F}{L_z L_x^2} \tag{22-46}$$

This equation applies locally at the point of closest approach. For the mean rate of heat evolution in a journal bearing or seal film near touchdown, eq. (22-39)

$$W_A = 0.919 \frac{\mu U^2}{(h' h_0)^{1/2}} \tag{22-47}$$

holds. This may be adapted in many ways using the other equations. An example is the friction coefficient of eq. (22-44), which drops as load is increased or as minimum film thickness is reduced. The most interesting combination results from combining frictional heating with its effect on curvature near the wave peak when operating under load. A runaway rise in curvature occurs when:

$$\frac{\varepsilon U F}{L_z K} > 0.69 \tag{22-48}$$

It is different from many thermoelastic instability phenomena in that load is a major influence, whereas that discovered by Dow and Burton (1972), and other related criteria are dependent only on speed. At some load the contact becomes elastohydrodynamic and load decreases the surface curvature at the peak. Furthermore, the long bearing line of contact will at some point become unstable and transform itself into a small patch of contact, as discussed in chapter 21.

23
Design Guides

To focus the results of the wide ranging derivations in this monograph, questions are posed and answered. For example:

Q What are the most likely kinds of thermoelastic failure?

A There are three effects that arise under reasonable operating conditions:
1. Quasi-static loss of clearance for differing materials in the bearing and journal
2. Start-up, particularly with a poorly conductive bearing
3. Surface wave growth in high-speed sliding, as in seals and brushes

Each is discussed in this chapter under a separate heading.

Avoiding Quasi-Static Seizure

Q What do you mean by quasi-static?

A A system may pass through a series of states where thermal gradients have equilibrated as though it operated at steady state. If it were true steady state, operating conditions could not change, so we use the words quasi-static and quasi-steady or possibly quasi-equilibrium. Often, real systems can drift up to such an operating condition over time intervals in hours.

Q What happens in seizure or failure?

A The system may reach an operating condition where quasi-steady operation is not possible.

Q Is this simply a running out of clearance? Doesn't the journal expand relative to the bearing as a smooth, monotonic function of temperature?

A No. At first the relative expansion advances smoothly with increases of operating speed, for example, but a threshold is reached for which this is no longer possible, and clearance rapidly disappears. In some cases this occurs when the film thickness reduces to half of the initial (rest) value; in other cases the

R. A. Burton, *Heat, Bearings, and Lubrication*

film may thin down further until a smaller critical thickness is finally reached. Monitoring of operating variables may not offer a hint that the threshold is going to be crossed until it is too late.

Q Why do you say this is most important for differing materials in the bearing and journal?

A In chapter 5 the single material system is examined, and found to reach criticality only at very high operating speed. In chapter 7 differing materials are shown to change the threshold greatly and lower the critical speed when a poor choice is made.

Q What is different about the two cases?

A The single-material system loses clearance only when the mean temperature of the bearing and housing is below that of the journal. This allows relative expansion by the journal and encroachment into the fluid film. When the bearing has the lower coefficient of expansion, an overall temperature rise causes the journal to expand more than the bearing; this is the principal source of relative expansion. Of course, a gradient in the bearing will exacerbate this. This is discussed in chapter 7.

Q What if the bearing is laminated from two materials, say a ceramic bushing in a steel housing?

A Chapter 16 gives some examples of this for cylindrical material sandwiches. Some are better than others, and the rules for estimating their performance are outlined.

Q What if the bearing and housing are of noncircular or asymmetric shapes?

A In the two-material problem, when gradient effects are small, shape does not matter. A uniformly heated body simply enlarges without changing shape. When gradients are present and the bearing exterior is not cylindrical, waviness may appear in the bearing bore. Chapter 19 shows, however, that reasonable values for the distortion do not change the critical film thickness for safe operation greatly, when compared with the axisymmetric case.

Q Do thermal effects on fluid viscosity change the seizure conditions?

A Yes. See chapter 5 for example.

Q Why do you use such crude viscosity models for your lubricant fluids?

A The important fluid properties in seizure prediction are viscosity at the operating temperature and the slope or rate of change of viscosity. We have found that a simple power law with zero fluidity at ambient temperature serves well and gives easily interpreted equations. One has to be careful with this kind of model, but with care it is useful.

Q Why don't you put the best model available into a computer simulation and not worry about being careful?

A We can do that, but often we have trouble picking apart the roles of the different design parameters and operating conditions. Furthermore, even though the chemist and rheologist carefully characterize selected fluids, the oils used in practice vary greatly from the models. This is true for oils that share the same SAE designation. Real refinement in modeling an oil calls for viscosity-temperature measurements on the test fluid. Because designers neither know nor specify the viscosity function, they are best off using the simplest model that is realistic in their expected operating range.

Q You spoke of the mean temperature of the bearing determining the bore size. Does the temperature distribution have a big influence? Does a temperature distribution dropping from the inner bore have the same effect as a distribution dropping inward from a maximum at the outside?

A For axisymmetric heat transfer, the radial variation of temperature does not affect inner or outer dimensions of a cylinder. The mean temperature determines both. There may be some distortion for large gradients in bodies that are not cylindrical. But remember the quasi-static seizure is most important when two materials are used and the bearing and journal rise together in temperature with small contributions from the gradient, and even smaller distortion effects.

Q What can one do about this kind of seizure?

A
1. Even when the bearing surface must be made of a poor expander, it may be pressed into a second material that gives a favorable expansion rate for the bearing bore.
2. Forced lubricant flow through the bearing serves as a coolant, which helps maintain moderate temperature for the system.

Q If quasi-static expansion is under control, will be system be expected to offer no further trouble from thermoelastic phenomena?

A No. Start-up problems may still fail the system in simple radial seizure; furthermore, surface waviness may be amplified and cause surface contact at hot spots.

Start-Up Problems

Q What do you mean by *start-up*?

A When a bearing and journal are allowed to equilibrate at rest, there is a clearance between them, and temperature is at environmental ambient, or at machine ambient, which is regulated by a thermostat. As sliding commences, lubricant is sheared and heat flows into the journal and bearing. If the mean temperature of the journal rises faster than the mean temperature of the bearing, a large relative expansion can occur for a short time, and this can take the film to a seizure threshold similar to that for quasi-static operation.

Q Does this happen in a few seconds? Can one start the machine carefully (say, quasi-statically) and avoid the special time-dependent expansion effects?

A In typical systems, start-up phenomena may be important for a large fraction of an hour. For large systems, this time can be extended greatly. Only in very special systems can careful ramping up of speed keep the system near to the static equilibrium states. Most systems are expected to rise quickly to operating conditions.

Q What are the main design features that affect clearance loss in start-up?

A The principal effect is caused by the expansion of the bearing lagging that of the journal. This can be caused by:

1. a bearing more massive than the journal
2. poor heat conduction into the bearing

The first can be controlled by good design, which increases journal mass or reduces that of the bearing and housing. The second can be exacerbated by use of a poorly conductive bushing material that acts as a thermal insulator.

Q Will increased lubricant flow help?

A Not much. Often the start-up expansion events occur before the film is raised to a greatly elevated temperature, and typical amounts of coolant flow are not effective. Of course, massive lubricant flow could keep the film at sump temperature and avoid the problem. This usually requires much more flow than a designer wishes to budget.

Q How about bearing geometry?

A Other than in keeping bearing mass low, geometry tends not to matter very much. The thermal resistance to a thin thermal boundary layer in the bearing serves to raise the film temperature sufficiently to drive heat into the journal, against low thermal resistance. The rest of the journal-bearing system can be thought of as resting at ambient temperature.

Q This thin thermal boundary layer sounds like that involved in the transient seizure phenomenon of chapter 9. Is it?

A There is a close relationship between the exponential growth of temperature and the rise during start-up. In fact, it is virtually impossible to separate the phenomena experimentally or in numerical simulation. The same guides on conductivity of the bearing and bearing mass apply to both phenomena.

Q How about those models of the thermoviscous lubricant?

A The temperature-viscosity model is important, but the change is small, and the rest viscosity of the lubricant serves as the worst case. Thinning-out (viscosity drop) with advancing temperature serves to moderate the seizure phenomenon in a small way.

Q So the worst case is an insulating polymer or ceramic as the bearing, with a metallic journal?

A Yes.

Q How can one keep the journal from expanding, aside from forced lubrication?

A Some effort has gone into using a liquid held centrifugally in a hollow journal, but this does not help much unless it gets hot enought to evaporate and recondense at some remote point. A heat pipe has been suggested, in which a hollow journal is stuffed with metal wool, and a low-boiling-point fluid is introduced before the system is sealed with fluid and vapor. Neither system seems to offer much promise.

There are metals that have a flat expansion curve (zero expansion) in fixed temperature ranges. If the system does not stray far from such a range, a journal made of that kind of material might help.

A laminated journal with a good wear material having low thermal couductivity could help.

There is a minimum lubricant-film thickness that permits operation without seizure. If this thickness is permissible, then the problem is avoided. Other problems may arise with large clearance, such as dynamic orbiting of the journal in the clearance, and lack of sufficient "stiffness" of the film, when the shaft must be located precisely.

Q If careful analysis and selection of design parameters (especially initial film thickness) precludes such seizure, and if quasi-static seizure is avoided, am I home free?

A No. The bearing or journal may still deform elliptically, by the wave-instability phenomenon.

Controlling Waviness

Q What do you mean by surface waviness?

A The nominal mean surface of a full journal bearing is a cylinder. The nominal surface of a thrust bearing or a seal may be flat. Departures from these reference conditions constitute a zero-average contribution of the film shape. This zero-average perturbation may be called a wave.

Q What do you mean by zero average?

A A zero-average function has peaks that extend into the film and troughs that thicken the film locally, and the two affects average out to zero around the full circumference.

Q Why this abstraction? Why not simply take the shape of the bearing or journal surface as it is and simulate its interaction in the film?

A There is nothing wrong with doing this. However, a thermoelastic body responds differently to uniform radial heat input and to zero-average waves of heat flux.

Separating these two effects aids in understanding what is taking place. For example, clever selection of materials can suppress clearance loss from quasi-static and start-up modes, as discussed above, and yet a surface can be excited to runaway growth of waviness and the eventual touchdown of the surfaces.

Q Explain the waviness a little better.

A The simplest wave has one wavelength exactly equal to the circumference of the bearing. This is called eccentricity. When the journal, even if perfectly cylindrical, is pushed to one side, it acts as a wave peak intruding into the film at that side, with a corresponding thick-film trough opposite to the eccentricty.

Q What happens when eccentricity causes unequal heating around the bearing?

A Three things:

1. There is thermal distortion of the bearing, which simply displaces the position of the bore but leaves it round.
2. Nonlinear heating can increase the uniform component of heat flux and affect the symmetric component of clearance. This is discussed in chapter 20.
3. The nonlinear heating can produce a component of ellipticity in the bearing, and this may be self-excited to grow.

Q Does ellipticity represent a wave?

A Yes. The elliptical bearing will have two points of nearest approach to the journal and two regions of increased film thickness between these. As a wave, it has wavelength equal to half the circumference of the bearing bore.

Q Flats as well as cylinders were mentioned as carrying zero-average waves. What are these?

A Two important flat or open systems are face seals and thrust bearings. In either case the flat ends of short cylinders may engage in circumferential sliding. Texturing of the surfaces can produce a mean film thickness that supports the axial load. In addition, clever exploitation of radial leakage can produce such lift in a seal. These methods are briefly discussed in chapter 22. The flat surfaces can carry circumferential waves. The single-peak, single-trough wave may be identified as tilt of the moving element relative to the stationary one. The two-peak wave may be identified as a saddle shape with peaks opposite one another separated by troughs. When compared with the full bearing, the saddle corresponds to ellipticity and the tilt corresponds to eccentricity.

Q On the flat surfaces, do the waves themselves give rise to load support?

A Yes. This is discussed in some detail in chapter 22. A sizable load may be sustained by the wave peak. There seems to be a failure of the film under sufficiently strenuous operating conditions (sufficiently high temperature).

Q Could you summarize the failure modes involving waves?

A An instability can cause runaway wave growth on the boundaries of a Couette flow. This is discussed in chapters 14 and 15. Such growth may mean failure when it applies to ellipticity in a full journal bearing because the wave encounters a firm constraint when its amplitude equals the initial film thickness. In the flat-surface systems, growth of the wave may lead to the surfaces being supported on thermal mounds; but if load is not too high, the concentrated contacts may not be fatal to the system. Chapter 21 provides means for modeling the final hot spot. So there are three criteria to review:

1. When is a small surface wave strongly amplified?
2. When does the hydrodynamic film near the peak become unstable and allow the film to be broken?
3. What are the conditions of the final concentrated contact? How hot is it?

The equations for each effect may suggest ways of avoiding this problem; however, speed, mean film thickness, and sliding speed are the principal variables. These may be dictated by independent design considerations. Lubricant choice may delay the instability, and extreme pressure additives may allow low-friction sliding once the hot spot forms. To increase operating film thickness, tiny step bearings may be formed in the sliding surfaces.

Q Do the external thermal resistances affect these mechanisms of potential failure?

A The temperature of the system in quasi-static operation is strongly influenced by both internal and external cooling. This is particularly important in systems where journal and bearing materials differ. When the bearing and journal are of the same material, improved external cooling does not affect operation greatly because the heat flow rate is determined by the heat generation rate, and this is what generates the temperature gradient. The start-up phenomena are scarcely affected by external cooling. This is true also of waves. In both cases, heat flow is restricted to a region near the film-solid interfaces.

Symbols

a	Parameter in the power-law equation for fluidity, eq. (3-1)
A	Constant in equation for turbulent friction coefficient
A	Coefficient in eq. (6-14)
A	Surface area
b	Parameter in the power law equation for fluidity, with ambient reference temperature
C_F	Friction coefficient for turbulent flow
C_P	Specific heat (J/kg-°C)
d	Distance from partition surface to a wall
D	Diameter of cylinder
E	Elastic modulus (MPa)
f	Friction coefficient (dimensionless)
F	Force (N)
$\mathbf{F}$	Dimensionless force
G	Dimensionless group defined in eq. (5-9)
G'	Dimensionless group in wave instability; see eq. (14-10)
h	Heat transfer coefficient (W/m^2-°C)
h	Thickness of fluid film
h'	Thermally induced change of film thickness
h''	Contribution to wave amplitude from thermal expansion
h_C	Mean film thickness for wavy-wall flow
h'_0	Initial amplitude of time-dependent expansion
h_W	Initial wave amplitude
H	Dimensionless film thickness (h/h_0)
k	Thermal diffusivity (m^2/s)
K	*In tables:* thermal conductivity (W/s-m)
K	*In equations:* thermal conductivity of fluid (W/s-m)
K_B	Thermal conductivity of bearing material (W/s-m)
K_C	Thermal conductivity of external coolant
K_J	Thermal conductivity of journal material (W/s-m)
K_S	Thermal conductivity of solid material (W/s-m)
L	Half wavelength of surface wave

ln	Natural logarithm
m	Measure of surface around contact patch, chapter 21
m	Exponent in the power law equation for fluidity with ambient reference temperature
m_B	Mass per unit length of bearing (Kg/cm)
m_J	Mass per unit length of journal (Kg/cm)
n	Parameter in the power-law equation for fluidity, eq. (3-1)
Nu	Nusselt number (hD/K), dimensionless
p	Pressure, N/cm^2
Pe	Peclet number, eq. (12-4)
r_B	Outer radius of bearing (m)
r_J	Journal radius (m)
r_S	Radius of bearing bore (m)
r_0	Alternative radius for bearing bore in numerical treatment; see chapter 17
R	Dimensionless radius
R	Reynolds number
s	dT/dy (°C/m)
S	Slope of fluidity-temperature curve at T_M (°C)
t	Temperature measured from zero at the ambient (°C)
t_B	Mean t for bearing (°C)
t_J	Temperature of journal surface (°C)
t_M	Maximum value of t in fluid film (°C)
t_S	Temperature on inner surface of bearing (°C)
T	Celsius temperature (°C)
T_A	Ambient temperature (°C)
T_J	Magnitude of t on journal surface (°C)
T_M	Maximum temperature in film (°C)
T_S	Film temperature at wall (°C)
$T^\star$	Intercept of slope of fluidity function from T_M, Fig. 3-1 (°C)
T_0	"Natural zero" for power-law viscosity equation, Eq. (3-1) (°C)
T_σ	Temperature at which shear stress is maximal
u	Velocity in fluid (m/s)
$u^\star$	Velocity in film where $T = T^\star$ (m/s)
u''	Mean velocity of the pressure-driven component of a Reynolds flow
U	Sliding speed (m/s)
$U^\star$	Critical speed for runaway growth of surface wave (m/s)
v	Specific volume (m^3/kg)
w	Viscous heating per unit of fluid volume (W/m^3)
W	Viscous heating in film per unit of wall surface area (W/m^2)
W''	Viscous heating from the pressure-driven component of Reynolds flow
W_P	Viscous heating at the peak of a surface wave on the bearing
W_T	Viscous heating at the trough of a surface wave on the bearing
x	Coordinate in direction of sliding (m)
y	Coordinate normal to surface (m)

$y^\star$	Coordinate where temperature in fluid is $T^\star$ (m)
y_M	Coordinate where temperature in fluid is T_0 (m)
z	Coordinate parallel to surface and normal to U
α	Contact patch radius, chapter 21
α	Exponent in equation for turbulent friction coefficient
α	Parameter in linearized solution, eq. (3-12)
β	Exponent in eq. (6-16)
δ	Thermal resistance, as an equivalent fluid thickness (m)
δ_A	Thermal resistance external to bearing as a thickness of solid material (m)
δ_B	Thermal resistance of bearing as a thickness of solid material (m)
δ_{BL}	Thickness of velocity boundary layer (m)
δ_C	Thermal resistance, as a thickness of external coolant (m)
δ_{SA}	Combined thermal resistance between film and ambient as an equivalent thickness of fluid (m)
δ_{SL}	Thickness of laminar sublayer (m)
ε	Coefficient of thermal expansion (1/°C)
ϕ	Fluidity, reciprocal of viscosity (m^2/N-s)
Φ_E	Dimensionless parameter that accounts for property differences in bearing and journal
Φ_L	Correction applied to linear temperature drop in bearing
Γ_E	Dimensionless parameter for exponential disturbance in clearance
ν	Poisson's ratio
τ	Time (s)
μ	Viscosity (N-s/cm^2)
σ	Shear stress on plane parallel to a wall (Pa)
σ_{xy}	Stress in the tangential direction (Pa)
σ_{zz}	Stress in the axial direction (Pa)
ζ	Dimensionless group for expansion of composite tubes; see eq. (16-7)
$()_L$	Subscript refers to laminar regime
$()_R$	Subscript refers to rough-wall condition
$()_T$	Subscript refers to turbulent regime
$()_\mu$	Subscript indicates constant viscosity
$()_+$	Subscript indicates condition in which thermal expansion brings clearance to zero

Bibliography

B. N. Banerjee and R. A. Burton, Thermoelastic instability in lubricated sliding between solid surfaces, *Nature, 121* (1976a) 399–400.

B. N. Banerjee and R. A. Burton, An instability for parallel sliding of solid surfaces separated by a viscous liquid film, *Trans. ASME, JOLT, 98* (1976b) 157–166.

B. N. Banerjee and R. A. Burton, Experimental studies on thermoelastic effects in hydrodynamically lubricated seals, *Trans. ASME, 101*, Series F (1979) 275–282.

J. R. Barber, The influence of thermal expansion on the friction and wear process, *Wear, 10* (1967) 155.

J. R. Barber, *Thermal Effects in Friction and Wear*, Dissertation St. John's College, Cambridge, England (1968).

J. R. Barber, Thermoelastic inatabilities in the sliding of conforming solids, *Proc. Roy. Soc., A312* (1969) 381–391.

J. R. Barber, Distortion of a semi-infinite solid due to transient surface heating, *Int. J. Mech. Sci., 14* (1972) 377–393.

J. R. Barber, Letter to the editor, *Wear, 26* (1975) 423–428.

J. R. Barber, The transient thermoelastic contact of a sphere sliding on a plane, *Wear 59* (1980) 21–29.

J. L. Bishop and C. M. McC. Ettles, The seizure of journal bearings by thermoelastic mechanisms, *Wear, 79* (1982) 37–52.

H. Blok, Viscosity of lubricating oils at high rates of shear, *De Ingenieur, Netherlands, 60* (1948) 58–63.

R. A. Burton, Thermal aspects of bearing seizure, *Wear, 8* (1965).

R. A. Burton and H. J. Carper, An experimental study of annular flows with applications in turbulent film lubrication, *Trans. ASME, 89*, Series F (1967) 381–391.

R. A. Burton, V. Nerlikar, and S. R. Kilaparti, Thermoelastic instability in a seal like configuration, *Wear, 24* (1973) 177–188.

R. A. Burton, An axisymmetric contact patch configuration for two slabs in frictionally heated contact, In *The Mechanics of Contact between Deformable Bodies*, DePater, Ed., Delft University Press, Delft (1975) 191–205.

R. A. Burton, High speed seal flows with temperature sensitive viscosity, *ASLE Trans., 23* (1989) 48–52.

R. A. Burton, The thermal boundary condition for high-speed seal flow, *STLE Trans. 34* (1991) 155–160.

R. A. Burton and R. G. Burton, Interaction of multiple brushes on a slipring, *IEEE Trans., CMTH, 18* (1992) 328–331.

R. A. Burton, The coupling of waviness and heating in a seal, *STLE Trans. 35* (1992) 751–755.

R. A. Burton, The effects of wall perturbations on thermoturbulent Couette flow, *Tribology Trans., 37* (1994a) 415–419.

R. A. Burton, Convection of heat in short bearings and face seals, *Tribology Trans., 37* (1994b) 876–880.

R. A. Burton and V. Nerlikar, Clearance, leakage, and temperature in thermoelastically deformed frictionally heated contact, *ASME Trans., Series F, 97* (1975) 546–551.

M. Couette, Etudes sur le frottement des liquides, *Ann. Chem. Phys., 21* (1890) 433.

H. B. Dakshima-Murthy, Limitations to non-isothermal flow in lubricant films due to frictional heating, *Dissertation WTDH*, Technical University of Delft, Netherlands (1985).

H. M. de Groff, On viscous heating, *J. Aero. Sci., 23* (1956) 395–396.

T. G. Doust and A. Parmer, Experimental study of pressure and thermal distortions in mechanical seals, *ASLE Trans, 29* (1991) 151–159.

T. A. Dow and R. A. Burton, Investigation of thermoelastic instabilities of sliding contact in the absence of wear, *Wear, 19*, (1972) 315–328.

T. A. Dow and R. A. Burton, The role of wear in the initiation of thermoelastic instabilities of rubbing contact, *Trans. ASME, Series 7, 95* (1973) 71–75.

T. A. Dow and R. D. Stockwell, Experimental verification of thermoelastic instabilities in sliding contact, *Trans. ASME, Series F, 99* (1977) 359.

T. A. Dow, R. D. Stockwell, and J. W. Kannel, Thermal effects in rolling/sliding EHD contacts—Part 1: Experimental measurements of surface pressure and temperature, *ASME Journal of Tribology, 109* (1987) 503.

D. Dowson, J. Hudson, B. Hunter, and C. March, An experimental investigation of thermal equilibrium of steadily loaded journal bearings, *Proc. I. Mech. E., 181, part 3B* (1966–67) 70–80.

K. Dufrane and J. Kannell, Thermally induced seizure of journal bearings, *Trans. ASME, Series F, 111* (1989) 177–182.

J. Dundurs, Distortion of a body caused by a free thermal expansion, *Mechanics Research Communications, 1* (1974) 121–124.

G. A. Etemad, Free convection heat transfer from a rotating horizontal cylinder in ambient air with interferometric study of flow, *Trans. ASME, 67* (1955) 1283–1289.

I. Etsion and Y. Dan, An analysis of mechanical face seal vibration, *Trans. ASME, Series F, 103* (1981) 428–435.

I. Etsion, Accuracy of the isoviscous solution for the Reynolds equation in mechanical seals, *J. Eng. Tribology, I. Mech. E., 210* (1996) 153–156.

I. Etsion and M. D. Pascovici, A thermohydrodynamic analysis of a misaligned mechanical face seal, *Tribology Trans. STLE, 31* (1993) 589–596.

I. Etsion, Thermohydrodynamic analysis of a mechanical face seal, *Trans. ASME, Series F, 114* (1992) 639–645.

C. M. McC. Ettles, Transient thermoelastic effects in fluid film bearings, *Wear, 79* (1982) 53–71.

N. Fillon, J. Frene, and R. Boncompain, Etude experimentale de I'affect thermique dans les paliers a patins oscillants, *Congres International de Tribologie, EUROTRIBE 85*, Lyon (1985).

E. Georgopoulos, Thermal convection effects in a thin viscous film, *Wear, 59* (1980) 111–120.

D. T. Gethen, An investigation into plain journal bearing behavior including deformation of the bearing, *Proc. I. Mech. E., C3* (1985) 215–223.

E. J. Hahn and C. F. Kettleborough, Solutions for the pressure and temperature in an infinite slider bearing of arbitrary profile, *Trans. ASME, Series F, 89* (1967) 445–452.

E. J. Hahn and C. F. Kettleborough, The effects of thermal expansion in infinitely wide slider bearings—free thermal expansion, *Trans. ASME, Series F, 90* (1968) 223–239.

T. L. Hazlett and M. Khonsari, Finite element model of journal bearings undergoing rapid thermally induced seizure, *Tribology International, 25* (1992a) 177–182.

T. L. Hazlett and M. Khonsari, Thermoelastic behavior of journal bearings undergoing seizure, *Tribology International, 25* (1992b) 183–187.

R. Holm, *Electrical Contacts Handbook*, Springer Verlag, Berlin (1958).

Y. C. Hsu and R. A. Burton, Exact thermoelastic solutions for clearance variation in a short cylindrical bearing configuration with unsymmetrical frictional heating, *Trans. ASME, Series F, 89* (1967) 19–25.

K. L. Johnson, *Contact Mechanics*, Cambridge University Press, Cambridge, England (1985) 391–396.

R. R. Johnson, T. A. Dow, and Y. Y. Zhang, Thermoelastic instability in elliptical contact between two sliding surfaces, *Trans. ASME, Journal of Tribology, 110* (1988) 80.

F. E. Kennedy and F. F. Ling, A thermal thermoelastic and wear simulation of a high energy sliding contact problem, *Trans. ASME, Series 7, 96* (1974) 496–507.

F. E. Kennedy Jr., C. K. Chuah, and F. O. W. Brote, Thermomechanical contact phenomena in face seals, *Wear, 102* (1985) 127–140.

S. R. Kilaparti and R. A. Burton, Pressure distribution for patchlike contact in seals with frictional heating, thermal expansion, and wear, *Trans. ASME, Series F, 100* (1978) 65–69.

M. Khonsari and H. J. Kim, On thermally induced seizure in journal bearings, *Trans. ASME, Series D, 111* (1989) 661–667.

J. D. Knight and P. Ghademi, Effects of modified effective length models of the rupture zone in the analysis of a fluid journal bearing, *Tribology Trans. 35* (1992) 29–36.

F. F. Ling, Contact and surface mechanics, *Achievements in Tribology 90*, (1990) 129–149.

F. F. Ling and V. C. Mow, Surface displacement of a convective elastic half space, *Trans. ASME, Series D, 87* (1966) 814–816.

F. F. Ling, *Surface Mechanics*, John Wiley and Sons, New York (1973).

J. D. Medwell and D. T. Gethen, An investigation into plain journal bearing behavior including thermal deformation, *Proc. I. Mech. E., 199* (C3) (1985) 215–223.

R. Nahme, Betrage zur hydrodynamischen Theorie der Lagerreibung, *Ing. Arch., 11* (1940) 191–209.

A. Nica, Contributions to the determination of the real clearance in sliding bearings, *Trans ASME, Series D, 87* (1965) 781–784.

J. Nikuradse, Stromungsgesetze in rauhen Rohren, (Flow laws in rough tubes) *Verein deutsche Ing., Forshungheft, 361* (1933).

F. W. Ocvirk, Short bearing approximation for full journal bearings, *NACA Tech. Note 2008* (1952).

M. Pascovici, Aspura influentei transferului calurii la miscarea fluidor in filme subtire, *St. Cerc. Cec. Apl.* (Romania) *28* (1969) 1041–1051.

O. Pinkus, *Thermal Aspects of Fluid Film Tribology*, ASME Press, New York (1990).

J. L. M. Poiseuille, Recherches experimentelles sur le mouvement des liquides dans le tubes de tres petits diametres, *Comptes Rendus, 11* (1840) 961 and 1041; and *Comptes Rendus, 12* (1841) 112.

O. Reynolds, On the therory of lubrication and its appliction to Mr. Beauchamp Tower's experiments, *Phil. Trans. Royal Soc., A, 177* (1886) 157–234.

Ernst Schmidt, Über die Anwendung der Differenzenrechnung auf technische Anhelzund Abkühlungsprobleme, *Beitrage zur Technischen Mechanik und Technischen Physik* (Foppls Festschrift), Springer, Berlin (1924) 179–189.

K. F. Slotta, Über die innere Reibung der lösungen einer Chromate. *Ann. Phys. Chem., Series 3, 14* (1881) 13–22.

J. M. Robertson, On turbulent plane-Couette flow, *Proc. 6th Midwestern Conference on Fluid Mechanics*, Univ. of Texas Press, Austin, Texas (1959) 169–182.

F. Sadeghi and T. A. Dow, Thermal effects in rolling/sliding EHD contacts - Part 2: analysis of thermal effects in fluid film, *ASME Journal of Tribology, 109* (1987) 512.

F. Sadeghi, T. A. Dow, and R. R. Johnson, Thermal effects in rolling sliding contacts - Part 3, an approximate method for prediction of mid-film temperature and sliding friction, *Trans ASME, Series D*, 105 (1983).

R. F. Salant and S. E. Hassan, Large scale thermoelastic instability in hydrostatic mechanical seals, *Proc. 12th Int. Conf. Fluid Sealing, BHRA* (1989) 75–88.

H. Schlichting, *Boundary Layer Theory*, (Trans. J. Kestin), McGraw-Hill Book Company, New York (1968).

E. Schmidt, *Foppls Festschrift*, Springer, Berlin (1924) 179.

K. F. Slotte, *Wied. Ann. 14* (1881) 13.

M. I. Smith and D. D. Fuller, Journal bearing operation at super laminar speeds, *Trans. ASME, Series F, 78* (1956) 469–474.

H. J. Sneck, Thermal effects in face seals, *Trans. ASME, Series F, 91* (1969) 434–437.

A. Sommerfeld, Zur Hydrodynamischen Theorie der Schmiermittelreibung, *Z. Angew. Phys., 50* (1904) 57–58.

H. E. Staph and R. A. Burton, Thermally activated seizure of angular contact bearings, *ASLE Trans., 10* (1967).

M. J. Stefan, Versuche ueber die scheinbare Adhaesion, *Sitzberichte der Mathematische Naturwissenschaftliche Classe*, Akademie der Wissenschaften in Wein, 1 (1874) 713, 735.

G. I. Taylor, Fluid friction between rotating cylinders, *Scientific Papers of G. I. Taylor, Vol. II*, Cambridge University Press, Cambridge, England (1960).

S. P. Timoshenko and J. N. Goodier, *Theory of Elasticity*, McGraw-Hill Book Company, New York (1970).

B. Tower, First report on friction experiments, *Proc. Inst. Mech. Engs.*, (1883) 632–659.

B. Tower, Second report on friction experiments, *Proc. Inst. Mech. Engs.*, (1885) 58–70.

G. Vogelpohl, Der Ubergang der Reibungswarme von Lagern aus der Schmierschicht in die Gleitflachen, *VDI Forschungheft, 425* (1949).

Y. T. Wu and R. A. Burton, Thermoelastic and dynamic phenomena in seals, *Trans. ASME, Series F, 103* (1981) 253–260.

Index